Crossing Bridges: Synthetic and Charge Transfer Studies of Linear and Cross-Conjugated Systems

KEVIN BARRY VINCENT

Department of Chemistry

Crossing Bridges: Synthetic and Charge Transfer Studies of Linear and Cross-Conjugated Systems

Kevin Barry Vincent MChem (Hons)

Department of Chemistry

A Thesis submitted in part fulfilment of the requirements for the degree of Doctor of Philosophy at Durham University

Statement of Copyright

Declaration

The work described in this thesis was carried out at the University of Durham, Department of Chemistry, between October 2010 and December 2013. All the work is that of the author unless otherwise stated, and it has not been submitted for a degree at this or any other university.

Memorandum

Part of this work has been the subject of the following published articles:

1. **Synthesis and redox properties of mono-, di- and tri-metallic Platinum-ethynyl complexes based on the *trans*-Pt($C_6H_4N\{C_6H_4OCH_3$-$4\}_2$)(C≡CR)(PPh_3)$_2$ motif.**

   K.B. Vincent, M. Parthey, D. S. Yufit, M. Kaupp, P. J. Low. *Polyhedron*, 2014, Manuscript submitted.

2. **A Combined Computational and Spectroelectrochemical Study of Platinum-Bridged Bis-Triarylamine Systems.**

   M. Parthey, K. B. Vincent, M. Renz, P. A. Schauer, D. S. Yufit, J. A. K. Howard, M. Kaupp, P. J. Low. *Inorg. Chem*, 2014, *53*, 1544-1554.

3. **Syntheses, Spectroelectrochemical Studies, and Molecular and Electronic Structures of Ferrocenyl Ene-diynes.**

   K. B. Vincent, Q. Zeng, M. Parthey, D. S. Yufit, J. A K. Howard, F. Hartl, M. Kaupp, P. J. Low. *Organometallics*, 2013, *32*, 6022-6032.

4. **Synthesis, structure and electrochemical properties of triarylamine bridged dicobaltdicarbon tetrahedrane clusters.**

   W.Y. Man, K.B. Vincent, H.J. Spencer, D.S. Yufit, J.A.K. Howard, P.J. Low, *J. Cluster Sci*, 2012, *23*, 853.

Part of this work has been the subject of the following presentations:

1. 2013: Poster and Flash presentation: International School and Symposium on Molecular Materials (ISSMM2013): Tokyo Institute of Technology: Tokyo, Japan. “Synthesis and Spectroelectrochemical Studies of Ferrocenyl ene-diynes”

2. 2012: Poster: International School and Symposium on Molecular Materials (ISSMM2012): Durham University: Durham, UK. “Platinum Bridged Mixed Valence Compounds”
3. 2012: Poster: RSC Dalton Summer School 2012; Electronic Structural Methods in Inorganic Chemistry: University of Edinburgh: Edinburgh, UK.
4. 2012: Poster: RSC Inorganic Chemistry 2012; A Joint Meeting of Dalton Division Interest Groups: Warwick University: Warwick, UK.
5. 2011: Poster: Electrochemistry Horizons: University of Bath: Bath, UK. “ ‘Inverse’ Mixed Valence Complexes”

Abstract

This thesis sets out to explore the electronic structure and properties of organometallic complexes. The mixed valence states generated on one-electron oxidation are investigated based on the theory developed in Chapter 1, which provides an introduction to the general area and electron transfer.

Further Chapters in this thesis set out to explore the communication between redox states spanning linear and branched architectures and draw on the ideas presented in Chapter 1 to draw conclusions as to the degree of communication between the sites. To this extent a series of platinum-acetylide complexes bearing the unusual triarylamine ligand, containing one to four redox centres, were prepared and the electronic properties probed with IR and UV-vis NIR spectroelectrochemistry. The results show that there is only very weak communication between the centres. In Chapter 3 the work looks at symmetrical analogues of these compounds and builds on previously published work to explore in more detail the electronic structure of a series of *trans*-$[Pt(C{\equiv}CC_6H_4NAr'_2)_2(PR_3)_2]$ complexes to explore the effect of the triarylamine and ancillary phosphine ligands. The results show modest communication between the centres and little effect of the phosphine ligand.

The later chapters in this thesis focus on developing synthetic routes and analyses of branched-conjugated materials. Chapter 4 develops the synthesis of a range of compounds based on the $FcCH{=}C(C{\equiv}CR)_2$ with organic R groups. The results show that, despite proposals of such systems being able to act as transistors, the ferrocene moiety is electronically isolated. Chapter 5 builds on this work and

develops the synthesis of $FcCH=C(C\equiv CC_6H_4C\equiv CML_n)_2$, ML_n= $Ru(PPh_3)_2Cp$ or Ru(dppe)Cp*. Spectroelectrochemical analysis has shown weak communication between the –Ru-(C≡C)- centres. Finally, Chapter 6 addresses the interactions within multi-ferrocenyl compounds. Analysis by IR SEC studies have shown that in compounds bearing either 2, 3 or 4 ferrocene groups that each centre is essentially electronically isolated despite electrochemical studies highlighting that in the right conditions a degree of through-space communication can be observed.

Acknowledgements

Firstly, I would like to thank Prof. Paul Low for giving me this great opportunity to carry out my PhD under his supervision and for the continued patience, support and guidance over the duration of my studies. I would also like to offer my thanks to Dr. Mark Fox for the many helpful discussions, on both theoretical and synthetic chemistry, we have had over the course of my studies as well as the invaluable discussions on the merits of why Arsenal are a better team than Liverpool. I would also like to express my thanks to the EPSRC for the funding to carry out this work.

I would also like to thank all of the members of the PJL research group, past and present, for all of the support and help that has been provided, especially in the 'Library' on Friday afternoons. In particular I would like to thank Dr. Phil Schauer who has provided some of the most interesting and insightful conversations on such occasions and for his continued aid in the pursuit to identify Durham's best pint. I would also like to offer my thanks to all of Durham's analytical services, who help to make all of this work achievable; In particular I would like to thank Dr. Dmitry S. Yufit of the crystallography service and Mrs Catherine Heffernan of the NMR service, not only for all of the help with NMR but for all of the conversations we have had over the years.

I would also like to thank all of my family and friends for the love, support and patience they have shown me over the years, in particular I would like to thank my parents, who without all of your support and belief through both this work and

previous times I would not be writing this today. I would also like to thank Dr. Antonis Messinis who proved great support and good laughs through the time we lived together. Finally I would like to thank Hannah for having to deal with me on the days that things went wrong, the days when nothing worked and the days that were never ending as well as for all the help you have given through proof-reading this thesis.

This thesis is dedicated to my grandparents.

Abbreviations

°	degrees
°C	degrees Celsius
$[BArF_4]^-$	$[B(C_6H_3(3,5\text{-}CF_3)_2)_4]$- anion
α	alpha
A	acceptor
A	amps
Å	angstrom
AcOH	acetic acid
Ar	aryl
ASAP	Atmospheric Solids Analysis Probe
β	beta
B	bridge
BL	bridging ligand
bpy	2,2'-bipyridine
BS	broken symmetry
ca.	circa
$CDCl_3$	deuterated chloroform
CH_2Cl_2	dichloromethane
cm^{-1}	wavenumber (reciprocal centimeters)
COD	cyclooctadiene
COSY	homonuclear correlation spectroscopy
Cp	cyclopentadienyl
Cp*	pentamethylcyclopentadienyl
CT	charge transfer
CV	cyclic voltammetry
δ	chemical shift
D	donor
d	doublet
ΔE_p	$E_{1/2}(2)$-$E_{1/2}(1)$ potential difference
DFT	density functional theory
dppe	1,2-bis(diphenylphosphino)ethane
dppf	1,1'-bis(diphenylphosphino)ferrocene
ε	extinction coefficient
E	cell potential

E^*_{th}	thermal activation energy
$E_{1/2}$	half wave potential
ET	electron transfer
Et	ethyl
EtOH	ethanol
eV	electron volt
F	Faraday constant
Fc	$(C_5H_5)Fe(C_5H_4)$
GC-MS	gas chromatography mass spectrometry
H_{ab}	electronic coupling value
HMBC	Heteronuclear multiple-bond correlation spectroscopy
HOMO	highest occupied molecular orbital
HOSO	highest occupied spin orbital
HSQC	Heteronuclear Single Quantum Correlation Spectroscopy
Hz	hertz
I	current
IC	interconfigurational
i_{pa}	peak anodic current
i_{pc}	peak cathodic current
IR	infra-red
IVCT	intervalence charge transfer
K	Kelvin
K_c	comproportionation constant
kJ	kilo joule
λ	wavelength
LMCT	ligand-to-metal charge transfer
M	metal
m	multiplet
M	molar concentration
m/z	mass per unit charge
MALDI	matrix assisted laser desorption ionisation
mL	millilitre
MLCT	metal-to-ligand charge transfer
mmol	millimol
MO	molecular orbital
MS	mass spectrometry
MV	mixed valence

mV	millivolt
NBu_4	tetra-butyl ammonium
NIR	near infra-red
NIS	N-iodo succinimide
NMR	nuclear magnetic resonance
NOESY	Nuclear Overhauser effect spectroscopy
OTf	triflate
OTTLE	optically transparent thin layer electrode
PF_6^-	hexafluorophosphate
Ph	phenyl
PPh_3	triphenylphosphine
ppm	parts per million
prep TLC	preparative thin layer chromatography
pz	pyrazine
R	gas constant
R	general organic group
s	singlet (NMR)
s	strong (IR)
SEC	spectroelectrochemistry
sh	shoulder (IR)
$SiMe_3$	trimethylsilyl group
SOMO	singularly occupied molecular orbital
t	triplet
T	temperature
TCNQ	tetracyanoquinodimethane
TDDFT	time-dependent density functional theory
TEE	tetraethynylethene
THF	tetrahydrofuran
TLC	thin layer chromatography
TMS	trimethylsilyl group
TMSA	trimethylsilyl acetylene
TOF	time of flight
TTF	tetrathiafulvalene
UV-vis NIR	UV-visible near infra-red
V	voltage
w	weak (IR)
X	halide, pseudo-halide

Table of Contents

1. Introduction

In 1965 it was observed by Gordon Moore, a co-founder of Intel, that the number of chips on a transistor was doubling at a rate of 18 – 24 months.[1] This observation was to become what is now known as Moore's law and, although Moore believed this prediction would hold for a decade, it has essentially held true for over 40 years. However, as we now reach a point where the physical limits of maintaining this rate due to problems with the construction[2] of the devices, then the rate of increase will only double every three years.[3] The inherent problems associated with the manufacture of smaller devices has led to concern that the solid state devices based on Moore's Law rates of progress will soon reach a failure point[4] and, as such, the electronics industry searches for improved techniques and solutions to these problems *in silico*n based devices. Consequently, a significant body of research has been directed towards a different route in the pursuit for smaller devices with higher levels of integration by looking at alternatives based on a molecular electronics technology.[5]

1.1. Electronics of Molecules

What is largely considered to be the key breakthrough[6] in molecular electronics came in 1974 when Aviram and Ratner proposed a molecular device in which charge could be transferred between electrodes through a molecular bridge.[7] The rectifier molecule proposed was of a donor-bridge-acceptor (D-B-A) construction with the tetrathiafulvalene (TTF) donor connected to tetracyanoquinodimethane

(TCNQ) acceptor through a saturated organic bridge system (Figure 1). However, despite decades of work, and many promising results that have led to molecular devices capable of current rectification,[8] there are still many challenges centred on the deposition of single molecules between electrode surfaces.[9] As such, there has been much wider interest in the study of the electronic properties of molecules with potential for device technology, and in particular a re-focussing of studies concerning conceptually simpler, wire-like systems.[10]

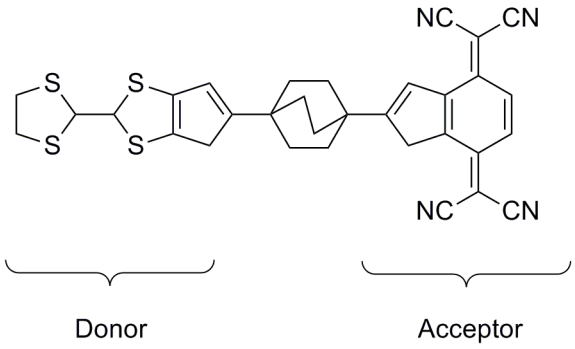

Figure 1: The Aviram-Ratner rectifier.

There are many examples of compounds that have been proposed as molecular wires based on their structural properties,[2b, 11] and a growing array of methods for the study of single molecule junctions.[12] However, spectroscopic and spectroelectrochemical techniques also allow facile studies of intramolecular electron transfer in solutions of the compound of interest. The simplest systems that can be considered as wire-like systems ar those which consist of molecules where two redox centres are connected via a conjugated bridge. These compounds are ideal molecular systems with which to explore intramolecular electron transfer reactions. For the compound to act as a prototypical wire, one terminus must be able to act as a source of electrons and the other end as a source of holes (also

known as a drain).[13] The most common systems have two identical metal-ligand fragments, M, serving as the termini, linked by a bridging ligand. In suitable cases, one-electron oxidation (or reduction), leads to a mixed valence (MV) complex, where the metal centre in the lower oxidation state serves as the source, the site in the higher oxidation state as the drain. Thermal- or photo-induced electron transfer is in principle possible between the two sites providing avenues for the study of the 'wire-like' nature of the bridge (Figure 2).

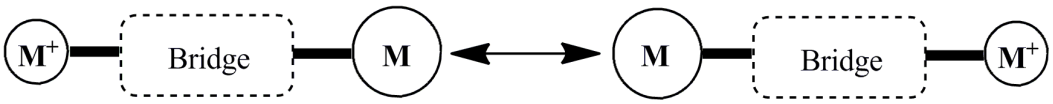

Figure 2: Basic description of a mixed-valence model of a molecular wire capped with two metal groups. Left; original configuration, right; configuration after electron transfer

1.1.1. Two Site Electron Transfer

Mixed valency has been extensively studied,[14] with the archetypal mixed valence system the Creetz-Taube ion[15,16] $[\{Ru(NH_3)_5\}_2(\mu\text{-pz})]^{5+}$ (pz = pyrazine) (Figure 3) serving as a representative example. The thermodynamic stability of the MV state relative to the analogous homo-valent states can be determined using electrochemical techniques under a given set of experimental conditions, with a number of different factors contributing to the relative stabilities, including electrostatic and / or solvation factors, ion-pairing interactions, structural changes and resonance stabilisation of the MV state.[17]

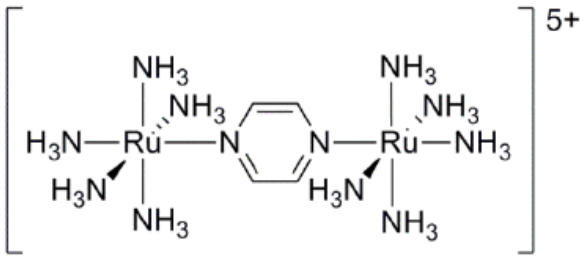

Figure 3: Cruetz Taube ion.

From electrochemical data, the comproportionation constant (K_c) can be determined. The magnitude of K_c reflects the thermodynamic stability of the MV state, that is, the stability of the complex $[M\text{-}M]^+$ relative to M-M and the dicationic $[M\text{-}M]^{2+}$.

$$[M-M] + [M-M]^{2+} \underset{}{\overset{K_c}{\rightleftharpoons}} 2[M-M]^{+}$$

K_c can be derived from the Nernst equation, which is discussed in more detail in Chapter 2, and as such the specific concentrations of the neutral, mono- and di-cationic species at equilibrium can be determined from ΔE between the redox events in the generation of $[M\text{-}M]^+$ and $[M\text{-}M]^{2+}$ (see Chapter 2, UV-vis NIR spectroelectrochemistry).

Recent work by Geiger *et al* on tetraferrocenyl(nickeldithioline) has shown that it is possible to affect the degree of separation of redox events, and hence K_C and the stability of the MV state relative to disproportionation, by alteration of the electrolyte (Figure 4). The effects are caused by the difference in ion-pairing strength between the different anions, and similar results can be achieved through altering the donor properties of the solvent.[18-20] This effect enables us to differentiate between through-bond (which are largely medium-independent) and

through-space effects between redox centres by comparison of the ΔE in solutions containing the $[PF_6]^-$ anion to results from electrolytes containing a weakly coordinating $[B(C_6F_5)_4]^-$ or $[B(C_6H_3(3,5\text{-}CF_3)_2)_4]^-$ anion. A change in ΔE in response to a change in the medium is consistent with through-space communication, conversely, if there is little change in the magnitude of ΔE then this is indicative of through-bond communication.[21] This phenomenon is also of great interest when it comes to the study of compounds that contain multiple-redox centres that in conventional electrolyte solutions have no thermodynamic stability of the MV states such that a single redox process is observed or the formal potentials are so close together that different processes are unresolved. It is clear that if the thermodynamic stability of these states can be manipulated by use of a larger, weakly coordinating anion then their properties should be examinable by spectroscopic methods.

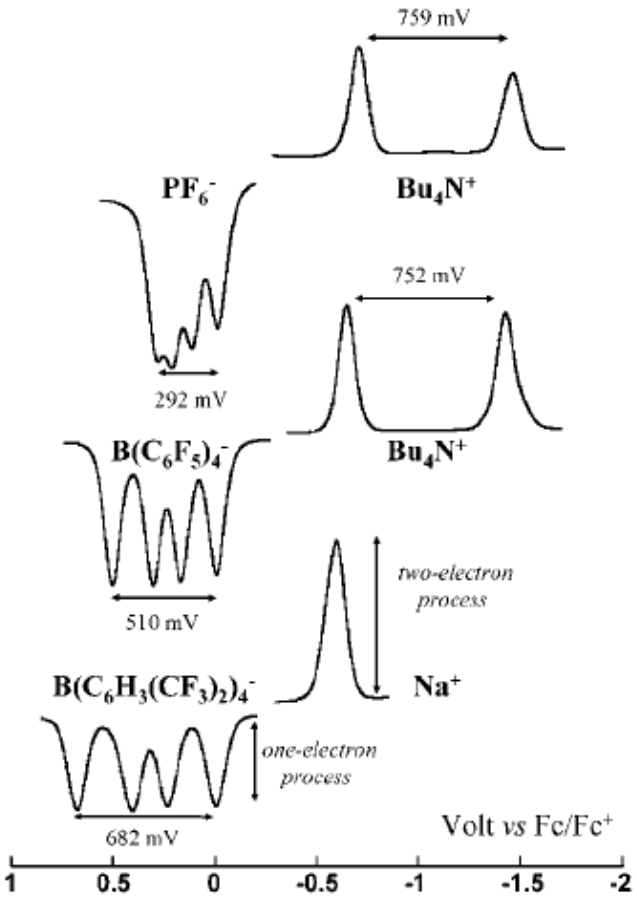

Figure 4: Electrolyte effects on a tetra-ferrocenyl nickel dithioline complex. Reproduced from [19] (reproduced by permission of American Chemical Society (ACS)).

In complementary fashion, the spectroscopic properties of MV complexes may be used to extract details of the underlying electronic structure and charge transfer characteristics.[22]

Mixed valence complexes of this nature give rise to potential energy surfaces that can be considered as two diabatic states with minima that represent the prospective location of the unpaired electron, i.e. at which terminus the electron is sitting. In systems where there is no communication between the redox termini the energy profile will retain this diabatic state, however, in systems where there is interaction between the two termini the two diabatic states can mix to give a set of

adiabatic surfaces in which the ground state shows mixing of the two minima to allow a pathway between them and an upper state that corresponds to an excited state. Robin and Day have devised a system of classification for MV complexes based on the structural and electronic properties so that compounds can be labelled according to the degree of interaction between the redox centres.[23] There are three original classes proposed by Robin and Day: Class (I), Class (II) and Class (III) where the degree of communication between the sites increases through each class.

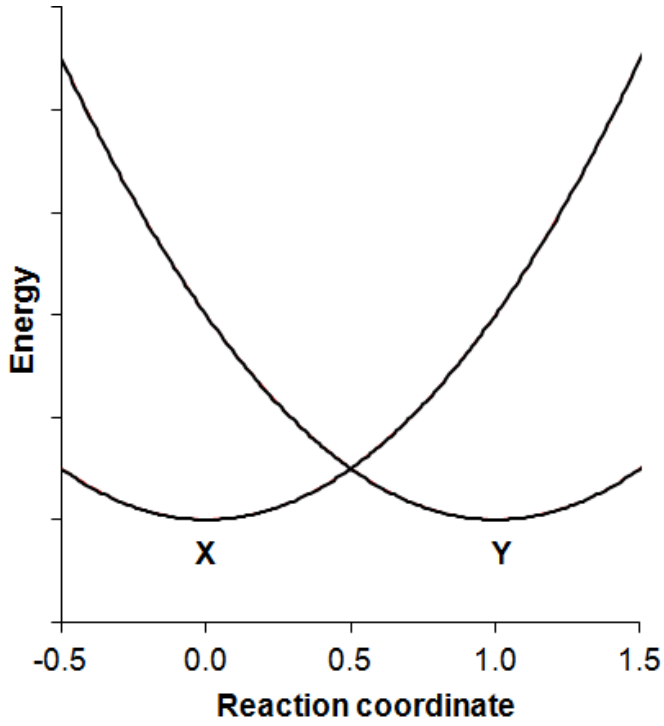

Figure 5: Potential surface for an elementary Class (I) system.

Class I MV systems have the least amount of communication between the redox sites and, as such, the properties of each individual centre can be observed (Figure 5), i.e. M^{+1}-B-M^{0}. Upon oxidation / reduction the charge becomes isolated on a single redox centre and there is no communication between the redox active moieties. Although MV complexes are often considered to be derived from two identical electrophores, such a restriction is not necessary to meet the broad

definition of a MV complex (i.e. one in which an element is present in two (or more) distinct oxidation states). Many Class I systems feature quite distinct and rigid coordination spheres that impose significant differences on the constituent metal centres in order to engineer distinct properties at each site.

Class (III) systems are those that exhibit full delocalization of the imparted charge, that is to say that $M^{+0.5}$-B-$M^{+0.5}$. The delocalisation of the charge across the whole molecule now gives rise to a potential surface that has a merged ground state (XY) and an accessible excited state (Z), from which an optical transition can occur (Figure 6). It is important here to note that extraction of any data based on the electrochemistry of Class (III) compounds can be hampered by ion-pairing effects in the MV and dicationic states. Logic suggests that if there is a high degree of communication between the redox sites then the second oxidation event should be shifted to higher potential in comparison to the first, due the fact it is less favourable to remove the second electron from the species. As noted earlier, the use of electrochemistry as a technique from which to garner information on the coupling between redox sites is complicated by many factors. As such it is possible that the charge localisation of the dicationic state can lead to increased stabilisation through solvation and ion-pairing effects and the second oxidation can become shifted close to the first oxidation, even giving rise to what can appear as a single redox event.[24]

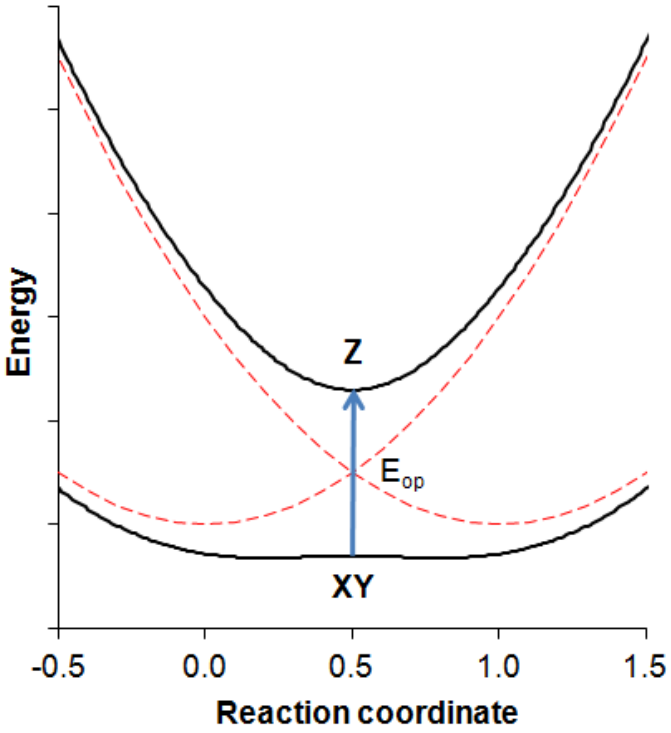

Figure 6: Potential surface for a Class (III) system.

Of greater interest is the Class II group of compounds that are deemed to have 'weakly-coupled' redox centres. The potential surface for these systems now gives a ground state with a double minima (XY) arising from an intermediate degree of mixing between the diabatic states. These two minima represent the two different locations that the hole can reside in the compound, as well as an accessible excited state (Z) from which interconversion between the states M-B-M^+ and M^+-B-M can occur (IVCT) (Figure 7). In this Class of compounds the electronic coupling, H_{ab}, is the same as twice the energy gap between the two states at the minima of Z.

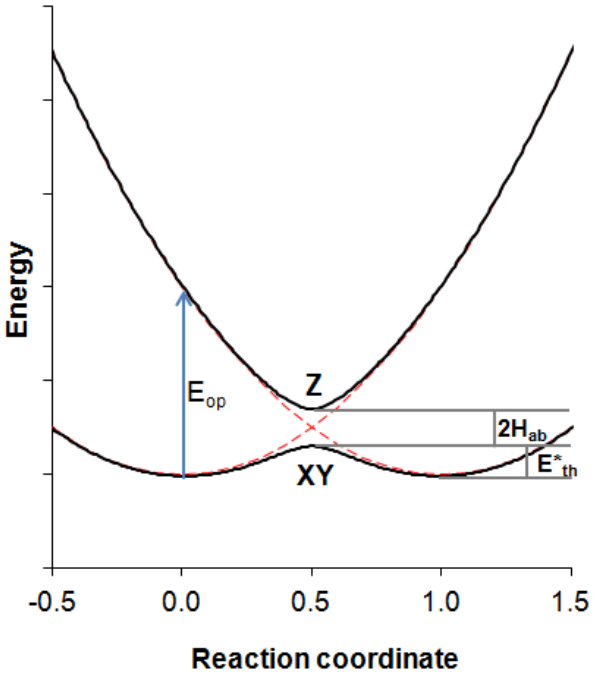

Figure 7: Potential surface for a Class (II) system.

Electron transfer between the two sites can now pass through either an optical or thermal pathway. The thermal pathway is governed by the Franck-Condon principle, which states that nuclear motion (10^{-13} s) is much slower than electron motion (10^{-15} s) and, as such, the immediate transfer of an electron is forbidden.[25] In order for the electron transfer to follow the thermal pathway (bottom path; Figure 8) there has to be a reorganisation of the inner and outer sphere of the system (local and solvent geometries) that facilitates the electron transfer and hence gives rise to the thermal activation energy E^*_{th} (Figure 7).

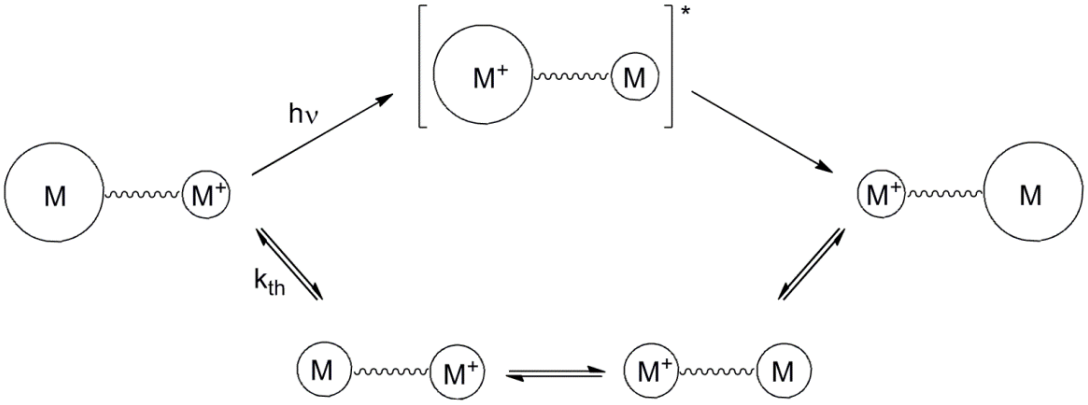

Figure 8: Electron transfer pathways in a Class (II) system.

It is the optically induced pathway that is of most interest in such systems as this is accompanied by a spectral band associated with the transition, IVCT. This band, often found in the NIR, has been shown by Hush (derived from Marcus theory) to be intrinsically related to the electronic coupling within the molecule and, as such, gives an experimental probe from which more accurate data can be extracted.[26] From this model it is possible to consider the parameters of the IVCT transition with respect to the inner and outer sphere reorganisation energies, λ_i and λ_o, and the energy contributions from the difference between the initial and final states, ΔE_0, and from the effects of spin orbit coupling and ligand effects, $\Delta E'$.[27]

$$\nu_{max} = \lambda_i + \lambda_o + \Delta E_0 + \Delta E'$$

For a symmetrical species the relationship between the IVCT band that occurs at optical absorption energy, E_{op}, and the thermal activation energy barrier for the electron transfer, ΔE_{th}^*, shows a linear four-fold relationship.

$$E_{op} = 4\Delta E_{th}^*$$

The band position is also governed by E_{op} and is related to the solvent effects on the CT in the mixed valence systems through:

$$E_{op} = E_{in} + E_{out}$$

$$E_{in} = n\left(\frac{2f_n f_{n+1}}{f_n + f_{n+1}}\right)(d_n^0 - d_{n+1}^0)^2$$

$$E_{out} = e^2\left(\frac{1}{2a_n} + \frac{1}{2a_{n+1}} - \frac{1}{r}\right)(\frac{1}{D_{op}} - \frac{1}{D_s})$$

n is the number of ligands per metal centre, f_n and f_{n+1} are the force constants for the redox site in oxidation state n and n^{+1} respectively, a_n and a_{n+1} are the metal-ligand bond lengths, *r* is the distance between the 2 redox sites and D_{op} and D_s are the optical and static dielectric constants for the solvent medium. The charge transfer band can also be used to extract the electronic coupling value (H_{AB}) between the two centres. The absorbance of the charge transfer band can be used to calculate the molar absorptivity from the Beer-Lambert law; in turn the molar absorptivity can be used to calculate H_{AB} using the respective equations below.

$$A = \varepsilon c l$$

$$H_{AB} = 2.05 \text{ x } 10^{-2}\frac{(\bar{\nu}_{max}\varepsilon_{max}\Delta\bar{\nu}_{\frac{1}{2}})^{1/2}}{r} \quad \text{cm}^{-1}$$

ε is the molar absorptivity at the charge transfer band maximum, A is the absorbance at the band maximum, *c* is the concentration of the solution and *l* is the path length of the cell for the Beer-Lambert law and $\bar{\nu}_{max}$ and $\Delta\bar{\nu}_{1/2}$ are the band maximum and the band width at half intensity for the transfer band. The

band maximum and band width at half intensity can also be used to determine the class of the mixed valence species (Class II or Class III). In a Class II system the transition from the ground to excited state occurs such that the excited state is formed at a steeply sloping part of the optical pathway, as such Class II systems often exhibit broad charge transfer bands. For Class III systems, where there is no clear distinction between the oxidation states of the two redox sites and the system is considered fully delocalized, the lower pathway of the potential energy diagram comes to form a single minima at X=0.5. For these systems there is a single transition available and the excited state is formed on a much shallower part of the optical pathway than for Class (II) systems, for this reason the charge transfer bands associated with Class (III) systems tend to be considerably sharper than those of Class (II) systems. It thus stands that if the band width at half intensity for the observed IVCT band is equal to or greater than the theoretical value obtained from the band maximum (using the equation below) then the system can be classified as a Class (II) system. If, however, $\Delta\bar{\nu}_{1/2}$ for the intervalence band is less than the calculated theoretical value then the system belongs to the Class (III) group.

$$\Delta\bar{\nu}_{1/2} = (2310\bar{\nu}_{max})^{1/2} \quad \text{cm}^{-1}$$

Other means of determining the class of the compounds also exist as the CT band exhibited in both Class (II) and Class (III) systems are of different nature. It stands that the band in Class (II) systems is dependent on the rearrangement of the solvent sphere, however, in Class (III) systems the electron density becomes delocalised and as such there is no rearrangement of the solvent required. In practical terms this allows the dependence of an IVCT band from Class (II)

systems to be identified due to the solvatochromic nature of transition.[27] Furthermore, because of the different origins of these transitions the relationships between H_{ab} and the spectroscopic profile outlined for class (II) systems no longer hold for Class (III)[16] and the coupling parameter is now given by:

$$H_{ab} = \lambda/2$$

While classes of compounds can be defined using these parameters the experimental results are often less well defined and recently there has been a new class of compounds proposed, Class (II-III), where the behaviour of the CT band exhibits both Class (II) and Class (III) properties and the compound exhibits electron transfer at a rate greater than the solvent reorganisation time.[28] It has been shown that small variations in the length of the bridging ligand, BL, in $[\{Ru(bpy)_2\}_2(\mu\text{-BL})]^{5+}$ (bpy=2,2'-bipyridine; BL= di-bidentate polypyridyl) gives rise to a range of compounds that cover the Class (II) and Class (III) descriptions as well as compounds that that are on the border of both classes.[29] Further to the proposal of a Class (II-III) assignment for such compounds, Chisholm *et al.* have prepared and studied a series of oxalate bridged complexes of the general form $[\{(^tBuCO_2)_3MM\}_2\text{-}(\mu_2\text{-}O_2CCO_2)]$ where MM = Mo_2, MoW and W_2, where both solvent independent IVCT and MLCT transitions can be seen in the spectroscopic data.[30] This observation has led to the proposal for a new class of MV systems, Class (IV).

While there are many factors that contribute to the appearance of an IVCT band, there are also intrinsic problems with the use of metal groups as the redox

components as spin orbit coupling can lead to the presence of multiple IVCT bands close in energy and overlapping in the experimental spectrum.[31-34]

In reality the lack of abrupt transitions between different classes of compounds means that there is, in fact, a sliding scale between what describes Class (II) and Class (III) and this can be seen in Figure 9, where the band shapes of the transitions are predicted according to the degree of coupling present.[28]

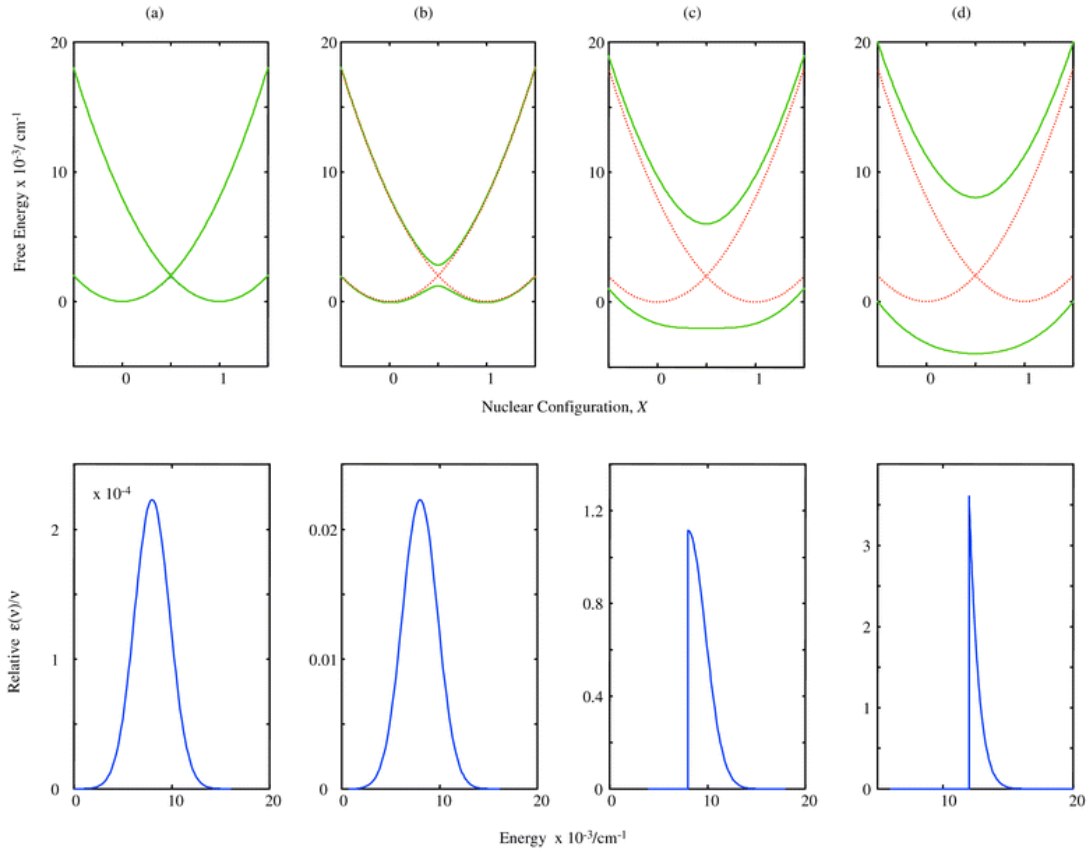

Figure 9: Simulated NIR transitions based on the two state model with the weakest coupling (left) and the strongest coupling (right). Reproduced from [28]. (reproduced by permission of Royal Society of Chemistry (RSC)).

All of the considerations given above have assumed symmetrical compounds where the two redox sites are the same. Often this is not the case as introducing

two different redox active groups, which in turn will have different redox potentials, can aid in the formation of compounds with similarities to those of MV compounds. Barlow has studied a number of different ferrocene / cobaltocene compounds in which the pseudo mixed valence states are generated through oxidation of one (cobalt) and not the other metal fragment (left, Figure 10).[35] Similar results have been seen by Molina and Tarraga in a ferrocene / ruthenocene triad (right, Figure 10).[36]

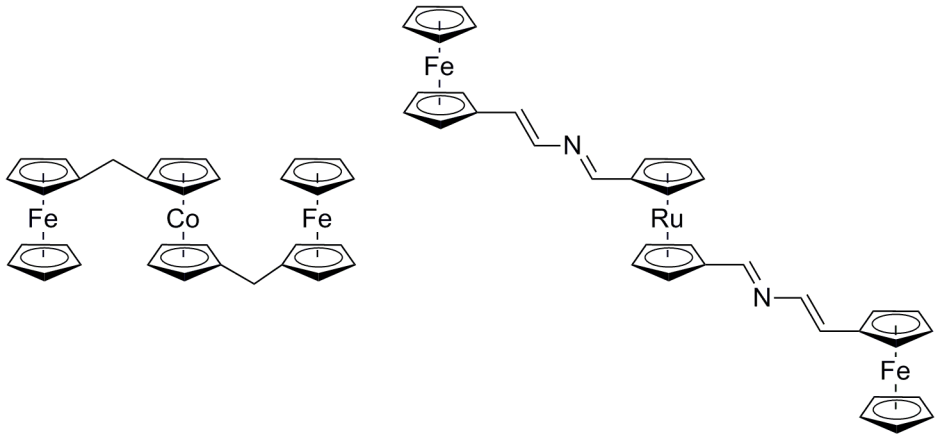

Figure 10: Examples of ferrocene / cobaltocene complexes as studied by Barlow (left) and ferrocene / ruthenocene complexes as studied by Molina and Tarraga (right).

In such asymmetric systems it can be seen that the potential surface for these systems now gives a ground state with a double minima, in which the electronic potential of the two curves differs, as well as a degenerate excited state (Figure 11).

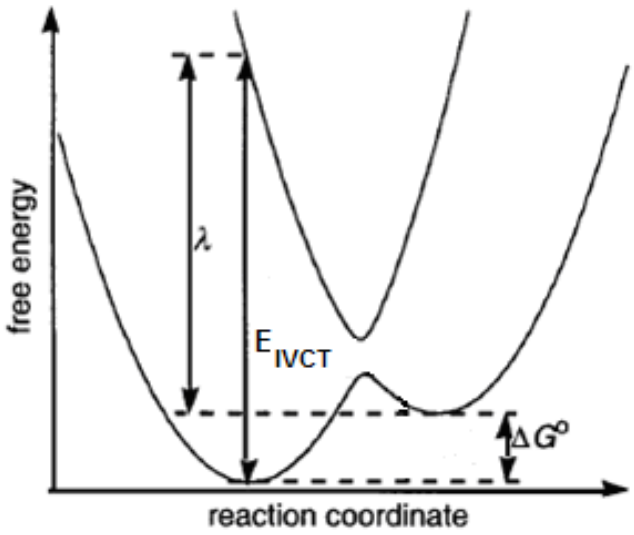

Figure 11: Potential surface for an asymmetric Class (II) system. Reproduced from [19b]. (reproduced by permission of American Chemical Society (ACS)).

It can be seen that the reorganisation energy is no longer equal to the energy of the observed transition, thus, the parameters set out above for estimating the characteristics of the IVCT band in a Class (II) system are no longer valid. The transition now has an energy equal to the reorganizational energy plus a free energy term, measured from electrochemistry, see Chapter 2.

$$\Delta G^0 = -RT \ln K_c$$

While there have been further developments in the two state model, including that of Bonvoisin and Launay, where a third equivalent redox centre is considered and all sites are believed to behave independently then the electronic coupling can be considered to be only a factor of √2 different to that of Class (II) systems with two redox sites.[37, 38]

$$H_{AB} = 2.05 \text{ x } 10^{-2} \frac{(\bar{\nu}_{max} \varepsilon_{max} \Delta \bar{\nu}_{\frac{1}{2}})^{1/2}}{r\sqrt{2}} \quad \text{cm}^{-1}$$

Further developments were made in 1978 when the PKS model was published; this adaptive model takes in to consideration the vibronic modes of the mixed valence complex and can be used to generate the potential surfaces based on different parameters.[39] The results of this model on the Creutz-Taube ion show an improved matching towards the experimental features and as such are suitable for analysis of results in strongly coupled systems.

In all of the systems above the treatment only considers involvement of the two redox centre. In practice systems are often more complicated than this and can contain redox non-innocent bridging fractions. Often in organometallic complexes the description of metal termini and an organic bridge is misleading, especially in the case of ruthenium which is often exploited in linear systems due to the ability in manipulation of its octahedral geometry and as such can be used as either a bridging or capping moiety. The synthesis of Ru(II) acetylides and their subsequent oxidation has now been exploited for many years.[40] Further to the stability of the different oxidation states of ruthenium it has also been shown that there is efficient mixing of the Ru (d) and sp^2 and sp carbon orbitals in the π system. The efficient mixing of the Ru and ligand orbitals means that any charge imparted on the Ru centre will be delocalised over the metal and C≡C moiety. The reason for the efficient mixing is the lower energy of the Ru 4d orbitals and as such increased overlap with the π orbitals of the sp and sp^2 hybridised C, which in turn gives rise to much more ligand character in the HOMO in the neutral species and thus much more ligand character to the hole when oxidised.[41] In cases where

the bridging moiety is involved in the transitions it is necessary to consider a third surface (W). Given the degree of delocalisation and the properties of the bridging ligand it is possible that this state can differ in energy and can be found at higher or lower energy than the MV state (XY). This corresponds to situations in which the hole is located either on a metal; leading to a MV state with the order of surfaces as depicted in Figure 12, or on the bridge, in which case W lies below XY. Often in Ru compounds the bridge state W is found at lower energy than the MV state.

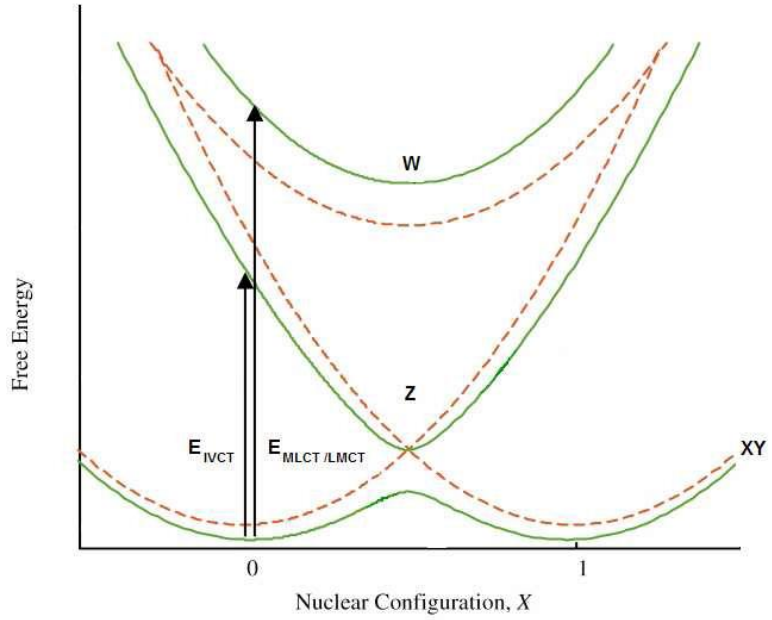

Figure 12: Three state potential surface for a Class (II) system. Reproduced from [28]. (reproduced by permission of Royal Society of Chemistry (RSC)).

It is clear that the introduction of a new state in the potential surface gives rise to a new set of transitions that can be attributed to a MLCT or LMCT. As can be seen the intensity of the MLCT / LMCT transitions decreases from Class (I) to Class (II) systems and is not present in the strongly coupled Class (II-III) / Class (III) systems. In contrast the IVCT band gains in intensity on moving through Class (I)

to Class (II) and as with the two-state model becomes extremely narrow in the Class (III) systems (Figure 13).[28, 42, 43]

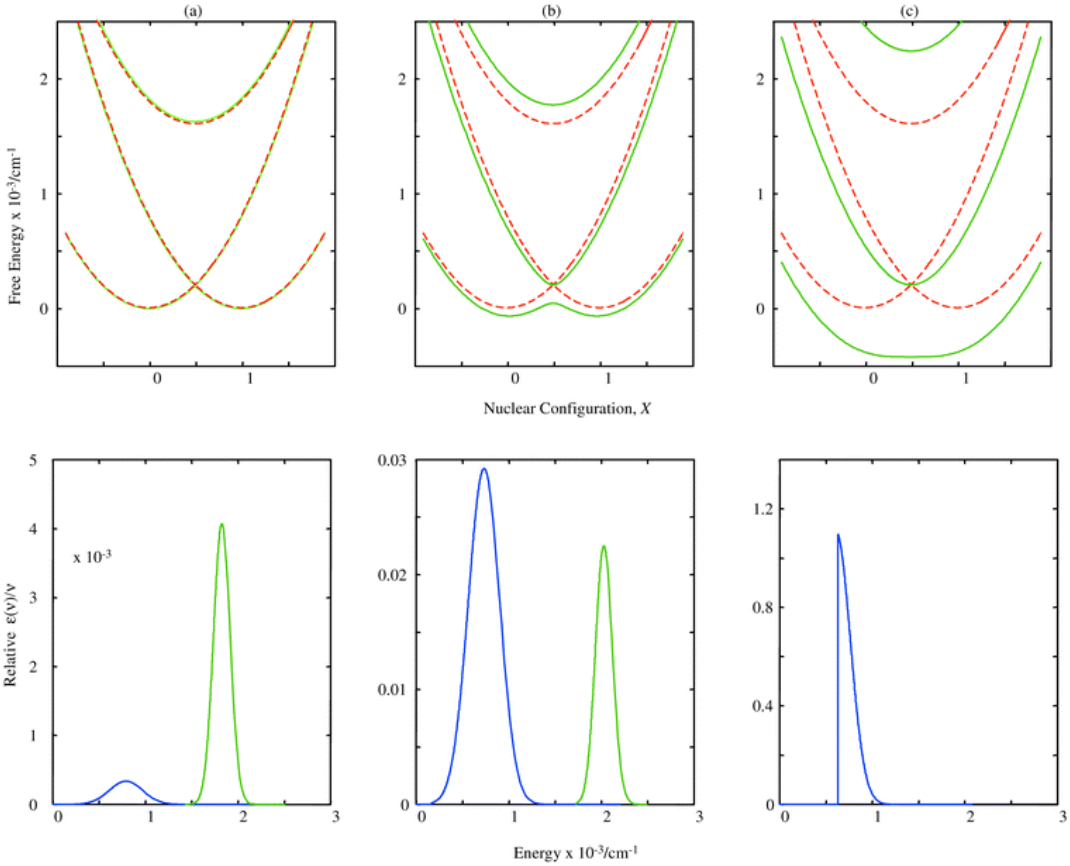

Figure 13: Simulated NIR transitions based on the three state model with the weakest coupling (left) and the strongest coupling (right). The blue band represents the IVCT and the green band the MLCT/LMCT. Reproduced from [28]. (reproduced by permission of Royal Society of Chemistry (RSC)).

While the majority of work considered here has focused on the archetypal metal-bridge-metal architecture the principles are equally applicable to less well studied systems. Fully organic mixed valence compounds have also been shown to display IVCT type transitions, the Lambert group has studied this extensively with triarylamine redox groups bridged by conjugated organic systems (Figure 14) and have shown that the results are comparable to those demonstrated earlier for organic bridged metal-capped systems.[44] While other groups have shown that 'inverse' MV complexes with metal bridges can also serve to facilitate IVCT

between two organic redox sites, this subject is considered in more detail in Chapter 2 and Chapter 3.

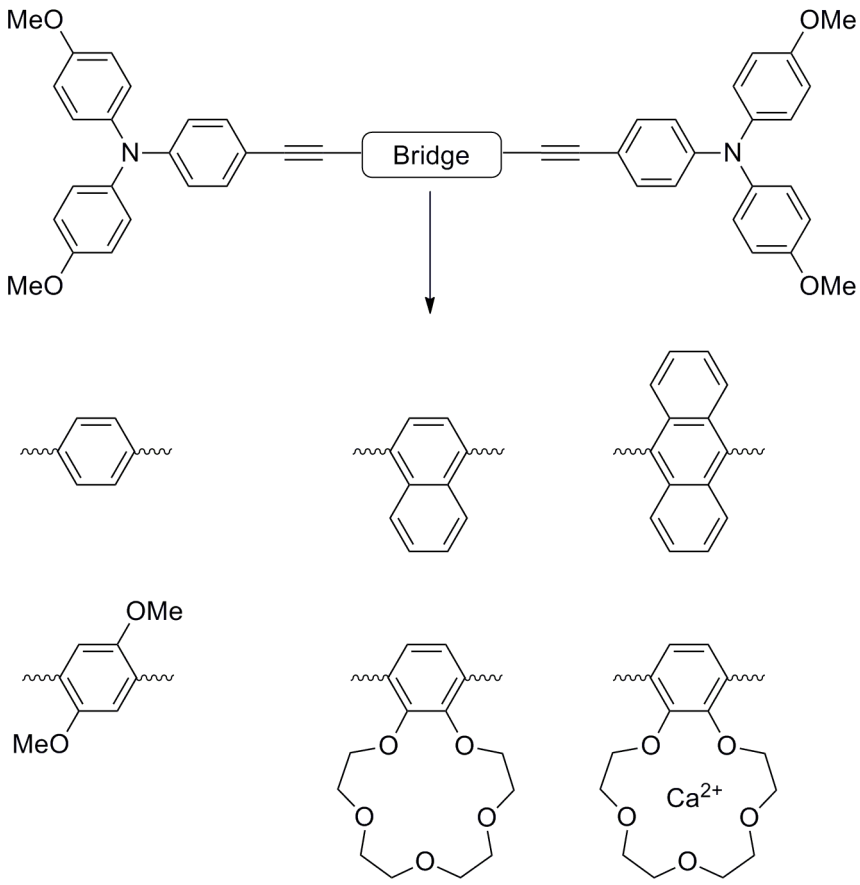

Figure 14: Examples of linear organic MV systems as studied by Lambert.

1.1.2. Multi-site Electron Transfer

Despite the interest in developing linear compounds to act as wire-like systems there has also been considerable interest in developing systems using the 1,3-diethynylbenzene linker as a 'bent' bridge to produce wire-like compounds that have a non-linear geometry. Unfortunately, the level of coupling between the redox centres in these compounds has been shown to be consistently below that of the *para* substituted analogue,[45] as such there has been considerable interest in the preparation of similar compounds with multiple redox centres. One of the most

studied architectures for this is the 1,3,5-triethynylbenzene core that allows three redox groups to be appended to the system. Given the propensity for charge transfer in 1,4-diethynylbenzene systems moving to higher substitution patterns appended with metal acetylides should allow charge transfer between the remote centres.[46] The preparation of a range of different organometallic analogues has been reported including those capped with $Ru(PPh_3)_2Cp$,[47] Fe(dppe)Cp*,[48] and Fc (reviewed in more detail in Chapter 6). Electrochemical analysis of the ruthenium analogue (A, Figure 15) gives rise to three sequential oxidation processes that can be attributed to the successive oxidations of the three –Ru-(C≡C)- fragments. The results suggest that it should be possible to study the MV species $[A]^+$ and $[A]^{2+}$ by IR and UV-vis NIR spectroelectrochemistry in order to determine the coupling between the centres, however, on the longer timeframe of spectroscopic analysis the compound decomposes and as such no reliable data on the interactions within this system are reported.[47]

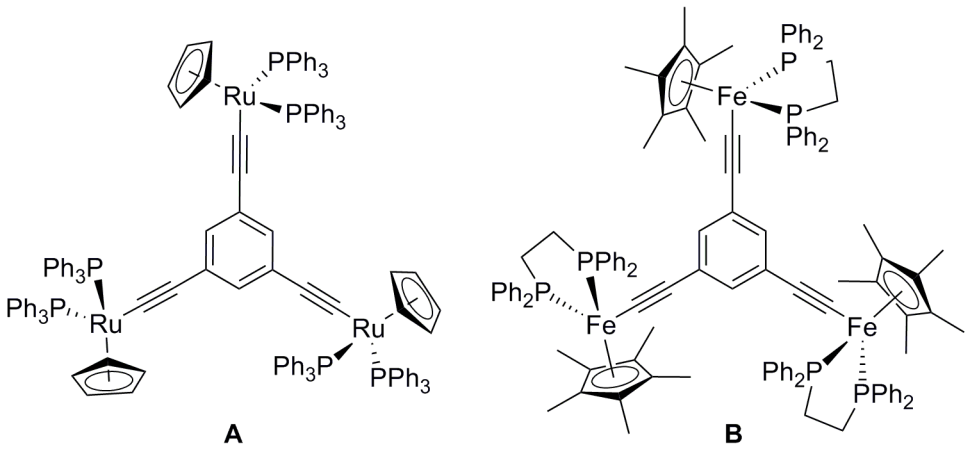

Figure 15: Ruthenium and iron analogues of 1,3,5-triethynylbenzene.

In similar fashion to A the Fe(dppe)Cp* analogue (B, Figure 15) also undergoes three reversible one-electron oxidation processes in the CV, however whereas A

was unable to be investigated by SEC, B was able to be isolated as the dicationic MV complex, $[\{Cp^*(dppe)Fe(C{=}C)\}_3(1,3,5\text{-}C_6H_3)][PF_6]_2$ and as such, IR and UV-vis NIR investigations were possible. The results have shown that there are two NIR transitions that correspond to IVCT transitions from the inequivalent Fe moieties. While the observation of two separate transitions could have easily been ascribed to the transitions to the two oxidised centres, TDDFT carried out by Lapinte et al. have shown that the transitions are in fact caused by the singlet and triplet states in the MV complex.[48] While observations such as this are scarce in the literature the results can be explained in terms of the electronic nature of the singlet and triplet states giving rise to transitions that occur at different energy.[49]

While the preparation of 1,2,4,5-tetraethynylbenzene is well known, further reactions of the compound are largely limited to cyclisation reactions to form larger systems of fused rings[50] and the preparation of large starburst polymer compounds.[51] The study of such compounds as molecular wires / junctions has only recently been explored with compounds bearing Co clusters[52] and Fc groups having been prepared, the tetraferrocenyl derivative is considered in more detail in Chapter 6. Despite previous reports of Co cluster compounds being explored through electrochemical and spectroelectrochemical studies[53] the related cluster compound of 1,2,4,5,-tetraethynylbenzene has not been investigated by these techniques.

1.2. Thesis Outline

As outlined above there are many challenges in the synthesis of MV compounds and the analysis of the interactions between the redox sites. Perhaps the most important parameter in assigning the class of a MV complex is the NIR band associated with IVCT transitions that can be experimentally measured. It is also important to understand the degree of delocalisation of the hole in the correct assignment of the transitions observed.

This thesis will set out to explore the electronic character of a series of linear and branched organometallic complexes bearing either redox active organic or metal fragments. Chapter 2 will explore the interactions in a series of platinum(II) triarylamine compounds in which the organic fragment serves as the redox probe and the metal fragment serves as the bridge. The compounds feature the *trans*-$Pt\{C_6H_4N(C_6H_4OCH_3\text{-}4)_2\}(PPh_3)_2$ moiety and with 1-4 amine centred redox sites that can be used to explore the communication through the unusual -$Pt(PPh_3)_2$-C≡C- bridge. This will then be continued in to Chapter 3 where the more traditional -C≡C-$Pt(PPh_3)_2$-C≡C- bridge is used in a series of *trans*-$[Pt(C{\equiv}CC_6H_4NAr'_2)_2(PR_3)_2]^{n+}$ complexes and the level of communication assessed by comparing different triarylamine moieties and changing the electronic nature of the phosphine ligand.

In Chapter 4 the work moves away from linear systems and explores the synthesis and electrochemical responses of a series of 2-ferrocenyl-1,1-diethynylethenes appended with either donor or acceptor groups. The results are considered in light of proposals of such systems to act as transistors. In Chapter 5 we investigate the

synthesis of metal acetylide analogues, $FcCH=C(C\equiv CML_n)_2$ (ML_n= $Ru(PPh_3)_2Cp$, Ru(dppe)Cp* and Fe(dppe)Cp*), of the compounds studied in Chapter 4, and explore the extended systems, $Ph_2C=C(C\equiv CC_6H_4C\equiv CH)_2$ and $FcCH=C(C\equiv CC_6H_4C\equiv CH)_2$, in an attempt to alleviate synthetic issues with steric congestion. These compounds are studied by electrochemistry and the MV states explored by spectroelectrochemistry in order to try and understand the degree of communication in the system. Finally in Chapter 6 the synthesis of a range of multi-ferrocenyl complexes containing two, three or four ferrocene groups is explored and the compounds studied by spectroelectrochemistry.

1.3. References

1. Moore, G. E. *Electronics*, **1965**, *38*, 114.
2. (a) Tour, J. M. *Acc. Chem. Res.*, **2000**, *33*, 791. (b) Robertson, N; McGowan, C. A. *Chem. Soc. Rev.*, **2003**, *32*, 96.
3. International Technology Roadmap for semiconductors. (2011)
4. Kisch, L. B. *Phys. Lett. A*. **2002**, *305*, 144.
5. Wenger, O. S., *Acc. Chem. Res.*, **2010**, *44*, 25.
6. Hitt, E. *P. Natl. Acad. Sci. USA*. **2004**. *101*. 7213.
7. Aviram, A; Ratner, M. A. *Chem. Phys. Lett.*, **1974**, *29*, 277.
8. Metzger, R. M. *Chem. Rev*. **2003**, *103*, 3803.
9. Tour, J. M; Kozaki,M; Seminario, J. M. *J. Am. Chem. Soc, 1998, 120*, 8486.
10. (a) Grelaud, G; Cifuentes, M. P; Paul, F; Humphrey, M. G; *J. Organomet. Chem*. **2014**, *751*, 181. (b) Sakamoto, R; Katagiri, S; Maeda, H; Nishihara, H. *Coord. Chem. Rev*. **2013**, *257*, 1493. (c) Launay, J. P. *Coord. Chem. Rev*. **2013**, *257*, 1544. (d) Halet, J. F; Lapinte, C. *Coord. Chem. Rev*. **2013**, *257*, 1584.
11. (a) Dembrinski, R; Bartik, T; Bartik, B; Jaeger, M; Gladysz, J. A. *J. Am. Chem. Soc.* **2000**, *122,* 810. (b) Grozema, F. C; Berlin, Y. A; Siebbeles, L. D.

A. *J. Am. Chem. Soc.* **2000**, *122,* 10903. (c) Crossley, M. J; Burn, P. L. *J. Chem. Soc. Chem. Commun*. **1991**. 1569.

12. (a) Nichols, R. J.; Haiss, W.; Higgins, S. J.; Leary, E.; Martin, S.; Bethell, D., *Phys. Chem. Chem. Phys.*, **2010**, *12*, 2801. (b) Haiss, W.; Wang, C.; Grace, I.; Batsanov, A. S.; Schiffrin, D. J.; Higgins, S. J.; Bryce, M. R.; Lambert, C. J.; Nichols, R. J., *Nat Mater*, **2006**, *5*, 995.
13. Ward, M. D. *J. Chem. Ed.* **2001**, *78*, 321.
14. Day, P; Hush, N. S; Clark, R. J. H. *Philosophical Transactions of the Royal Society A: Mathematical, Physical and Engineering Sciences*, **2008**, *366*, 5.
15. Creutz, C; Taube, H. *J. Am. Chem. Soc.*, **1969**, *91*, 3988.
16. Creutz, C. *Prog. Inorg. Chem.* **1983**, *30*, 1.
17. Low, P. J.; Brown, N. J. *J. Cluster Sci.* **2010**, *21*, 235. Marcus, R. A; *Rev. Mod. Phys*. **1993**, *65*, 599.
18. Barrière, F.; Camire, N.; Geiger, W. E.; Mueller-Westerhoff, U. T.; Sanders, R. *J. Am. Chem. Soc.* **2002**, *124*, 7262.
19. (a) Barriere, F.; Geiger, W. E. *J. Am. Chem. Soc.* **2006**, *128*, 3980. (b) Naffaday, A; Chin, T. T; Geiger, W. E. *Organometallics*, **2006**, *25*, 1654.
20. Geiger, W. E.; Barriere, F. *Acc. Chem. Res.* **2010**, *43*, 1030.
21. Diallo, A. K.; Daran, J.-C.; Varret, F.; Ruiz, J.; Astruc, D. *Angew. Chem. Int. Ed.* **2009**, *48*, 3141.
22. (a) Brunschwig, B. S; Creutz, C; Sutin, N. *Coord. Chem. Rev*. **1998**, *177*, 61. (b) Creutz, C; Brunschwig, B. S; Sutin, N. *Chem. Phys*. **2006**, *324*, 244. (c) Adams, D. M; Brus, L; Chidsey, C. E. D; Creager, S; Creutz, C; Kagan, C. R; Kamat, P. V; Lieberman, M; Lindsay, S; Marcus, R. A; Metzger, R. M; Michel-Beylerle, M. E; Miller, J. R; Newton, M. D; Rolison, D. R; Sankey, O; Schanze, K. S; Yardley, J; Zhu, X. Y. *J. Phys. Chem. B*. **2003**, *107*, 6668. (d) Heckmann, A; Lambert, C. *Angew. Chem. Int. Ed.* **2012**, *51*, 326. (e) Heckmann, A; Lambert, C. *J. Am. Chem. Soc*. **2007**, *129*, 5515.
23. (a) Robin M. B; Day, P. *Adv. Inorg. Chem. Radiochem.*, **1967**, *10*, 247. (b) Cowan, D. O; LeVanda, C; Park, J; Kaufman, F. *Acc. Chem. Res*., **1973**, *6*, 1.
24. D'Allesandro, D. M; Keene, R. *Dalton. Trans*. **2004**, 3950.
25. Libby, W. F. *J. Phys. Chem*. **1952**, *56*, 863.
26. (a) Allen, G. C.; Hush, N. S. *Prog. Inorg. Chem.* **1967**, *8*, 357. (b) Hush, N. S. *Prog. Inorg. Chem.* **1967**, *8*, 391.

27. D'Alessandro, D. M; Keene, F. R. *Chem. Soc. Rev.* **2006**, *35*, 424.
28. Brunschwig, B. S; Creutz, C; Sutin, N. *Chem. Soc. Rev.* **2002**, *31*, 168.
29. D'Allesandro, D. M; Topley, A. C; Davies, M. S; Keene, F. R. *Chem. Eur. J.* **2006**, *12*, 4873.
30. Lear, B. J.; Chisholm, M. H. *Inorg. Chem.* **2009**, *48*, 10954.
31. Chen, P. Y; Meyer, T. J. *Chem. Rev*. **1998**, *98*, 1439.
32. Demadis, K. D; Hartshorn, C. M; Meyer, T. J. *Chem. Rev*. **2001**, *101***,** 2655.
33. Concepcion, J. J; Dattelbaum, D. M; Meyer, T. J; Rocha, R. C. *Phil. Trans. R. Soc. A.* **2008**, *366*, 163.
34. Rocha, R. C.; Rein, F. N.; Jude, H.; Shreve, A. P.; Concepcion, J. J.; Meyer, T. J. *Angew. Chem.* **2008**, *120*, 513.
35. Barlow, S. *Inorg. Chem*. **2001**, *40*, 7047.
36. Caballero, A; Espinosa, A; Tarraga, A; Molina, P. *J. Org. Chem.* **2007**, *72*, 6924.
37. Bonvoisin, J; Launay, J. P; Van der Auweraer, M; de Schryver, F. C. *J. Phys. Chem.* **1994**, *98*, 5052.
38. Bonvoisin, J; Launay, J.P; Verbouwe, W; Van der Auweraer, M; de Schryver, F. C. *J. Phys. Chem.* **1996**, *100*, 17079.
39. Piepho, S. B; Krausz, E. R; Schatz, P. N. *J. Am. Chem. Soc*. **1978**, *10*, 2996. Rice, M. J. *Phys. Rev. Letters*, **1976**, *37*, 36.
40. For example: (a) Colbert, M. C. B; Lewis, J; Long, N. J; Raithby, P. R; White, A. J. P; Williams, D. J. *J. Chem. Soc., Dalton Trans*. **1997**, 99. (b) Zhu, Y; Clot, O; Wolf, M. O; Yap, G. P. A. *J. Am. Chem. Soc.* **1998**, *120*, 1812. (c) Klein, A; Lavastre, O; Fiedler. J. *Organometallics*. **2006**, *25*, 635.
41. (a) Pevny, F; Di Piazza, E; Norel, L; Drescher, M; Winter, R. F; Rigaut, S. *Organometallics.* **2010**, *29*, 5912. (b) Evans, C. E. B; Naklicki, M. L; Rezvani, A. R; White, C. A; Kondratiev, V. V; Crutchley, R. J *J. Am. Chem. Soc.* **1998**, *120*, 13096. (c) Fox, M. A; Farmer, J. D; Roberts, R. L; Humphrey, M. G; Low, P. J. *Organometallics.* **2009**, *28*, 5266. (d) Olivier, C; Kim, B; Touchard, D; Rigaut, S. *Organometallics*. **2008**, *27*, 509.
42. Brunschwig, B. S; Sutin, N. *Coord. Chem. Rev.* **1999**, *187*, 233.
43. Launay, J. P; Coudret, C; Hortholary, C. *J. Phys. Chem. B.* **2001**, *111*, 6788.
44. (a) Lambert, C.; Nöll, G. *J. Am. Chem. Soc.* **1999**, *121*, 8434. (b) Lambert, C.; Noll, G.; Schelter, J. *Nat. Mat.,* **2002**, *1*, 69. (c) Lambert, C.; Amthor, S.;

Schelter, J. *J. Phys. Chem. A* **2004**, *108*, 6474. (d) Heckmann, A.; Lambert, C. *Angew. Chem. Int. Ed.*, **2012**, *51*, 326.

45. (a) Uno, M; Dixneuf, P. H. *Angew. Chem. Int. Ed.* **1998**, 37, 1714. (b) Irwin, M. J; Manojlovic-Muir, L; Muir, K. W; Puddephatt, R. J; Yufit, D. S. *Chem. Commun.* **1997**, 219. (c) Weyland, T; Costuas, K; Mari, A; Halet, J. F; Lapinte, C. *Organometallics*, **1998**, *17*, 5569.
46. Long, N. J; Martin, A. J; de Biani, F. F; Zanello, P. *J Chem. Soc. Dalton Trans.* **1998**. 2017.
47. Cifuentes, M. P; Powell, C. E; Humphrey, M. G; Heath, G. A; Samoc, M; Luther-Davies, B. *J. Phys. Chem. A*, **2001**, *105*, 9625.
48. Weyland, T; Costuas, K; Toupet, L; Halet, J. F; Lapinte, C. *Organometallics*, **2001**, *19*,4228.
49. (a) Patoux, C; Coudret, C; Launay, J. P; Joachim, C; Gourdon, A. *Inorg. Chem.* **1997**, *36*, 5037. (b) Karafiloglou, P; Launay, J. P. *Chem. Phys.* **1999**, *250*, 1.
50. (a) Eikmeier, C; Junga, H; Matzger, A. J; Scherlag, F; Shim,M; Vollhardt, K. P. C. *Angew. Chem. Int. Ed*, **1997**, *36*, 2103. (b) Goldfinger, M. B; Khusrav, B.C; Swager, T. M. *J. Am. Chem. Soc.* **1997**, *119*, 4578. (c) Goldfinger, M. B; Khusrav, B. C; Swager, T. M. *J Org. Chem.*, **1998**, *63*, 1676.
51. (a) Honda, K; Maruyama, T; Yamamoto, T. *Synth. Met*, **1997**, *90*, 153. (b) Li ,H; Powell, D. R; Hayashi, K; West, R. *Macromolecules*, **1998**, *31*, 52, (c) Jones, K. M; Keller, T. M. *Polymer*, **1995**, *36*, 187.
52. Constable, E. C; Gusmeroli, D; Housecroft, C. E; Neuburger, M; Schaffner, S. *Polyhedron*, **2006**, *25*, 421.
53. (a) Canzi, G; Kubiak, C. P. *Small*, **2011**, *7*, 1967. (b) Goeltz, J. C; Benson, E. E; Kubiak, C. P. *J. Phys. Chem. B*, **2010**, *114*, 14729. (c) Glover, S. D; Goeltz, J. C; Lear, B. J; Kubiak, C. P. *Coord. Chem. Rev*. **2010**, *254*, 331. (d) Goeltz, J. C; Hanson, C. J; Kubiak, C.P. *Inorg. Chem*. **2009**, *48*, 4763. (e) Glover, S. D; Lear, B. J; Salsman, J. C; Londergan, C. H; Kubiak, C. P. *Phil. Trans. R. Soc. A.* **2008**, *366*, 177.

Chapter 2: Synthesis and Spectroelectrochemistry of Triarylamine-Platinum(II) Compounds

2.1. Synopsis

A previously reported, but much overlooked, oxidative addition reaction of $Pt(PPh_3)_4$ with aryl iodides, Ar′-I, has been used to prepare *trans*-$Pt(Ar')I(PPh_3)_2$ compounds in good yield. These halide complexes undergo CuI-catalysed dehydrohalogenation reactions with 1-alkynes to form *trans*-$Pt(C{\equiv}CR)(Ar')(PPh_3)_2$ (Ar′ = aryl) compounds which can then undergo further reactions to form *trans*-$[Pt(C{\equiv}CR)_2(PPh_3)_2]$. In reactions starting with *trans*-$Pt(C_6H_4COOCH_3\text{-}4)I(PPh_3)_2$, methyl benzoate can be identified by GC-MS, to indicate that the second alkynylation occurs through an unanticipated second transmetallation reaction.

In order to explore the synthetic utility of *trans*-$Pt(Ar')I(PPh_3)_2$ complexes, *trans*-$Pt\{C_6H_4N(C_6H_4OCH_3\text{-}4)_2\}I(PPh_3)_2$ was prepared from $Pt(PPh_3)_4$ and $N(C_6H_4I\text{-}4)(C_6H_4OCH_3\text{-}4)_2$. Reactions of *trans*-$Pt\{C_6H_4N(C_6H_4OCH_3\text{-}4)_2\}I(PPh_3)_2$ with 1-alkynes under standard CuI-catalysed dehydrohalogenation conditions allow the preparation of a range of asymmetric platinum ethynyl compounds containing up to four organic redox centres. The compound *trans*-$Pt\{C_6H_4N(C_6H_4OCH_3\text{-}4)_2\}\{C{\equiv}CC_6H_4N(C_6H_4OCH_3\text{-}4)_2\}(PPh_3)_2$ is of particular interest as an example of a bis(triarylamine) compound featuring an unusual -$Pt(PPh_3)_2$-C≡C- organometallic bridge. The redox products derived from these NAr'_3 derivatives have been explored using both electrochemical and SEC studies. The complete reversibility of the redox chemistry associated with the larger systems means that

they can be used for charge storage materials with up to +4 charge. However, the -$Pt(PPh_3)_2$-C≡C- fragment is less effective at promoting electronic interactions between remote NAr'_3 electrophores than the -C≡C-$Pt(PPh_3)_2$-C≡C- bridge explored in Chapter 3 of this thesis.

2.2. Introduction

Linear molecules containing redox-active fragments bridged by some conjugated fragment continue to be well studied due to their potential for use in, or as models of, molecular electronic devices.[1] Many studies are concerned with the mixed valence (MV) compounds that are associated with the cationic radicals generated either by chemical or electrochemical oxidation.[2] While the majority of research has focussed on complexes featuring metal fragments as the electrophore with a π-conjugated organic bridging ligand, there is a growing interest in using redox-active organic fragments in such systems, although the majority of these are purely organic molecules.[3-9] Compounds containing redox-active organic end-caps with metal / organometallic bridges remain scarce in the literature.[10-15]

Complexes of the general form $Pt(Ar')X(PR_3)_2$ (X = halide, pseudo halide; Ar′ = aryl; R = aromatic, alkyl) have a long history, and can be prepared by numerous synthetic methods, including reactions of [PtX_2{bis(olefin)}] with aryl Grignard reagents and phosphine,[16-18] from $PtX_2(PR_3)_2$ with Ar′Li,[19] by disproportionation reactions of $Pt(MPh_2)Cl(PPh_3)_2$ (M = Sn, Pb),[20] reaction of *cis*-$Pt(Ph)(PPh_3)_2(PbPh_3)$ with Br_2 or HBr,[21] decarbonylation of $Pt(COAr')X(PR_3)_2$,[22] ligand exchange reactions of $\{Pt(tht)(C_6F_5)\mu\text{-}Cl\}_2$,[23] and perhaps most simply by oxidative addition of arylhalides to $Pt(PR_3)_n$ (R = Ph, Et; n = 3, 4).[24, 25] These aryl

platinum(II) complexes have served as models through which to explore key reaction steps in various catalytic transformations,[26] and structurally well-defined building blocks for the assembly of molecular nanostructures,[27] scaffolds and redox-innocent end-caps for polyynes, some of quite extraordinary length.[28]

Alkynyl complexes *trans*-Pt(C≡CR)(Ar')$(PR_3)_2$ have also demonstrated a range of interesting and potentially useful optoelectronic properties, leading to the design of soluble and processable materials with low band-gaps for solar cell applications,[29] significant two-photon absorption cross-sections,[30] whilst the heavy atom effect leads to effective intersystem crossing[31] and efficient triplet sensitised processes such as visible light induced ring-closing of Irie-style molecular switches,[32] efficient optical limiting[33] and (electro)phosphorescence.[34] The preparation of a penta-(platinum alkynyl) complex of corannulene (Figure 16) further demonstrates the vast scope for use of the *trans*-PtX(Ar)$(PR_3)_2$ motif to assemble and stabilise complex structures.[35]

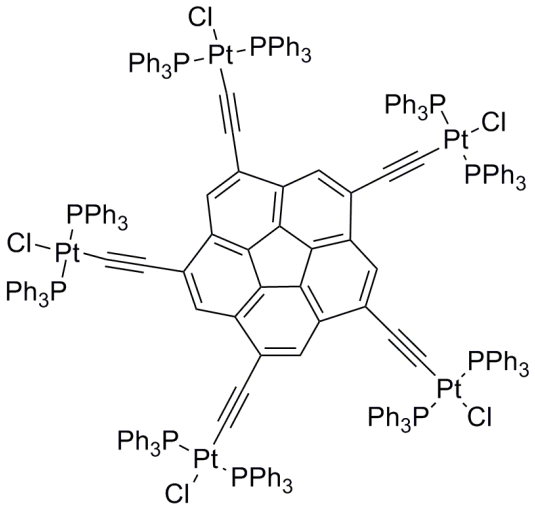

Figure 16: Platinum Corannulene complex

Given the attraction of developing systems where two or more organic electrophores[36] can be connected to form larger structures, the synthesis of the novel redox-active building block *trans*-Pt($C_6H_4NAr_2$)I(PPh_3)$_2$ (**9**, Ar = C_6H_4OMe-4) was developed, and its readiness to undergo CuI catalysed reactions with terminal alkynes exploited for the preparation of mono-, bi- and trimetallic complexes. Electrochemical and spectroelectrochemical investigations, supported by DFT calculations on representative examples, have been used to explore the redox chemistry and electronic structures of these complexes and their redox products. These studies reveal sequential oxidation of the {$Ar_2NC_6H_4$-} and {-C≡C-$C_6H_4NAr_2$} centres, which are only very weakly coupled through the *trans*-Pt(PPh_3)$_2$ bridge.

2.3. Results and discussions

2.3.1. Synthesis

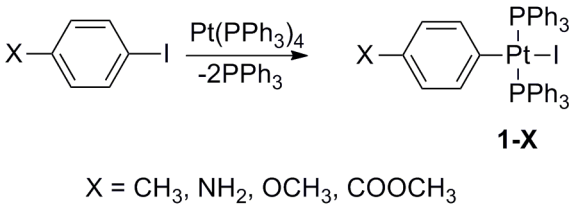

Scheme 1: Oxidative addition of aryl halides to Pt(PPh_3)$_4$.

A series of aryl platinum halide compounds of the form *trans*-Pt(Ar')I(PPh_3)$_2$, were synthesised via oxidative addition of the appropriate aryl iodide to the precursor Pt(PPh_3)$_4$ (Scheme 1).[37] Compounds **1-CH$_3$**, **1-OCH$_3$** and **1-COOCH$_3$** were chosen as representative examples, featuring substituents with different electron-donating and electron-withdrawing nature, and **1-NH$_2$** was chosen as the

amine feature can act as a surface binding group with a view to future studies.[38] The reactions proceed in good yields and the products are precipitated from the reaction mixtures as pure, white solids. ASAP MS for the compounds gave the $[M\text{-}I]^+$ ion in each case. The $^{31}P\{^1H\}$ NMR spectrum for each compound shows the expected singlet resonance with platinum satellites; **1-CH$_3$** δ 20.43 ($J_{P\text{-}Pt}$ = 3100 Hz), **1-NH$_2$** 20.26 ($J_{P\text{-}Pt}$ = 3083 Hz), **1-OCH$_3$** 23.70 ($J_{P\text{-}Pt}$ = 3071 Hz) and **1-COOCH$_3$** 19.92 ($J_{P\text{-}Pt}$ = 3021 Hz); other spectroscopic data were consistent with reported data.[37]

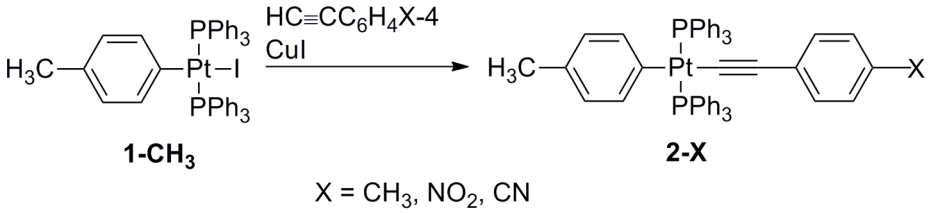

Scheme 2: The synthesis of mono-ethynyl platinum complexes 2-X from CuI-catalysed reactions of 1-CH$_3$.

Complexes of general form *trans*-Pt(Ar')X(PR$_3$)$_2$ are known to undergo CuI-catalysed dehydrohalogenation reactions with terminal alkynes in the presence of amine solvents (X = Cl;[17, 18, 23, 28, 25, 39]). Compounds **2-CH$_3$**, **2-OCH$_3$**, **2-NO$_2$** and **2-CN** (Scheme 2) were prepared from the reaction of **1-CH$_3$** with the respective 1-alkyne using standard CuI-catalysed dehydrohalogenation reactions.[40] The compounds were isolated in moderate to good yield after purification and characterised by the usual spectroscopic methods. ASAP or MALDI MS(+) for the compounds gave signals corresponding to either the $[M]^+$ or $[M+H]^+$ molecular ions. The $^{31}P\{^1H\}$ NMR spectrum for each compound shows the expected singlet resonance with platinum satellites; **2-CH$_3$** δ 20.31 ($J_{P\text{-}Pt}$ = 3000 Hz), **2-OCH$_3$** 20.29 ($J_{P\text{-}Pt}$ = 3003 Hz), **2-NO$_2$** 20.27 ($J_{P\text{-}Pt}$ = 2976 Hz) and **2-CN** 20.31 ($J_{P\text{-}Pt}$ = 2995 Hz). In the preparation of compounds **2-CH$_3$** and **2-OCH$_3$** it

was observed that, along with the desired product, a considerable amount of the bis-ethynyl compounds **3-CH$_3$** and **3-OCH$_3$** (Scheme 3) were produced as well. In order to explore the viability of **1-X** as precursors to bis-ethynyl platinum compounds, the reactions to make **3-CH$_3$** and **3-OCH$_3$** were undertaken in a one-pot reaction of **1-CH$_3$** with an excess of the alkyne, and also from reactions of isolated **2-CH$_3$** or **2-OCH$_3$** with an extra portion of 1-alkyne. In both methods the bis-ethynyl platinum compounds were formed in good yields and the spectroscopic data for the bis-ethynyl complexes **3-X** are consistent with those previously reported.[41, 42] ASAP or MALDI MS(+) for the compounds gave isotopic patterns corresponding to either the $[M]^+$ or $[M+H]^+$ molecular ions. The $^{31}P\{^1H\}$ NMR spectrum for each compound shows the expected resonance with platinum satellites; **3-CH$_3$** δ 17.70 ($J_{P\text{-}Pt}$ = 2654 Hz), **3-OCH$_3$** 17.76 ($J_{P\text{-}Pt}$ = 2665 Hz).

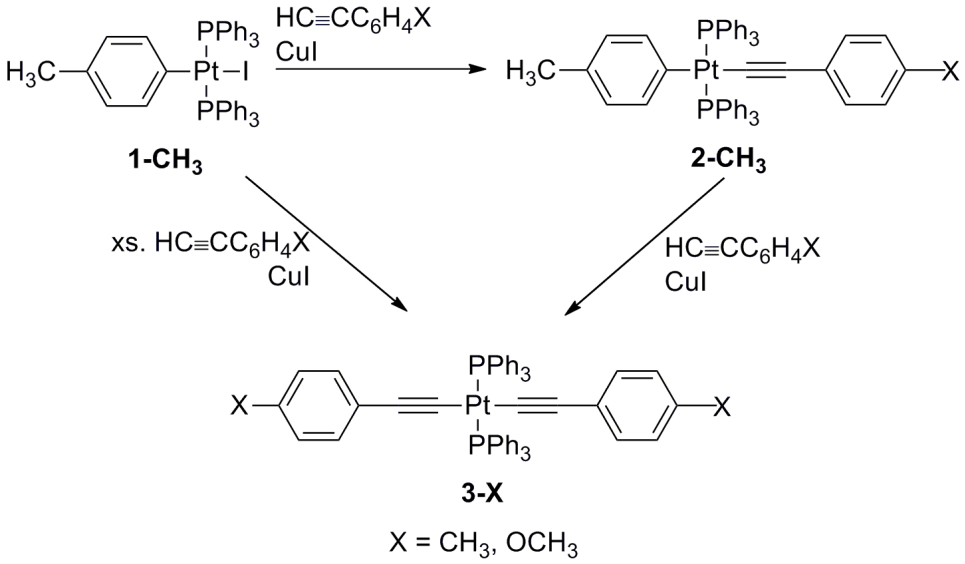

Scheme 3: Synthesis of bis-ethynyl platinum compounds from aryl-platinum halides.

Reaction of **1-COOCH$_3$** with an excess of the 1-alkyne 4-ethynylanisole (HC≡CC$_6$H$_4$OCH$_3$-4) was used as a test platform to try and understand the

sequence of reactions leading to the formation of **3-OCH_3**. Following the typical conditions described above, the reaction was left to react at reflux overnight and the platinum product **3-OCH_3** collected by filtration from the reaction mixture. GC-MS of the supernatant solution revealed the presence of $C_6H_5COOCH_3$ (methyl benzoate) (Figure 17 and Figure 18) in the reaction solution, which suggests that the second alkynylation is caused by trans-metallation from the Cu-alkyne intermediate (Scheme 4).

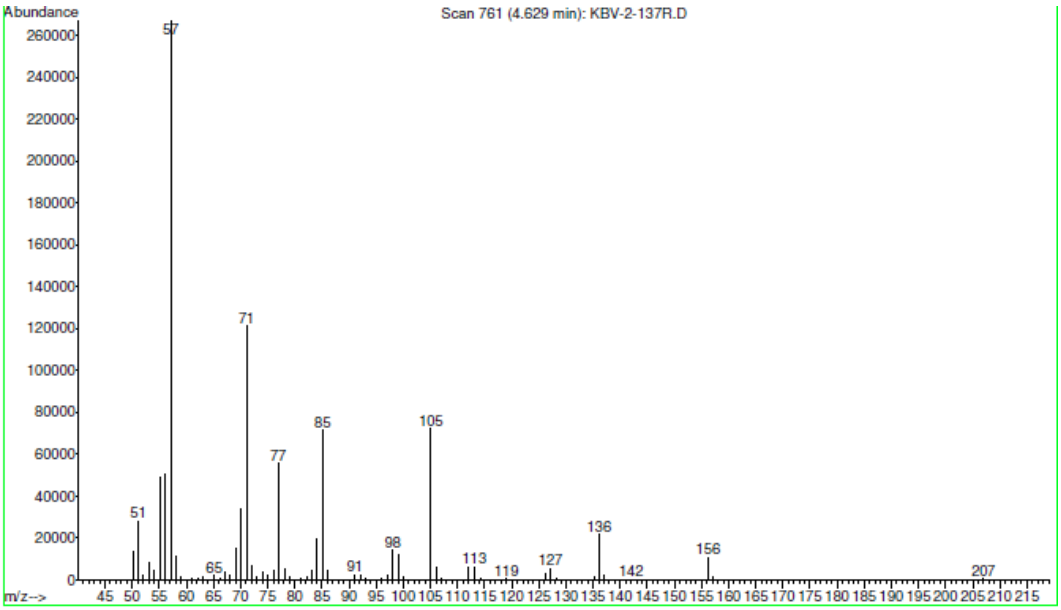

Figure 17: MS trace obtained of methyl benzoate from reaction mixture

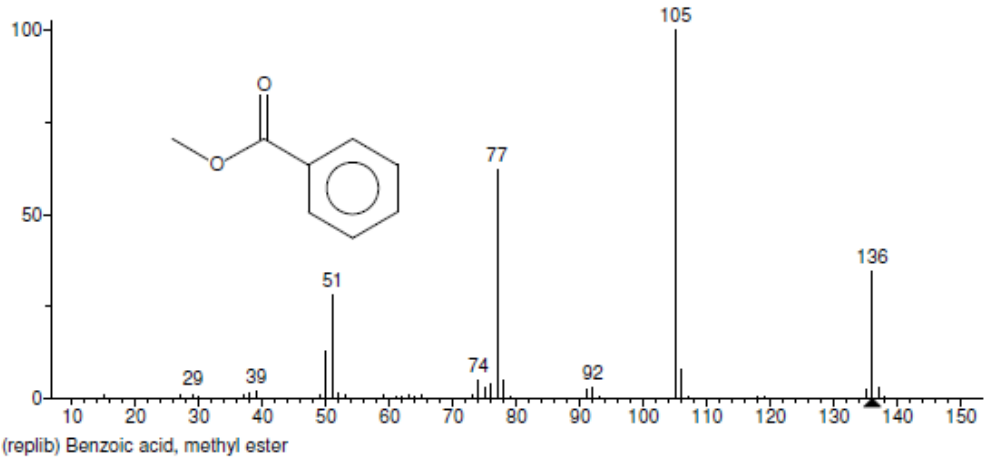

Figure 18: MS trace of methyl benzoate obtained from the NIST Mass Spectrometry Data Centre

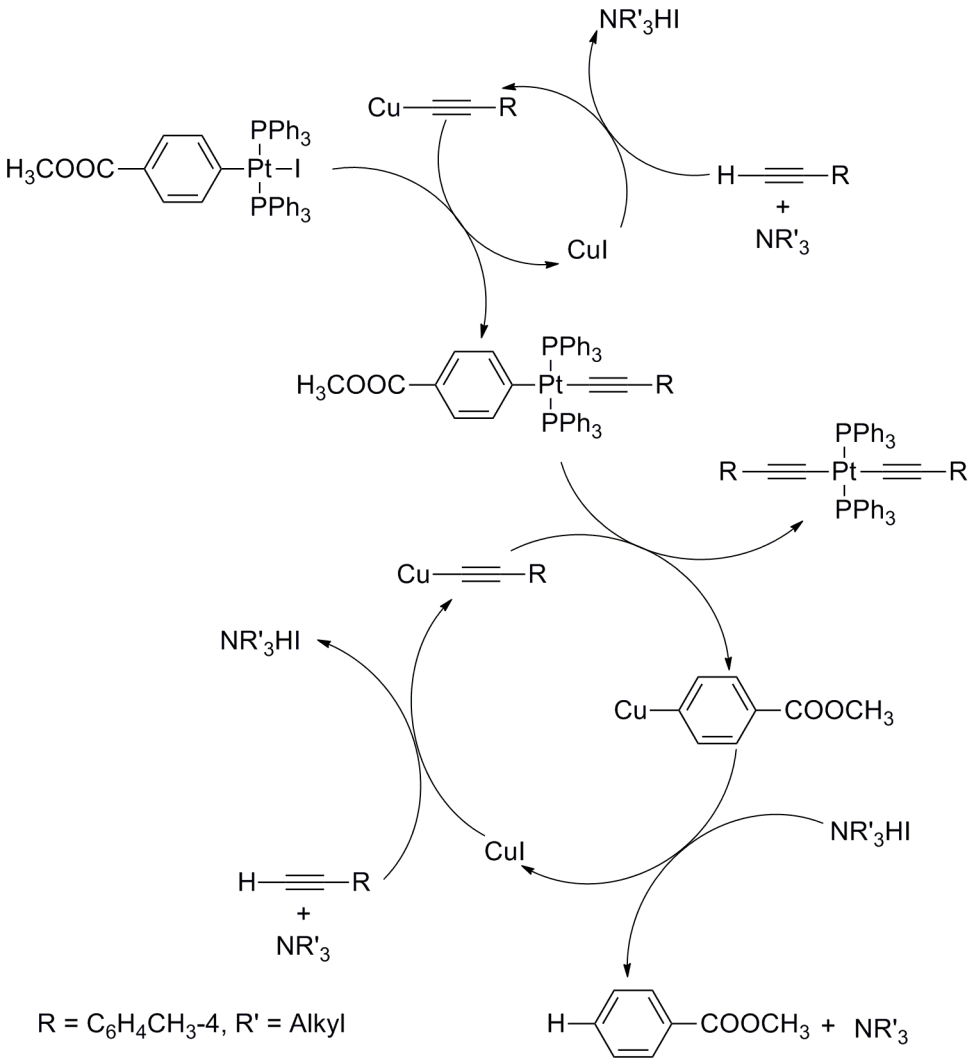

Scheme 4: Proposed transmetallation cycle in synthesis of bis-ethynyl compounds.

To further explore synthetic diversity of the compounds **1**, by way of example **1-CH$_3$** was converted to the fluoride (**4**) or chloride (**5**) compounds through halide exchange reactions (Scheme 5).[43, 44] The halide exchange reactions were carried out with slight modifications of previously reported literature preparations and the chloride reaction proceeds through extraction of the iodide with silver triflate to form the active species, Pt(Ar')(OTf)(PPh$_3$)$_2$, which then under goes a triflate/halide exchange reaction with NBu$_4$Cl to form the platinum chloride complex **5**. ASAP MS for the compounds gave isotopic envelopes corresponding to either the [M-F]$^+$ or [M-Cl]$^+$ molecular ions. The ^{31}P{^{1}H} NMR spectrum for

each compound shows the expected doublet or singlet resonance with platinum satellites; **4** 21.84 ($J_{P\text{-}F}$ = 20 Hz , $J_{P\text{-}Pt}$ = 3280 Hz), **5** 23.17 ($J_{P\text{-}Pt}$ = 3164 Hz).

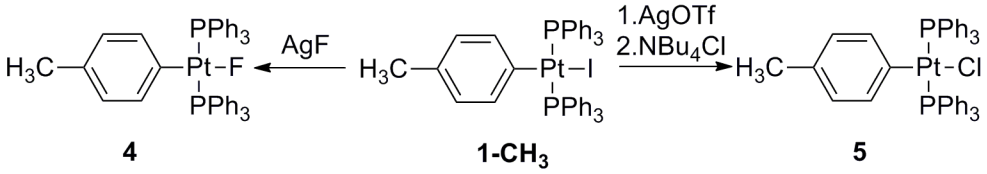

4 **1-CH$_3$** **5**

Scheme 5: Halide exchange reactions

Compound **5** and similar aryl-platinum halides have been used by the group of Gladysz[12, 13, 28] to produce a range of polyyne bridged, bimetallic platinum compounds using classic dehydrohalogenation reactions, however, despite repeated attempts to carry out similar reactions with arylethynyl ligands and **5** no reaction was observed and the starting materials could be isolated quantitatively. Despite the inability of **5** to undergo alkynylation reactions with the arylethynyl ligands in our hands, the route to preparing the metal precursor has considerable advantages over that used by Gladysz (Scheme 6) which requires the use of hygroscopic Pt(COD)Cl_2 and moisture-sensitive p-toylmagnesiumbromide solutions, both of which are expensive when obtained from commercial sources.

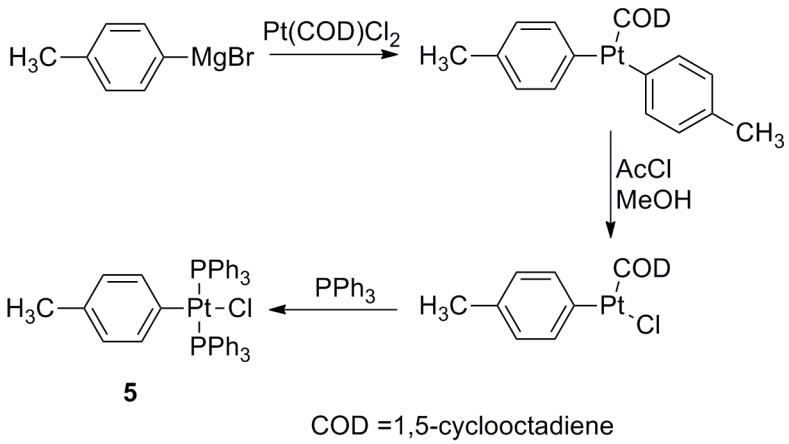

5

Scheme 6: Gladysz synthetic route to 5

Attention was next turned to the synthesis of unsymmetrical bis-ethynyl platinum compounds, with a view to building on the chemistry leading to the preparation of **3-X** from **1-X** or **2-X** (Scheme 7). D'Amato has recently shown that a range of different unsymmetrical compounds can be prepared through selective synthesis of initially *trans*-Pt(C≡CR)Cl(PPh_3)$_2$ from *cis*-$PtCl_2(PPh_3)_2$ and HC≡CR, and subsequent reaction with a second equivalent of a different 1-alkyne.[42] Following this example, the one pot synthesis of *trans*-Pt(C≡C$C_6H_4CH_3$-4)(C≡C$C_6H_4OCH_3$-4)(PPh_3)$_2$ (**6**) was attempted with equimolar amounts of the alkynes HC≡C$C_6H_4CH_3$-4, HC≡C$C_6H_4OCH_3$-4 and **1-CH$_3$** under the usual CuI catalysed reaction conditions. After reaction, the precipitated solid was collected by filtration and ASAP-MS(+) confirmed a mixture of the homo-bis-ethynyl complexes (**3-CH$_3$** and **3-OCH$_3$**) and the hetero-bis-ethynyl product (**6**). Unfortunately due to the poor solubility of the complexes comprising the mixture, no purification or separation of the compounds was possible.

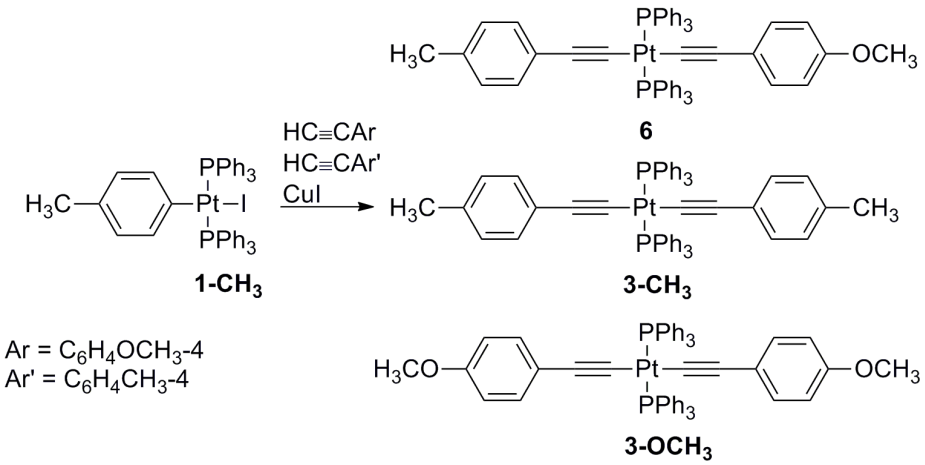

Scheme 7: Synthesis of unsymmetrical bis-ethynyl Pt compounds.

While the aryl-platinum compounds **1** – **6** are not redox-active in common solvents and within usual potential ranges, the -C≡C-Pt(PR_3)$_2$-C≡C- motif has been used as a largely redox inert bridge to prepare an organic mixed valence

compound *trans*-[Pt(C≡C$C_6H_4NAr_2$)$_2$(PEt_3)$_2$]$^+$, which has been examined in solutions generated by stoichiometric chemical oxidation and by gas-phase calculations on the homo-valence parent compound.[11] Having exploited the oxidative addition route to mono-ethynyl platinum compounds with a range of aryl iodides, the synthesis of a redox-active aryl-platinum moiety was undertaken in order to extend this family of metal-bridged organic MV complexes.

The synthesis of the redox-active pro-ligand, **8**, was achieved through sequential Ullmann cross coupling reactions of 4-iodoanisole with aniline, to give N(C_6H_5)Ar_2 (**7**) as a white solid, [45] and iodination of the triarylamine with NIS in chloroform (with the exclusion of light) to give N(C_6H_4I-4)Ar_2 (**8**) (Scheme 7). Compound **8** was isolated after purification as an off-white coloured solid in good yield. Spectroscopic data for these compounds were consistent with those previously reported.[46]

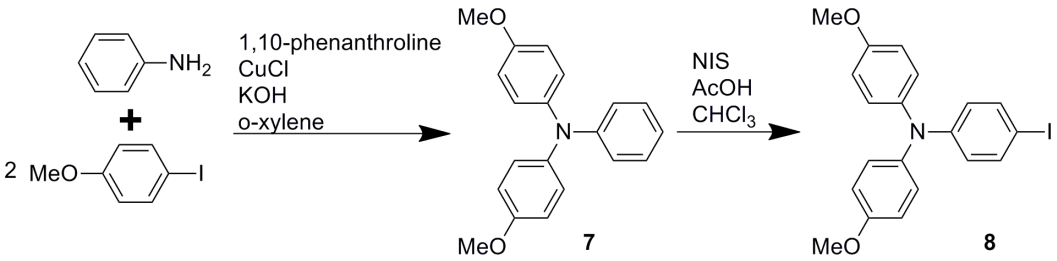

Scheme 8: Synthetic routes to 7 and 8

Compound **8** reacted smoothly with $Pt(PPh_3)_4$ [47] in refluxing toluene to give *trans*-Pt($C_6H_4NAr_2$)I(PPh_3)$_2$ (**9**) in excellent (95%) isolated yield (Scheme 9). The *trans*-geometry of **9** was established by the observation of a singlet in the ^{31}P NMR spectrum at δ 20.67 ppm with Pt satellites (J_{Pt-P} = 3070 Hz). The complex was further characterised by ^{1}H and ^{13}C NMR spectroscopies, which were fully

assigned on the basis of NOESY, COSY, HSQC and HMBC methods, although several of the anisole and phenylene ^{1}H resonances were found to be overlapped. MALDI-MS and elemental analytical results were also fully consistent with the proposed structures.

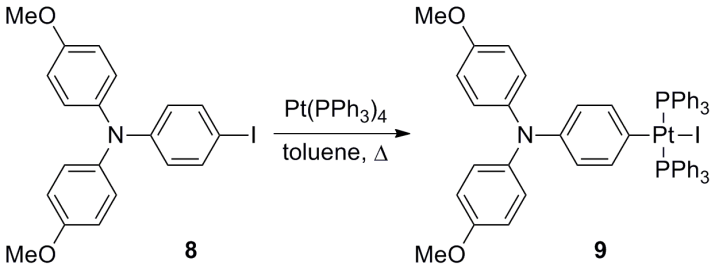

Scheme 9: Synthesis of 9

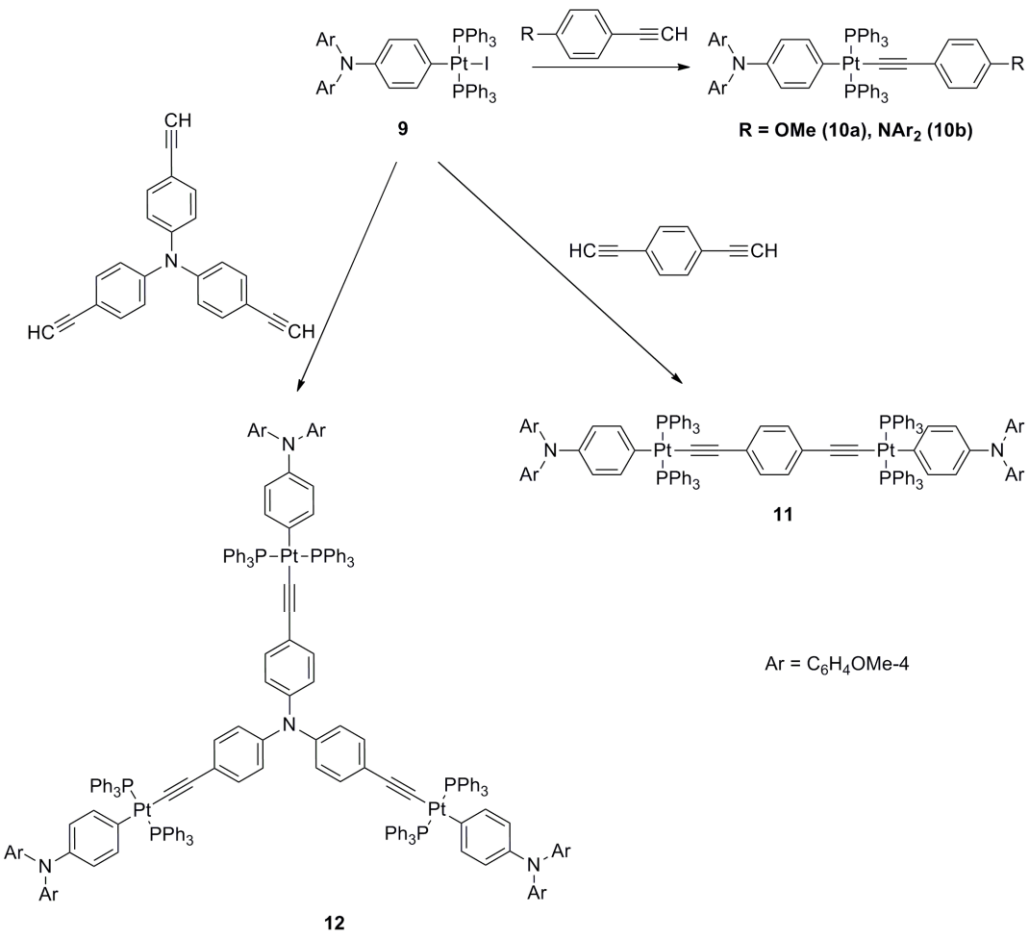

Scheme 10: The preparation of 10a, 10b, 11 and 12.

Compounds **10a, 10b, 11** and **12** (Scheme 10) were synthesised from compound **9** and the respective 1-alkyne using standard CuI catalysed dehydrohalogenation reactions.[48] The compounds were isolated in moderate to good yield after purification and characterised by the usual spectroscopic methods. Compounds **10a, 10b, 11** and **12** all give rise to a single ν(C≡C) absorption band near 2100 cm^{-1}. MALDI or ASAP MS for the compounds gave isotopic envelopes corresponding to either the $[M]^+$ or $[M+H]^+$ molecular ions. The $^{31}P\{^1H\}$ NMR spectrum for each compound shows the expected singlet resonance with platinum satellites; **10a** 20.84 ($J_{P\text{-}Pt}$ = 2985 Hz), **10b** 20.95 ($J_{Pt\text{-}P}$ = 2981Hz), **11** 20.73 ($J_{Pt\text{-}P}$ = 2971Hz) and **12** 20.93 ($J_{P\text{-}Pt}$ = 2998 Hz). The ^{13}C NMR all show triplet resonances for the Pt bound *ipso* C for the triarylamine moiety at ca. 140 ppm with $J_{C\text{-}Pt}$ = 120 Hz. Due to the poor solubility of the compounds signals for C≡C could not be seen.[49]

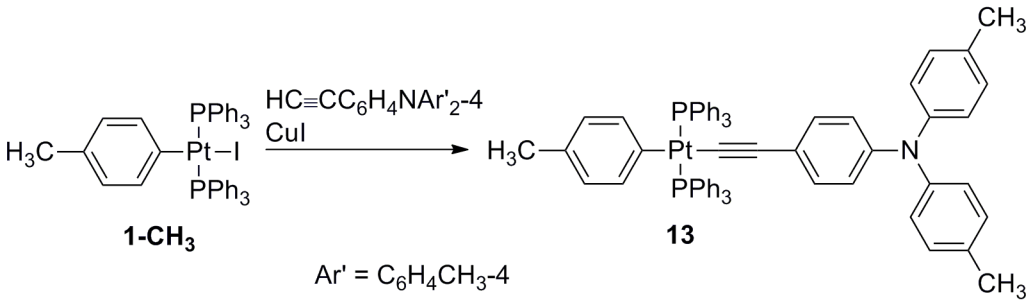

Scheme 11: Synthesis of model compound 13.

In order to better understand the electronic structure of the redox-active compounds **10a-b** – **12** the model compound **13** (Scheme 11) which contains the redox innocent aryl ligand and the redox-active ethynyl triarylamine ligand was prepared by an analogous synthetic route to that described previously from **1-CH$_3$** and $HC{\equiv}CC_6H_4N(C_6H_4CH_3\text{-}4)_2$, and purified by silica column chromatography.

Compound **13** gives a single ν(C≡C) absorption band around 2100 cm^{-1} while ASAP MS contained $[Pt(C_6H_4CH_3)(PPh_3)_2+H]^+$ as the highest molecular mass fragment. The $^{31}P\{^1H\}$ NMR spectrum showed a singlet resonance with platinum satellites: δ 20.25 (s, $^1J_{P\text{-}Pt}$ = 3003 Hz). ASAP-HRMS was used to unambiguously confirm the presence of the desired compound.

2.3.2. Molecular Structures

Crystals of **1-CH$_3$**, **2-CH$_3$**, **5**, **10a, 10b** and **13** were all grown by slow diffusion of EtOH in to a CH_2Cl_2 solution of the compound to give pale yellow crystals that were suitable for X-ray diffraction (Figure 19 - Figure 24). The molecular structures of all compounds confirm the anticipated connectivity and *trans*-geometry of the complexes. The Pt centre displays the expected square-planar arrangement whilst the triarylamine fragments are arranged in the usual propeller-like geometry.[53-55] The greatest significant differences in the structures of **10a** and **10b** arise in the alkynyl fragments with some evidence for a degree of cumulenic character in the N2-C26…C22-C21 portion of **10b** (Table 1). The Pt1-C21 bonds in **10b** and **13** are slightly shorter than in **2-CH$_3$** and **10a**, perhaps reflecting a greater degree of electrostatic attraction between Pt1-C1 brought about by the electron-donating triarylamine moiety over the OCH_3 group. This is consistent with the longer C≡C bond in compounds **10b** and **13** compared to **2-CH$_3$** and **10a.**

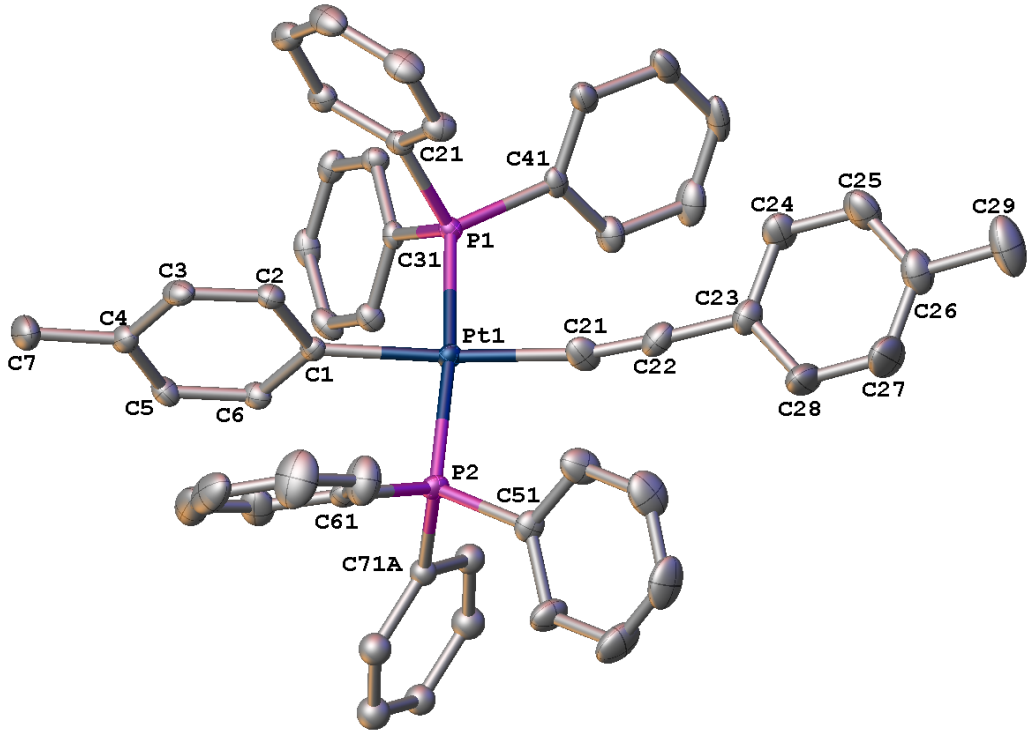

Figure 19: A plot of a molecule of 2-CH_3 showing the atom labelling scheme, with thermal ellipsoids plotted at 50 %. Hydrogen atoms have been omitted for clarity.

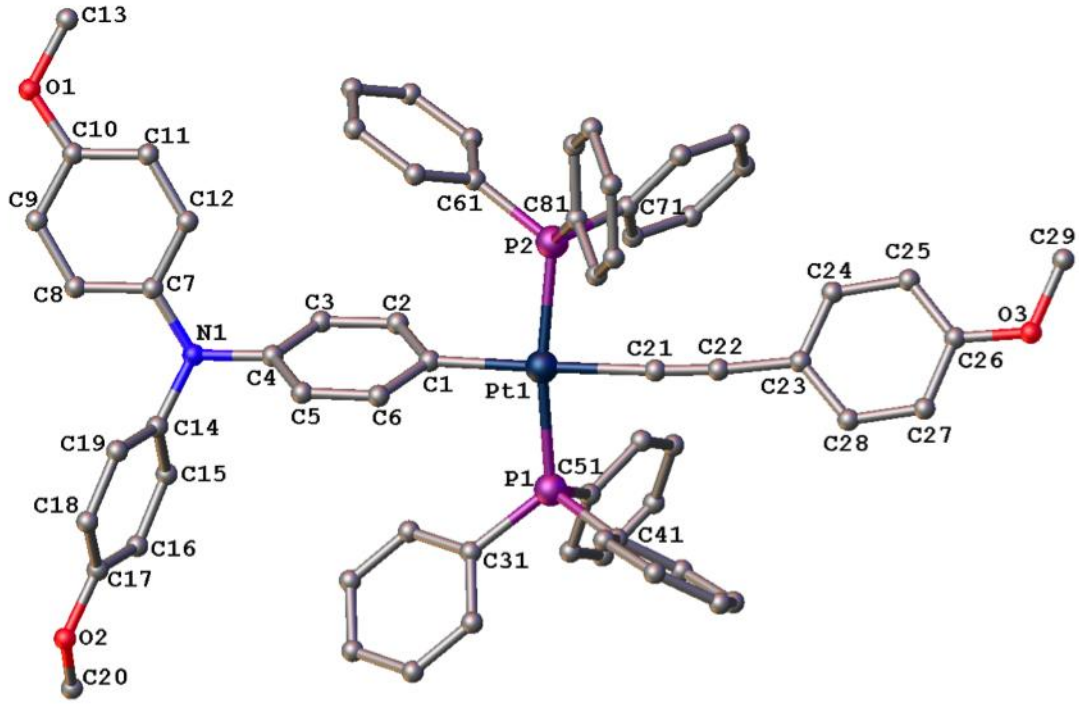

Figure 20: A plot of a molecule of 10a showing the atom labelling scheme. Hydrogen atoms have been omitted for clarity.

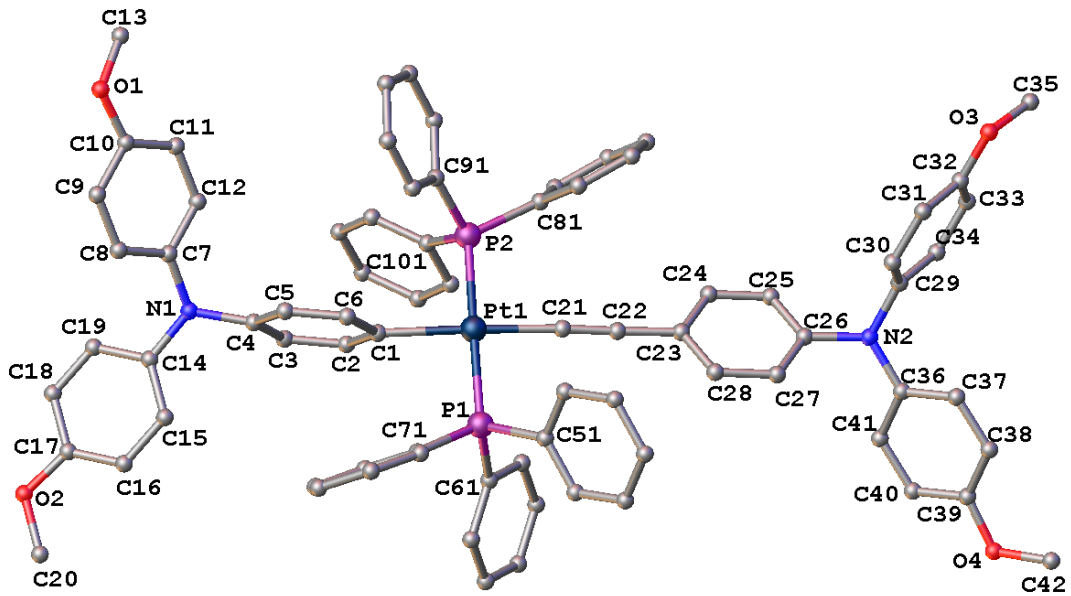

Figure 21: A plot of a molecule of 10b showing the atom labelling scheme. Hydrogen atoms have been omitted for clarity.

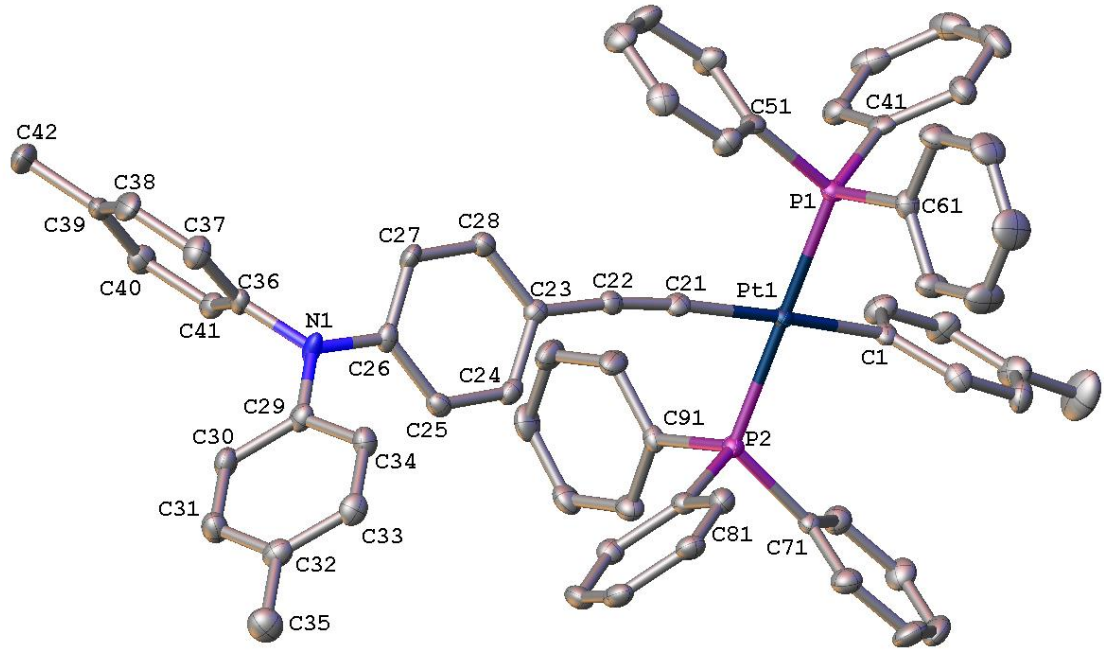

Figure 22: A plot of a molecule of 13 showing the atom labelling scheme, with thermal ellipsoids plotted at 50 %. Hydrogen atoms have been omitted for clarity.

Table 1: Selected bond lengths, bond and torsion angles for 2-CH_3, 10a, 10b and 13.

	2-CH_3	**10a**	**10b**	**13**		**2-CH_3**	**10a**	**10b**	**13**
Pt1-P1	2.2921(6)	2.2944(7)	2.286(3)	2.2860(9)	C1-Pt1-C21	174.09(11)	178.66(10)	176.6(3)	174.76(13)
Pt1-P2	2.3076(7)	2.2892(7)	2.313(3)	2.2920(9)	P1-Pt1-P2	174.27(2)	169.73(3)	175.48(10)	175.97(3)
Pt1-C1	2.073(2)	2.057(3)	2.144(5)	2.063(3)	C1-Pt1-P1	87.79(7)	94.14(7)	90.90(19)	92.69(9)
Pt1-C21	2.030(3)	2.072(3)	1.993(10)	2.005(3)	C1-Pt1-P2	87.14(7)	93.44(7)	89.88(19)	89.77(9)
N1-C4		1.438(4)	1.464(9)		P1-Pt1-C21	91.12(8)	87.20(7)	88.1(3)	91.14(9)
N1-C7		1.415(4)	1.431(10)		P2-Pt1-C21	94.20(8)	85.22(7)	90.8(3)	86.61(9)
N1-C14		1.438(4)	1.418(9)						
C21-C22	1.180(4)	1.138(4)	1.236(12)	1.213(5)	C2-C1-C23-C24		41.49	55.48	
C22-C23	1.461(4)	1.479(4)	1.435(10)	1.436(4)	C3-C4-C7-C8		120.47	144.59	
N2-C26			1.457(8)	1.411(4)	C3-C4-C14-C15		42.10	79.69	
N2-C29			1.460(8)	1.420(4)	C25-C26-C29-C30			101.11	
N2-C36			1.414(9)	1.436(4)	C25-C26-C36-C37			121.26	

The structures of *trans*-Pt($C_6H_4CH_3$-4)X(PPh_3)$_2$ (X= I (**1-CH$_3$**), Cl (**5**)) are unremarkable, with Pt-aryl bond lengths (**1-CH$_3$** 2.025(5) Å; **5** 2.024(2) Å) consistent with previously reported structures such as 1,4-[Pt(PEt_3)$_2$I]$_2$$C_6H_4$ (2.021(5) Å)[50] and *trans*-Pt(C_6F_5)Cl(PPh_3)$_2$ (2.017(4) Å).[51C] There is little difference between the structures of **1-CH$_3$** and **5,** with the most noticeable being the Pt-X bond length, which is much shorter in **5**, reflecting the smaller size of the chloride ligand. As with the Pt-aryl bonds the Pt-X bonds are consistent with those reported previously for Pt-I[24c and 50] and Pt-Cl[51] bonds in compounds such as 1,4-[Pt(PEt_3)$_2$I]$_2$$C_6H_4$, 4,4'-bis[*trans*-PtI($PEt_3$)$_2$]biphenyl, *trans*-Pt($C_6F_5$)Cl($PPh_3$)$_2$ and *trans*-Pt(o-tolyl)Cl(PEt_3)$_2$.

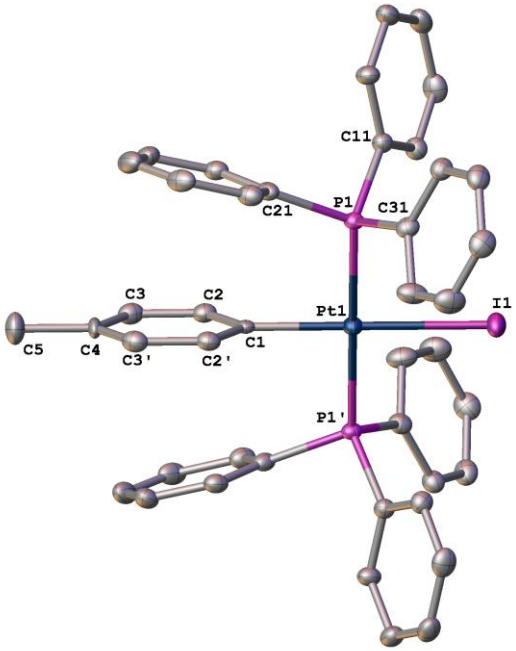

Figure 23: A plot of a molecule of 1-CH$_3$ showing the atom labelling scheme, with thermal ellipsoids plotted at 50 %. Hydrogen atoms have been omitted for clarity.

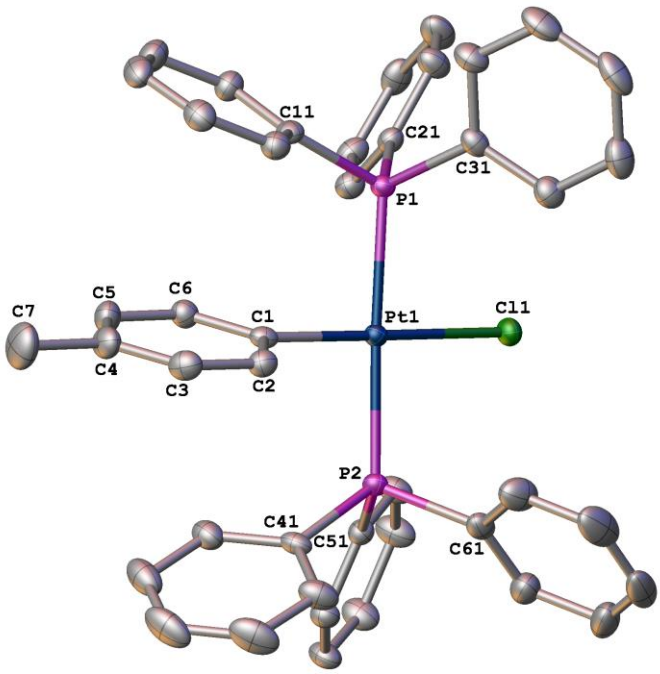

Figure 24: A plot of a molecule of 5 showing the atom labeling scheme, with thermal ellipsoids plotted at 50 %. Hydrogen atoms have been omitted for clarity.

Table 2: Selected bond lengths, and bond angles for 1-CH_3 and 5

	1-CH_3	**5**		**1-CH_3**	**5**
Pt1-P1	2.3058(7)	2.2996(5)	C1-Pt1-X	180.0	179.58(5)
Pt1-C1	2.025(5)	2.024(2)	C1-Pt1-P1	90.035(18)	91.75(5)
Pt1-X	2.7100(3)	2.4093(5)	X-Pt1-P1	89.965(18)	87.841(17)

2.3.3. Electrochemistry

Electrochemical techniques have long been used to assess the redox properties of organic and organometallic species. By far the most common technique is cyclic voltammetry (CV) where a current response caused by transfer of electrons at the working electrode surface is measured as a function of the applied potential.[52] For the most simple and reversible of these systems the mechanism for electron transfer is a purely heterogeneous electron transfer (ET) mechanism, $\vec{E}$. The current measurement

for $\vec{E}$ systems is dependent on: (1) the heterogeneous ET rate from the electrode to the electroactive species; and (2) the rate of diffusion of the charged species in the diffusion layer to the bulk solution. For a fully reversible process the diffusion rate is large and the measured current is dependent on (2). The Randles-Sevcik equation (Equation 1) shows that the relationship between current and scan rate is dependent on $\sqrt{\upsilon}$ where i_p = current maximum (amps), n = number of electrons transferred in the redox event, A = electrode area (cm^2), F = Faraday constant ($C\ mol^{-1}$), D = diffusion coefficient (cm^2/s), C = concentration (mol/cm^3), υ = scan rate (V/s). Thus, for a redox event where n, A and C remain constant (i.e. the typical conditions in a cyclic voltammetry experiment), for a fully reversible process (with $i_{pa} = i_{pc}$) the current produced should be linear with respect to $\sqrt{\upsilon}$.

$$i_p = 0.4463\ nFAC\left(\frac{nF\nu D}{RT}\right)^{\frac{1}{2}}$$

Equation 1: Randles-Sevcik equation

One drawback from drawing conclusions of reversibility from the current: scan rate relationship alone is the failure to include any consideration of the kinetics of both forward *and* back reactions which is expressed in the peak-peak separation $E_{pc} - E_{pa} = \Delta E_p$. The Nernst equation (Equation 2), where E is the experimental potential (V), $E°$ is the standard potential (V) which is dependent on the identity of the process, R is the gas constant (J/molK), T is temperature (K), n is the number of electrons transferred (mol e/mol), F is Faraday's constant, [ox] is the activity of the oxidised form of the analyte and [red] is the activity of the reduced form of the analyte, can be used to relate the concentration of the oxidised and reduced species to the voltage applied, and in turn to the diffusion controlled equilibrium processes of both forward and back reactions.

$$E = E^o + \frac{0.05916}{n} log_{10} \frac{[ox]}{[red]}$$

Equation 2: Nernst equation

Thus for a diffusion controlled process the formal redox potential is the midpoint between the E_{pa} and E_{pc} and the peak-peak separation E_{pc} - E_{pa} = ΔE_p = 59/*n* mV and that for a redox process in which a single electron (*n* = 1) is transferred then ΔE_p should be 59 mV and is independent of scan rate. For reactions that are not diffusion controlled, i.e. the rate of transfer from the electrode to the analyte is now the defining parameter, then ΔE_p will be dependent on υ and > 59 mV; these reactions are referred to as quasi-reversible and refer to the case when forward and reverse electron transfer reactions occur with different rates. Whilst at sufficiently slow scan rates quasi-reversible processes may appear fully reversible, on increases to the scan rate the rates of reaction are not sufficiently well match to maintain Nernstian equilibrium and ΔE_p increases. In an irreversible case the electrochemical reactions are not diffusion controlled and the reverse electrochemical reaction does not take place at any measureable rate. The sluggish electrode kinetics leads to broadening of the observed wave and the forward peak potential, E_p, is sensitive to the scan rate. Peak currents are also usually lower than for reversible systems as the rate of diffusion of material away from the electrode can relax the concentration of the redox species during the time course of the potential scan. It is often therefore desirable to consider a range of different parameters when considering the reversibility of redox processes in CV (Table 3).

Table 3: Summary of features used to determine reversibility of electrochemical one-electron processes. Where N = transfer coefficient (a measure of the symmetry of the energy barrier) and v = scan rate

Reversible	Quasi-reversible	Irreversible
E_{pa} independent of scan rate	E_{pa} dependent on scan rate	E_{pa} dependent on scan rate
$\Delta E_p = 59$ mV	$\Delta E_p > 59$ mV	unobserved
$i_{pa}/i_{pc} = 1$	$i_{pa}/i_{pc} = 1$ when N'=0.5 $i_{pa}/i_{pc} < 1$ when N'>0.5 $i_{pa}/i_{pc} > 1$ when N'<0.5	-
i_{pa} vs $\sqrt{\upsilon}$ = linear	i_{pa} vs $\sqrt{\upsilon}$ = non-linear	i_{pa} vs $\sqrt{\upsilon}$ = linear

It is important to note that despite consideration of all criteria when assigning reversibility the theoretical ΔE_p value of 59 mV is not often observed due to uncompensated internal solution resistance. As such comparison with an internal reference that has been shown to be fully reversible, such as $FeCp^*_2$ / $FeCp_2$ etc., can be used, with the other criteria, to determine the reversibility in each independent case.

Electrochemical studies of compounds **10a, 10b, 11, 12** and **13** show either one (**10a**, **11** and **13**) or two (**10b** and **12**) reversible oxidation processes dependent on the number of different triarylamine groups in the compound (Table 4). All compounds show a linear dependence on the scan rate and peak-current ratios (i_{pc}/i_{pa}) values of between 0.98 and 1. The relatively low oxidation potentials are consistent with the oxidation of triarylamine moieties reported elsewhere.[53-56] The values of ΔE_p observed here are all slightly greater than expected for an ideal process (Table 4), but are, however, consistent with the values observed for the internal reference in each case, and as such the redox processes can be considered reversible.

Table 4: Oxidation potentials for platinum complexes 11 – 13. CV in CH_2Cl_2 with 0.1 M $NBu_4[PF_6]$ at a scan rate of 100 mV/s and referenced against $FeCp^*_2$ at -0.48 V *vs* $FeCp_2$ ($FeCp_2$ = +0.0 V).

Compound	$E_{1/2}(1)$/ V	$\Delta E_p(1)$/ V	$E_{1/2}(2)$/ V	$\Delta E_p(2)$/ V	$\Delta E(1\text{-}2)$/ V	$\Delta E_p(FeCp^*_2)$/ V
10a	0.004	0.087				0.083
10b	0.044	0.084	0.189	0.083	0.145	0.078
11	0.012	0.093				0.088
12	0.038	0.080	0.204	0.076	0.166	0.077
13	0.370	0.098				0.089

Compound **10a** and **13** give voltammograms with single oxidation processes consistent with the single redox-active amine moiety present in the compound (Figure 25 and Figure 26). The low potential of the oxidation in **10a** (+0.004 V) supports the description of the aryl bound amines oxidising first in compounds **11** ($E_{1/2}(1)$ 0.012 V) and **12** ($E_{1/2}(1)$ 0.038 V). The more positive oxidation potential of the model compound **13** ($E_{1/2}(1)$ 0.37 V) is consistent with other examples of ethynyl-substituted triarylamine compounds,[53-55] highlighting the difference between redox potentials of the ethynyl and non-ethynyl appended triarylamine groups.

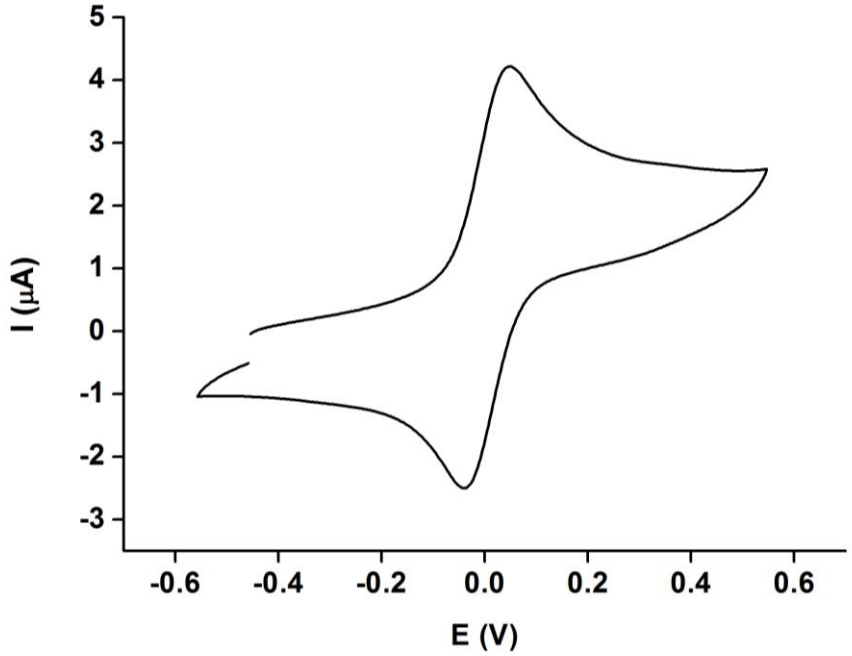

Figure 25: Cyclic voltammogram of 10a in CH_2Cl_2/0.1 M NBu_4PF_6; scan rate (v) = 100 mV s^{-1}. Potentials are reported against ferrocene ($FeCp_2/FeCp_2^+$ = 0.0 V) by reference against an internal decamethylferrocene/decamethylferricenium couple ($FeCp^*_2$/ $FeCp^*_2{}^+$ = −0.48 V vs $FeCp_2/FeCp_2^+$)

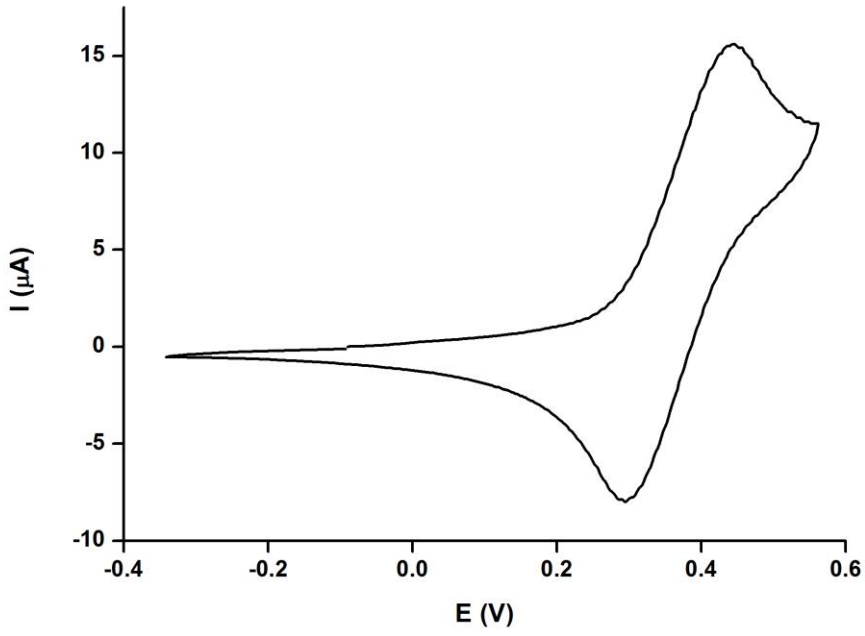

Figure 26: Cyclic voltammogram of 13 in CH_2Cl_2/0.1 M NBu_4PF_6; scan rate (v) = 100 mV s^{-1}. Potentials are reported against ferrocene ($FeCp_2/FeCp_2^+$ = 0.0 V) by reference against an internal decamethylferrocene/decamethylferricenium couple ($FeCp^*_2$/ $FeCp^*_2{}^+$ = −0.48 V vs $FeCp_2/FeCp_2^+$)

The single reversible redox process in compound **11** shows simultaneous oxidation of both triarylamine groups in the compound in NBu_4PF_6 electrolyte (Figure 27). As noted above the observation of ΔE_p values consistent with the internal standard and considerably greater than would be expected for a single $2e^-$ process (ca. 30 mV) indicate that the redox couple is more consistent with two closely positioned $1e^-$ processes. Studies in electrolyte containing the very weakly coordinating $[B\{C_6H_3\text{-}3,5\text{-}(CF_3)_2\}_4]^-$ ($[BAr^F{}_4]^-$) anion[57] also show no separation of the two oxidation waves, and as such there is no strong evidence for through-space communication in the systems. The challenges of extrapolating the electrochemical data, which is thermodynamic in nature, to the underlying electronic structure, are well known and without recourse to a wider range of data it is difficult to draw definitive conclusions on the degree or nature of electronic interactions between redox centres based on electrochemical data from a single compound alone.[58] Qualitative conclusions may, however, be made when data are considered alongside reference potentials from a suitable range of model systems.

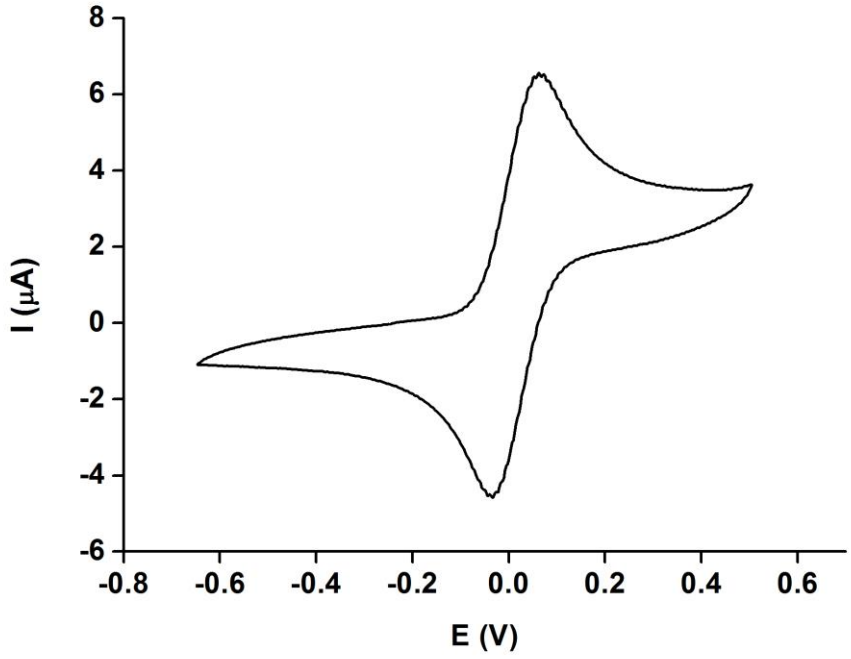

Figure 27: Cyclic voltammogram of 11 in CH_2Cl_2/0.1 M NBu_4PF_6; scan rate (v) = 100 mV s^{-1}. Potentials are reported against ferrocene ($FeCp_2/FeCp_2^+$ = 0.0 V) by reference against an internal decamethylferrocene/decamethylferricenium couple ($FeCp^*_2$/ $FeCp^*_2{}^+$ = −0.48 V vs $FeCp_2$/ $FeCp_2^+$)

The potentials of the two redox processes present in compound **10b** relative to the mono-amine models **10a** and **13** suggest that there is a modest degree of communication between the two triarylamine moieties. The first oxidation potential $E_{1/2}(1)$ in **10b** is some 40 mV higher compared to the model compound **10a** (Figure 28) suggesting that not only is the ethynyl triarylamine moiety a weaker electron donor than the anisole moiety, but *also* that the electronic influence of the ethynyl ligand substituent is propagated to the Pt-ligated triarylamine electrophore. In contrast, the second redox process in **10b** ($E_{1/2}(2)$ = 0.189 V), which is assigned to the ethynyl-substituted triarylamine, is considerably less positive than the model system **13** ($E_{1/2}$ = 0.37 V) and suggests that the oxidised triarylamine moiety in [**10b**]$^+$ is still a stronger electron donor than the tolyl group in **13**. Thus, not only do the relative potentials serve to highlight that the order of oxidation is the platinum bound

triarylamine followed by the ethynyl triarylamine ligand, but also evidences some degree of ground state interaction across the Pt-C≡C bridge.

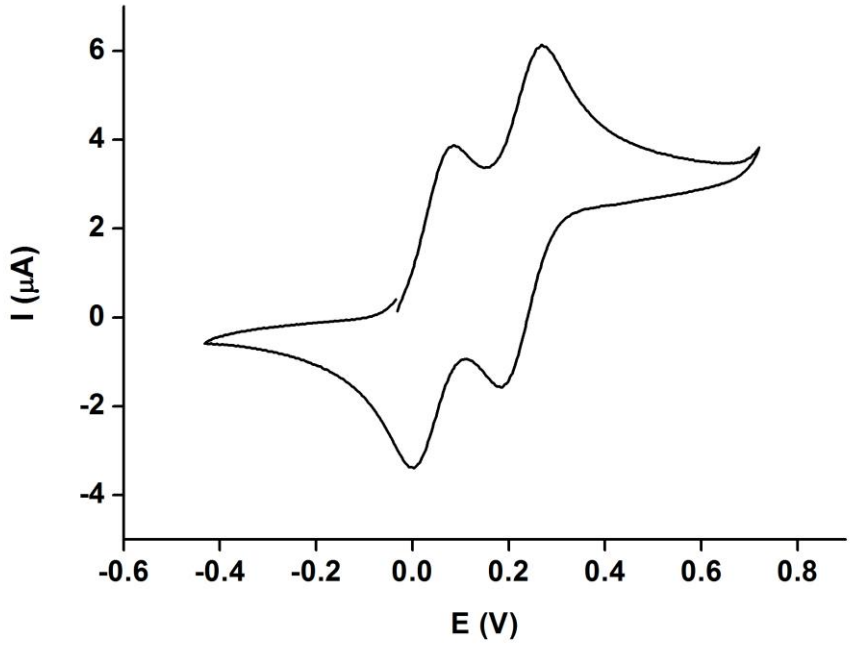

Figure 28: Cyclic voltammogram of 10b in CH_2Cl_2/10^{-1} M NBu_4PF_6; scan rate (v) = 100 mV s^{-1}. Potentials are reported against ferrocene ($FeCp_2/FeCp_2^+$ = 0.0 V) by reference against an internal decamethylferrocene/decamethylferricenium couple ($FeCp^*_2$/ $FeCp^*_2{}^+$ = −0.48 V vs $FeCp_2/FeCp_2^+$)

Compound **12** gives rise to two reversible processes with relative peak currents of 3:1 in the CV, but each with the shape of a $1e^-$ process (Figure 29). These can be attributed to the near simultaneous, independent oxidations of the three triarylamine groups on the periphery of the molecule (ΔE_p = 80 mV) followed by the oxidation of the triarylamine moiety at the core of the compound. As noted previously, the observation of ΔE_p values consistent with the internal standard and considerably greater than would be expected for a single $3e^-$ (ca. 20 mV) process indicate that the redox couple is consistent with either three independent 1e processes that take place at the same potential, or at least three closely positioned $1e^-$ processes. The

pronounced similarity of the half-wave potentials in the larger compound **12** with those observed for the structurally related bis(triarylamine) compound **10b** suggests a similar degree of electronic interaction is taking place along the three Pt-C≡C bridges in each case.

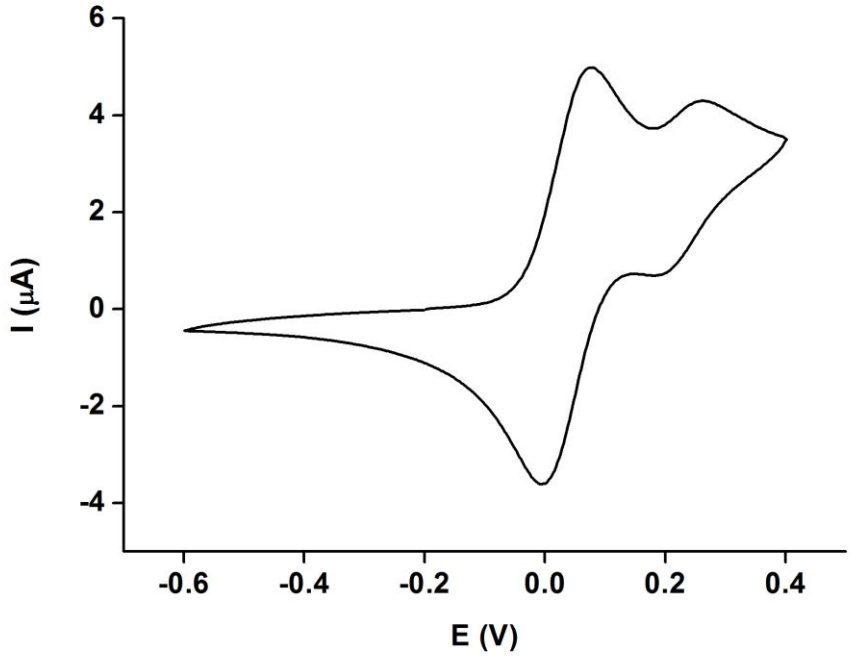

Figure 29: Cyclic voltammogram of 12 in CH_2Cl_2/10^{-1} M NBu_4PF_6; scan rate (v) = 100 mV s^{-1}. Potentials are reported against ferrocene ($FeCp_2/FeCp_2^+$ = 0.0 V) by reference against an internal decamethylferrocene/decamethylferricenium couple ($FeCp^*_2$/ $FeCp^*_2{}^+$ = −0.48 V vs $FeCp_2/FeCp_2^+$)

2.3.4. IR Spectroelectrochemistry

In order to better understand the electronic properties of compounds **10a, 10b, 11**, **12** and **13** and their redox products, spectroelectrochemical studies have been carried out. IR spectroelectrochemical investigations carried out in ca. 1 mM solutions in 0.1 M NBu_4PF_6 / CH_2Cl_2 show that the neutral complexes **10a, 10b, 11**, **12** and **13** all give rise to single ν(C≡C) absorption band near 2100 cm^{-1} (Table 5). This

characteristic feature can be used as a handle to explore the changes in physical structure, and hence to some degree electronic structure, accompanying the *in situ* oxidation of the triarylamine moieties.[59]

Table 5: Experimental ν(C≡C) frequencies for complexes [4a – 6]$^{n+}$.

Compound	n = 0	n = 1	n = 2
[10a]$^{n+}$	2107(s)	2107(m)	
[10b]$^{n+}$	2105(s)	2105(m)	2071(vs)
		2071(s)	2052(sh)
		2052(sh)	2027(sh)
		2027(sh)	
[11]$^{n+}$	2103(s)		2105(m)
[13]$^{n+}$	2103(s)	2076(s)	
		2047(sh)	
		2013(sh)	
	n = 0	n = 3	n = 4
[12]$^{n+}$	2105(s)	2107(m)	2068(s)
			2027(sh)

Upon oxidation the ν(C≡C) band profile for compounds **10a** (Figure 30) and **11** (Figure 31) shows a small decrease in intensity, which in the case of **11** is accompanied by a very small blue shift. The lack of any discernable concentration of a one-electron oxidation product [**11**]$^{+}$ is consistent with the electrochemical results described above, i.e. the indiscernible separation of the redox processes associated with the two amine moieties and hence the limiting value of $K_c = 4$. In contrast [**13**]$^{+}$ shows large shift of the ν(C≡C) to lower energy on oxidation to lower energy with the growth of a band envelope that is consistent with previous reports of oxidised triarylamine compounds and the complex band envelope could be a result of Fermi coupling, as often observed by the Rennes group in studies of iron acetylide complexes.[62]

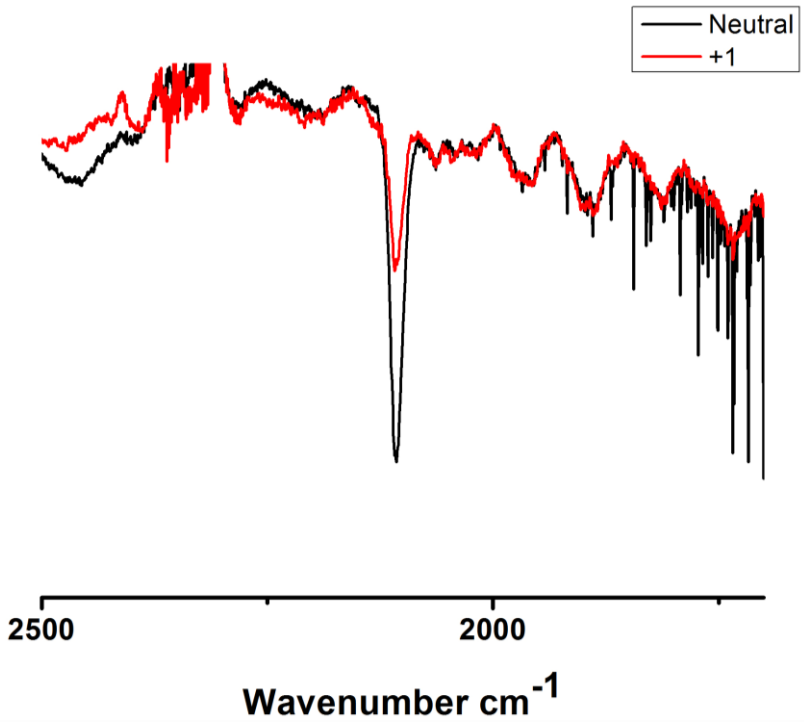

Figure 30: IR spectra of 10a showing the ν(C≡C) band in the different oxidation states generated by *in situ* electrochemical oxidation in CH_2Cl_2 / 0.1 M NBu_4PF_6 in an OTTLE cell

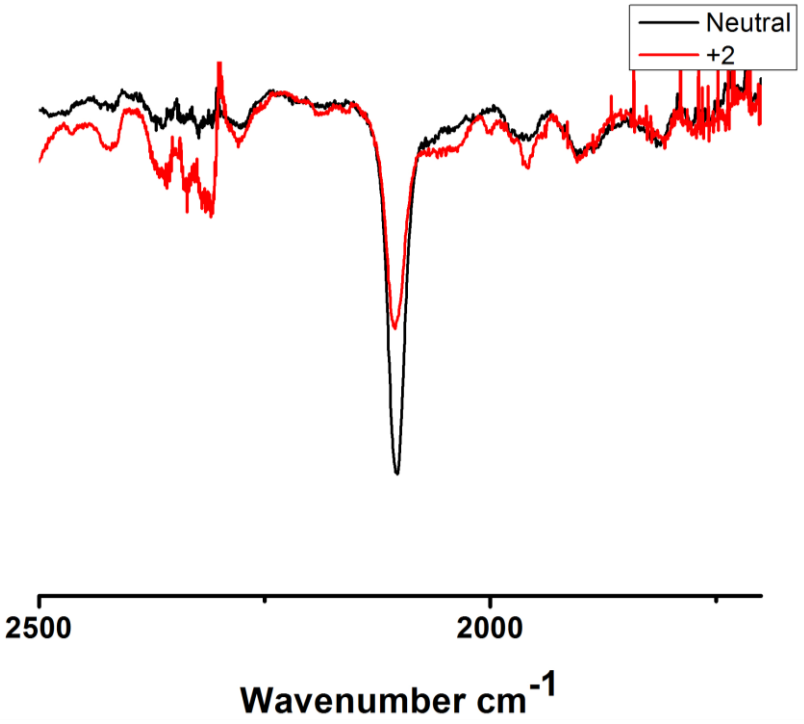

Figure 31: IR spectra of 11 showing the ν(C≡C) band in the different oxidation states generated by *in situ* electrochemical oxidation in CH_2Cl_2 / 0.1 M NBu_4PF_6 in an OTTLE cell

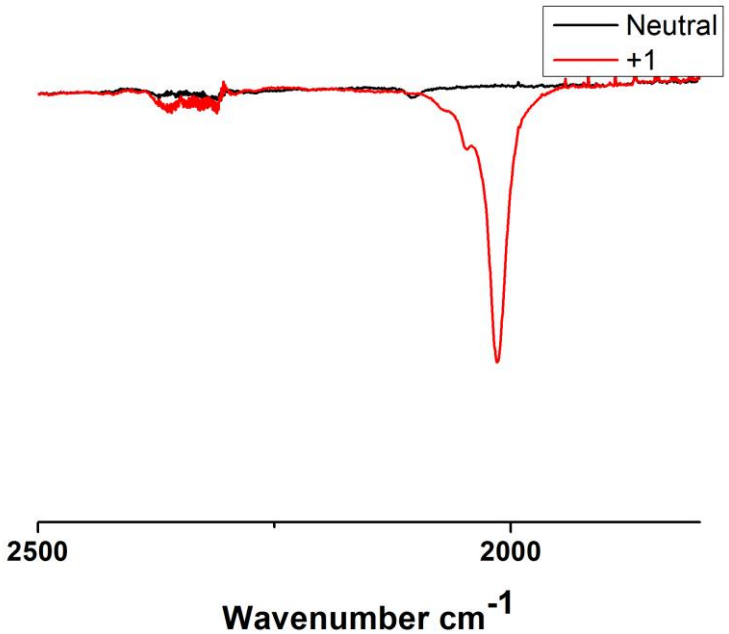

Figure 32: IR spectra of 13 showing the ν(C≡C) band in the different oxidation states generated by *in situ* electrochemical oxidation in CH_2Cl_2 / 0.1 M NBu_4PF_6 in an OTTLE cell

Oxidation of **10b** to [**10b**]$^+$ results in both a small decrease in intensity of the initial ν(C≡C) band, together with the appearance of a broad, poorly structured ν(C≡C) band envelope between 2071 - 2027 cm^{-1} (Figure 33). Further oxidation to [**10b**]$^{2+}$ results in a substantial increase in the intensity of this lower energy band envelope. This pattern of IR bands associated with **10b**, [**10b**]$^+$ and [**10b**]$^{2+}$ is consistent with an initial oxidation event more or less at the Pt-ligated triarylamine moiety but which perturbs the remote C≡C moiety. The second oxidation is more clearly associated with the alkynyl-bound triarylamine and is consistent with the band pattern shown in the model compound [**13**]$^+$.

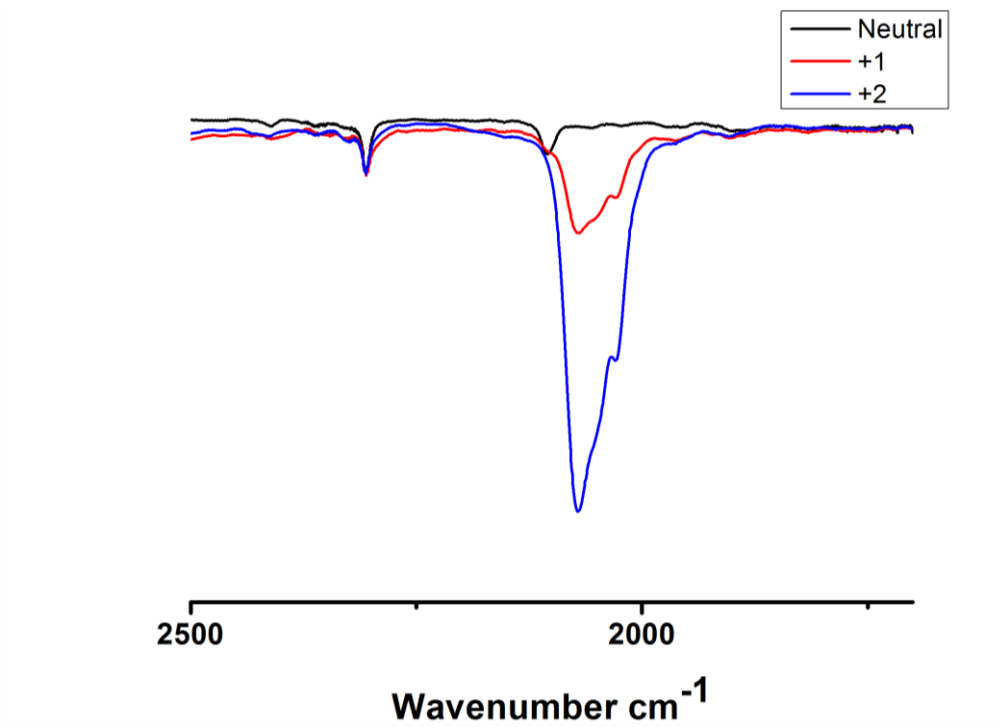

Figure 33: IR spectra of 10b showing the ν(C≡C) band in the various oxidation states generated by *in situ* electrochemical oxidation in CH_2Cl_2 / 0.1 M NBu_4PF_6 in an OTTLE cell

These IR features are accompanied by the appearance of a weak NIR band unique to [**10b**]$^+$ with an apparent band centre at 8000 cm^{-1}, which collapses on oxidation to [**10b**]$^{2+}$ (Figure 34). This behaviour is suggestive of $\{Ar_2NC_6H_4C{\equiv}C\}\rightarrow\{PtC_6H_4N^+Ar_2\}$ IVCT character in this low-energy electronic transition, and hence description of [**10b**]$^+$ as a weakly coupled mixed valence complex. Rudimentary analysis of the NIR band using the Hush expressions[60] (See Chapter 1) and taking the crystallographically determined N1-N2 distance as a proxy for the electron-transfer distance gives H_{ab} = 170 cm^{-1}.

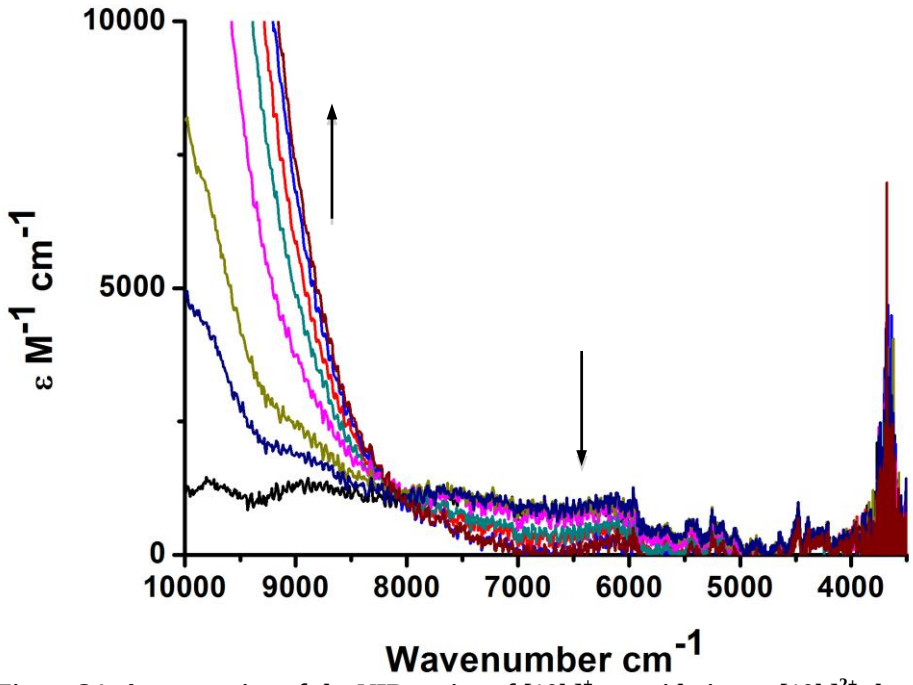

Figure 34: An expansion of the NIR region of $[10b]^{+}$ on oxidation to $[10b]^{2+}$ showing the collapse of the IVCT band

Table 6: Estimated coupling parameters for the IVCT band in 10b

	$\varepsilon/M^{-1}\ cm^{-1}$	$V_{1/2}/cm^{-1}$	V_{max}/cm^{-1}	r/Å	H_{ab}/cm^{-1}
10b	1000	2200	7200	15.231	170

Oxidation of **12** to $[\mathbf{12}]^{3+}$ gives the same pattern of behaviour as observed for oxidation of **10b** to $[\mathbf{10b}]^{+}$, with oxidation accompanied by a decrease in intensity of the ν(C≡C) band and a shift to higher wavenumbers, but now with a weaker ν(C≡C) band envelope at lower wavenumber accompanied by the appearance of a NIR band (ν_{max} = 8700 cm^{-1}) of much more appreciable intensity. Assuming that the NIR band is caused by an IVCT type transition between the amine moieties then a small coupling constant, H_{ab}, value of ca. 130 cm^{-1} (allowing for the three possible transitions) can be estimated from spectral data.

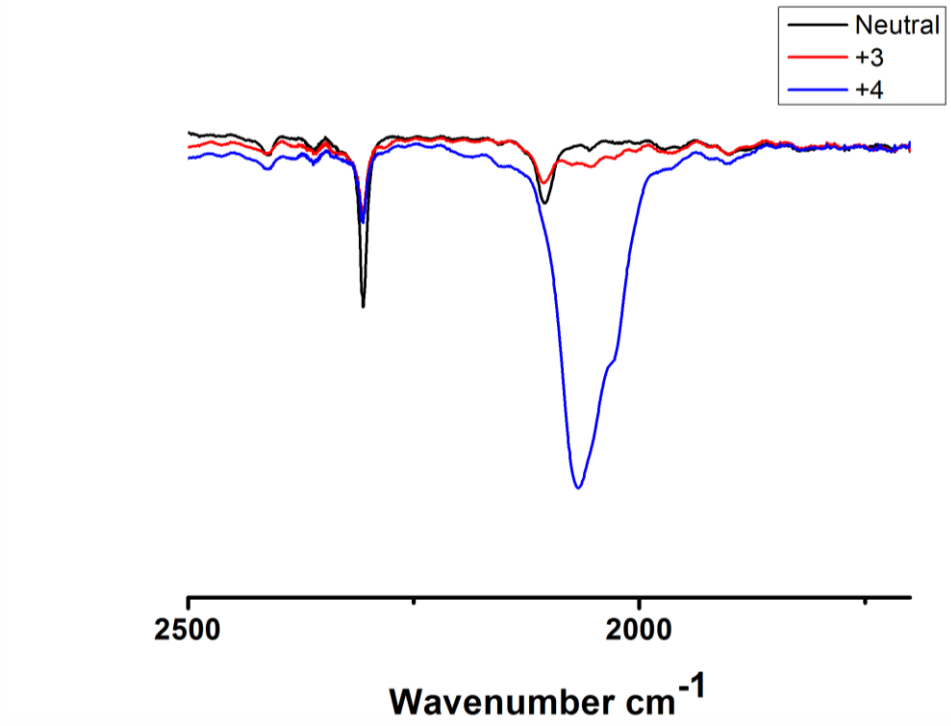

Figure 35: IR spectra of 12 showing and the ν(C≡C) band in the various oxidation states generated by *in situ* electrochemical oxidation in CH_2Cl_2 / 0.1 M NBu_4PF_6 in an OTTLE cell

The ν(C≡C) IR band envelope of [**12**]$^{4+}$ is similar to that of the linear model [**10b**]$^{2+}$. The observation of multiple ν(C≡C) features in these highly charged systems could be a result of Fermi coupling, as often observed by the Rennes group in studies of iron acetylide complexes.[62] The NIR transitions in [**12**]$^{4+}$ are complicated however with the appearance of the tail of low energy optical bands; these are discussed in more detail below.

2.3.5. UV-vis NIR Spectroelectrochemistry

The UV-vis-NIR spectra of [**10a, 10b, 11**, **12** and **13**]$^{n+}$ (n = 0, 1, 2, 3 or 4) were collected using spectroelectrochemical methods from ca. 1 mM solutions in 0.1 M NBu_4PF_6 / CH_2Cl_2. Spectra for the neutral complexes **10a, 10b, 11**, **12** and **13** are consistent throughout the series and are each characterised by two distinct bands at ca. 33000 cm^{-1} and 27000 cm^{-1} (Figure 36 and Table 7). These transitions are

characteristic of triarylamine compounds and can be attributed to two different N→π* transitions. [53-55] The intensity of these transitions increases with the number of triarylamine groups in the molecule. There are no features in the lower energy (vis-NIR) region of the spectrum for the neutral complexes.

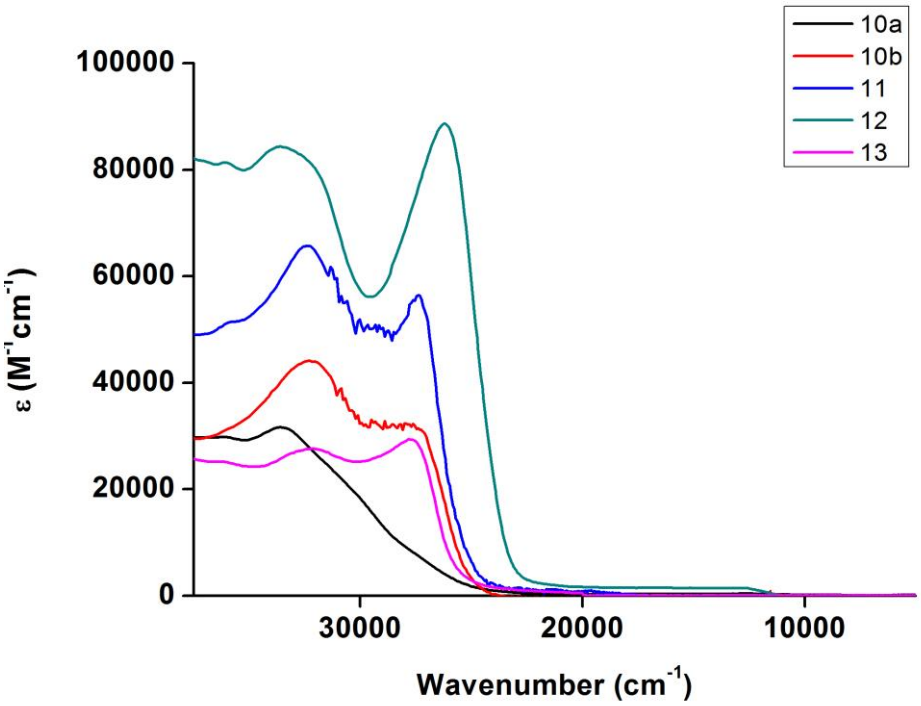

Figure 36: UV-vis NIR spectra of 10-13 in CH_2Cl_2 / 0.1 M NBu_4PF_6 in an OTTLE cell.

Table 7: Characteristic UV-vis NIR absorption maxima (cm^{-1}) of 10-13 observed in spectroelectrochemical studies by *in situ* oxidation of a $CH_2Cl_2/10^{-1}$ M $NBu_4[PF_6]$ solution for $[10\text{-}13]^{n+}$ (n = 0, 1, 2, 3, 4).

Compound	absorption maxima (cm^{-1})
10a	36800, 33500, 27200
[10a]$^+$	36800, 28600, 15700, 12600
10b	32300, 27800
[10b]$^+$	36700, 32600, 26700, 15500, 12500, 7200
[10b]$^{2+}$	36700, 26200, 23900, 22300, 14500, 12800, 10300
11	36100, 32500, 27300
[11]$^{2+}$	37200, 33200, 26800, 15600, 12500, 9800
12	36700, 33500, 26200
[12]$^{3+}$	32300, 25800, 15400, 12500, 7800
[12]$^{4+}$	33700, 31000, 26100, 23000, 21400, 15200, 12700, 8700, 6000
13	32300, 27800,
[13]$^+$	33400, 27700, 24000, 22300, 17900, 9900

On oxidation of compounds **10a, 10b, 11, 12** and **13** to give [**10a**]$^+$ (Figure 37), [**10b**]$^+$, [**11**]$^{2+}$ (Figure 38), [**12**]$^{3+}$ and [**13**]$^+$ (Figure 39) the spectra all show a decrease in the intensity of the highest energy band at ca. 33000 cm^{-1} and an increase in the lower energy band at ca. 27000 cm^{-1} accompanied by a small blue shift to ca. 26000 cm^{-1}. There are significant changes in the visible region of the spectra for all the compounds with the growth of a high intensity band centred at ca. 12000 cm^{-1} and a less intense band overlapping this transition at higher energy centred at ca. 16000 cm^{-1}. These changes in the spectra are consistent with previous reports of amine radical species and platinum bridged triarylamine compounds.[11] Interestingly the low energy band in compounds [**10a**]$^+$, [**11**]$^{2+}$ and [**12**]$^+$ are at lower energy than in compound **13** consistent with the oxidation of the triarylamine moiety not bound directly to the platinum centre.

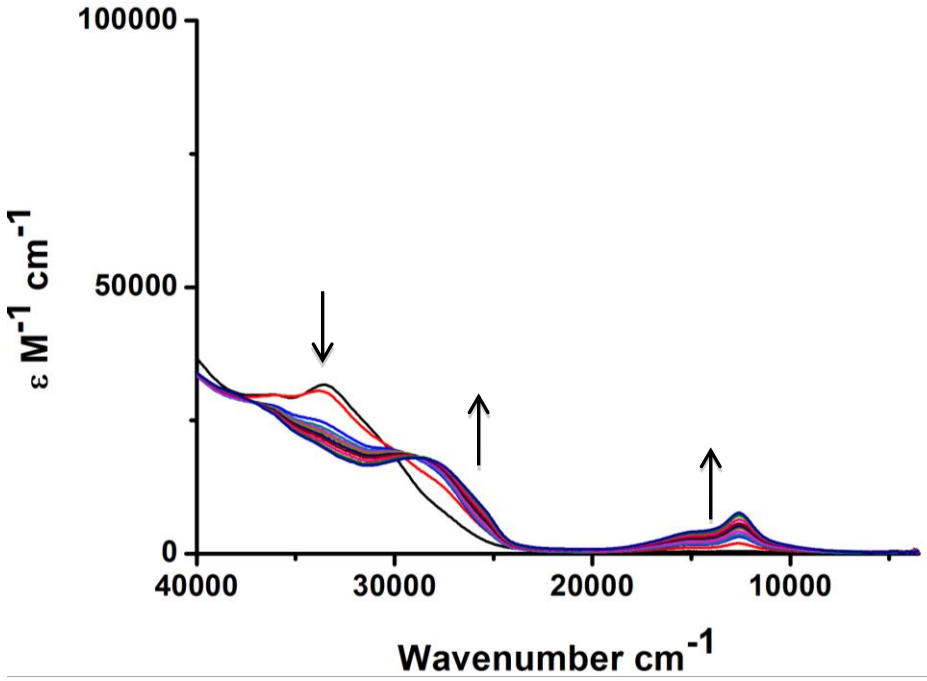

Figure 37: UV-vis-NIR spectra of 10a showing the spectral changes upon oxidation generated by *in situ* electrochemical oxidation in CH_2Cl_2 / 0.1 M NBu_4PF_6 in an OTTLE cell

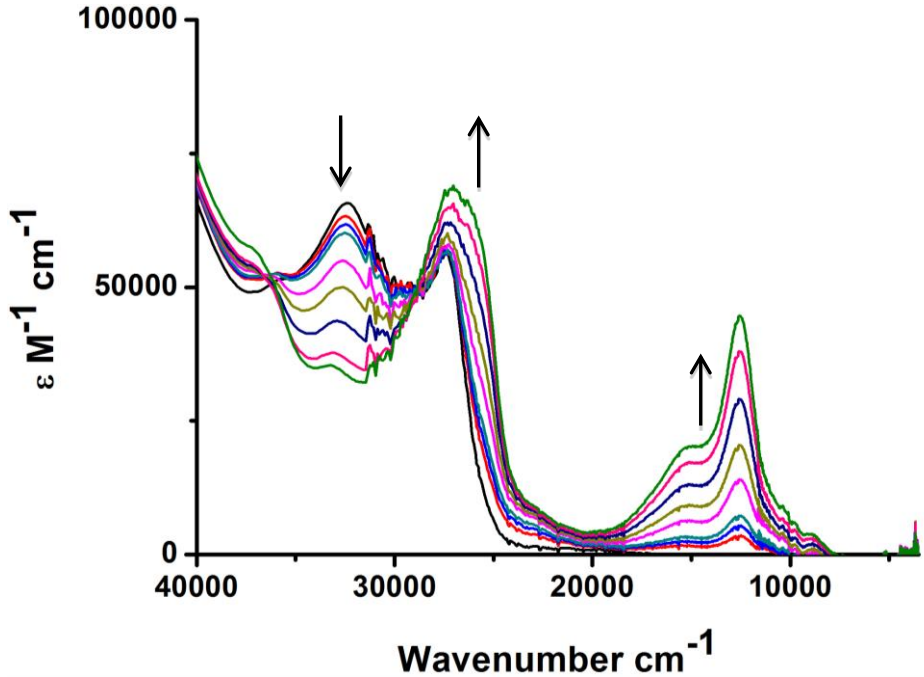

Figure 38: UV-vis-NIR spectra of 11 showing the spectral changes upon oxidation generated by *in situ* electrochemical oxidation in CH_2Cl_2 / 0.1 M NBu_4PF_6 in an OTTLE cell

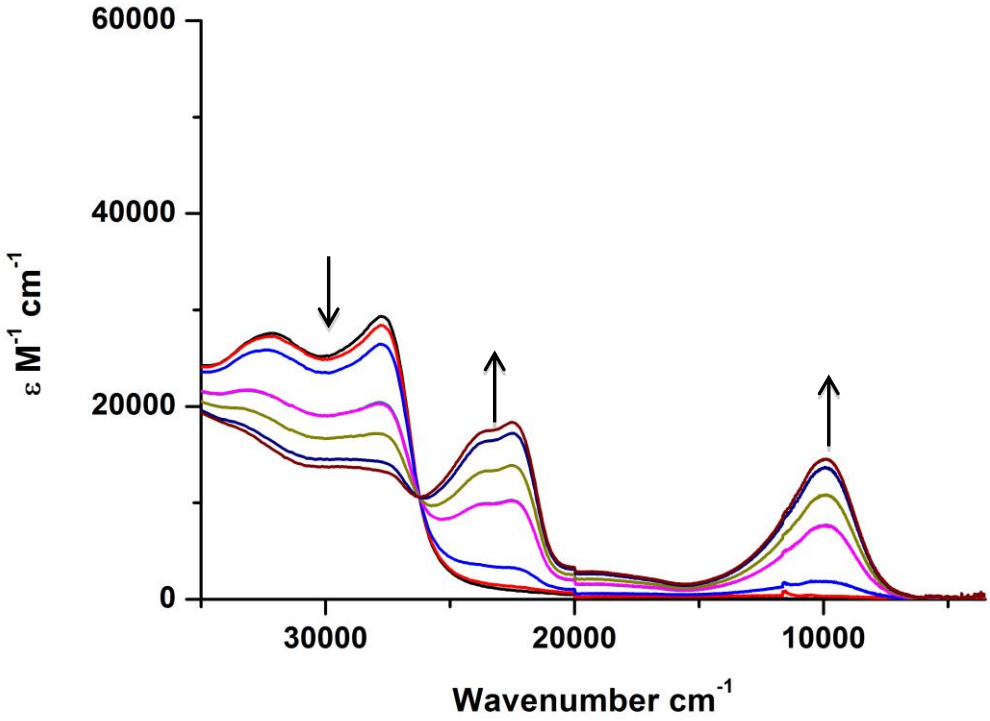

Figure 39: UV-vis-NIR spectra of 13 showing the spectral changes upon oxidation generated by *in situ* electrochemical oxidation in CH_2Cl_2 / 0.1 M NBu_4PF_6 in an OTTLE cell

As discussed above, in the case [**10b**]$^+$ (Figure 24, Figure 40) and [**12**]$^{3+}$ (Figure 41) there is also a very weak transition below 10000 cm^{-1} in the NIR region of the spectra, which is consistent with an IVCT band of the nature N→N$^+$ from the 'mixed valence' nature of the amine oxidations (Figure 42).

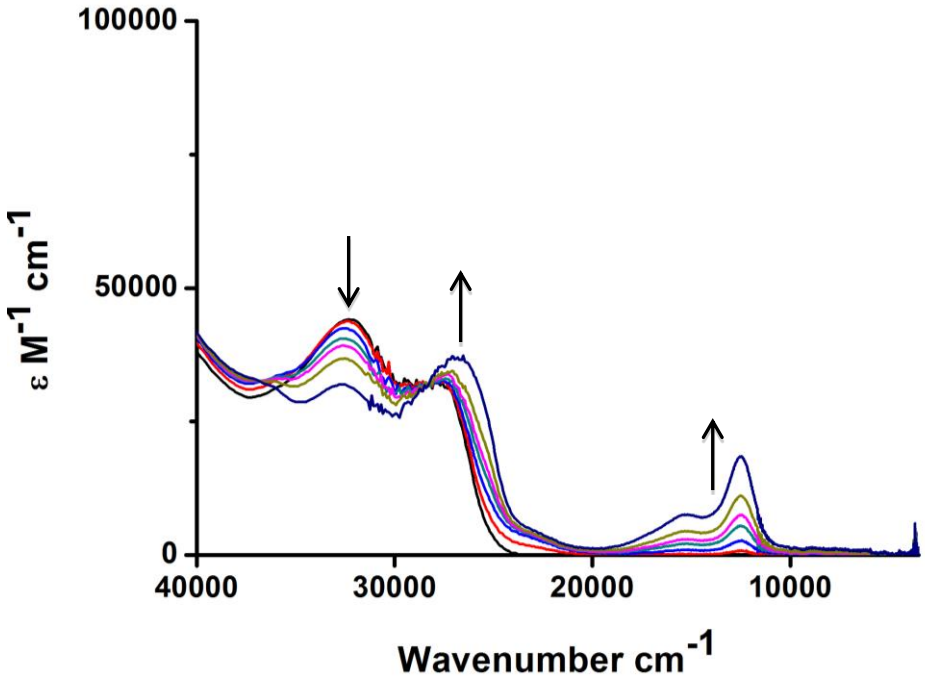

Figure 40: UV-vis-NIR spectra of 10b→[10b]$^{+}$ showing the spectral changes upon oxidation generated by *in situ* electrochemical oxidation in CH_2Cl_2 / 0.1 M NBu_4PF_6 in an OTTLE cell

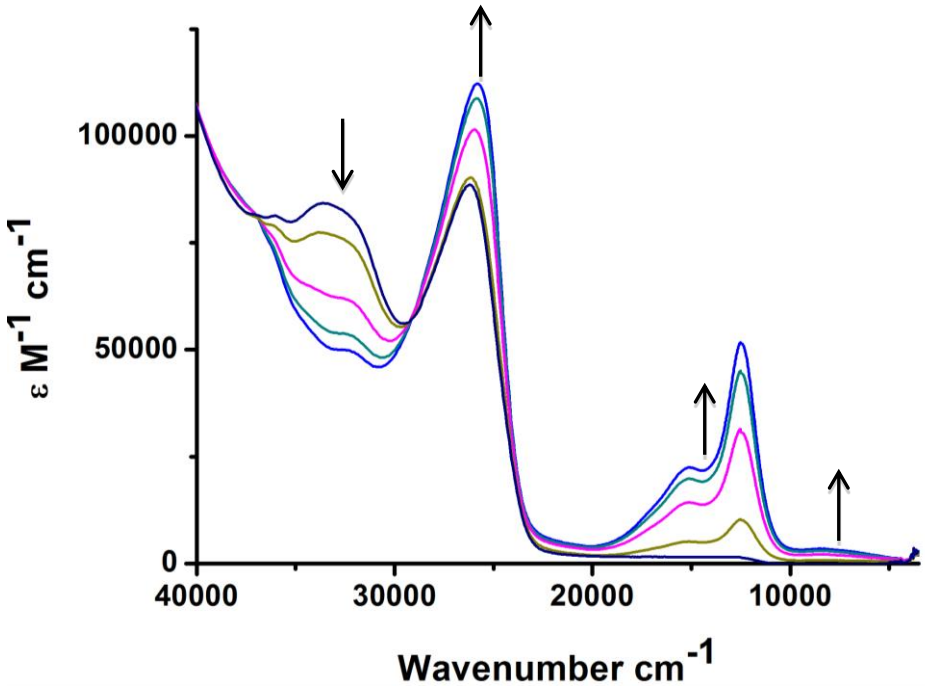

Figure 41: UV-vis-NIR spectra of 12→[12]$^{3+}$ showing the spectral changes upon oxidation generated by *in situ* electrochemical oxidation in CH_2Cl_2 / 0.1 M NBu_4PF_6 in an OTTLE cell

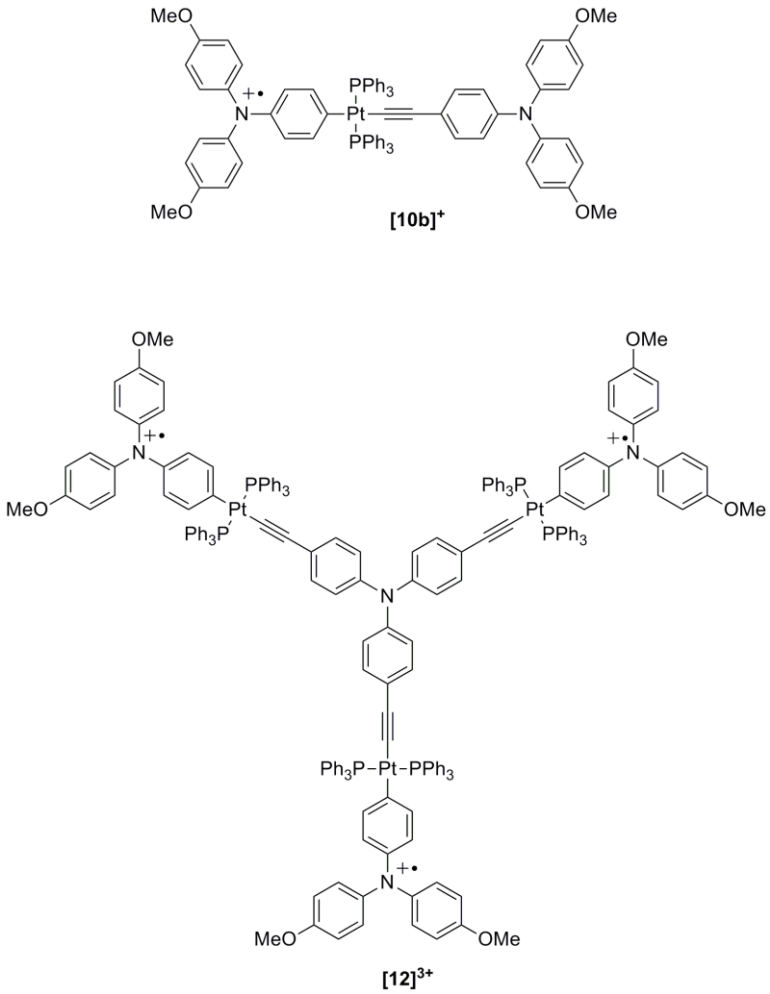

Figure 42: Schematic of compounds $[10b]^+$ and $[12]^{3+}$ showing the mixed valence nature of the triarylamines.

Further oxidation of [**10b**]$^+$ to [**10b**]$^{2+}$ (Figure 43) shows a small collapse of the band at ca. 26000 cm^{-1} accompanied by the growth of a series of unresolved transitions between 17000 and 25000 cm^{-1}, the transitions at 15000 and 12500 cm^{-1} both increase in intensity and the signal at 12500 cm^{-1} undergoes a small blue shift. The changes in the spectra on progression from [**10b**]$^+$ to [**10b**]$^{2+}$ are accompanied by the growth of a new signal at ca. 10000 cm^{-1}, consistent with a second set of $NAr'_3{}^+$, with energy the same as those seen for the ethynyl-triarylamine oxidation in **13**. It is clear that the two different signals are consistent with transitions from the chemically distinct amine

moieties, and the complete collapse of the weak band at ca. 6000 cm^{-1} consistent with the IVCT assignment.

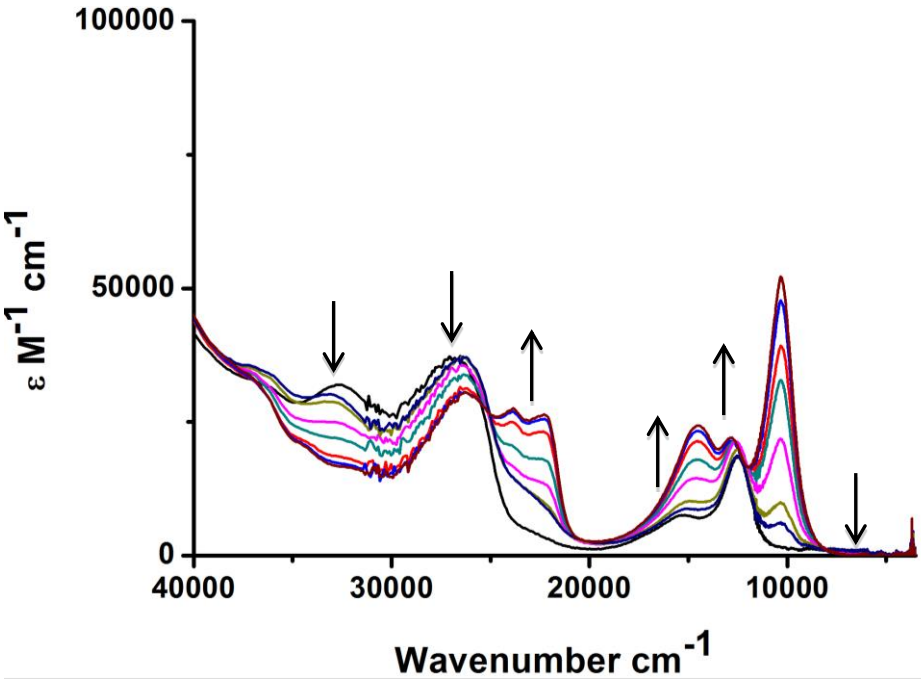

Figure 43: UV-vis-NIR spectra of $[10b]^{+}$→$[10b]^{2+}$ showing the spectral changes upon oxidation generated by *in situ* electrochemical oxidation in CH_2Cl_2 / 0.1 M NBu_4PF_6 in an OTTLE cell

Further oxidation of $[\mathbf{12}]^{3+}$ to $[\mathbf{12}]^{4+}$ (Figure 44) shows a collapse of the band at ca. 26000 cm^{-1} accompanied by the growth of a series of unresolved transitions between 17000 and 25000 cm^{-1}, the transitions at 15000 and 12500 cm-1 both increase in intensity and the signal at 12500 cm^{-1} undergoes a small blue shift. The changes in the spectra are accompanied by the growth of a new signal at ca. 10000 cm^{-1} with equal intensity as the signal at 12500 $cm^{-1,}$ consistent with a second set of $NAr'_3{}^{+}$ transitions with the same origin as those in $[\mathbf{10b}]^{2+}$ and $[\mathbf{13}]^{+}$ and a slight increase and change in shape of the signal at 6000 cm^{-1}, which remains of low intensity.

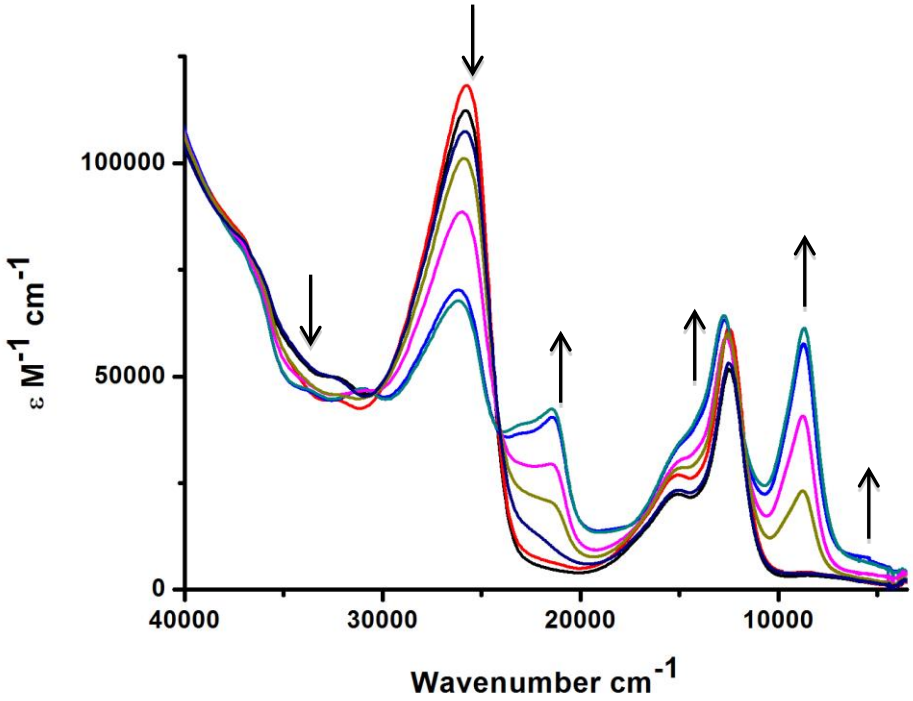

Figure 44: UV-vis-NIR spectra of $[12]^{3+}$→ $[12]^{4+}$ showing the spectral changes upon oxidation generated by *in situ* electrochemical oxidation in CH_2Cl_2 / 0.1 M NBu_4PF_6 in an OTTLE cell

2.3.6. Quantum Chemical Calculations

To complete the description of these redox-active Pt-ethynyl/triarylamine assemblies, quantum-chemical calculations using the BLYP35 functional and COSMO (dichloromethane) solvent model were carried out by Matthias Parthey in the group of Professor Martin Kaupp in TU Berlin, Germany. The combination of a high amount of direct exchange in the functional and the inclusion of a solvent model has been shown to allow the accurate description of charge localisation/delocalisation now in a wide range of organic and organometallic mixed-valence complexes spanning the weakly to strongly coupled regime.[61]

As expected, complexes [**10a**]$^+$, [**10b**]$^+$, [**11**]$^+$ and [**13**]$^+$ all exhibit spin densities localised at one triarylamine unit in their monocationic forms (Table 8 - Table 12). In the case of [**10b**]$^+$ this localisation takes place at the triarylamine moiety which is

directly connected to the platinum centre. The localised (Class II) behaviour of all complexes investigated here is in agreement with previous studies of platinum-bridged triarylamine systems and the work described later in Chapter 3. Vibrational analysis within a harmonic framework provides excellent agreement between the computed ν(C≡C) frequency at 2075 cm^{-1} and the experimental at 2071 cm^{-1} for [**10b**]$^{+}$ after scaling by an empirical factor of 0.95.[81] In contrast for [**10a**]$^{+}$ no intensity is calculated for ν(C≡C), consistent with the decrease in intensity of this band observed experimentally.

Table 8: Orbital energies (E_{orb}) and contributions from Mulliken population analysis for [10a]$^+$.

Orbital	E_{orb} [eV]	Contributions [%]			
		$Ar_2NC_6H_4$	$Pt(PPh_3)_2$	C≡C	C_6H_4OMe
spin density	/	99	1	0	0
263 β*	-0.93	10	74	0	0
263 α*	-0.97	36	50	0	0
262 β*	-4.05	92	2	0	0
262 α	-5.90	0	9	36	49
261 β	-5.91	0	8	37	50
261 α	-6.44	87	3	3	0
260 β	-6.84	1	16	66	2
260 α	-6.88	0	13	68	2
259 β	-7.20	50	24	5	0
259 α	-7.32	0	81	0	0
258 β	-7.37	4	85	0	0
258 α	-7.38	4	83	0	0
257 β	-7.40	14	64	1	4
257 α	-7.56	12	22	8	43
256 β	-7.43	92	0	0	0
256 α	-7.64	28	29	0	29
255 β	-7.59	0	32	6	52
255 α	-7.69	91	0	0	0
254 β	-7.70	0	30	2	54
254 α	-7.71	1	40	2	40
253 β	-7.79	3	79	2	8
253 α	-7.79	0	83	2	6
252 β	-7.81	10	78	0	0
252 α	-7.82	1	88	0	0
251 β	-7.85	0	81	0	5
251 α	-7.85	0	86	0	6
250 β	-7.87	3	67	6	7
250 α	-7.90	6	76	3	1
249 β	-7.92	29	56	0	0
249 α	-7.96	16	73	0	0

* unoccupied orbital

Table 9: Orbital energies (E_{orb}) and contributions from Mulliken population analysis for [10b]$^+$.

Orbital	E_{orb} [eV]	Contributions [%]			
		$Ar_2NC_6H_4$	C≡C	$Pt(PPh_3)_2$	$C_6H_4NAr_2$
spin density	/	0	0	1	100
315 β*	-0.93	0	0	73	11
315 α*	-0.96	0	0	48	37
314 β*	-4.05	0	0	2	92
314 α	-5.31	81	12	2	0
313 β	-5.30	81	12	2	0
313 α	-6.36	15	13	7	52
312 β	-6.45	52	32	9	0
312 α	-6.54	28	22	5	31
311 β	-6.84	2	67	17	0
311 α	-6.87	3	68	14	0
310 β	-6.96	92	0	0	0
310 α	-6.96	92	0	0	0
309 β	-7.20	0	4	28	49
309 α	-7.32	0	0	80	0
308 β	-7.37	0	0	84	4
308 α	-7.38	0	0	85	4
307 β	-7.40	0	1	61	18
307 α	-7.55	86	0	6	0
306 β	-7.43	0	0	0	92
306 α	-7.61	48	2	13	22
305 β	-7.55	86	0	6	0
305 α	-7.65	34	1	24	25
304 β	-7.63	75	2	9	0
304 α	-7.68	0	0	0	89
303 β	-7.70	38	1	45	0
303 α	-7.70	36	1	46	0
302 β	-7.78	1	0	76	6
302 α	-7.79	3	0	81	0
301 β	-7.81	0	0	80	8
301 α	-7.82	0	0	84	0
300 β	-7.84	23	0	62	0
300 α	-7.84	24	0	62	0
299 β	-7.86	63	0	22	0
299 α	-7.87	70	0	17	0
298 β	-7.88	15	4	56	3
298 α	-7.90	2	3	74	3
297 β	-7.91	0	0	57	27
297 α	-7.95	0	0	74	16

* unoccupied orbital

Table 10: Orbital energies (E_{orb}) and contributions from Mulliken population analysis for $[11]^+$.

Orbital	E_{orb} [eV]	Contributions [%]				
		$Ar_2NC_6H_4$	$Pt(PMe_3)_2$	$C{\equiv}CC_6H_4C{\equiv}C$	$Pt(PMe_3)_2$	$C_6H_4NAr_2$
spin density	/	99	0	0	0	0
296 β*	-0.79	96	0	0	0	0
296 α*	-0.92	95	0	0	0	0
295 β*	-4.10	92	2	0	0	0
295 α	-5.14	0	0	0	2	72
294 β	-5.14	0	0	0	2	72
294 α	-5.79	0	3	86	5	0
293 β	-5.79	0	3	86	5	0
293 α	-6.46	89	4	0	0	0
292 β	-6.64	0	0	39	30	2
292 α	-6.64	0	0	39	31	2
291 β	-6.71	0	0	19	19	15
291 α	-6.72	0	0	18	19	15
290 β	-6.78	0	0	0	0	83
290 α	-6.78	0	0	0	0	83
289 β	-6.95	0	0	0	83	0
289 α	-6.95	0	0	0	83	0
288 β	-6.95	0	32	59	0	0
288 α	-6.97	0	32	61	0	0
287 β	-7.12	15	12	49	7	0
287 α	-7.13	0	0	0	1	13
286 β	-7.13	0	0	0	1	13
286 α	-7.17	0	9	63	10	0
285 β	-7.30	43	20	19	3	0
285 α	-7.41	5	91	0	0	0
284 β	-7.40	5	87	0	0	0
284 α	-7.50	0	0	0	0	97
283 β	-7.42	88	4	0	0	0
283 α	-7.54	53	33	0	0	0
282 β	-7.50	0	0	0	0	97
282 α	-7.63	0	0	98	0	0
281 β	-7.63	0	0	98	0	0
281 α	-7.63	0	0	26	21	0
280 β	-7.63	0	0	26	21	0
280 α	-7.70	0	0	0	0	93

* unoccupied orbital

Table 11: Orbital energies (E_{orb}) and contributions from Mulliken population analysis for [13′]$^+$.

Orbital	E_{orb} [eV]	Contributions [%]			
		$Ar_2C_6H_4$	C≡C	$Pt(PPh_3)_2$	C_6H_4Me
spin–density	/	73	23	5	–1
251 β*	–1.12	55	12	23	0
251 α*	–1.45	72	14	7	0
250 β*	–4.25	69	21	5	0
250 α	–6.38	12	8	10	57
249 β	–6.41	0	2	11	78
249 α	–6.60	49	13	5	24
248 β	–6.93	53	23	11	3
248 α	–7.08	0	0	5	89
247 β	–7.07	0	0	6	88
247 α	–7.33	1	7	73	0
246 β	–7.33	1	12	73	1
246 α	–7.37	0	0	72	17
245 β	–7.35	0	0	72	18
245 α	–7.46	44	25	21	0
244 β	–7.55	14	24	47	1
244 α	–7.58	22	15	46	1
236 β	–8.03	65	0	15	0
236 α	–8.04	0	2	86	3

*unoccupied orbital.

To characterise the UV-vis-NIR transitions TDDFT calculations employing the same BLYP35/COSMO(CH_2Cl_2) combination as for the ground-state analysis were carried out. All complexes exhibit localised charge distributions in the ground-state, and the reasonable agreement between experimental bands and calculated excitations is consistent with previous observations at this level for Class II systems. The compounds [**10a**]$^+$ and [**10b**]$^+$ exhibit a typical β-HOMO - β-SOMO transition at 9996 cm^{-1} ([**10a**]$^+$, exp. ca. 10,000 cm^{-1}), and at 6514 cm^{-1} ([**10b**]$^+$, exp. ca. 7000 cm^{-1}), respectively. These transitions arise from charge transfer between the alkynyl

ligand and its substituent to the oxidised triarylamine moiety directly coordinated to Pt. At higher energies characteristic excitations associated with the oxidised triarylamine unit and MLCT transitions are computed (Table 12 and Table 13). Interestingly the ethynyl unit contributes more to the orbitals involved in the excitations for [**10a**]$^+$ than [**10b**]$^+$ (Table 8 and Table 9).

As expected, TDDFT calculations from the monocation [**13´**]$^+$ (Table 13) do not exhibit any transitions below 10000 cm^{-1}. The absorption pattern above 10000 cm^{-1} exhibits the same features as [**12´**]$^+$. The first excitation of [**13´**]$^+$ is calculated at 10543 cm^{-1}, which is red shifted by about 700 cm^{-1} compared to [**12´**]$^+$ (11295 cm^{-1}). This can be explained by the nature of the involved orbital. For [**12´**]$^+$ this transition occurs from a delocalised orbital, which has significant contributions from the second triarylamine group (Table 10). As this group is absent in [**13´**]$^+$, the orbital is destabilised in the ground state (–6.41 eV compared to –6.60 eV for [**12´**]$^+$) and is predominantly localised at the tolyl ligand (78 %).

Table 12: Calculated excited state parameters: UV-vis-NIR transition energies E_{trans}, transition dipole moments μ_{trans} and main MO contributions for [10a]$^+$.

#	E_{trans} [cm^{-1}]	μ_{trans} [D]	contributions [%]
1	9996	4.3	261 β -> 262 β 97.6
2	14733	6.9	259 β -> 262 β 45.9, 260 β -> 262 β 39.8
3	16577	4.3	256 β -> 262 β 79.7, 249 β -> 262 β 5.2
4	17128	1.7	260 β -> 262 β 52.4, 259 β -> 262 β 35.6
5	17752	1.8	258 β -> 262 β 55.6, 256 β -> 262 β 9.6
6	18442	2.1	249 β -> 262 β 27.2, 258 β -> 262 β 26.5
7	20298	0.3	257 β -> 262 β 79.7
8	9996	4.3	261 β -> 262 β 97.6

Table 13: Calculated excited state parameters: UV-vis-NIR transition energies E_{trans}, transition dipole moments μ_{trans} and main MO contributions for [10b]$^+$.

#	E_{trans} [cm^{-1}]	μ_{trans} [D]	contributions [%]
1	6514	4.8	313 β-> 314 β 97.8
2	14116	6.5	312 β -> 314 β 52.8, 309 β -> 314 β 28.3
3	15338	3.5	311 β -> 314 β 43.6, 312 β -> 314 β 34.5
4	16600	4.2	306 β -> 314 β 78.3, 297 β -> 314 β 5.3
5	17135	2.1	311 β -> 314 β 41.6, 309 β -> 314 β 39.0
6	17700	1.8	308 β -> 314 β 60.7, 306 β -> 314 β 9.5
7	18421	2.2	297 β -> 314 β 26.8, 308 β -> 314 β 22.5
8	20290	0.3	307 β -> 314 β 78.5, 309 β -> 314 β 12.4
9	20961	0.2	310 β -> 314 β 99.4
10	20977	0.2	313 β -> 329 β 9.8, 313 β -> 319 β 9.7
11	22429	0.3	289 β -> 314 β 35.5, 291 β -> 314 β 13.0
12	22872	0.1	288 β -> 314 β 92.6
13	23668	0.4	302 β -> 314 β 29.3, 300 β -> 314 β 16.8
14	24120	0.2	303 β -> 314 β 27.5, 296 β -> 314 β 24.0
15	24520	0.3	305 β -> 314 β 37.6, 286 β -> 314 β 35.4

Table 14: Calculated excited state parameters: UV-vis-NIR transition energies E_{trans}, transition dipole moments μ_{trans} and main MO contributions for [13]$^+$.

#	E_{trans} [cm^{-1}]	μ_{trans} [D]	contributions [%]
1	10543	7.0	249 β –> 250 β 70.1, 244 β –> 250 β 8.1
2	11532	8.7	248 β –> 250 β 70.9, 246 β –> 250 β 8.8
3	13892	1.9	249 β –> 250 β 28.1, 246 β –> 250 β 17.9
4	15968	0.3	245 β –> 250 β 72.9, 247 β –> 250 β 18.4
5	18088	0.1	247 β –> 250 β 80.2, 245 β –> 250 β 17.4
6	18920	0.5	246 β –> 250 β 53.4, 244 β –> 250 β 38.1
7	19800	1.4	236 β –> 250 β 28.7, 227 β –> 250 β 26.9

Although [**11**]$^+$ was not sufficiently thermodynamically stable to be observed in the spectroelectrochemical experiments, some information concerning this unusual mixed-valence complex can be obtained from quantum chemical calculations, using a truncated model in which the PPh_3 ligands have been replaced by PMe_3 ([**11-Me**]$^+$). The compound [**11-Me**]$^+$ is calculated to exhibit a N→N$^+$ IVCT transition at 6692 cm^{-1} with only modest intensity (μ_{trans} = 0.8 D) as expected for a weakly coupled system. The β-HOMO–1 - β-SOMO charge transfer excitation at 9808 cm^{-1} (μ_{trans} = 3.8 D) from the oxidised triarylamine moiety to the diethynylbenzene bridge is responsible for the next lowest-energy excitation. The two most intense transitions are computed at 14966 cm^{-1} (μ_{trans} = 7.4 D) and 16258 cm^{-1} (μ_{trans} = 5.5 D) as is commonly observed for oxidised triarylamine compounds. The first corresponds to a π→N$^+$ CT excitation with one triarylamine unit (43%), the neighbouring platinum (20%) and the diethynylbenzene (19%) contributing significantly to the π-type orbital. The second excitation is best described in terms of an IC excitation at the charged triarylamine.

Table 15: Calculated excited state parameters: UV-vis-NIR transition energies E_{trans}, transition dipole moments μ_{trans} and main MO contributions for [11-Me]$^+$.

#	E_{trans} [cm^{-1}]	μ_{trans} [D]	contributions [%]
1	6692	0.8	294 β -> 295 β 99.6
2	9808	3.8	293 β -> 295 β 97.4
3	14966	7.4	285 β -> 295 β 43.3, 287 β -> 295 β 26.2
4	16258	5.5	283 β -> 295 β 88.7, 284 β -> 295 β 5.8
5	16770	1.2	288 β -> 295 β 67.6, 287 β -> 295 β 12.1
6	18085	0.4	284 β -> 295 β 89.2, 283 β -> 295 β 5.9
7	18141	0.1	292 β -> 295 β 84.6, 291 β -> 295 β 8.9
8	18923	0.4	291 β -> 295 β 84.6, 292 β -> 295 β 8.5
9	19061	1.7	276 β -> 295 β 90.4
10	20025	0	290 β -> 295 β 99.8
11	20141	0.1	294 α -> 299 α 32.4, 293 β -> 297 β 30.4
12	20759	0	289 β -> 295 β 100.0
13	21003	0.3	287 β -> 295 β 55.8, 285 β -> 295 β 36.5
14	22420	0.3	270 β -> 295 β 79.9, 271 β -> 295 β 13.5
15	22593	0	286 β -> 295 β 99.7

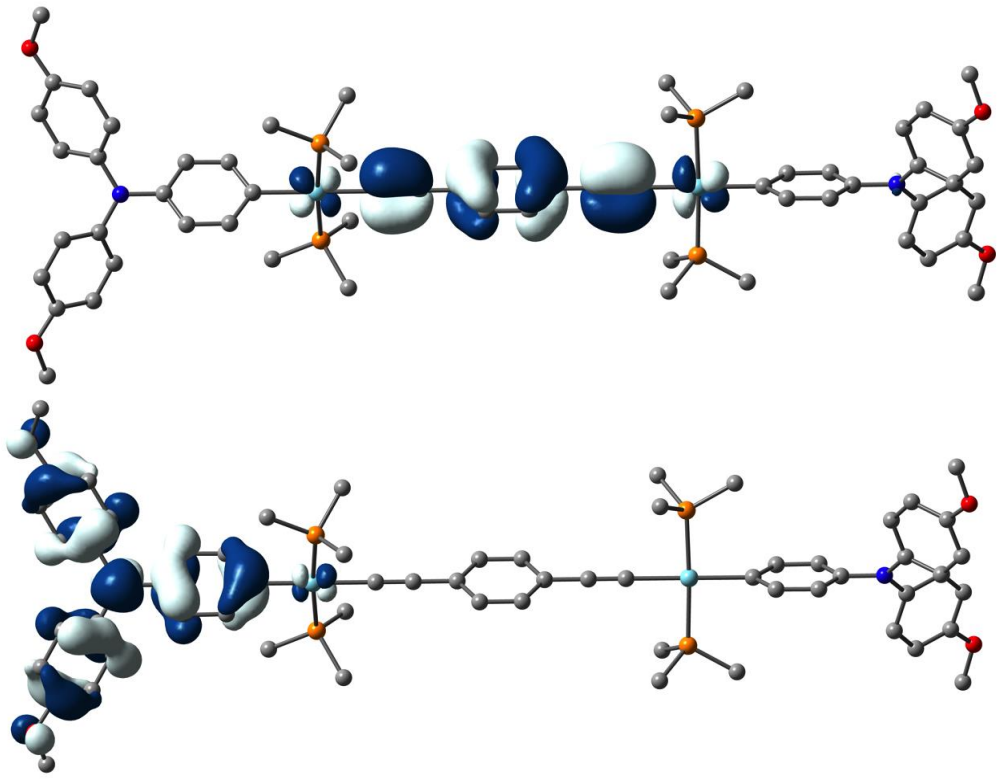

Figure 45: Isosurface plots (± 0.03 a.u.) of the β-SOMO (top) and β-HOMO–1 (bottom) of [11-Me]$^+$. Hydrogen atoms have been omitted for clarity.

For [**11-Me**]$^{2+}$, which was observed in the spectroelectrochemical experiments the calculations provide almost degenerate broken-symmetry (BS, "open-shell singlet") and triplet state, with the former being slightly lower. Keeping in mind that hybrid functionals with increased exact exchange admixture tend to favour high-spin states, the negligible energy difference of only 0.04 kJ/mol (calculated using the Yamaguchi spin projection procedure) in combination with the onset of spin-contamination ($<S^2>_{singlet}$ = 1.06) indicate that both states likely contribute significantly to the spectra. But as expected, the two spin states exhibit very similar spectral features both in the ground- (e.g. $\nu(C{\equiv}C)_{singlet}$ = 2124 cm^{-1} and $\nu(C{\equiv}C)_{triplet}$ = 2124 cm^{-1}) and the excited state. TDDFT gives very similar transition energies for the BS (e.g. 11057 cm^{-1}, μ_{trans} = 5.9 D) and triplet state (e.g. 11073 cm^{-1}, μ_{trans} = 6.1 D), which likely correspond to the low energy shoulder observed near 10000 cm^{-1} (Figure 38). But while excitations arise mainly from and to α-orbitals for the BS state, transitions involve almost exclusively β-orbitals for the triplet. The lowest-energy transition arises in both cases from orbitals located at the diethynylbenzene unit. But while the charge is transferred upon excitation from one triarylamine in the case of the BS state, both triarylamine moieties contribute significantly (30% and 41%) to the orbital involved in the transition for the triplet.

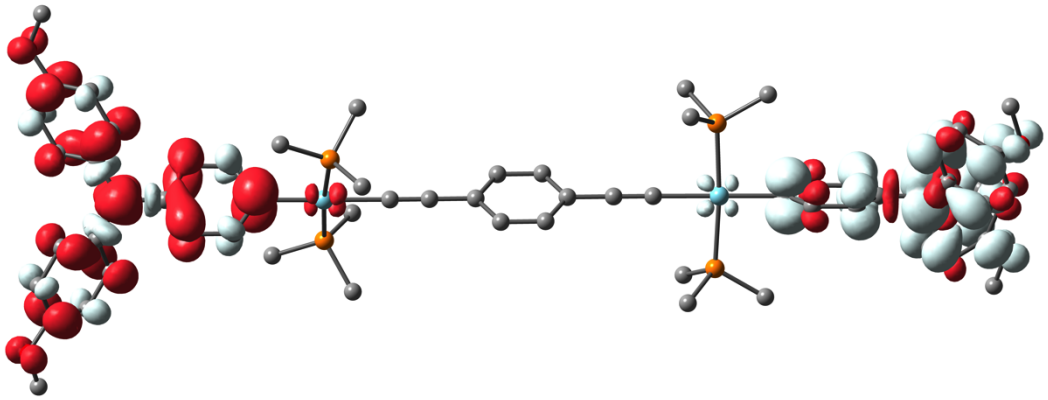

Figure 46: Spin density isosurface plot (± 0.002 a.u.) of the (broken-symmetry) low-spin state of [11-Me]$^{2+}$. Hydrogen atoms have been omitted for clarity.

With this background understanding of the spectroscopic features of the smaller model complexes [**10a**]$^{+}$, [**10b**]$^{+}$ and the computational model [**11-Me**]$^{+}$ it is possible to readily assign the spectroscopic features in the larger systems [**12**]$^{3+}$ and [**12**]$^{4+}$ for which no quantum chemical calculations were performed due to the size of the compound and potential complications from the many possible spin states of these highly charged compounds. The observation of the characteristic intense triarylamine bands between 10000 – 20000 cm^{-1} together with the current ratios described in the electrochemistry section are consistent with the oxidation of the peripheral amine moieties in [**12**]$^{3+}$, with the less intense NIR feature at 5500 cm^{-1} arising from IVCT like processes from the inner to outer amines, all of which are similar to the analogous transitions in [**10b**]$^{+}$. Further oxidation of the central amine moiety in [**12**]$^{4+}$ gives rise to a second set of amine based transitions similar to those observed in [**10b**]$^{2+}$.

2.3.7. Conclusions

The syntheses of mono-ethynyl platinum species with redox-active triarylamine ligands, **10a**, **10b**, **11**, **12** and **13** have successfully been achieved through the oxidative addition of the iodo-triarylamine with the platinum precursor $Pt(PPh_3)_4$ and then coupling to the respective 1-alkyne. These compounds have been studied electrochemically and show that the aryl bound amine moiety has a lower oxidation potential than either the 4-ethynylenephenylenedi-*p*-anisylamine or the tris-(4-ethynylenephenyl)amine moieties.

Spectroelectrochemical investigations have been used to probe the nature of the electronic transitions and in the case of **10b** and **12** low intensity NIR bands are present in the mixed valence species $[\mathbf{10b}]^+$ and $[\mathbf{12}]^{3+}$. TDDFT on compound **10b** has been used to confirm that the nature of this transition is of IVCT character from the ethynyl-triarylamine to the oxidised triarylamine in character. The TDDFT studies have also shown that the extended linear compound, $[\mathbf{11\text{-}Me}]^+$, has similar properties to that of compound $[\mathbf{10b}]^+$ and complexes of this type would exhibit similar low energy transitions if thermodynamically stable and observed on the SEC timescale.

2.4. Experimental

2.4.1. General Conditions

All reactions were carried out under an atmosphere of nitrogen using standard Schlenk techniques as a matter of routine, although no special precautions were taken to exclude air or moisture during work-up. Dry solvents were purified and dried using an Innovative Technology SPS-400, and degassed before use. 4-

ethynylenephenylenedi-*p*-anisylamine,[31] $Pt(PPh_3)_4$,[29] $Pd(PPh_3)_4$[63] and NBu_4BArF_4[64a] were prepared by the literature methods.

NMR spectra were recorded on a Bruker Avance (^1H 400.13 MHz, ^{13}C 100.61 MHz, ^{31}P 161.98 MHz) spectrometer from $CDCl_3$ solutions unless otherwise indicated, and referenced against solvent resonances ($CDCl_3$ ^1H 7.26 ^{13}C 77.0). IR spectra (CH_2Cl_2) were recorded using a Nicolet 6700 spectrometer from cells fitted with CaF_2 windows. Electrospray ionisation mass spectra were recorded using Thermo Quest Finnigan Trace MS-Trace GC or WATERS Micromass LCT spectrometers. Samples in dichloromethane (1 mg/mL) were 100 times diluted in either methanol or acetonitrile, and analysed with source and desolvation temperatures of 120 °C, with cone voltage of 30 V. ASAP mass spectra were recorded from solid aliquots on LCT Premier XE mass spectrometer (Waters Ltd, UK) or Xevo QToF mass spectrometer (Waters Ltd, UK) in which the aliquot is vaporised using hot N_2, ionised by a corona discharge and carried to the TOF detector (working range 100-1000 m/z).

Electrochemical analyses were carried out using an EcoChemie Autolab PGSTAT-30 potentiostat, with platinum working, platinum counter and platinum pseudo reference electrodes, from solutions in CH_2Cl_2 containing 0.1 M supporting electrolyte, ν = 100 mV s^{-1}. The decamethylferrocene/decamethylferricenium ($FeCp^*_2$/ $FeCp^*_2{}^+$) couple was used as an internal reference for potential measurements such that the $FeCp_2$/ $FeCp_2{}^+$ couple falls at 0.00 V ($FeCp^*_2$/ $FeCp^*_2{}^+$ = –0.48 V). Spectroelectrochemical measurements were made in an OTTLE cell of Hartl design from CH_2Cl_2 solutions containing 0.1 M $[NBu_4][PF_6]$ or $[NBu_4][BArF_4]$ electrolyte. The cell was fitted into the sample compartment of the Thermo Nicolet 6700 IR or

Lambda 900 UV-Vis NIR spectrophotometer, and electrolysis in the cell was performed with a PGSTAT-30 potentiostat.

2.4.2. Preparation of $PtI(C_6H_4CH_3\text{-}4)(PPh_3)_2$ (1-CH_3)

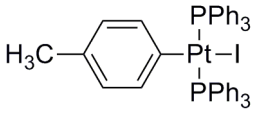

An oven dried flask was charged with dry toluene (15 mL) and the solvent degassed. To this solution, $Pt(PPh_3)_4$ (1.00 g, 0.802 mmol) and 4-iodotoluene (0.350 g, 1.608 mmol) were added and the mixture was stirred under reflux for 24 hours to give a white precipitate. After cooling to ambient temperature the solid was filtered and washed with hexane (2 x 10 mL). Yield 655 mg, 87 %. Crystals suitable for X-ray diffraction were grown from CH_2Cl_2:EtOH. ^{1}H NMR ($CDCl_3$) δ 1.88 (3H, s), 5.95 (2H, d, J = 8 Hz), 6.46 (2H, d, J = 8 Hz), 7.23 (12H, m), 7.31 (6H, m), 7.54 (12H, m); ^{31}P NMR ($CDCl_3$) 20.43 (s, $J_{P\text{-}Pt}$ = 3100 Hz) ASAP-MS(+): calculated for ($C_{43}H_{37}P_2Pt$) 810.20 m/z, found 810.2 m/z.

2.4.3. Preparation of $PtI(C_6H_4NH_2\text{-}4)(PPh_3)_2$ (1-NH_2)

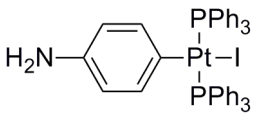

An oven dried Schlenk flask was charged with dry toluene (20 mL) and the solvent degassed. To this solution, $Pt(PPh_3)_4$ (0.50 g, 0.402 mmol) and 4-iodoaniline (0.265 g, 1.20 mmol) were added and the mixture stirred under reflux for 16 hours to give a white precipitate. After cooling to ambient temperature the solid was filtered and wash with hexane (2 x 10 mL). Yield 349 mg, 93 %. ^{1}H NMR ($CDCl_3$) δ 5.72 (2H, d, J = 8 Hz), 6.37 (2H, d, J = 8Hz), 7.25 (12H, m), 7.33 (6H, m), 7.55 (12H, m); ^{31}P

NMR ($CDCl_3$) 20.26 (s, J(P-Pt) = 3083Hz). ASAP-MS(+): calculated for ($C_{42}H_{36}NP_2Pt$) 811.20 m/z, found 811.2 m/z

2.4.4. Preparation of $PtI(C_6H_4OCH_3\text{-}4)(PPh_3)_2$ (1-OCH_3)

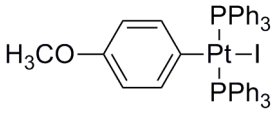

An oven dried Schlenk flask was charged with dry toluene (20 mL) and the solvent degassed. To this solution, $Pt(PPh_3)_4$ (0.50 g, 0.402 mmol) and 4-iodoaniline (0.282 g, 1.20 mmol) were added and the mixture stirred under reflux for 16 hours. After cooling to ambient temperature the mixture was treated with hexane (50 cm^3) to facilitate precipitation of a white solid. The solid was filtered and washed with hexane (2 x 10 mL). Yield 322 mg, 85 %.^{1}H NMR ($CDCl_3$) δ 3.48 (3H, s), 5.81 (2H, d, J = 8 Hz), 6.48 (2H, d, J = 8Hz), 7.25 (12H, m), 7.32 (6H, m), 7.55 (12H, m); ^{31}P NMR ($CDCl_3$) 23.70 (s, J(P-Pt) = 3071Hz). ASAP-MS(+): calculated for ($C_{43}H_{37}OP_2Pt$) 826.20 m/z, found 826.2 m/z.

2.4.5. Preparation of $PtI(C_6H_4COOCH_3\text{-}4)(PPh_3)_2$ (1-$COOCH_3$)

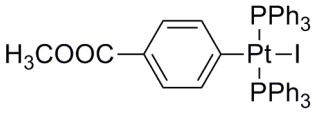

An oven dried Schlenk flask was charged with dry toluene (20 mL) was added and the solvent degassed. To this solution, $Pt(PPh_3)_4$ (0.50 g, 0.402 mmol) and methyl 4-iodobenzoate (0.316 g, 1.20 mmol) were added and the mixture stirred under reflux for 16 hours. After cooling to ambient temperature the solid was filtered and washed with hexane (2 x 10 mL). Yield 331 mg, 84 %.^{1}H NMR ($CDCl_3$) δ 3.75 (3H, s), 6.56 (2H, d, J = 8 Hz), 7.18 (2H, d, J = 8Hz), 7.24 (12H, m), 7.32 (6H, m), 7.55 (12H, m);

^{31}P NMR (CD_3Cl) 19.92 (s, J(P-Pt) = 3021Hz). ASAP-MS(+): calculated for ($C_{44}H_{37}O_2P_2Pt$) 855.20 m/z, found 855.2 m/z.

2.4.6. Preparation of Pt(C≡C$C_6H_4CH_3$-4)($C_6H_4CH_3$-4)(PPh_3)$_2$ (2-CH_3)

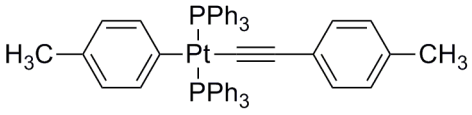

An oven dried Schlenk flask was charged with dry CH_2Cl_2 (6 mL) and $^{i}Pr_2NH$ (4 mL) and the solution degassed. To this solution, **1- CH_3** (150 mg, 0.160 mmol) CuI (12 mg) and 4-ethynyl toluene (21 µL, 0.160 mmol) were added and the solution stirred for 90 minutes. The solvent was removed under reduced pressure and the residue purified by preparative TLC (silica; hexane:CH_2Cl_2). Yield 87 mg, 58 %. ^{1}H NMR ($CDCl_3$) δ 1.95 (3H, s), 2.12 (3H, s), 6.06-6.15 (4H, m), 6.43 (2H, d, J = 8 Hz), 6.66 (2H, d, J = 8Hz), 7.21 (12H, m), 7.30 (6H, m), 7.54 (12H, m); ^{31}P NMR ($CDCl_3$) 20.31 (s, J(P-Pt) = 3000Hz) ASAP-MS(+): calculated for ($C_{43}H_{37}P_2Pt$) 925.2 m/z, found 925.2 m/z.

2.4.7. Preparation of Pt(C≡C$C_6CH_4OCH_3$-4)($C_6H_4CH_3$-4)(PPh_3)$_2$ (2-OCH_3)

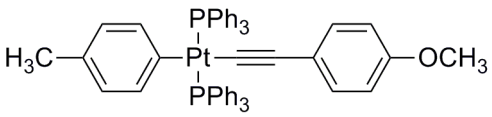

An oven dried Schlenk flask was charged with dry CH_2Cl_2 (6 mL) and $^{i}Pr_2NH$ (4 mL) and the solution degassed. To this solution, **1- CH_3** (100 mg, 0.106 mmol) CuI (4 mg) and 4-ethynyl anisole (14 µL, 0.106 mmol) were added and the solution stirred for 3 h. The solvent was removed under reduced pressure and the residue purified by preparative TLC (silica; hexane:CH_2Cl_2). Yield 49 mg, 49 %. ^{1}H NMR ($CDCl_3$) δ

1.97 (3H, s), 3.65 (3H, s), 6.10-6.15 (4H, m), 6.40-6,46 (4H, m), 7.23 (12H, m), 7.31 (6H, m), 7.55 (12H, m); ^{31}P NMR ($CDCl_3$) 20.29 (s, J(P-Pt) = 3003Hz) MALDI-MS(+): calculated for [M-$C_2C_6H_4OCH_3$($C_{43}H_{37}P_2Pt$)] 810.20 m/z, found 810.2 m/z.

2.4.8. Preparation of Pt(C≡C$C_6CH_4NO_2$-4)($C_6H_4CH_3$-4)(PPh_3)$_2$ (2-NO_2)

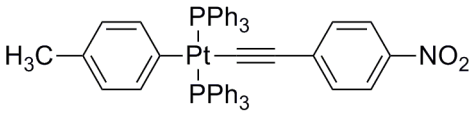

An oven dried Schlenk flask was charged with dry CH_2Cl_2 (6 mL) and $^{i}Pr_2NH$ (4 mL) and the solution degassed. To this solution, **1- CH_3** (050 mg, 0.053 mmol) CuI (4 mg) and 4-ethynylnitrobenzene (8 mg, 0.053 mmol) were added and the solution stirred for 43 hours. The solvent was removed under reduced pressure and the residue purified by preparative TLC (silica; hexane:CH_2Cl_2). Yield 28 mg, 55 %. ^{1}H NMR ($CDCl_3$) δ 1.97 (3H, s), 6.10-6.20 (4H, m), 6.42 (2H, d, J = 8 Hz), 7.24 (12H, m), 7.33 (6H, m), 7.50 (12H, m), 7.71 (2H, d, J = 8Hz); ^{31}P NMR ($CDCl_3$) 20.27 (s, J(P-Pt) = 2976Hz) ASAP-MS(+): calculated for ($C_{51}H_{41}NO_2P_2Pt$+ H) 957.3 m/z, found 957.3 m/z

2.4.9. Preparation of Pt(C≡CC_6H_4CN-4)($C_6H_4CH_3$-4)(PPh_3)$_2$ (2-CN)

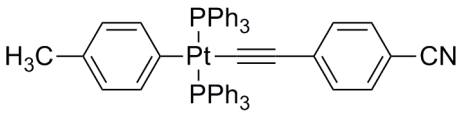

An oven dried Schlenk flask was charged with dry CH_2Cl_2 (6 mL) and $^{i}Pr_2NH$ (4 mL) and the solution degassed. To this solution, **1- CH_3** (050 mg, 0.053 mmol) CuI (4 mg) and 4-ethynylbenzonitrile(7 mg, 0.053 mmol) were added and the solution stirred for 43 hours. The solvent was removed under reduced pressure and the residue purified by preparative TLC (silica; hexane:CH_2Cl_2). Yield 29 mg, 58 %. Crystals suitable for

X-ray diffraction were grown from slow evaporation of a CH_2Cl_2:$CDCl_3$ solution. ^1H NMR ($CDCl_3$) δ 1.96 (3H, s), 6.10-6.18 (4H,m), 6.41 (2H, d, J = 8Hz), 7.10 (2H, d, J = 8Hz), 7.23 (12H, m), 7.32 (6H, m), 7.50 (12H, m) ASAP-MS(+): calculated for ($C_{52}H_{41}NP_2Pt$+H) 937.3 m/z, found 937.3 m/z

2.4.10. Preparation of Pt(C≡C$C_6CH_4CH_3$-4)$_2$(PPh_3)$_2$ (3-CH_3)

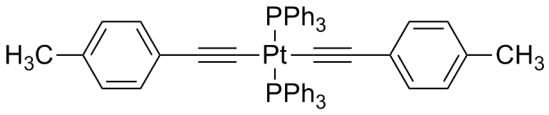

Method A: An oven dried Schlenk flask was charged with dry CH_2Cl_2 (6 mL) and $^iPr_2NH$ (4 mL) and the solution degassed. To this solution, **1-CH_3** (050 mg, 0.053 mmol) CuI (4 mg) and 4-ethynyltoluene (7 µL, 0.053 mmol) were added and the solution stirred for 16 hour. Further 4-ethynyltoluene (7 µL, 0.053 mmol) was added and the mixture stirred for a further 24 hours. The solvent was removed under reduced pressure and the residue dissolved in CH_2Cl_2 (3 mL) and treated with methanol (10 mL) and the solvent carefully removed *in vacuo* to yield a bright yellow precipitate in the methanol that was filtered and washed with methanol (2 x 5 mL). Yield 42 mg, 84 %. ^1H NMR ($CDCl_3$) δ 2.16 (6H, s), 6.17 (4H, d, J = 8 Hz), 6.71 (4H, d, J = 8Hz), 7.30-7.45 (18H, m), 7.81 (12H, m); ^{31}P NMR ($CDCl_3$) 17.70 (s, J(P-Pt) = 2654Hz) ASAP-MS(+): calculated for ($C_{43}H_{37}P_2Pt$) 950.2 m/z, found 950.2 m/z.

Literature: ^1H NMR ($CDCl_3$): δ 2.17 (6H, s), 6.19 (4H, d, J =8.0 Hz), 6.72 (4H, d, J = 8.0 Hz), 7.41–7.33 (18H, m), 7.84–7.74 (12H, m).

Method B: An oven dried Schlenk flask was charged with dry CH_2Cl_2 (6 mL) and $^iPr_2NH$ (4 mL) and the solution degassed. To this solution, **2- CH_3** (040 mg, 0.043

mmol) CuI (4 mg) and 4-ethynyltoluene (5.5 µL, 0.043 mmol) were added and the solution stirred for 18 hours. The solvent was removed under reduced pressure and the residue dissolved in CH_2Cl_2 (3 mL) and treated with methanol (10 mL) and the solvent carefully removed *in vacuo* to yield a bright yellow precipitate in the methanol that was filtered and washed with methanol (2 x 5 mL) and hexane (2 x 5mL). Yield 36 mg, 88 %. ^{1}H NMR ($CDCl_3$) δ 2.16 (6H, s), 6.17 (4H, d, J = 8 Hz), 6.71 (4H, d, J = 8Hz), 7.30-7.45 (18H, m), 7.81 (12H, m); ^{31}P NMR ($CDCl_3$) 17.70 (s, J(P-Pt) = 2654Hz) ASAP-MS(+): calculated for ($C_{43}H_{37}P_2Pt$) 950.2 m/z, found 950.2 m/z

2.4.11. Preparation of Pt(C≡C$C_6H_4OCH_3$-4)$_2$(PPh_3)$_2$ (3-OCH_3)

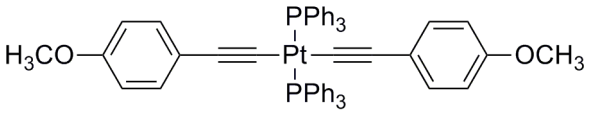

An oven dried Schlenk flask was charged with dry CH_2Cl_2 (6 mL) and $^iPr_2NH$ (4 mL) and the solution degassed. To this solution, **1- CH_3** (050 mg, 0.053 mmol) CuI (4 mg) and 4-ethynylanisole (7 µL, 0.053 mmol) were added and the solution stirred for 16 hours. Further 4-ethynylanisole (7 µL, 0.053 mmol) was added and the mixture stirred for a further 24 hours. The solvent was removed under reduced pressure and the residue dissolved in CH_2Cl_2 (3 mL) and treated with methanol (10 mL) and the solvent carefully removed *in vacuo* to yield a bright yellow precipitate in the methanol that was filtered and washed with methanol (2 x 5 mL). Yield 49 mg, 94 %. ^{1}H NMR ($CDCl_3$) δ 3.70 (6H, s), 6.23 (4H, d, J = 8 Hz), 6.48 (4H, d, J = 8Hz), 7.30-7.45 (18H, m), 7.84 (12H, m); ^{31}P NMR ($CDCl_3$) 17.66 ($J_{P\text{-}Pt}$ = 2665 Hz)

Literature: ^{1}H NMR ($CDCl_3$): δ 3.65 (6H, s), 6.16- 6.45 (8H, dd), 7.30-7.80 (30H, m).

2.4.12. Preparation of $PtF(C_6H_4CH_3\text{-}4)(PPh_3)_2$ (4)

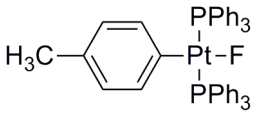

An oven dried Schlenk flask was charged with dry CH_2Cl_2 (15 mL) and **1- CH_3** (150 mg, 0.16 mmol) and the solution degassed. To this solution, AgF (81 mg, 0.640 mmol) was added and the mixture sonicated in an ice cooled sonicator for 3 hours with exclusion of light. The mixture was filtered through celite to remove the residual silver and washed with CH_2Cl_2 (2 x 10 mL). Yield 84 mg, 62 %. ^{1}H NMR ($CDCl_3$) δ 1.91 (3H, s), 5.94 (2H, d, J = 8Hz), 6.40 (2H, d, J = 8Hz), 7.24 (12H, m), 7.34 (6H, m), 7.55 (12H, m); ^{31}P NMR ($CDCl_3$) 21.84 (d, J(P-F) = 20Hz, J(P-Pt) = 3280Hz) ASAP-MS(+): calculated for ($C_{43}H_{37}P_2Pt$) 810.20 m/z, found 810.2 m/z

2.4.13. Preparation of $PtCl(C_6H_4CH_3\text{-}4)(PPh_3)_2$ (5)

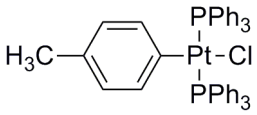

An oven dried Schlenk flask was charged with dry toluene (25 mL) and the solution degassed. To this solution, **1- CH_3** (500 mg, 0.53 mmol) and AgOTf (0.137 g, 0.533 mmol) were added and the solution stirred for 2 hours until complete by ^{31}P NMR. The solution was cannula filtered in to a dry degassed flask containing NBu_4Cl (0.178 g, 0.640 mmol) and stirred for 1 hour. The solution was filtered and the white precipitate washed with MeOH (3 x 15 mL) and dried under airflow. Yield 314 mg, 70 %. Crystals suitable for X-ray diffraction were grown from CH_2Cl_2:EtOH. ^{1}H NMR ($CDCl_3$) δ 1.91 (3H, s), 5.96 (2H, d, J = 8 Hz), 6.48 (2H, d, J = 8Hz), 7.23 (12H, m), 7.33 (6H, m), 7.52 (12H, m); ^{31}P NMR ($CDCl_3$) 23.17 (s, J(P-Pt) = 3164Hz). ASAP-MS(+): calculated for ($C_{43}H_{37}P_2Pt$) 810.20 m/z, found 810.2 m/z

2.4.14. Preparation of Pt(C≡CC$_6$CH$_4$CH$_3$-4) (C≡CC$_6$CH$_4$OCH$_3$-4) (PPh$_3$)$_2$ (6)

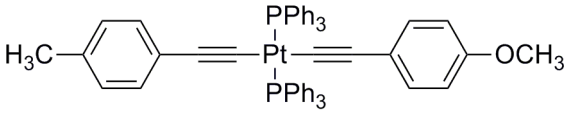

An oven dried Schlenk flask was charged with dry CH_2Cl_2 (6 mL) and $^iPr_2NH$ (4 mL) and the solution degassed. To this solution, **2- CH_3** (250 mg, 0.270 mmol), CuI (12 mg) and 4-ethynylanisole (35. µL, 0.270 mmol) were added and the solution stirred for 20 hours. The solvent was removed under reduced pressure and the residue dissolved in CH_2Cl_2 (3 mL) and treated with methanol (10 mL) and the solvent carefully removed *in vacuo* to yield a bright yellow precipitate in the methanol that was filtered and washed with methanol (2 x 5 mL) and hexane (2 x 5mL). Analysis of the sample by mass spectrometry shows that the reaction yields a statistical mixture of the 2 homo-bis-ethynyls and the hetero-bis-ethynyl products.

2.4.15. Preparation of N(C$_6$H$_5$)(C$_6$H$_4$OCH$_3$-4)$_2$ (7)

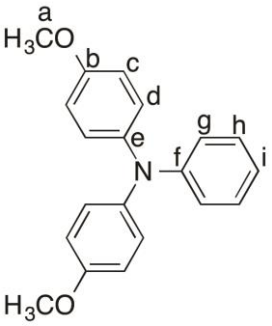

An oven dried Schlenk flask was charged with o-xylene (30 mL) and the solvent degassed. To this solution, 4-iodoanisole (15.00 g, 64.1 mmol), CuCl (0.201 g, 2.03 mmol), 1,10-phenanthroline (0.274 g, 1.5 mmol) and aniline (2.78 mL, 30.5 mmol) were added, the mixture was heated at reflux for 35 minutes, KOH (13.70 g, 244

mmol) was added and the mixture heated at reflux for 28 hours, cooled, poured in to H_2O (150 mL) and extracted with CH_2Cl_2 (3 x 60 mL). The organic layers were combined and dried over $MgSO_4$, filtered and the solvent removed in vacuo. The residue was suspended in hexane and purified by silica column chromatography eluting with hexane increasing to hexane:CH_2Cl_2 (50:50), removal of the solvent and crystallisation from hot hexane gives the title compound as a white solid. Yield 3.29 g, 32 %. ^{1}H NMR ($CDCl_3$) δ 7.16 (d, *J* = 7 Hz, 2H), 7.05 (d, *J* = 9 Hz, 4H), 6.94 (d, *J* = 7 Hz, 2H), 6.90 - 6.85 (m, 1H), 6.82 (d, *J* = 9 Hz, 4H), 3.80 (s, 6H). Literature: ^{1}H NMR ($CDCl_3$): δ = 7.25−6.79 (m, 13H, Ar), 3.79 ppm (s, 6H, OCH3). ESI-MS: 305.6 $[M]^+$

2.4.16. Preparation of $N(C_6H_4I\text{-}4)(C_6H_4OCH_3\text{-}4)_2$ (8)

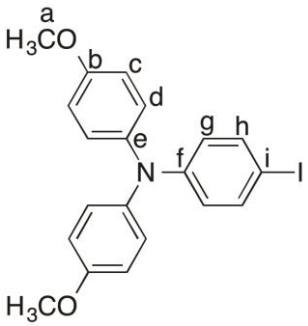

An oven dried Schlenk flask was charged with chloroform (90 mL) and the solvent degassed. To this solution, **7** (3.00 g, 9.8 mmol) and NIS (2.430 g, 10.8 mmol) were added with the exclusion of light followed by acetic acid (60 mL) and the mixture stirred at room temperature for 30 hours and quenched with aqueous sodium thiosulphate (300 mg in 30 mL H_2O) and extracted with CH_2Cl_2 (3 x 30 mL). The organic layers were combined and dried over $MgSO_4$, filtered and the solvent removed in vacuo to give an off-white solid. Yield 3.14 g, 75 %). ^{1}H NMR (400

MHz, $CDCl_3$) δ 7.40 (d, *J* = 8 Hz, 2H), 7.02 (d, *J* = 8 Hz, 4H), 6.82 (d, *J* = 8 Hz, 4H), 6.67 (d, *J* = Hz, 2H), 3.79 (s, 6H).Literature: ^{1}H NMR (250 MHz, $CDCl_3$): δ 7.40/6.67 (m, AA`, 2 H/m, BB`, 2H; I-C_6H_4), 7.03/6.82 (m, AA`±BB', 8H; MeO-C_6H_4), 3.79 (s, 6H; MeO) ESI-MS: 431.5 $[M]^+$

2.4.17. Preparation of *trans*-PtI{$C_6H_4N(C_6H_4OCH_3$-4)$_2$}(PPh_3)$_2$ (9)

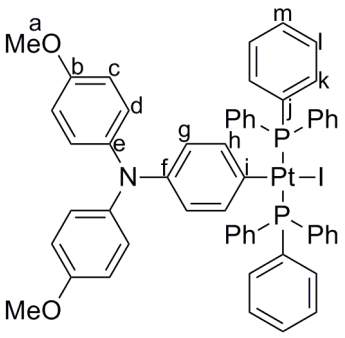

An oven dried Schlenk flask was charged with dry toluene (20 mL) and the solvent degassed. To this solution, $Pt(PPh_3)_4$ (1.00 g, 0.804 mmol) and 4-iodophenylene-*p*-dianisylamine (0.693 g, 1.60 mmol) were added and the mixture stirred for 16 hours at reflux. The mixture was cooled to ambient temperature and added to vigorously stirred hexane (150 mL) and the off-white precipitate was filtered and washed with hexane (2 x 10 mL). Yield 880 mg, 95 %. ^{1}H NMR (CD_2Cl_2) δ 3.76 (s, 6H, H*a*), 5.98 (d, J = 8Hz, 2H, H*h*), 6.71 (m, 10H, H*c*,*d* and *g*) 7.34 (vt, J = 8Hz, 12H, H*k*), 7.41 (t, J = 8Hz, 6H, H*m*), 7.62 (m, 12H, H*l*). ^{31}P NMR (CD_2Cl_2): 20.67 ($J_{Pt\text{-}P}$ = 3074Hz). ^{13}C NMR (CD_2Cl_2): 154.72 (C*b*, s), 142.22 (C*e*, s), 141.78 (C*f*, s), 136.17 (C*g*, s), 135.08 (C*l*, t, $J_{C\text{-}P}$ = 5Hz), 131.80 (C*j*, t, $J_{C\text{-}P}$ = 28Hz), 129.88 (C*m*, s), 127.58 (C*k*, t, $J_{C\text{-}P}$ = 5Hz), 125.19 (C*c*, s), 122.99 (C*h*, s), 113.99 (C*d*, s), 55.39 (C*a*, s). ASAP-MS(+) *m*/*z*:

1151.1 $[M+H]^+$. Analysis found (calculated) %: C 58.60 (58.44), H 4.04 (4.20), N 1.29 (1.22).

2.4.18. Preparation of *trans*-Pt(C≡CAr)($C_6H_4NAr_2$)(PPh_3)$_2$ (10a)

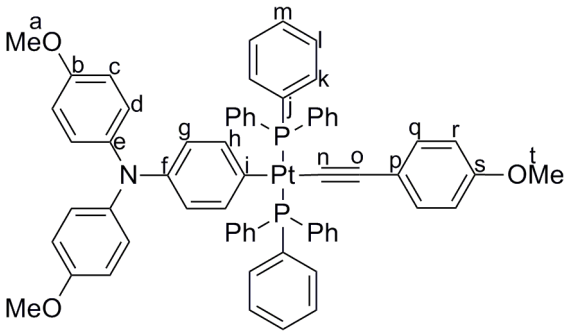

An oven dried Schlenk flask was charged with dry $HNEt_2$ (10 mL) and the solvent degassed. To this solution, 4-ethynylanisole (0.017 g, 0.13 mmol), **3** (150 mg, 0.13 mmol) and CuI (4 mg) were added and the solution stirred at room temperature for 17 hours. The precipitate was filtered, washed with ethanol (3 x 5 mL) and methanol (3 x 5 mL) and dried under airflow for 1 h. Yield 131 mg, 87 %. ^{1}H NMR (CD_2Cl_2): δ 3.64 (s, 3H, H*t*), 3.76 (s, 6H, H*a*), 6.11 (d, J = 8Hz, 2H, H*h*), 6.15 (d, J = 9Hz, 6H, H*r*), 6.43 (d, J = 9Hz, 2H, H*q*), 6.71 (d, J = 8Hz, 2H, H*g*), 6.73 (m, 8H, H*c and d*) 7.32 (vt, J = 8Hz, 12H, H*k*), 7.40 (t, J = 8Hz, 6H, H*m*), 7.64 (m, 12H, H*l*). ^{31}P NMR (CD_2Cl_2): 20.84 ($J_{Pt\text{-}P}$ = 2985Hz). ^{13}C NMR (CD_2Cl_2): 156.77 (C*s*, s), 154.29 (C*b*, s), 142.31 (C*e*, s), 141.55 (C*f*, s), 139.55 (C*g*, s), 134.84 (C*l*, t, $J_{C\text{-}P}$ = 5Hz), 131.79 (C*j*, t, $J_{C\text{-}P}$ = 28 Hz), 131.35 (C*q*, s),129.75 (C*m*, s), 127.58 (C*k*, t, $J_{C\text{-}P}$ = 5Hz), 124.10 (C*c*, s), 123.94 (C*h*, s), 121.74 (C*p*, s), 113.92 (C*d*, s), 112.71 (C*r*,s), 55.40 (C*a*, s), 54.96 (C*t*, s). MALDI-MS(+) *m*/*z*: 1155.3 $[M+H]^+$. IR (CH_2Cl_2) ν(C≡C) 2107 cm^{-1}. Analysis found (calculated) %: C 67.45 (67.58), H 4.74 (4.80), N 1.17 (1.21).

2.4.19. Preparation of *trans*-Pt(C≡C$C_6H_4NAr_2$)($C_6H_4NAr_2$)(PPh_3)$_2$ (10b)

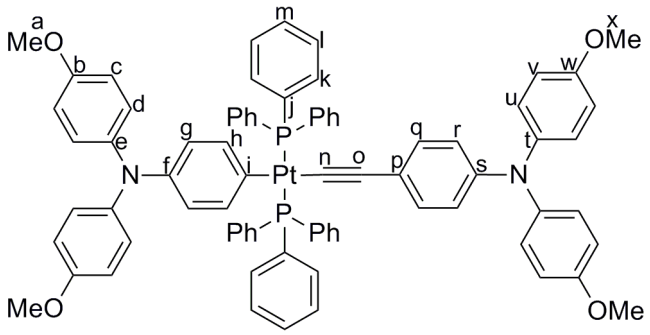

An oven dried Schlenk flask was charged with 4-ethynylenephenylenedi-*p*-anisylamine (0.043 g, 0.13 mmol) in dry CH_2Cl_2 and the solvent removed *in vacuo*. Dry $HNEt_2$ (10 mL) was added and the solvent degassed. To this solution, *trans*-PtI($C_6H_4N(C_6H_4OCH_3$-4)$_2$)(PPh_3)$_2$ (150 mg, 0.130 mmol) and CuI (4 mg) were added and the solution stirred at room temperature for 2 hours. The precipitate was filtered, washed with ethanol (3 x 5 mL), hexane (3 x 5 mL) and methanol (3 x 5 mL) and dried under airflow for 1 h. Yield 109 mg, 63 %. ^{1}H NMR (CD_2Cl_2): δ 3.76 (s, 12H, Ha and *x*), 6.03 (d, J = 8Hz, 2H, H*q*), 6.11 (d, J = 8Hz, 2H, H*h*), 6.44 (d, J = 8Hz, 2H, H*r*), 6.68 (d, J = 8Hz, 2H, H*g*), 6.73 (m, 8H, H*c and d*), 6.76 (d, J = 8Hz, 4H, H*v*), 6.89 (d, J = 8Hz, 4H, H*u*), 7.32 (vt, J = 8Hz, 12H, H*k*), 7.39 (t, J = 8Hz, 6H, H*m*), 7.64 (m, 12H, H*l*). ^{31}P NMR (CD_2Cl_2): 20.95 ($J_{Pt\text{-}P}$ = 2981Hz). ^{13}C NMR (CD_2Cl_2): 155.48 (C*w*, s), 154.29 (C*b*, s), 145.33 (C*t*, s), 142.31 (C*e*, s), 141.59 (C*f*, s), 141.12 (C*s*, s), 139.53 (C*g*, s), 134.84 (C*l*, t, $J_{C\text{-}P}$ = 5Hz), 131.781 (C*j*, t, $J_{C\text{-}P}$ = 28 Hz), 130.97 (C*q*, s), 129.76 (C*m*, s), 127.59 (C*k*, t, $J_{C\text{-}P}$ = 5Hz), 125.86 (C*u*, s), 124.11 (C*c*, s), 123.93 (C*h*, s), 120.45 (C*r*, s), 114.37 (C*v*, s), 113.92 (C*d*, s), 55.40 (C*a*, s), 55.36 (C*x*, s). MALDI-MS(+) *m*/*z*: 1352.3 $[M+H]^+$. IR (CH_2Cl_2) ν(C≡C) 2105 cm^{-1}. Analysis found (calculated) %: C 69.05 (69.27), H 4.84 (4.92), N 2.11 (2.07).

2.4.20. preparation of {*trans*-Pt($C_6H_4NAr_2$)(PPh_3)$_2$}$_2$(μ-C≡C-1,4-C_6H_4C≡C) (11)

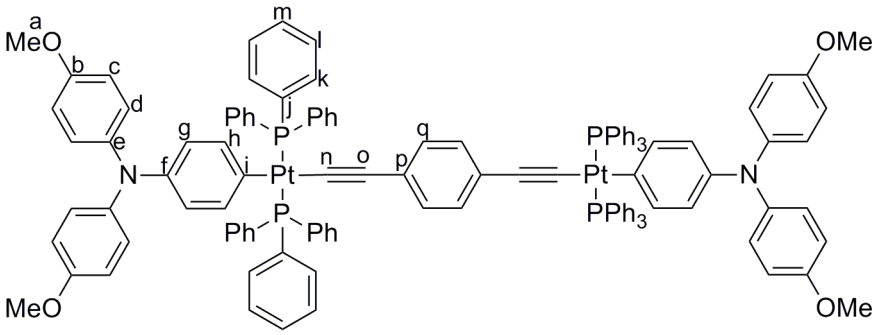

An oven dried Schlenk flask was charged with dry $HNEt_2$ (10 mL) and the solvent degassed. To this solution, **9** (100 mg, 0.087 mmol), CuI (3 mg) and 1,4-diethynylbenzene (5 mg, 0.043 mmol) were added and the solution stirred at room temperature for 16 hours. The precipitate was filtered, washed with ethanol (3 x 5 mL), hexane (3 x 5 mL) and methanol (3 x 5 mL) and dried under airflow for 1 h. Yield 50 mg, 54 %. ^{1}H NMR (CD_2Cl_2): δ 3.74 (s, 12H, H*a*), 5.72 (s, 4H, H*q*), 6.08 (d, J = 8Hz, 4H, H*h*), 6.67 (d, J = 8Hz, 4H, H*g*), 6.71 (m, 16H, H*c and d*) 7.28 (vt, J = 8Hz, 24H, H*k*), 7.37 (t, J = 8Hz, 12H, H*m*), 7.59 (m, 24H, H*l*). ^{31}P NMR (CD_2Cl_2): 20.73 ($J_{Pt\text{-}P}$ = 2971Hz). ^{13}C NMR (CD_2Cl_2): 154.27 (C*b*, s), 142.29 (C*e*, s), 141.42 (C*f*, s), 139.50 (C*g*, s), 134.78 (C*l*, t, $J_{C\text{-}P}$ = 5Hz), 131.70 (C*j*, t, $J_{C\text{-}P}$ = 28 Hz), 129.71 (C*q*, s), 129.23 (C*m*, s), 127.55 (C*k*, t, $J_{C\text{-}P}$ = 5Hz), 124.08 (C*c*, s), 123.90 (C*h*, s), 113.90 (C*d*, s), 55.39 (C*a*, s). MALDI-MS(+) *m*/*z*: 2170.6 $[M]^+$. IR (CH_2Cl_2) ν(C≡C) 2103 cm^{-1}.

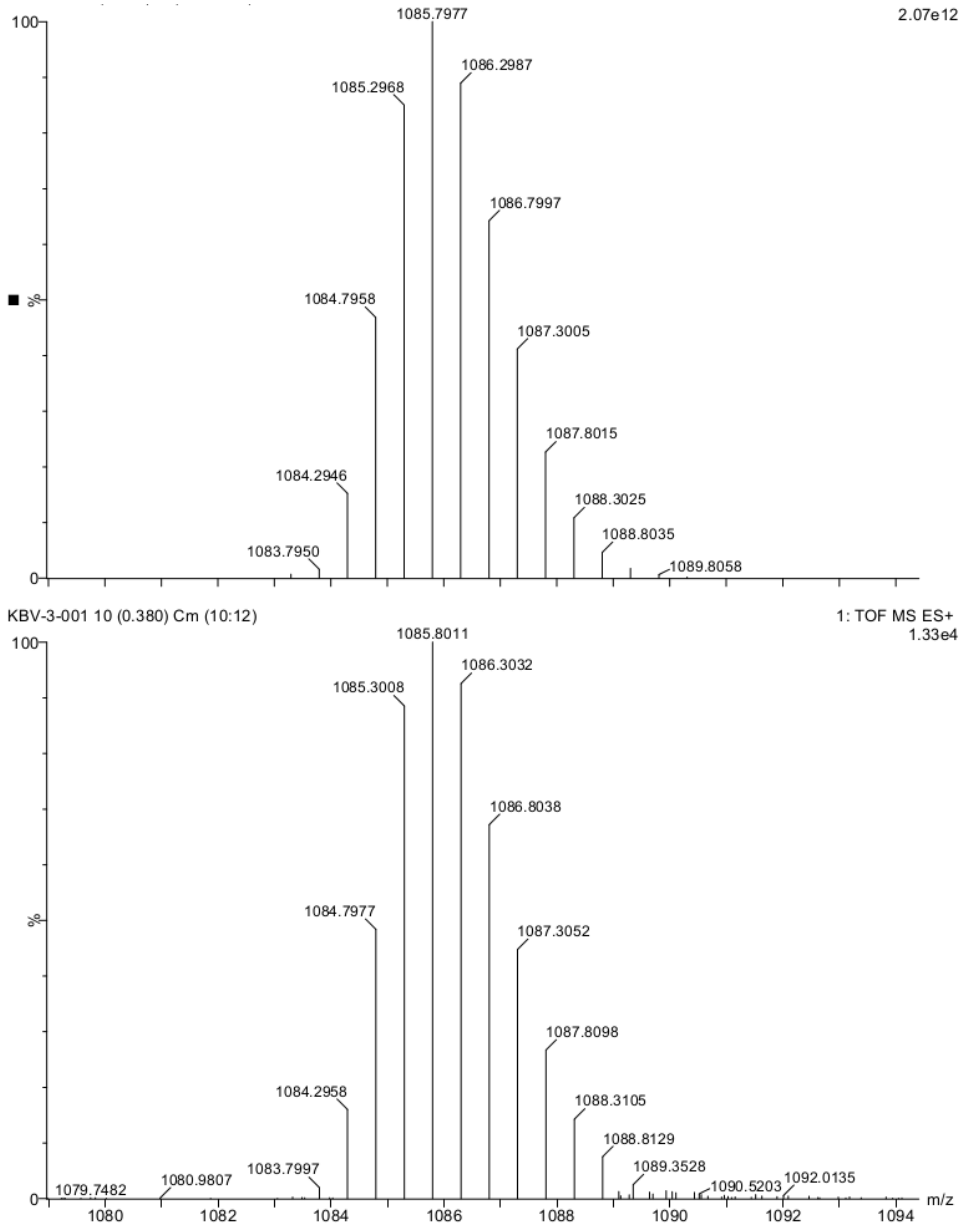

Figure 47: ESI-HRMS of 5 showing the predicted (top) and observed (bottom) spectra for $[M]^{2+}$

2.4.21. Preparation of $N\{C_6H_4C{\equiv}CPt(C_6H_4NAr_2)(PPh_3)_2\}_3$ (12)

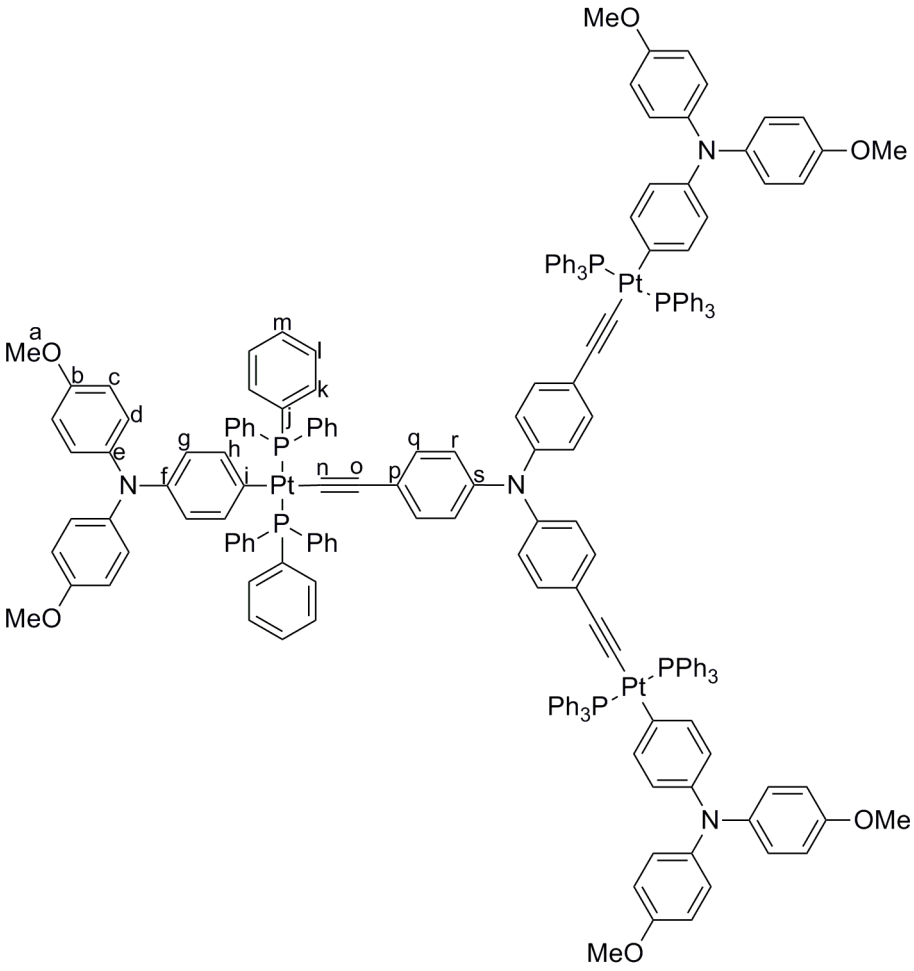

An oven dried Schlenk flask was charged with dry $HNEt_2$ (10 mL) and the solvent degassed. To this solution, **9** (150 mg, 0.130 mmol), CuI (3 mg) and triethynylphenylamine (13 mg, 0.043 mmol) were added and the solution stirred at room temperature for 16 hours. The precipitate was filtered, washed with ethanol (3 x 5 mL), hexane (3 x 5 mL) and methanol (3 x 5 mL) and dried under airflow for 1 h. Yield 98 mg, 67 %. ^{1}H NMR (CD_2Cl_2): δ 3.76 (s, 18H, H*a*), 5.93 (d, J = 9Hz, 6H, H*r*), 6.11 (d, J = 8Hz, 6H, H*h*), 6.31 (d, J = 9Hz, 6H, H*q*), 6.69 (d, J = 8Hz, 6H, H*g*), 6.73 (m, 24H, H*c and d*) 7.32 (vt, J = 8Hz, 36H, H*k*), 7.39 (t, J = 8Hz, 18H, H*m*), 7.62 (m, 36H, H*l*). ^{31}P NMR (CD_2Cl_2): 20.93 ($J_{Pt\text{-}P}$ = 2998Hz). ^{13}C NMR (CD_2Cl_2): 154.29 (C*b*, s), 142.30 (C*e*, s), 143.90 (C*s*, s), 141.66 (C*f*, s), 139.55 (C*g*, s), 134.83 (C*l*, t, $J_{C\text{-}P}$ = 5Hz), 131.76 (C*j*, t, $J_{C\text{-}P}$ = 28 Hz), 130.96 (C*r*, s), 129.78 (C*m*, s), 127.60

(C*k*, t, J_{C-P} = 5Hz), 124.11 (C*c*, s), 123.93 (C*h*, s), 122.73 (C*q*, s), 113.92 (C*d*, s), 55.40 (C*a*, s). MALDI-MS(+) *m*/*z*: 3385.6 $[M+H]^+$. IR (CH_2Cl_2) ν(C≡C) 2105 cm^{-1}. Analysis found (calculated) %: C 67.87 (68.10), H 4.48 (4.64), N 1.69 (1.65).

2.4.22. Preparation of *trans*-Pt{C≡C$C_6H_4N(C_6H_4CH_3$-4)$_2$}($C_6H_4CH_3$-4)(PPh_3)$_2$ (13)

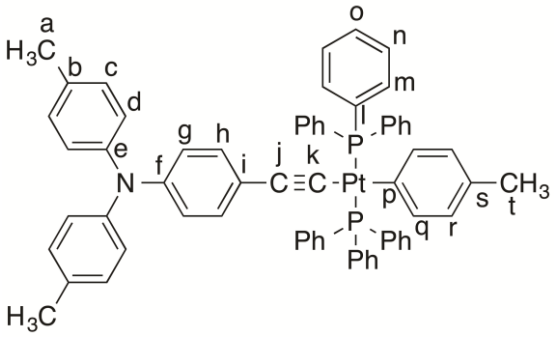

An oven dried Schlenk flask was charged with CH_2Cl_2 (6 mL) and HN^iPr_2 (4 mL) and the solvent degassed. To this solution, **1- CH_3** (100 mg, 0.106 mmol), 4-ethynylenephenylenedi-*p*-tolylamine (7 mg, 0.053 mmol) and CuI (4 mg) were added and the solution stirred for 3 hours at room temperature. The solvent was removed in vacuo and the residue dissolved in CH_2Cl_2 and purified by preparative TLC (silica; hexane:CH_2Cl_2). Yield 42 mg, 36 %. ^{1}H NMR ($CDCl_3$) δ 1.96 (3H, s), 2.26 (6H, s), 6.00 (2H, d, J = 9Hz), 6.11 (2H, d, J = 8Hz), 6.41 (2H, d, J = 8Hz), 6.53 (2H, d, J = 9Hz), 6.84 (4H, d, J = 8Hz), 6.97 (4H, d, J = 9Hz), 7.21 (12H, m), 7.34 (6H, m), 7.53 (12H, m); ^{31}P NMR ($CDCl_3$) 20.25 (s, J(P-Pt) = 3003Hz). ^{13}C NMR ($CDCl_3$) δ 145.67 (C_e, s), 144.49 (C_f, s), 139.24 (C_q, s), 134.97 (C_n, t, *J* = 6 Hz), 131.74 (C_l, t, *J* = 28 Hz), 131.72 (C_h, s), 129.72 (C_c, s), 129.66 (C_o, s), 128.10 (C_s, s), 127.88 (C_r, s), 127.61 (C_m, t, *J* = 5 Hz), 124.08 (C_d, s), 122.69 (C_g, s), 20.88 (C_a, s), 20.62 (C_t, s) other quaternary ^{13}C were not observed in the spectra.; ASAP-MS(+) *m*/*z*: 850.3 [M-

$NC_{20}H_{18}+H]^{+}$.; IR (CH_2Cl_2) ν(C≡C) 2103 cm^{-1}.; ASAP-HRMS(+) *m/z*: 1105.3469 (calculated for $C_{65}H_{55}NP_2{}^{194}Pt$: 1105.3437)

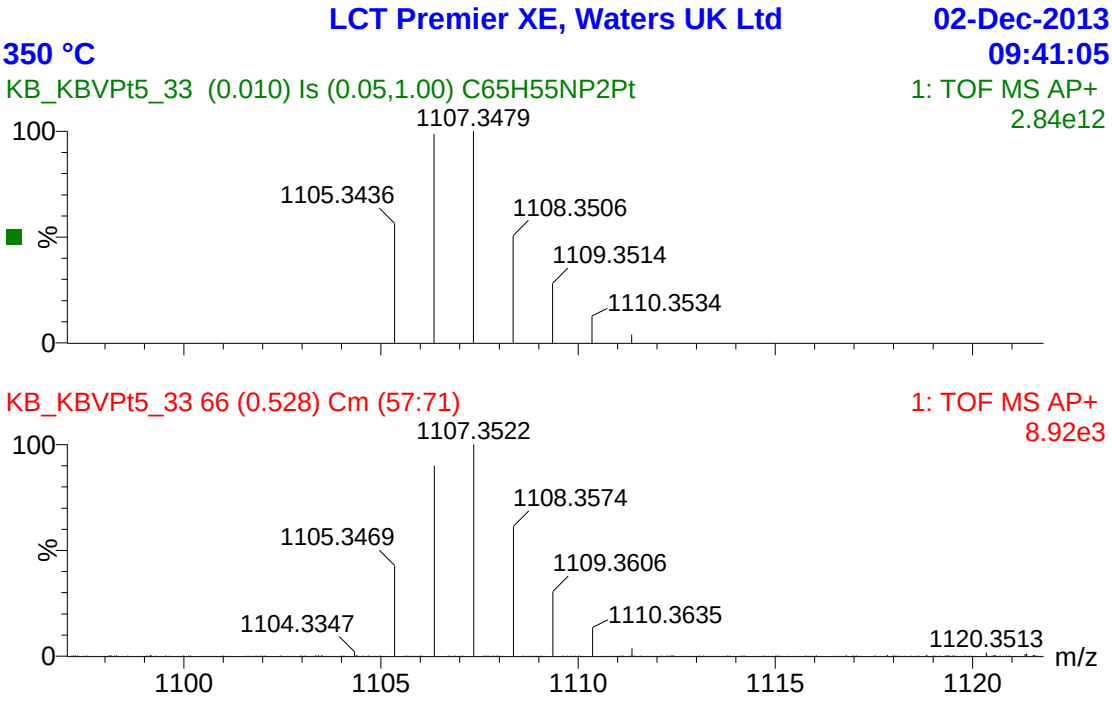

Figure 48: ASAP-HRMS plot for 5 showing the predicted (top) and observed (bottom) spectra

2.4.23. Preparation of Sodium tetrakis[(3,5-trifluoromethyl)phenyl]borate ($NaBArF_4$)[64b]

An oven dried flask was charged with dry THF (120 mL) and the solvent vigorously degassed. To this solution, bromo-3,5-bis(trifluromethyl)benzene (25 mL, 145 mmol) was added and the solution degassed again and cooled to -26 °C. To this solution, 2.0M ^{i}PrMgCl in THF (80 mL, 160 mmol) was added drop wise over 50 minutes. The cold bath was removed and the flask allowed to warm to room temperature followed by addition of anhydrous sodium tetrafluoroborate (2.680 g, 24 mmol) in one quick addition. The solution was stirred for 48 hours and poured in to solution of sodium hydrogencarbonate (20 g) and sodium carbonate (44 g) in water (600 mL) and

extracted in to ether (3 x 250 mL). The organic phases were combined, washed with brine (200 mL), dried over sodium carbonate and filtered. Removal of the solvent in vacuo gives a thick yellow residue containing white crystalline material that was treated with hot CH_2Cl_2 until a single homogenous phase was present and the solution slowly cooled to -28 °C. The white solid was filtered and washed with cold CH_2Cl_2 to give a white solid. Yield 19.7 g.

2.4.24. Preparation of tetrabutylammonium tetrakis[(3,5-trifluoromethyl)phenyl]borate (NBu_4BArF_4)[64a]

A round bottom flask was charged with methanol (50 mL) and $NaBArF_4$ (12.90 g, 12.09 mmol) and stirred till dissolved. To this solution, NBu_4Br (3.90 g, 12.90 mmol) was added and the solution stirred for 15 minutes followed by addition of H_2O (100 mL). The precipitate was filtered, dissolved in the minimum volume of hot methanol, treated with H_2O (0.2 mL) and cooled to -28 °C for 7 days. The white crystals were filtered and the crystallisation repeated two further times and the crystals dried under high vac at 70 °C for 72 hours. Yield 9.64 g (72 %). ^1H NMR ($CDCl_3$): δ 0.98 (m, 12H), 1.37 (m, 8), 1.52 (m, 8H), 3.01 (m, 8H), 7.55 (s, 4H), 7.70 (s, 8H).

Literature: δ 0.94 (t, *J*=7.4 Hz, 12H), 1.34 (m, 8), 1.52 (m, 8H), 2.99 (t, J=8.5 Hz, 8H), 7.53 (s, 4H), 7.69 (s, 8H).

2.4.25. Computational Details

Full structure optimizations and analysis of all ground and excited state[65-67] properties were performed using a locally modified version of the TURBOMOLE 6.4 program code[68] enabling the use of the BLYP35 hybrid functional[69] based on

$$E_{XC} = 0.65(E_X^{LSDA} + \Delta E_X^{B88}) + 0.35 E_X^{exact} + E_C^{LYP}$$

which has been shown to give accurate results for organic[70-73] and inorganic[74-77] MV systems. Split-valence def2-SVP basis sets were employed on all lighter atoms, together with the corresponding def2-SVP effective-core potential and a corresponding valence basis set for platinum.[78-80] Computed harmonic vibrational frequencies were scaled by an empirical factor of 0.95.[81,82] To account for solvent effects, the conductor-like-screening (COSMO) solvent model was employed for ground state structure optimizations and analysis as well as in subsequent TDDFT calculations of excitation energies and transition dipole moments.[83] Dichloromethane ($\varepsilon = 8.93$) was used, as experimental data were collected in this solvent (non-equilibrium solvation was assumed in the TDDFT calculations). Spin-density and molecular-orbital isosurface plots were generated with the GaussView program.[84] For complex $[\mathbf{5}]^+$ a truncated model $[\mathbf{5\text{-}Me}]^+$, in which the PPh_3 ligands were replaced by PMe_3, was used to reduce computational cost.

2.5. References

1. Low, P. J. *Dalton Trans.* **2005**, 2821.
2. For example: (a) Bruce, M. I; Low, P. J; Hartl, F; Humphrey, P. A; de Montigny, F; Jevric, M; Lapinte, C; Perkins, G. J; Roberts, R. L; Skelton, B. W; White, A. H. *Organometallics*, **2005**, *24*, 5241. (b) Guillevic, M. A; Toupet, L; Paul, F; Lapinte, C. *Organometallics*, **1997**, *16*, 5988. (c) Díez, A; Lalinde, E; Moreno, M. T; Sánchez, S. *Dalton Trans*, **2009**, *18*, 3434. (d) Touchard, D; Haquette, P; Guesmi, S; Le Pichon, L; Daridor, A; Toupet, L; Dixneuf, P. H. *Organometallics*. **1997**, *16*, 3640. (e) Albertin, G; Autoniutti, S; Bordignon, E; Cazzaro, F. *Organometallics*. **1995**, *14*, 4114. (f) Choi, M. Y; Chan, M. C. W; Peng, S. M; Cheung. KK. *Chem Comm.* **2000**, 1250. (g) Khan, MS; Kakkar, AK; Ingham, SL;

Raithby, PR; Lewis, J; Spencer, B; Wittmann, F; Friend. R. H. *J. Organomet. Chem*. **1994**, *472*, 247. (h) McDonagh, A. M; Cifuentes, M. P; Whittall, I. R. *J. Organomet. Chem.* **1996**, *526*., 99.

3. Hankache, J; Wenger O. S. *Chem. Rev*, **2011**, *111*, 5138.
4. Lipnická, S; Bělohradský, M; Kolivoška, V; Pospíšil, L; Hromadová, M; Pohl, R; Chocholoušová, JV; Vacek, J; Fiedler, J; Stará, IG; Starý, I. *Chem. Eur, J.* **2013**, *19*, 6108.
5. Yang, J; Zhang, W; Si, Y; Zhao, Y. *J. Phys. Chem B*. **2012**, *116*, 14126.
6. Barlow, S; Risko, C; Odom, S. A; Zheng, S; Coropceanu, V; Beverina, L; Brédas, J. L; Marder, S. R. *J. Am. Chem. Soc*. **2012**, *134*, 10146.
7. Lambert, C; Schelter, J; Fiebig, T; Mank, D; Trifonov, A. *J. Am. Chem. Soc*. **2005**, *127*, 10600.
8. Sakamoto, R; Kume, S; Nishihara, H. *Chem. Eur, J*. **2008**, *14*, 6978.
9. Heckmann, A; Lambert, C. *Angew. Chem., Int. Ed*, **2012**, *51*, 326.
10. Liddle, B. J.; Wanniarachchi, S.; Hewage, J. S.; Lindeman, S. V.; Bennett, B.; Gardinier, J. R. *Inorg. Chem*. **2012**, *51*, 12720.
11. Jones, S. C.; Coropceanu, V.; Barlow, S.; Kinnibrugh, T.; Timofeeva, T.; Bredas, J. L.; Marder, S. R. *J. Am. Chem. Soc*. **2004**, *126*, 11782.
12. Vacher, A.; Barriere, F.; Camerel, F.; Bergamini, J. F.; Roisnel, T.; Lorcy, D. *Dalton Trans*. **2013**, *42*, 383.
13. Vacher, A.; Barriere, F.; Roisnel, T.; Piekara-Sady, L.; Lorcy, D. *Organometallics* **2011**, *30*, 3570.
14. Cai, X. M.; Zhang, X. Y.; Savchenko, J.; Cao, Z.; Ren, T.; Zuo, J. L. *Organometallics* **2012**, *31*, 8591.
15. Bushby, R. J.; Kilner, C.; Taylor, N.; Williams, R. A. *Polyhedron* **2008**, *27*, 383.
16. Kistner, C. R; Hutchinson, J. H; Doyle, J. R; Storlie, J. C. *Inorg. Chem*. **1963**. *2*. 1255.
17. Peters, T. B; Zheng, G; Stahl, J; Bohling, J. C; Arif, A. M; Hampel, F; Gladysz, J. A. *J. Organomet. Chem*. **2002**, *641*. 53.
18. Zheng, Q; Bohling, J. C; Peters, T. B; Frisch, A. C; Hampel, F; Gladysz, J. A. *Chem. Eur. J*. **2006**, *12*, 6486.
19. Rosevear, D. T; Stone, F. G. A. *J. Chem. Soc*. **1965**. 5275.
20. Baird, M. C. *J. Inorg. Nucl. Chem*. **1967**, *29*, 367.

21. Crociani, B; Nicolini, M; Clemente, D. A; Bandoli, G. *J. Organomet. Chem*. **1973**, *49*, 249.
22. Mukhedkar, A. J; Green, M; Stone, F. G. A. *J. Chem. Soc. A*, **1970**, 947.
23. Stahl, J; Bohling, J. C; Peters, T. B; de Quadras, L; Gladysz, J. A. *Pure Appl. Chem*. **2008**, *80*, 459.
24. (a) Norris, A. R; Baird, M. C. *Can. J. Chem*. **1969**, *47*, 3003. Sato, M; Mogi, E; Katada, M. *Organometallics*, **1995**, *14*, 4837. (b) Manna, J; Whiteford, J. A; Stang, P. J; Muddiman, D. C; Smith, R. D. *J. Am. Chem. Soc*. **1996**, *118*, 8731. (c) Manna, J; Kuehl, CJ; Whiteford, J. A; Stang, P. J. *Organometallics*, **1997**, *16*, 1897.
25. Sato, M; Mogi, E. *J. Organomet. Chem*. **1996**, *508*, 159.
26. (a) Nilsson, P; Puxty, G; Wendt, O. F. *Organometallics*, **2006**, *25*, 1285. (b) Kuniyasu, H; Yamashita, F; Hirai, T; Ye, J. H; Fujiwara, SI. ; Kambe, N. *Organometallics*, **2006**, *25*, 566. (c) Nilsson, P; Plamper, F; Wendt, O. F. *Organometallics*, **2003**, *22*, 5235. (d) Kondo, T; Tsuji, Y; Watanabe, Y. *J. Organomet. Chem.* **1988**,*345*, 397.
27. (a) Manna, J; Kuehl, C. J; Whiteford, J. A; Stang, P. J; Muddiman, D. C; Hofstadler, S. A; Smith, R. D. *J. Am. Chem. Soc*. **1997**, *119*, 11611. (b) Stang, P. J; Persky, N. E; Manna, J. *J. Am. Chem. Soc*. **1997**, *119*, 4777. (c) Gallasch, D. P; Tiekink, E. R. T; Rendina, L. M. *Organometallics*, **2001**, *20*, 3373.
28. (a) Owen, G. R; Stahl, J; Hampel, F; Gladysz, J. A. *Chem. Eur. J*. **2008**, *14*, 73. (b) de Quadras, L; Shelton, A. H; Kuhn, H; Hampel, F; Schanze, K. S; Gladysz, J. A. *Organometallics*, **2008**, *27*, 4979. (c) Owen, G. R; Stahl, J; Hampel, F; Gladysz, J. A. *Organometallics*, **2004**, *23*, 5889. (d) Mohr, W; Stahl, J; Hampel, F; Gladysz, J. A. *Chem. Eur. J*. **2003**, *9*, 3324. (e) Mohr, W; Stahl, J; Hampel, F; Gladysz, J. A. *Inorg. Chem*. **2001**, *40*, 3263. (f) Peters, T. B; Bohling, J. C; Arif, A. M; Gladysz, J. A. *Organometallics*, **1999**, *18*, 3261.
29. (a) Zhan, H; Wong, W. Y; Ng, A; Djurisic, A. B; Chan, W. K. *J. Organomet. Chem*. **2011**, *696*, 4112. (b) Zhan, H. M; Lamare, S; Ng, A; Kenny, T; Guernon, H; Chan, W. K; Djurisic, A. B; Harvey, P. D; Wong, W. Y. *Macromol*. **2011**, *44*, 5155. (c) Liu, L; Chow, W. C; Wong, W. Y; Chui, C. H; Wong, R. S. M. *J. Organomet. Chem*. **2011**, *696*, 1189. (d) Wong, W. Y; Chow, W. C; Cheung, K. Y; Fung, M. K; Djurisic, A. B; Chan, W. K. *J. Organomet. Chem*. **2009**, *694*, 2717. (e) Wong, W. Y; Wang, X; Zhang, H. L; Cheung, K. Y; Fung, M. K;

Djurisic, A. B; Chan, W. K. *J. Organomet. Chem*. **2008**, *693*, 3603. (f) Wang, X. Z; Wong, W. Y; Cheung, K. Y; Fung, M. K; Djurisic, A. B; Chan, W. K. *Dalton Trans*. **2008**, 5484. (g) Liu, L; Ho, C. L; Wong, W. Y; Cheung, K. Y; Fung, M. K; Lam, W. T; Djurisic, A. B; Chan, W. K. *Adv. Funct. Mater*. **2008**, *18*, 2824. (h) Wong, W. Y; Wang, X. Z; He, Z; Chan, K. K: Djurisic, A. B; Cheung, K. Y; Yip, C. T; Ng, A. M. C; Xi, Y. Y; Mak, C. S. K; Chan, W. K. *J. Am. Chem. Soc*. **2007**, *129*, 14372.

30. Goudreault, T; He, Z; Guo, Y; Ho, C. L; Zhan, H; Wang, Q; Ho, K. Y. F; Wong, K. L; Fortin, D; Yao, B; Xie, Z; Wang, L; Kwok, W. M; Harvey, P. D; Wong, W. Y. *Macromol*. **2010**, *43*, 7936.
31. Liu, L; Poon, S. Y; Wong, W. Y. *J. Organomet. Chem*. **2005**, *690*, 5036.
32. Brayshaw, S. K; Schiffers, S; Stevenson, A. J; Teat, S. J; Warren, M. R; Bennett, R. D; Sazanovich, I. V; Buckley, A. R; Weinstein, J. A; Raithby, P. R. *Chem. Eur. J*. **2011**, *17*, 4385.
33. Zhou, G. J; Wong, W. Y; Lin, Z; Ye, C. *Angew. Chem., Int. Ed*. **2006**, *45*, 6189.
34. (a) Ho, Cl; Chui, C. H; Wong, W. Y; Aly, S. M; Fortin, D; Harvey, P. D; Yao, B; Xie, Z; Wang, L. *Macromol. Chem. Phys*. **2009**, *210*, 1786. (b) Aly, S. M; Ho, C. L; Wong, W. Y; Fortin, D; Harvey, P. D. *Macromol*. **2009**, *42*, 6902. (c) Khan, M. S; Al-Suti, M. K; Al-Mandhary, M. R. A; Ahrens, B; Bjernemose, J. K; Mahon, M. F; Male, L; Raithby, P. R; Friend, R. H; Koehler, A; Wilson, J. S. *Dalton Trans*. **2003**, 65. (d) Khan, M. S; Al-Mandhary, M. R. A; Al-Suti, M. K; Feeder, N; Nahar, S; Koehler, A; Friend, R. H; Wilson, P. J; Raithby, P. R. *J. Chem. Soc., Dalton Trans*. **2002**, 2441.
35. Choi, H; Kim, C; Park, K. M; Kim, J; Kang, Y; Ko, J. *J. Organomet. Chem*. **2009**, *694*, 3529.
36. Parthey, M; Vincent, K. B; Renz, M; Schauer, P. A; Yufit, D. S; Howard, J. A. K; Kaupp, M; Low, P. J. *Inorg. Chem*, **2014**, 52, 1544.
37. (a) Sugita, N.; Minkiewicz, J. V.; Heck, R. F. *Inorg. Chem*. **1978**, *17*, 2809. (b) Kawata, N.; Mizoroki, T.; Ozaki, A. *Bull. Chem. Soc. Jpn*. **1974**, *47*, 1807.
38. (a) Frei, M.; Aradhya, S. V.; Hybertsen, M. S.; Venkataraman, *J. Am. Chem. Soc*. **2012**, *134*, 4003. (b) González, M. T.; Díaz, A.; Leary, E.; García, R.; Herranz, M. A.; Rubio-Bollinger, G.; Martín, N.; Agraït, N. *J. Am. Chem. Soc*. **2013**, *135*, 5420. (c) Pera, G.; Martín, S.; Ballesteros, L. M.; Hope, A. J.; Low, P. J.; Nichols, R. J.; Cea, P. *Chem. Eur. J*. **2010**, *16*, 13398. (d) Marqués-González, S.; Yufit, D.

S.; Howard, J. A. K.; Martín, S.; Osorio, H. M.; García-Suárez, V. M.; Nichols, R. J.; Higgins, S. J.; Cea, P.; Low, P. J. *Dalton Trans*. **2013**, *42*, 338.

39. (a) Khan, M. S; Al-Mandhary, M. R. A; Al-Suti, M. K; Al-Battashi, F. R; Al-Saadi, S; Ahrens, B; Bjernemose, J. K; Mahon, M. F; Raithby, P. R; Younus, M; Chawdhury, N; Koehler, A; Marseglia, E. A; Tedesco, E; Feeder, N; Teat, S. J. *Dalton Trans*. **2004**, 2377. (b) Wong, W. Y; Lu, G. L; Ng, K. F; Choi, K. H; Lin, Z. *J. Chem. Soc., Dalton Trans*. **2001**, 3250.
40. Blatter, K; Schluter, A. D. *Synthesis*. **1989**, *5*, 356.
41. Sadowy, A. L; Ferguson, M. J; McDonald, R; Tykwinski, R. R. *Organometallics*, **2008**, *27*, 6321.
42. D'Amato, R; Furlani, A; Colapietro, M; Portalone, G; Casalboni, M; Falconieri, M; Russo, M. V. *J. Organomet. Chem*. **2001**. *627*, 13.
43. Nilsson, P; Plamper, F; Wendt, O. F. *Organometallics*, **2003**, *22*, 5235.
44. Nguyen, M. H; Wong, C. H; Kip, J. H. K. *Organometallics*, **2013**, *32*, 1620.
45. He, Z; Wong, W. Y; Yu, X. M; Kwok, H. S; Lin, Z. Y. *Inorg. Chem*. **2006**, *45*, 10922.
46. (a) Lambert, C; Noll, G. *Angew. Chem. Int. Ed*, **1998**, *37*, 2107. (b) Song, J. L; Amaladass, P; Wen, S. H; Pasunooti, K. K; Li, A; Yu, Y. L; Wang, X; Deng, W. Q; Liu, X. W. *New. J. Chem*. **2011**, *35*, 127.
47. Ugo, R; Cariati, F; Lamonica, G. *Inorg Synth*, **1990**, *28*, 123.
48. Blatter, K; Schluter, A. D. *Synthesis*. **1989**, *5*, 356.
49. Khairul, W. M; Fox, M. A; Zaitseva, N/ N; Gaudio, M; Yufit, D. S; Skelton, B. W; White, A. H; Howard, J. A. K; Bruce, M. I; Low, P. J. *Dalton Transactions*, **2009**, *4*, 610.
50. Gardinier, J. R; Clerac, R, Gabbai, F. P. *J. Chem. Soc*., *Dalton Trans*. **2001**, 3453.
51. (a) Conzelmann, W; Koola, J. D; Kunze, U; Strahle, J. *Inorg. Chim. Acta*, **1984**, *89*, 147. (b) Edelbach, B. L; Vicic, D. A; Lachiotte, R. J; Jones, W. D. *Organometallics*, **1998**, *17*, 4784. (c) Al-Fawaz, A; Aldridge, S; Coombs, D. L; Dickinson, A. A; Willcock, D. J; Ooi, L. L; Light, M. E; Coles, S. J, Hursthouse, M. B. *Dalton. Trans*, **2004**, 4030. (d) Khanna, A; Khandelwal, B. L; Saxena, A. K; Singh, T. P. *Polyhedron*, **1995**, *14*, 2705. (e) Rieger, A. L; Carpenter, G. B; Rieger, R. H. *Organometallics*, **1993**, *12*, 842.
52. Zanello, P. (2002). *Inorganic Electrochemistry Theory and Practice*. London: Royal Society of Chemistry. 630.

53. Low, P. J; Paterson, M. A. J; Goeta, A. E; Yufit, D. S; Howard, J. A. K; Cherryman, J. C; Tackley, D. R; Brown, B. *J. Mater. Chem*. **2004**, *14*, 2516.
54. Low, P. J.; Paterson, M .A. J; Puschmann, H; Goeta, A. E; Howard, J. A. K; Lambert, C; Cherryman, J. C; Tackley, D. R; Leeming, S; Brown, B. *Chem. Eur. J*. **2004**, *10*, 83.
55. Low, P. J; Paterson, M. A. J; Yufit, D. S; Howard, J. A. K; Cherryman, J. C; Tackley, D. R; Brook, R; Brown, B. *J. Mater. Chem*. **2005**, *15*, 2304.
56. Lambert, C; Nöll, G. *J. Am. Chem. Soc*. **1999**, *121*, 8434.
57. (a) Barriere, F; Camire, N; Geiger, W. E; Mueller-Westerhoff, U. T; Sanders, R. *J. Am. Chem. Soc*. **2002**, *124*, 7262. (b) Barriere, F; Geiger, W. E. *J. Am. Chem. Soc*. **2006**, *128*, 3980.
58. (a) D'Alessandro, D. M; Keene, R. *Dalton. Trans*. **2004**, 3950. (b) Low, P. J; Brown, N. J. *J. Clust. Sci*. **2010**, *21*, 235. (c) Arnold, D. P; Heath, G. A; James, D. A. *J. Porphyr. Phtalocya*. **1999**, *3*, 5.
59. Low, P. J; Bock, S. *Electrochimica Acta*. **2013**, *110*, 681.
60. Hush, N. S. *Prog. Inorg. Chem.* **1967**, *8*, 391.
61. (a) Renz, M; Theilacker, K; Lambert, C; Kaupp, M. *J. Am. Chem. Soc*. **2009**, *131*, 16292. (b) Kaupp, M; Renz, M; Parthey, M; Stolte, M; Wurthner, F; Lambert, C. *Phys. Chem. Chem. Phys*. **2011**, *13*, 16973.
62. (a) Richardson, D. E; Taube, H. *Coord. Chem. Rev*. **1984**, *60*, 107. (b) Denis, R; Toupet, L; Paul, F; Lapinte, C. *Organometallics* **2000**, *19*, 4240.
63. Coulson, D. R. *Inorg. Synth.* **1972**, *13*, 121.
64. (a) Ono, T; Ohta, M; Sada, K. *ACS. Macro. Lett.* **2012**, *1*, 1270. (b) Yakelis, N. A; Bergman, R. G. *Organometallics*, **2005**, *24*, 3579.
65. Bauernschmitt, R; Ahlrichs, R. *Chem. Phys. Lett.* **1996**, *256*, 454.
66. Bauernschmitt, R; Haser, M; Treutler, O; Ahlrichs, R. *Chem. Phys. Lett.* **1997**, *264*, 573.
67. Furche, F; Rappoport, D. *Density functional theory for excited states: equilibrium structure and electronic spectra, Vol. 16 of "Computational and Theoretical Chemistry"*, Elsevier, Amsterdam, **2005**.
68. TURBOMOLE V6.4 **2012**, a development of University of Karlsruhe and Forschungszentrum Karlsruhe GmbH, 1989-2007, TURBOMOLE GmbH, since 2007.

69. Renz, M; Theilacker, K; Lambert, C; Kaupp, M. *J. Am. Chem. Soc.* **2009**, *131*, 16292.
70. Kaupp, M; Renz, M; Parthey, M; Stolte, M; Würthner, F; Lambert, C. *Phys. Chem. Chem. Phys.* **2011**, *13*, 16973.
71. Renz, M; Kaupp, M. *J. Phys. Chem. A* **2012**, *116*, 10629.
72. Renz, M; Kess, M; Diedenhofen, M; Klamt, A; Kaupp, M. *J. Chem. Theory Comput.* **2012**, *8*, 4189.
73. Völker, S. F; Renz, M; Kaupp, M; Lambert, C. *Chem. Eur. J.* **2011**, *17*, 14147.
74. Parthey, M; Gluyas, J. B. G.; Fox, M. A; Low, P. J; Kaupp, M. *Chem. Eur. J.* **2014**, accepted.
75. Parthey, M; Gluyas, J. B. G; Schauer, P. A; Yufit, D. S; Howard, J. A. K; Kaupp, M; Low, P. J. *Chem. Eur. J.* **2013**, *19*, 9780.
76. Parthey, M; Vincent, K. B; Renz, M; Schauer, P. A; Yufit, D. S; Howard, J. A. K; Kaupp, M; Low, P. J. *Inorg. Chem.* **2014**, *53*, 1544.
77. Vincent, K. B; Zeng, Q; Parthey, M; Yufit, D. S; Howard, J. A. K; Hartl, F; Kaupp, M; Low, P. J. *Organometallics* **2013**, *32*, 6022.
78. Andrae, D; Häussermann, U; Dolg, M; Stoll, H; Preuss, H. *Theor. Chim. Acta* **1990**, *77*, 123.
79. Schäfer, A; Horn, H; Ahlrichs, R. *J. Chem. Phys.* **1992**, *97*, 2571.
80. Weigend, F; Ahlrichs, R. *Phys. Chem. Chem. Phys.* **2005**, *7*, 3297.
81. Scott, A. P; Radom, L. *J. Phys. Chem.* **1996**, *100*, 16502.
82. Roder, J. C; Meyer, F; Hyla-Kryspin, I; Winter, R. F; Kaifer, E. *Chem. Eur. J.* **2003**, *9*, 2636.
83. Klamt, A; Schüürmann, G. *J. Chem. Soc., Perkin Trans. 2*, **1993**, *5*, 799.
84. GaussView, Version 5, Dennington, R; Keith, T; Millam, J. Shawnee Mission KS, **2009**.

Chapter 3: Synthesis and Characterisation of Triarylamine Capped Bis-ethynyl Platinum Complexes

3.1. Synopsis

A range of bis-ethynyl platinum compounds of the general form *trans*-$[Pt(C{\equiv}CC_6H_4NAr'_2)_2(PR_3)_2]^{n+}$ (R = Et or Ph; Ar' = $C_6H_4CH_3$-4 or $C_6H_4OCH_3$-4; n = 0, 1, 2) have been prepared and characterised. Electrochemical studies of the bis-ethynyl compounds show that there is a moderate degree of through-bond communication between the redox-active moieties, as evidenced by the small, but almost identical, separation of the two consecutive amine centred oxidations (ΔE) in both NBu_4PF_6 and the weakly coordinating electrolyte $NBu_4[BArF_4]$.

UV-vis-NIR and IR spectroelectrochemical (SEC) studies show that, for the neutral compounds *trans*-$[Pt(C{\equiv}CC_6H_4NAr'_2)_2(PR_3)_2]$, there is a single $\nu(C{\equiv}C)$ band consistent with the identical environments at both C≡C moieties. On oxidation to the mono-cationic radical forms *trans*-$[Pt(C{\equiv}CC_6H_4NAr'_2)_2(PR_3)_2]^{+}$, the IR $\nu(C{\equiv}C)$ spectra change and resemble a superposition of the neutral and dicationic spectra, whilst the dications *trans*-$[Pt(C{\equiv}CC_6H_4NAr'_2)_2(PR_3)_2]^{n+}$ feature $\nu(C{\equiv}C)$ spectra which do not resemble any of the neutral $\nu(C{\equiv}C)$ features. Given that the $\nu(C{\equiv}C)$ spectra of the monocationic systems seem to be a superposition of the neutral and dicationic spectra, a description in terms of a localised MV complex appears appropriate. These changes are complimented by the rise and fall of a NIR band centred at ca. 6000 cm^{-1} through the oxidation states.

These results are supported by quantum chemical calculations performed by the Kaupp group at TU Berlin that show amine-centred HOMO valence orbitals and

TDDFT results that closely match the experimental IR frequencies and UV-vis NIR transitions that accurately reproduce the key spectral features of both the monocationic and dicationic species, including the low energy IVCT band in the MV mono-cations. Visible absorption bands centred at 10000 and 15000 cm^{-1} are shown to be comprised of a number of different ligand and metal-based transitions, which agree with the asymmetric appearance of bands in the experimental spectra.

3.2. Introduction

Conjugated molecules that can undergo redox processes and exhibit ET phenomena are often considered for advanced materials applications, and many examples contain multiple redox centres that are linked together through a conjugated backbone.[1] Such MV compounds are often metal-bridge-$metal^{+/-}$ in construct (see Figure 49) and are derived from the one-electron oxidation or reduction of the neutral species, metal-bridge-metal where the metal is a redox-active metal ligand moiety and the bridge is a conjugated organic / organometallic fragment. The mixed valence complexes are often characterised by an IVCT transition in the NIR region of the electromagnetic spectrum. The ability to use redox processes to open an optical CT event has led to consideration for MV complexes in advanced materials as well as providing platforms for the study of the fundamentals of intramolecular ET reactions.

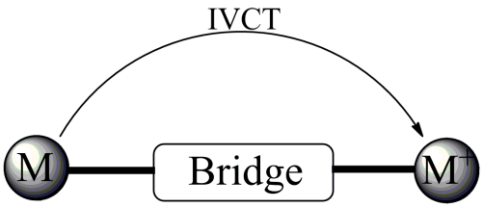

Figure 49: General schematic of a donor-bridge-acceptor molecule

While compounds in which metal electrophores are bridged by organic ligands have dominated studies of MV chemistry and the physical properties associated with them, there has been much recent interest in organic mixed valence systems,[2] no doubt in response to the growing interest in organic electronic materials. There are far fewer examples of systems containing organic redox centres joined through conjugated organometallic bridges. This is somewhat surprising when *trans*-bis-acetylides of Ru, Os and Pt have long been known,[3] and recent results have shown that it is possible to achieve greater levels of control over molecular conductivity in some metal-bridged systems than in purely organic systems.[4]

Nevertheless, a small number of 'inverted' MV complexes have been designed, in which organic redox systems are bridged by a metal-based complex that serves as a bridge.[5-10] Mono-metallic systems with organic redox termini connected through a platinum bridged organic redox centre are also good candidates to be studied as model compounds for larger oligomeric and polymeric species, given the general kinetic inertness of the Pt-C≡C bond. In seeking to design larger systems, understanding the electronic nature of smaller species and the electronic transitions / properties that can be exploited through optical / electrochemical methods can provide a deeper insight into the fundamental properties of such assemblies, and ultimately allow the design and synthesis of materials based on these predicted properties. Systems based on polymer compounds of Pt-polyyne and C_{60} are now being studied due to their potential applications in photocell technology.[11] It has also been shown that the fluorescence spectra of such compounds[6] show both singlet and triplet transitions comparable to the polymeric Pt species and, as such, understanding the effects of changing the alkynyl and ancillary ligands in these smaller species will

play a fundamental part in fully understanding the transitions involved in much larger systems.[12-18]

However, the observation of a simple, Gaussian-shaped IVCT band is rare in organometallic MV systems,[19,20] and more often the near-degeneracy of the d-orbitals, together with the range of possible conformations of molecules of low axial symmetry in solution,[18] can lead to a set of transitions close in energy and thus to a series of overlapping NIR bands, not all of which have IVCT character.[21] In addition, electronic absorption bands are typically complicated by solvent-induced band broadening. Despite these complications, excitation energies and bandwidth are often extracted from the experimental spectral envelopes by Gaussian deconvolution and used in analyses based on the methods and expression developed by Hush.[64] Further complications arise, however, as a unique analytical solution to the deconvolution is often not possible, leaving considerable ambiguity in the spectroscopic assignments and much space for individual interpretation. Another complication to Gaussian band-shaped based deconvolutions and spectral fitting occurs in strongly coupled systems, which often exhibit bands with a pronounced 'cut-off' on the low-energy side of the band leading to an asymmetric shape of the NIR band,[22] making the Gaussian-shape of sub-bands an invalid approximation. Furthermore the ability to modulate the ET phenomena present in such systems is possible through control of the metallic bridge. While compounds bridged by –C≡C-Ru-C≡C- fragments are known to give rise to highly delocalised orbitals,[23] previous studies have shown that the Pt centre is less strongly coupled to the backbone,[3] and as such give rise to systems of a more localised electronic structure of a MV nature that in principle should obey Hush rules better (Chapter 1).

An IVCT process has been identified in a mixed-valent bis-triarylamine Pt bridged rod-like system, [*trans*-$Pt(PEt_3)_2\{C{\equiv}CC_6H_4N(C_6H_4OCH_3\text{-}4)_2\}_2]^+$ by S.R. Marder *et al*. This metal-bridged organic MV complex showed only a small decrease in the intensity of the IVCT band in comparison to the organic analogue, $[\{C{\equiv}CC_6H_4N(C_6H_4OCH_3\text{-}4)_2\}_2]^+$, with more detailed analysis revealing similar coupling between the amine moieties via both organic and organometallic bridges.[6] It is therefore desirable to further investigate the ET process, and associated spectroscopic profiles, in metal-bridged organic mixed-valence complexes of this type through variation in the ancillary bridging ligands, phosphine co-ligands at Pt, and the electronic character of the redox centre through altering the aryl moiety at the N centre. Along with the control offered through manipulation of the electronic structure by systematic changes in the molecular structure it is also desirable to be able to characterise and predict these effects. Considering the fundamental difficulties in analytical treatment of the spectroscopic band envelopes, a quantum-chemical perspective is used to assist these analyses.[24, 25]

To these ends, a range of bis-ethynyl platinum compounds of the general form *trans*-$[Pt(C{\equiv}CC_6H_4NAr'_2)_2(PR_3)_2]^{n+}$ (R = Et or Ph, Ar = $C_6H_4CH_3$-4 or $C_6H_4OCH_3$-4, n = 0, 1, 2) have been synthesised and IR and UV-vis NIR spectroelectrochemical studies undertaken to fully determine the electronic properties of the molecules in all the accessible oxidation states. Quantum chemical calculations with the hybrid functional BLYP35 in combination with suitable (COSMO) solvent models have been used to model the UV-vis-NIR and IR spectroscopic properties of these complexes ([**17**- **20**]$^+$), to confirm the description of these compounds as examples of

metal-bridged organic mixed-valence compounds. Principal features of the electronic spectra have been assigned, including the triarylamine-based IVCT transition located in the NIR region.

3.3. Results and discussions

3.3.1. Synthesis

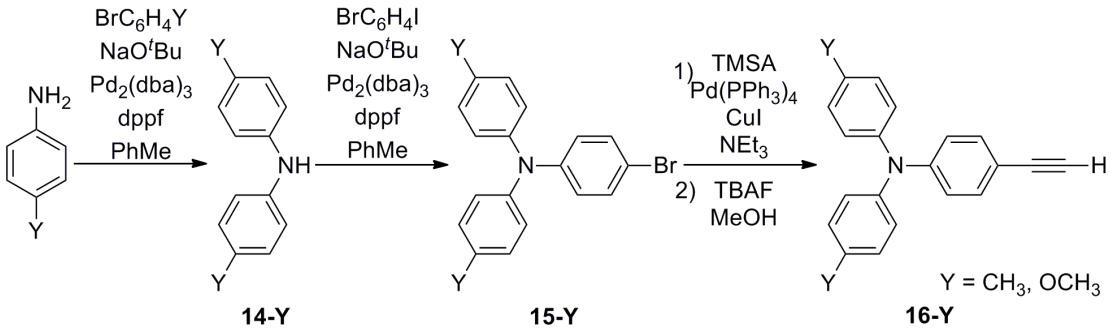

Scheme 12: Synthetic route of the organic ligands used in this work

Syntheses of both tolyl[26] and methoxy derivatives of the triarylamine pro-ligand (**16-CH_3** and **16-OCH_3**) were achieved through a series of palladium catalysed cross coupling reactions and fluoride mediated deprotection reactions (Scheme 12). The alkynes **14-CH_3** and **15-CH_3** were prepared from *para*-toluidine through sequential Hartwig-Buchwald amination[27, 28] and Sonogashira cross-coupling[29] reactions (Scheme **12**). There are numerous reports of the preparation of the ligand building block **14-CH_3** from arylation reactions of para-toluidine with 4-chloro[30–37], bromo[38, 39] or iodo-toluene[40]; the compounds are also available commercially. We elected to employ a simple combination of readily available palladium source [$Pd_2(dba)_3$], supporting phosphine (dppf) and base (NaO^tBu) in a Hartwig-Buchwald based methodology to cross couple 4-iodotoluene with *para*-toluidine, which gave **14-CH_3** in good (68 %) yield in an experimentally convenient fashion. The same conditions were employed to selectively couple the iodo moiety in 1-bromo-4-iodobenzene to

14-CH$_3$, which afforded the tertiary amine [N(C_6H_4Br-4)($C_6H_4CH_3$-4)$_2$] (**15-CH$_3$**) (Scheme **12**).

These compounds have been characterised by the usual spectroscopic techniques and the data are consistent with those reported previously in the literature.[41, 42] ES-MS (+) for all of the precursors give rise to the $[M+H]^+$ ion. ^{1}H-^{1}H (NOESY and COSY) and ^{1}H-^{13}C (HSQC and HMBC) 2D NMR experiments allowed assignment of all ^{1}H and ^{13}C signals. The ^{1}H NMR spectra of both **16-CH$_3$** and **16-OCH$_3$** show characteristic AB splitting patterns for the inequivalent protons of the Ar rings, with apparent coupling constants of 8 Hz for the methyl substituted rings (**16-CH$_3$**) and 9 Hz for the halide / ethynyl substituted rings.

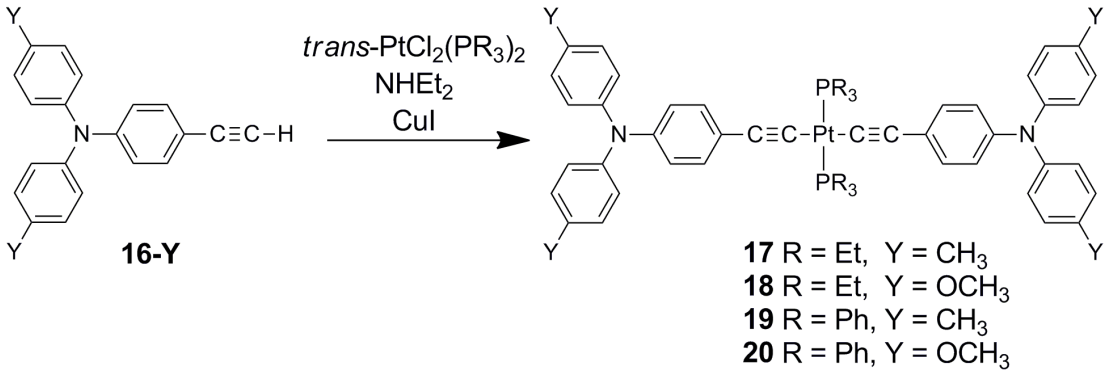

Scheme 13: Compounds studied in this work

Compounds **17** – **20** (Scheme 13) were synthesized via CuI catalysed dehydrohalogenation reactions of *trans*-$PtCl_2(PEt_3)_2$ or *cis*-$PtCl_2(PPh_3)_2$ and the corresponding ethynyl-substituted triarylamine.[6,43] Compounds **17** and **18** were purified by preparative TLC (silica) while compounds **19** and **20** were collected by filtration directly from the reaction mixture and extracted into CH_2Cl_2 to remove any remaining amine or Cu salts. Compounds **17** – **20** were each characterized by a single

ν(C≡C) absorption around 2100 cm^{-1}. MALDI or ASAP MS for compounds **17** – **20** gave signals corresponding to the $[M]^+$ or $[M+H]^+$ molecular ions. The $^{31}P\{^1H\}$ NMR spectrum for each compound showed a singlet resonance with platinum satellites: **17** 11.0 (s, $^1J_{P\text{-}Pt}$ = 2385 Hz); **18** 9.93 (s, $^1J_{P\text{-}Pt}$ = 2373 Hz); **19** 18.73 (s, $^1J_{P\text{-}Pt}$ = 2663 Hz); **20** 17.69, (s, $^1J_{P\text{-}Pt}$ = 2671 Hz). The $^{13}C\{^1H\}$ NMR spectra of **17** and **18** showed characteristic resonances for alkynyl carbons at 109.05 and 106.13 (**17**), 108.90 and 105.40 (**18**) and 113.11 and 108.81 (**20**), however, the poor solubility gives rise to spectra with low signal to noise ratios and the $J_{C\text{-}P}$ and $J_{C\text{-}Pt}$ satellites expected for these compounds are not seen. However not all of the quaternary carbons of **19** could be observed; the poor solubility of these compounds has been noted previously in the literature.[44] For compounds **10**, **19** and **20** successful elemental analyses have been obtained. In the case of the literature compound **18** no further analysis was attempted.

3.3.2. Molecular Structure

Pale yellow, needle-like crystals of **17** suitable for X-ray diffraction were grown by slow diffusion of EtOH in to a CH_2Cl_2 solution of the complex (Figure 50), and selected bond lengths (Å) and angles (°) are given in Table 16. In each case, the Pt atom of these *trans*-geometry molecules is located on an inversion centre. The coordination geometry at the platinum centre is square planar with the near linear C3-C2-C1-Pt1-C1'-C2'-C3' chain confirming the rigid rod-like structure of the complexes. The structures also show the characteristic propeller arrangement of the phenyl moieties and trigonal planar nitrogen geometry associated with the triarylamine moiety.[45-47] In **17** the ethyl moieties on the phosphine ligands are disordered in all cases. The bond lengths and angles are common with the other known examples of *trans*-$Pt(PR_3)_2$ bis-ethynyl systems,[48-53] such as *trans*-

$[Pt\{C{\equiv}CC_6H_4N(C_6H_4OCH_3\text{-}4)_2\}_2(PEt_3)_2]$ **(18)**,[6] and *trans*-$[Pt\{C{\equiv}CC_6H_4NPh_2\}_2(PBu_3)_2]$.[54]

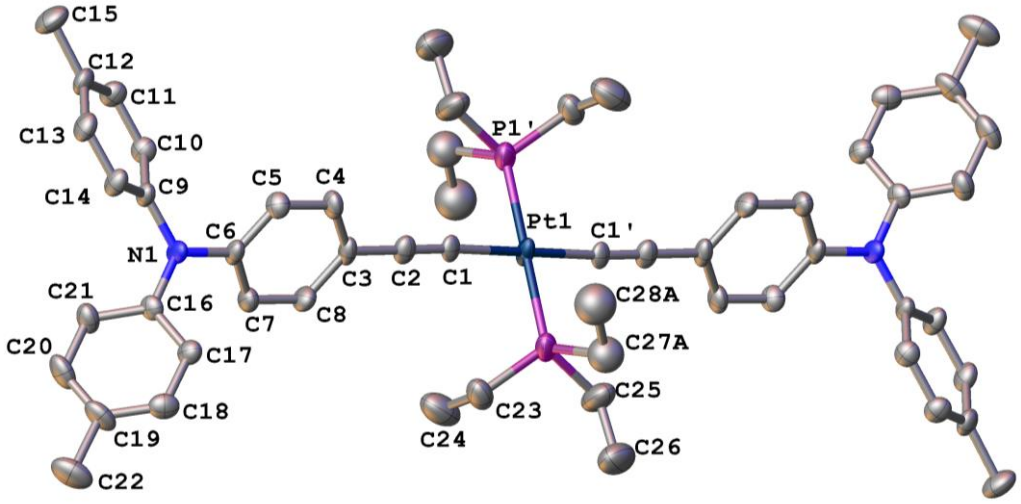

Figure 50: A plot of a molecule of 17 showing the atom labeling scheme, with thermal ellipsoids plotted at 50 %. Hydrogen atoms have been omitted for clarity.

Table 16: Selected bond lengths (Å) and angles (°) for 17

Pt1-P1	2.2667(19)	Pt1-C1-C2	175.9(6)
Pt1-C1	1.999(6)	C1-C2-C3	178.5(7)
C1-C2	1.194(8)	C1-Pt1-P1	87.82(18)
C2-C3	1.453(8)	C1'-Pt1-P1	92.17(18)
N1-C6	1.423(7)	C31-Pt1-P1	
N1-C9	1.423(7)	C1'-Pt1-C1	180.00(13)
N1-C16	1.409(8)	C31-Pt1-C1	N1-C16

3.3.3. Electrochemistry

The observation of two overlapping one-electron redox processes in bis-triarylamine complexes is well established, and is consistent through both organic and metal bridged systems.[45-47, 55] The degree of separation between these waves, $\Delta E(1\text{-}2) = |E_{1/2}(1)\text{-}E_{1/2}(2)|$, can be used to calculate the comproportionation constant, K_c, and hence the thermodynamic stability of individual redox states with respect to disproportionation. These values have often been used to describe the level of electronic communication between the redox sites, however, the challenges of extrapolating the electrochemical data, which is thermodynamic in nature, to the underlying electronic structure, is well known and without recourse to a wider range of data it is difficult to draw definitive conclusions on the degree or nature of electronic interactions between the amine centres based on electrochemical data alone.[56] As such, extraction of such data is best obtained through analysis of the electronic absorption spectra.

The CV of compounds **17** – **20** each exhibit two reversible redox processes (Table 17). It can be seen that there are two general trends for compounds **17** – **20** with the potential of the first redox process, $E_{1/2}(1)$ occurring at low potential for the anisyl derivatives **18** and **20**, which can be attributed to the more electron-donating nature of the OCH_3 groups over the tolyl groups. The second trend is the decrease in ΔE for the anisyl systems compared to the tolyl systems. The increased stability offered to the amine-centred radical cation by the anisyl groups compared to the tolyl groups suggests that the dication is more stabilised and as such there is a smaller peak-to-peak separation. The peak-to-peak separation can be determined from the CV or the differential pulse voltammetry (DPV) (Table 17). Despite the low value of ΔE and

hence small K_c for **17** - **20** the mixed valence state; *trans*-$[Pt(C{\equiv}CC_6H_4NAr'_2)_2(PR_3)_2]^+$, can be studied as the comproportionated mixture with the neutral and dicationic species. Interestingly, the electrochemical results are consistent in both 0.1 M NBu_4PF_6 and the 'Geiger electrolyte' 0.1 M $NBu_4[B\{C_6H_3\text{-}3,5\text{-}(CF_3)_2\}_4]$, which features the very weakly coordinating $[B\{C_6H_3\text{-}3,5\text{-}(CF_3)_2\}_4]^-$ ($[BAr^F{}_4]^-$) anion.[57,58] Given the likely similar energies of solvation, ion pairing, and electronic factors across the series of complexes, the absence of any increased separation in ΔE on changing the electrolyte is likely consistent with a moderate degree of through-bond interaction between the amine centres.[59]

Table 17: Oxidation potentials for platinum complexes 17 – 20 and related organic bis-triarylamines. CV in CH_2Cl_2 with 0.1 M $NBu_4[X]$ in CH_2Cl_2 at a scan rate of 100 mV/s and referenced against $FeCp^*_2$ at -0.48 V *vs* $FeCp_2$ ($FeCp_2$ = +0.0 V).

Compound	$[X]^-$	$E_{1/2}(1)$ / V	$E_{1/2}(2)$ / V	$\Delta E(1\text{-}2)$ / V	K_c
$\{C{\equiv}CC_6H_4N(C_6H_4OMe\text{-}4)_2\}_2$[41]	$[PF_6]^-$	0.29	0.39	0.10	50
$[C_6H_4\{C{\equiv}CC_6H_4N(C_6H_4OMe\text{-}4)_2\}_2]$[41]	$[PF_6]^-$	0.28	0.34	0.06	10
17	$[PF_6]^-$	0.27	0.40	0.13	160
	$[BAr^F{}_4]^-$	0.25	0.39	0.14	
18	$[PF_6]^-$	0.17	0.23	0.06	10
	$[BAr^F{}_4]^-$	0.20	0.26	0.06	
19	$[PF_6]^-$	0.24	0.36	0.12	108
	$[BAr^F{}_4]$	0.25	0.36	0.11	
20	$[PF_6]^-$	0.21	0.27	0.06	10
	$[BAr^F{}_4]^-$	0.22	0.29	0.07	

3.3.4. IR Spectroelectrochemistry

To get a more detailed understanding of the nature of the electronic properties of compounds **17** – **20** in their various electrochemically accessible redox states, IR and UV-vis NIR SEC and DFT calculations were carried out (the latter in collaboration with Matthias Parthey of the Kaupp group at TU Berlin). As noted above, the IR spectra of the neutral complexes **17** – **20** are characterized by a single weak ν(C≡C) band (Table 18). The observation of a single band for both C≡C bonds is consistent with the highly symmetric distribution of electron density over the molecular backbone. During oxidation the IR band profile evolves from a single ν(C≡C) band for the neutral complexes, through a more complex pattern of multiple bands associated with the comproportionated equilibrium mixture of the neutral, monocationic and dicationic states, to a strong absorption feature characteristic of the dicationic state (Figure 51 (**17**), Figure 52 (**18**, **19**, **20)**). The observation of multiple ν(C≡C) bands associated with the monocation, perhaps due to the effects of Fermi coupling,[60] in combination with the low comproportionation constant, which ensures solutions of the monocations also contain appreciable amounts of the neutral and dicationic forms, makes the assignment of the spectra for [**17** – **20**]$^{+}$ more complicated. However assignment of the spectra was aided by the growth of a NIR band associated with the mono-cationic, mixed-valence, state at ca. 5000 cm^{-1}. When this electronic transition reached peak intensity, the maximum composition of the monocationic (MV) form of the complex in the mixture was assumed to have been reached. The nature of this NIR band is discussed in more detail later.

Table 18: Experimental and calculated C≡C stretching frequencies/cm^{-1} for complexes [17 - 20]$^{n+}$ (n = 0, 1, 2).[a]

	17			**18**			**19**			**20**		
	0	+1	+2	0	+1	+2	0	+1	+2	0	+1	+2
exp	2100(s)	2018 2046 (sh) 2070 (sh) 2100	2018 2046 (sh) 2070 (sh)	2100	2025 2046 (sh) 2065 (sh) 2100	2025 2046 (sh) 2065 (sh) 2073	2106	2024 2049 (sh) 2079 (sh) 2106	2024 2049 (sh) 2079 (sh)	2106	2030 2050 (sh) 2070 (sh) 2106	2030 2050 (sh) 2070 (sh)
BLYP35	2119	2031 2098	2043	2119	2048 2110	2072	2131	2029 2111	2043	2130	2050 2126	2075
B3LYP	2100	2018 2046 2070 2100	2018 2046 2070									

a. Calculated IR frequencies were scaled by an empirical factor of 0.95.[58,59] b. sh denotes shoulder on major peak.

Further oxidation of this equilibrium mixture resulted in a collapse of the NIR band associated with the monocation and the ν(C≡C) band continued to develop into an envelope of higher intensity transitions associated with the dicationic state, the frequency of which was consistent with the lowest energy band observed in the ν(C≡C) spectra of the equilibrium mixture. The observation of band profiles for the monocationic species as a superposition of the neutral and dicationic species further supports the assignment of the singly oxidised species as being of localised MV origin.

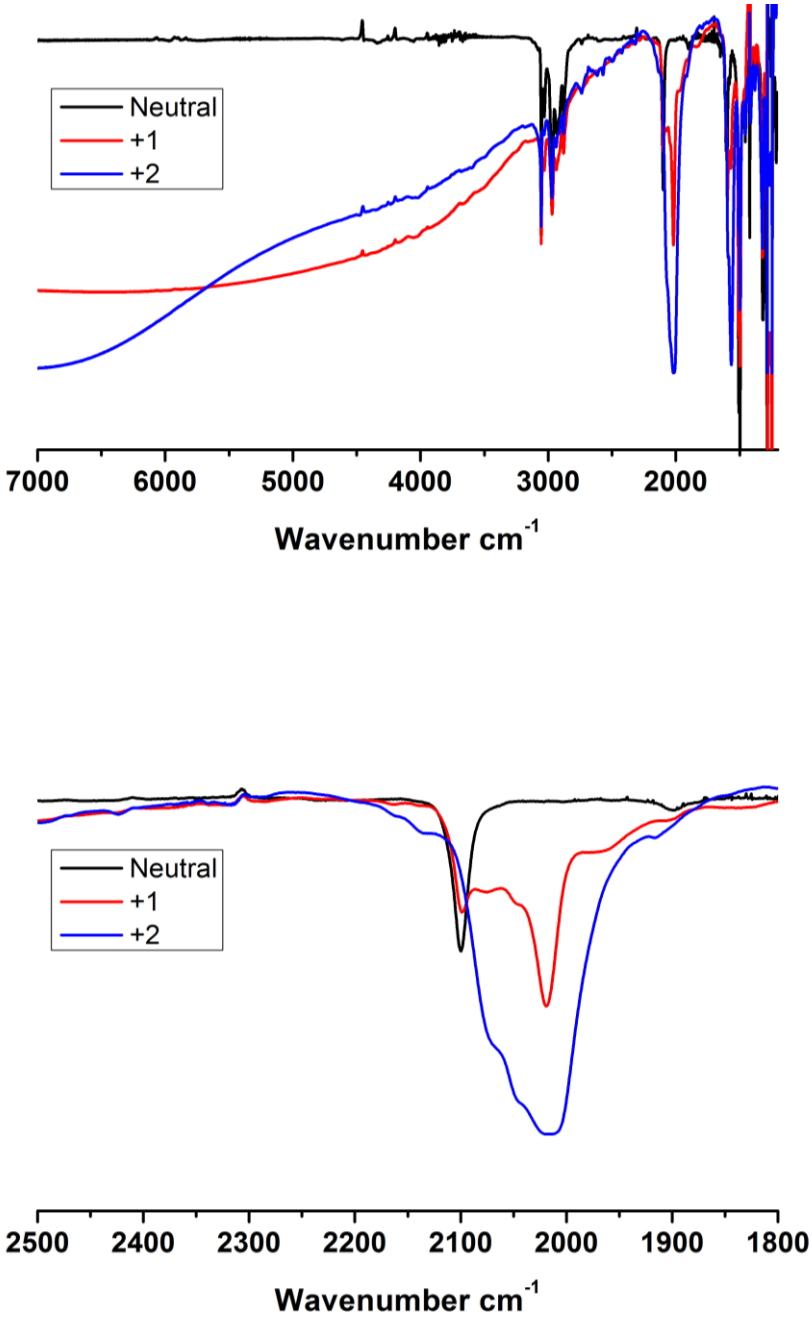

Figure 51: IR spectra of 17 showing the IR-NIR spectra in various oxidation states (top) and an expansion of the ν(C≡C) region in the various oxidation states (bottom) generated by *in situ* electrochemical oxidation in CH_2Cl_2 / 0.1 M NBu_4PF_6 in an OTTLE cell

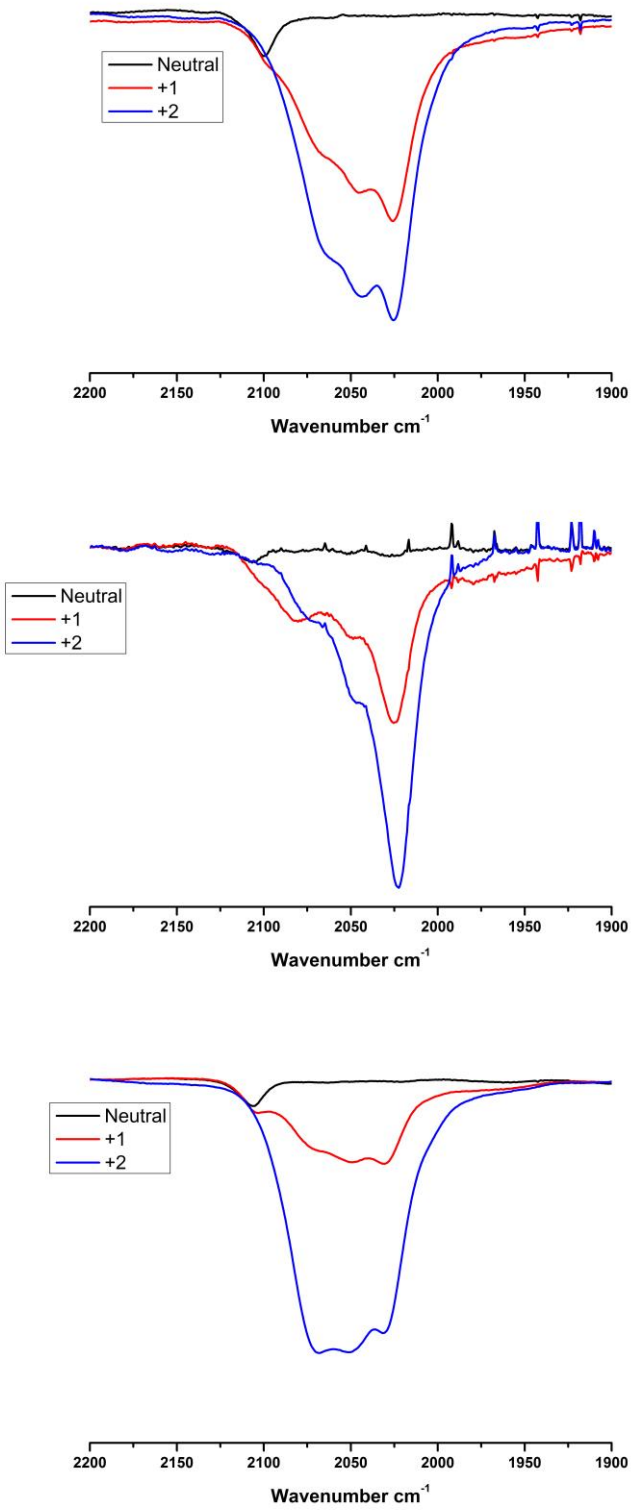

Figure 52: IR spectra of 18 (left), 19 (centre) and 20 (right) showing the IR-NIR spectra of the ν(C≡C) region in the various oxidation states (bottom) generated by *in situ* electrochemical oxidation in CH_2Cl_2 / 0.1 M NBu_4PF_6 in an OTTLE cell.

3.3.5. UV-vis NIR Spectroelectrochemistry

The UV-vis-NIR spectra of [**17** – **20**]$^{n+}$ (n = 0, 1, 2) were collected using spectroelectrochemical methods from ca. 1 mM solutions in 0.1 M NBu_4PF_6 / CH_2Cl_2 and data for the mixed-valence state were corrected for the comproportionation equilibria, Table 19.[61] Given that the mixture is in equilibrium it can be seen that the concentrations of each species are given by:

$$[M] + [M]^{2+} \rightleftarrows 2[M]^{+}$$

Where K_c is then:

$$K_c = \frac{([M]^{+})^2}{[M].[M]^{2+}}$$

Total concentration of all species = c, therefore the concentration of each species can be expressed as a factor of *x* to give:

$$[M]^{+} = c - 2x$$

$$[M] = [M]^{2+} = x$$

which allows Kc to be calculated in terms of x with:

$$K_c = \frac{(c - 2x)^2}{x^2}$$

and thus:

$$K_c = \frac{c^2 - 4cx + 4x^2}{x^2}$$

which can be rearranged to give:

$$K_c x^2 = c^2 - 4cx + 4x^2$$

and hence:

$$(K_c - 4)x^2 + 4cx - c^2 = 0$$

and solved for x by:

$$x = \frac{-4c \mp \sqrt{(4c)^2 + 4(K_c - 4)c^2}}{(2K_c - 8)}$$

with the only physically realistic solution being given in Table 19.

Table 19: Concentration of [M], $[M]^+$ and $[M]^{2+}$ at maximum equilibrium concentration of $[M]^+$

	c mol	[M] mol	$[M]^+$ mol	$[M]^{2+}$ mol
17	1.1×10^{-3}	37.51×10^{-5}	7.51×10^{-5}	0.95×10^{-3}
18	0.45×10^{-3}	8.72×10^{-5}	8.72×10^{-5}	0.276×10^{-5}
19	0.364×10^{-3}	2.89×10^{-5}	2.89×10^{-5}	0.306×10^{-3}
20	1.337×10^{-3}	2.59×10^{-4}	2.59×10^{-4}	0.819×10^{-3}

Spectra for neutral complexes **17 – 20** are consistent throughout with each displaying two pronounced bands at 33000 cm^{-1} and 25000 cm^{-1} arising from the two N→π* transitions commonly observed in triarylamine complexes of general form $ArNAr'_2$ (Table 20).[45-47] There are no other features associated with the UV-vis NIR absorption spectra for the neutral complexes.

Table 20: Electronic absorption spectra of 17 - 20 and their $1e^-$ oxidised forms in CH_2Cl_2/NBu_4PF_6.

Compound	Wavenumber (cm^{-1})
17	32567, 26980
$[17]^+$	28574, 22994, 17011, 9966, 5506
$[17]^{2+}$	22660, 17209, 9632
18	32682, 26800
$[18]^+$	26929, 23651, 22115, 14627, 9807, 6492
$[18]^{2+}$	26714, 23651, 22115, 14422, 9702
19	32097, 25917
$[19]^+$	27845, 23396, 21863, 9966, 5779
$[19]^{2+}$	27647, 23457, 21863, 16480, 9632
20	32233, 25522
$[20]^+$	26653, 23525, 21733, 14756, 9966, 6444
$[20]^{2+}$	26714, 23457, 21863, 14551, 9836

On oxidation of compounds **17 – 20** to the comproportionated mixtures containing the mixed-valence species ([**17 - 20**]$^{+}$) a broad, low intensity IVCT band near 6000 cm^{-1} and a distinct absorption band near 10000 cm^{-1} is observed in each case. The visible region also shows distinct differences between the tolyl (**17** and **19**) and the anisyl (**18** and **20**) derivatives, where the tolyl derivatives (**17** and **19**) give rise to an absorption band envelope between 15000 and 20000 cm^{-1} that has no distinct features (Figure 53 and Figure 54).

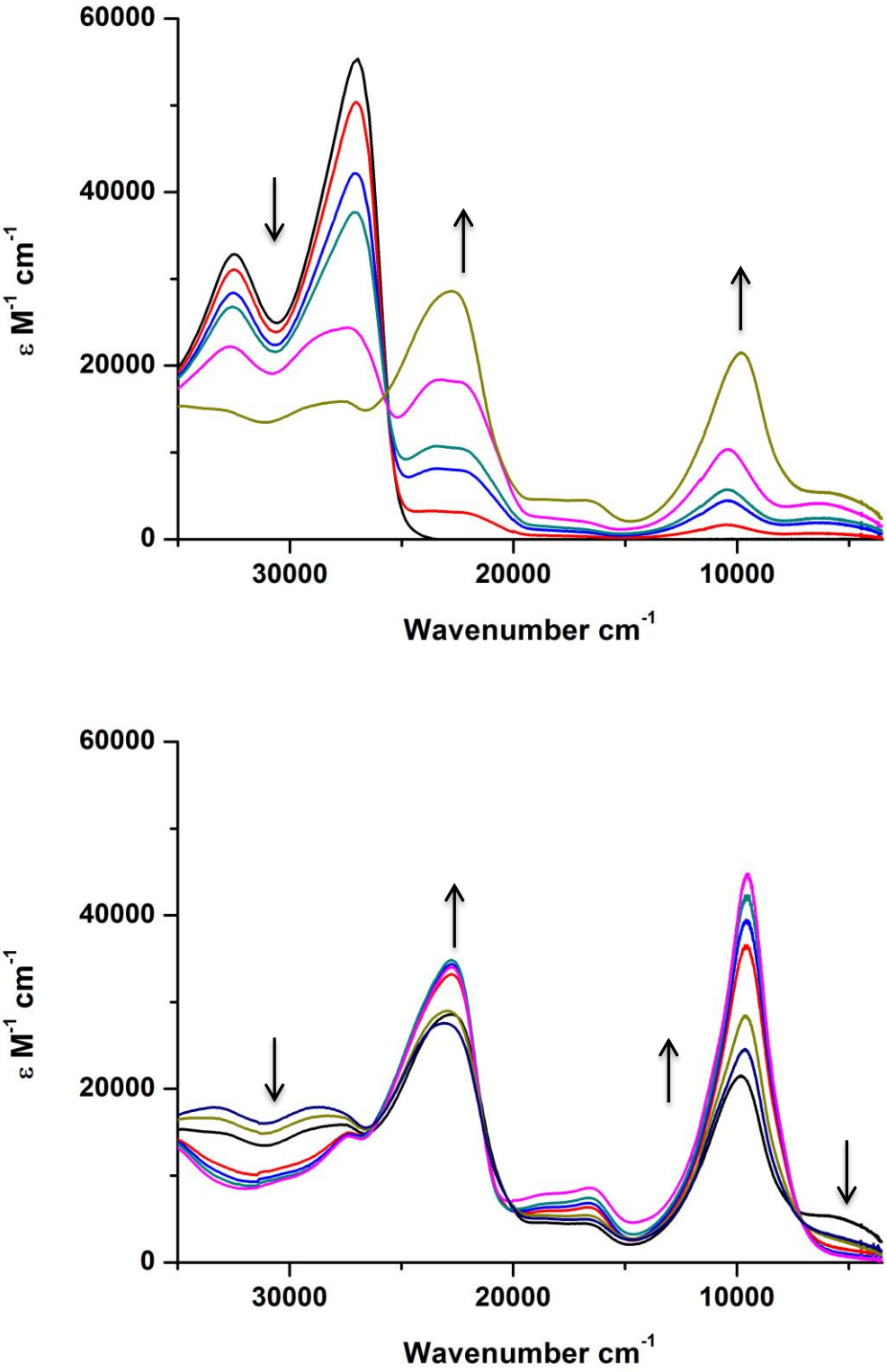

Figure 53: UV-vis-NIR spectra of 17 showing the [17]to $[17]^{+}$ (top) and $[17]^{+}$ to $[17]^{2+}$ (bottom) generated by *in situ* electrochemical oxidation in CH_2Cl_2 / 0.1 M NBu_4PF_6 in an OTTLE cell.

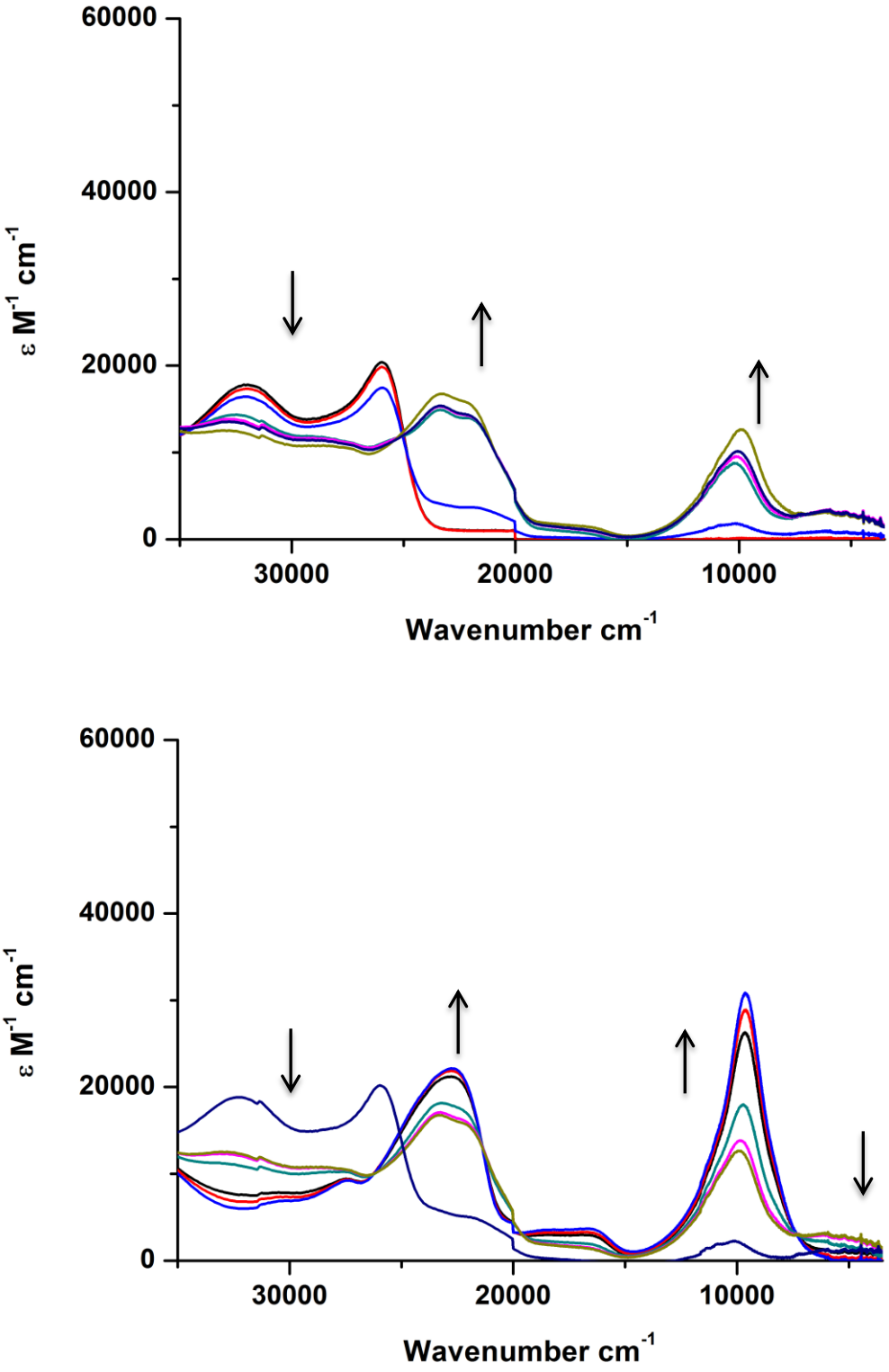

Figure 54: UV-vis-NIR spectra of 19 showing the [19] to $[19]^{+}$ (top) and $[19]^{+}$ to $[19]^{2+}$ (bottom) generated by *in situ* electrochemical oxidation in CH_2Cl_2 / 0.1 M NBu_4PF_6 in an OTTLE cell.

Conversely the anisyl derivatives give rise to a better resolved band apparent below 15000 cm^{-1} in addition to an unresolved band envelope at higher energy that are similar to those seen in the tolyl derivatives (Figure 55 and Figure 56). At higher energy the two absorptions at 25000 cm^{-1} and 33000 cm^{-1} become less intense for all complexes and new features arise between 20000 cm^{-1} and 25000 cm^{-1}. This change in shape for the localised amine transitions is consistent with previous studies of the electronic spectra of triarylamine radical cations indicating that the new features at the high energy end of the spectra are caused by transitions that occur from localised amine orbitals involved with the oxidised region of the mixed valence state.[45-47, 62 and 63]

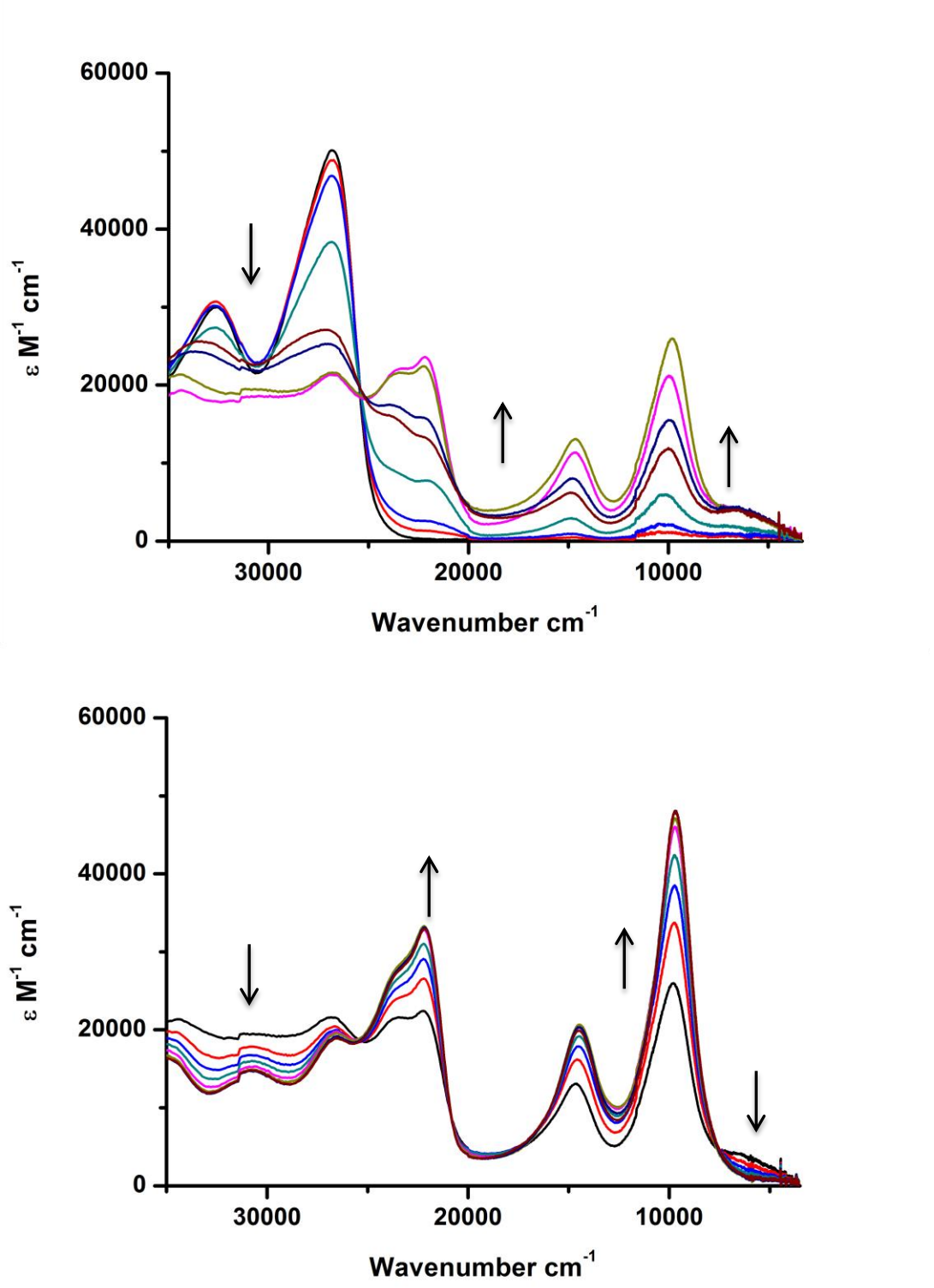

Figure 55: UV-vis-NIR spectra of 18 showing the [18] to $[18]^+$ (top) and $[18]^+$ to $[18]^{2+}$ (bottom) generated by *in situ* electrochemical oxidation in CH_2Cl_2 / 0.1 M NBu_4PF_6 in an OTTLE cell.

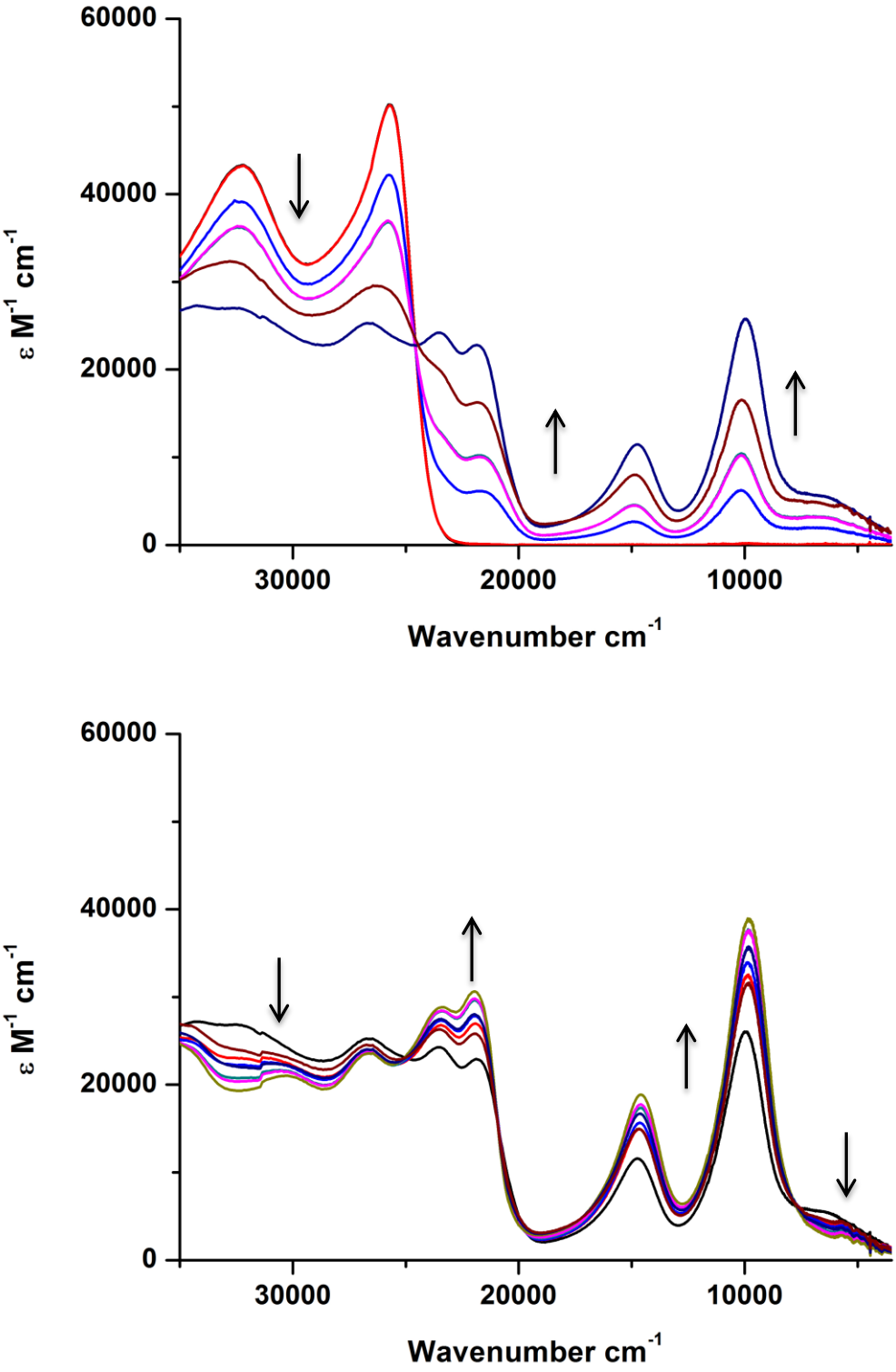

Figure 56: UV-vis-NIR spectra of 20 showing the [20] to $[20]^{+}$ (top) and $[20]^{+}$ to $[20]^{2+}$ (bottom) generated by *in situ* electrochemical oxidation in CH_2Cl_2 / 0.1 M NBu_4PF_6 in an OTTLE cell.

Following further oxidation to [**17 - 20**]$^{2+}$ the low energy bands between 5000 and 7000 cm^{-1} collapse, supporting the IVCT assignment of this transition, and all of the other absorptions below 25000 cm^{-1} gain intensity.

Table 21: Hush analysis and deconvolution parameters of the IVCT transition in [17 - 20]$^{+}$

Compound	ε/M^{-1} cm^{-1}	$\nu_{1/2}$/cm^{-1}	ν_{max}/cm^{-1}	r/Å	H_{ab}/cm^{-1}
[17]$^{+}$	5660	4097	5506	17.72	415
[18]$^{+}$	6575	3872	6492	17.78	471
[19]$^{+}$	5167	4836	5779	17.72	442
[20]$^{+}$	4741	4444	6444	17.78	427

Gaussian deconvolution of the IVCT band (corrected for the comproportionation constant) provides the parameters given in Table 21 for the mixed valence species [**17 – 20**]$^{+}$, with the charge transfer distance taken to be the crystallographic N-N distance, *r*. TDDFT calculations (vide infra) have shown that the low energy NIR band arises from orbitals centred largely on the nitrogen centre but with contributions from the ethynyl and aryl groups; as such the N-N distance should be an over-estimate of the charge transfer distance and hence the the electronic coupling parameter, H_{ab}, calculated through the Hush relationships (Chapter 1) will be under-estimated.[64] The modest level of communication between the amine redox centres is consistent with work published previously.[6,41]

3.3.6. Quantum Chemical Calculations

In order to further understand the ν(C≡C) bands in the IR spectra and the electronic absorption processes observed in the UV-vis NIR spectra, DFT calculations were carried out by Matthias Parthey in the Kaupp group at TU Berlin. Previous studies have inferred

the electronic properties of the monocationic state **[18]**$^{+}$ from gas-phase calculations on computational models of neutral **18** at the B3LYP level of theory. However to better understand the underlying electronic structure of these prototypical metal-bridged organic MV systems we turned to newer quantum-chemical methods to study the complete series of complexes [**17´ - 20´**]$^{n+}$ (n = 0, 1, 2), using the BLYP35 functional and the COSMO (CH_2Cl_2) solvent model (the prime notation is used to distinguish the computational systems from the experimental complexes). BLYP35 was chosen as the level of theory for these calculations as the increased amount of exact exchange (35%) in comparison to the B3LYP functional that employs ca. 20% exact exchange. Although other hybrid functionals are known such as BLYP (0%) or BHLYP (50%), the use of the COSMO solvent model reduces the amount of exact exchange needed in the functional to get reliable descriptions of localised valency and the excited state parameters that occur. Unrestricted structure optimization of [**17´ – 20´**]$^{n+}$ (n = 0, 1, 2) gave stable minima evidenced by the absence of imaginary frequencies.

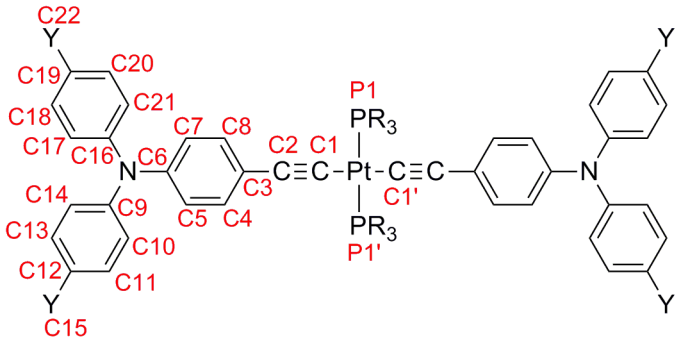

Figure 57: Atom numbering scheme for DFT calculations

The neutral and dicationic structures [**17´ – 20´**]$^{n+}$ (n = 0, 2) are effectively symmetric, and some general trends can be observed across the series. In general the distances between the amine nitrogen atom and the first carbon atom of the bridge C_6, d(N-C_6), are the most influenced by the oxidation state: they contract upon oxidation (Table 22; for

atom labelling, see Figure 57). The d(N-C_6) are slightly longer for the neutral tolyl systems **17´** and **19´** (1.411 Å and 1.413 Å) than for the anisyl complexes **18´** and **20´** (1.407 Å and 1.408 Å), and the d(N-C_6) bond lengths are significantly shorter in the dicationic state for [**18´**]$^{2+}$ and [**20´**]$^{2+}$ by some 0.012 - 0.016 Å (1.395 Å and 1.392 Å) and shorter still for the tolyl derivatives [**17´**]$^{2+}$ and [**19´**]$^{2+}$ by 0.031 - 0.036 Å (1.380 Å and 1.377 Å). For **17´**, **18´**, **19´**, [**17´**]$^{2+}$ and [**18´**]$^{2+}$ the two phenyl rings of the bridge and the P-Pt-P axis are in plane, as the averaged dihedral angle Ω (average of ∠(P_1-Pt-C_3-C_4) and ∠(P_2-Pt-C_3-C_8)) reaches a maximum value of 12.6 ° for [**18´**]$^{2+}$. In general this torsion angle is larger (> 23 °) for complexes with triphenylphosphine ligands **20´**, [**19´**]$^{2+}$ and [**20´**]$^{2+}$, as expected due to the increased steric interactions.

Table 22: Important computed bond lengths for [17-20]$^{n+}$

	17´	**18´**	**19´**	**20´**	**[17´]$^{+}$**	**[18´]$^{+}$**	**[19´]$^{+}$**	**[20´]$^{+}$**	**[17´]$^{2+}$**	**[18´]$^{2+}$**	**[19´]$^{2+}$**	**[20´]$^{2+}$**
d(N-C_6) /Å	1.411	1.407	1.413	1.408	1.403	1.401	1.405	1.404	1.380	1.395	1.377	1.392
	1.411	1.406	1.413	1.408	1.373	1.385	1.371	1.383	1.379	1.395	1.377	1.392
d(N-$C_{9/16}$) /Å	1.418	1.420	1.418	1.420	1.422	1.422	1.421	1.422	1.421	1.410	1.422	1.412
	1.419	1.421	1.418	1.420	1.426	1.416	1.427	1.417	1.421	1.410	1.422	1.412
d(C≡C) /Å	1.227	1.227	1.225	1.225	1.228	1.227	1.226	1.225	1.233	1.230	1.232	1.229
	1.227	1.227	1.225	1.225	1.238	1.234	1.237	1.233	1.233	1.230	1.232	1.229
d(Pt-C_1) /Å	2.028	2.029	2.029	2.029	2.017	2.021	2.017	2.021	2.010	2.016	2.011	2.015
	2.028	2.028	2.029	2.029	1.998	2.009	2.002	2.011	2.009	2.016	2.011	2.016

For the mixed-valence monocationic structures [**17´ – 20´**]$^+$, minima with clearly localised electronic structures were obtained. In each case a significant asymmetry in the two halves of the molecule was observed and the corresponding d(N-C_6) distances differed by at least 0.16 Å (Table 22), clearly pointing towards a localization of the redox event in [**17´ – 20´**]$^+$ to one amine. Spin density plots for [**17´ - 20´**]$^+$ are shown in Figure 58 and the orbital population data for the mixed valence compounds are given in Table 23 - Table 26.

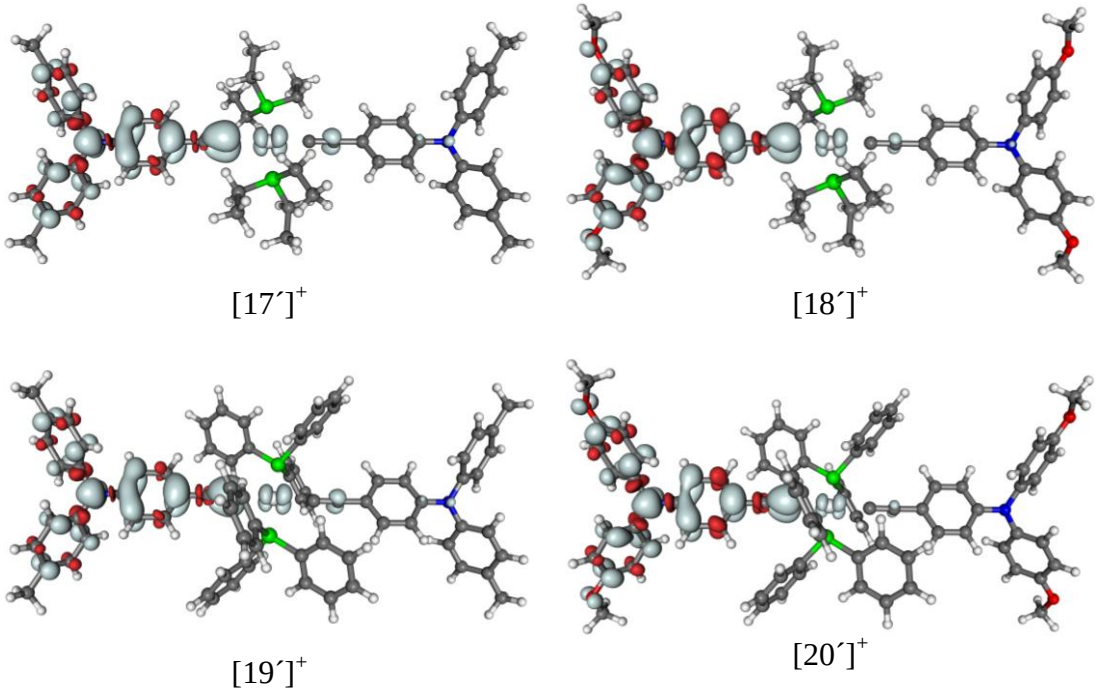

Figure 58: Spin density isosurface plots (±0.002 a.u.) of [17´ – 20´]$^+$.

Table 23: Orbital energies (E_{orb}) and contributions from Mulliken population analysis for [17′]$^+$.

Orbital	E_{orb}/eV	Contributions/%				
		$Ar_2C_6H_4$	C≡C	$Pt(PEt_3)_2$	C≡C	$C_6H_4Ar_2$
spin–density	/	68	19	7	3	6
233 β*	–1.25	52	14	18	5	7
233 α*	–1.50	65	15	9	2	1
232 β*	–4.36	64	19	6	2	0
232 α	–5.6	0	0	3	12	79
231 β	–5.55	3	0	2	11	74
231 α	–6.49	52	15	9	6	7
230 β	–6.64	17	7	13	19	34
230 α	–6.94	26	0	5	22	38
229 β	–7.15	0	6	24	62	3
229 α	–7.17	0	5	24	62	3
228 β	–7.22	37	17	2	9	26
228 α	–7.51	0	33	52	0	0
227 β	–7.49	0	34	50	0	0
227 α	–7.51	0	0	0	0	92
226 β	–7.50	0	0	0	0	93
226 α	–7.56	10	6	4	0	67

*unoccupied orbital.

Table 24: Orbital energies (E_{orb}) and contributions from Mulliken population analysis for $[18']^+$.

Orbital	E_{orb}/eV	Contributions/%				
		$Ar_2C_6H_4$	C≡C	$Pt(PEt_3)_2$	C≡C	$C_6H_4Ar_2$
spin–density	/	81	13	4	1	1
249 β*	–1.20	56	14	17	4	4
249 α*	–1.40	66	14	9	2	0
248 β*	–4.26	76	12	4	1	0
248 α	–5.41	0	0	3	11	81
247 β	–5.39	1	0	2	11	78
247 α	–6.31	49	15	9	7	7
246 β	–6.44	12	10	13	18	34
246 α	–6.70	35	0	5	19	33
245 β	–7.01	0	0	0	0	92
245 α	–7.01	0	0	0	0	93
244 β	–7.02	33	19	2	9	27
244 α	–7.03	0	8	23	62	3
243 β	–7.02	0	8	23	61	2
243 α	–7.36	38	23	8	2	19
242 β	–7.37	0	37	50	0	0
242 α	–7.38	0	36	50	0	0
241 β	–7.45	94	0	0	0	0
241 α	–7.66	93	0	0	0	0
240 β	–7.67	0	0	1	0	96
240 α	–7.68	0	0	0	0	96
239 β	–7.68	0	0	94	0	0
239 α	–7.70	0	0	2	0	94

*unoccupied orbital.

Table 25: Orbital energies (E_{orb}) and contributions from Mulliken population analysis for [19´]$^+$.

Orbital	E_{orb}/eV	Contributions/%				
		$Ar_2C_6H_4$	C≡C	$Pt(PPh_3)_2$	C≡C	$C_6H_4Ar_2$
spin–density	/	69	21	5	2	6
305 β*	–1.24	41	12	25	5	6
305 α*	–1.47	61	14	14	2	0
304 β*	–4.29	64	20	6	2	0
304 α	–5.54	0	0	3	13	78
303 β	–5.50	3	0	2	12	75
303 α	–6.45	51	16	8	6	8
302 β	–6.60	12	6	11	22	37
302 α	–6.87	24	1	4	23	37
301 β	–7.02	0	8	15	59	3
301 α	–7.04	0	8	15	62	2
300 β	–7.13	36	19	4	10	12
300 α	–7.34	0	7	75	0	0
299 β	–7.37	0	7	74	0	0
299 α	–7.47	0	0	0	0	93
298 β	–7.46	0	0	0	0	93
298 α	–7.54	7	6	3	0	66
297 β	–7.57	0	0	0	1	91
297 α	–7.64	29	13	7	2	32
296 β	–7.68	0	0	0	0	90
296 α	–7.68	0	0	0	0	91
295 β	–7.68	0	1	82	3	0
295 α	–7.69	0	1	83	2	0
287 β	–8.01	80	0	3	0	0
287 α	–8.07	0	1	84	3	0
277 β	–8.63	76	6	2	4	2
277 α	–8.71	97	0	0	0	0

*unoccupied orbital.

Table 26: Orbital energies (E_{orb}) and contributions from Mulliken population analysis for [20´]$^+$.

Orbital	E_{orb}/eV	Contributions/%				
		$Ar_2C_6H_4$	C≡C	$Pt(PPh_3)_2$	C≡C	$C_6H_4Ar_2$
spin–density	/	81	15	3	1	0
321 β*	–1.16	48	12	22	4	1
321 α*	–1.36	64	13	12	2	0
320 β*	–4.21	76	14	3	1	0
320 α	–5.35	0	0	2	12	81
319 β	–5.33	0	0	2	12	79
319 α	–6.28	49	15	8	7	6
318 β	–6.41	9	9	11	22	36
318 α	–6.62	24	0	3	21	34
317 β	–6.82	8	12	12	39	9
317 α	–6.87	0	12	16	57	2
316 β	–6.93	21	23	8	26	2
316 α	–6.98	0	0	0	0	92
315 β	–6.98	0	0	0	0	92
315 α	–7.23	20	16	46	0	0
314 β	–7.32	0	4	78	0	0
314 α	–7.4	18	13	39	1	8
313 β	–7.44	94	0	0	0	0
313 α	–7.58	0	4	21	0	60
312 β	–7.57	0	3	65	1	19
312 α	–7.58	0	1	80	0	7
311 β	–7.57	0	8	41	1	35
311 α	–7.62	0	24	23	8	25
310 β	–7.61	0	22	17	8	36
310 α	–7.64	92	0	0	0	0

*unoccupied orbital.

To gain more insight into the origin of the electronic transitions observed in the UV-vis-NIR SEC studies and to confirm the identity of the IVCT bands, TDDFT calculations were performed for the mixed-valence monocations [**17´** – **20´**]$^+$ using the same basis sets, functionals and solvent models as described above. The

assignment of the broad low-energy NIR-band of [**17´ - 20´**]$^{+}$, peak centre around 5000 to 6000 cm^{-1}, to an IVCT is straightforward on the basis of the quantum-chemical results (Figure 59, Table 21). The lowest energy transition (5572 cm^{-1}, β-HOMO→ β -LUMO 96% **(17)**, 5628 cm^{-1}, β-HOMO→ β-LUMO 96.8% **(18)**, 5716 cm^{-1}, β-HOMO→ β-LUMO 96% **(19)**, 5626 cm^{-1}, β-HOMO→ β-LUMO 97.1% **(20)**) has appreciable N→N^{+} character with a significant contribution from the ethynyl parts of the bridge. The mixing of platinum d-orbital character with the alkynyl π-system in the ground state is relatively limited, and there is only a small contribution from the Pt d-orbitals to the β-HOMO (2 %) and β-SOMO (6 %).

The TDDFT calculations also suggest that the intense asymmetric band envelope observed in the experimental spectrum at around 10000 cm^{-1} arises from two excitations, computed at 11252 cm^{-1} and 12046 cm^{-1} in [**17´**]$^{+}$. The transition at 11252 cm^{-1} is calculated to have substantial β-HOMO–1 (230β) → β-SOMO (69 % contribution) and β-HOMO–3 (228β) → β-SOMO (12 % contribution) character (Figure 13). The β-HOMO–1 and the 228β orbital are both unevenly distributed over the molecular backbone (Figure 6) and, whilst the β-HOMO–1 exhibits noticeable Pt(d)/ C≡C (13/26 %) character, there is substantially less d-orbital character (2 %) in 228β. Thus the transition at 11252 cm^{-1} also exhibits charge transfer character and is best described as a π→N^{+} excitation with considerably more bridge character in the donor orbital than for the IVCT transition at 5572 cm^{-1} (Figure 58). The transition at 12046 cm^{-1} arises from transitions between β-HOMO–4 (227β) (41 % contribution), β-HOMO–2 (229β) (34 % contribution) and the β-SOMO (Figure 58). Both donor orbitals are mainly localised in the metal coordination sphere (50 % and 24 %) and the ethynyl parts of the bridge (34 % and 67 %) whilst the acceptor orbital

is triarylamine centred, giving this transition significant MLCT (Pt→N^+) character. Four low-intensity excitations are computed for [**17′**]$^+$ between 15000 and 20000 cm^{-1}, consistent with the observation of multiple transitions in this range (Figure 59). The calculated transitions at 15790 cm^{-1} (μ_t = 1.0 D) and 17548 cm^{-1} (μ_t = 0.2 D) have significant MLCT character, while the excitation at 16162 cm^{-1} (μ_t = 1.3 D) corresponds to a π→N^+ transition. The highest energy calculated excitation at 19679 cm^{-1} (μ_t = 1.7 D) can be attributed to an intra-ligand transition associated with the oxidised triarylamine moiety.

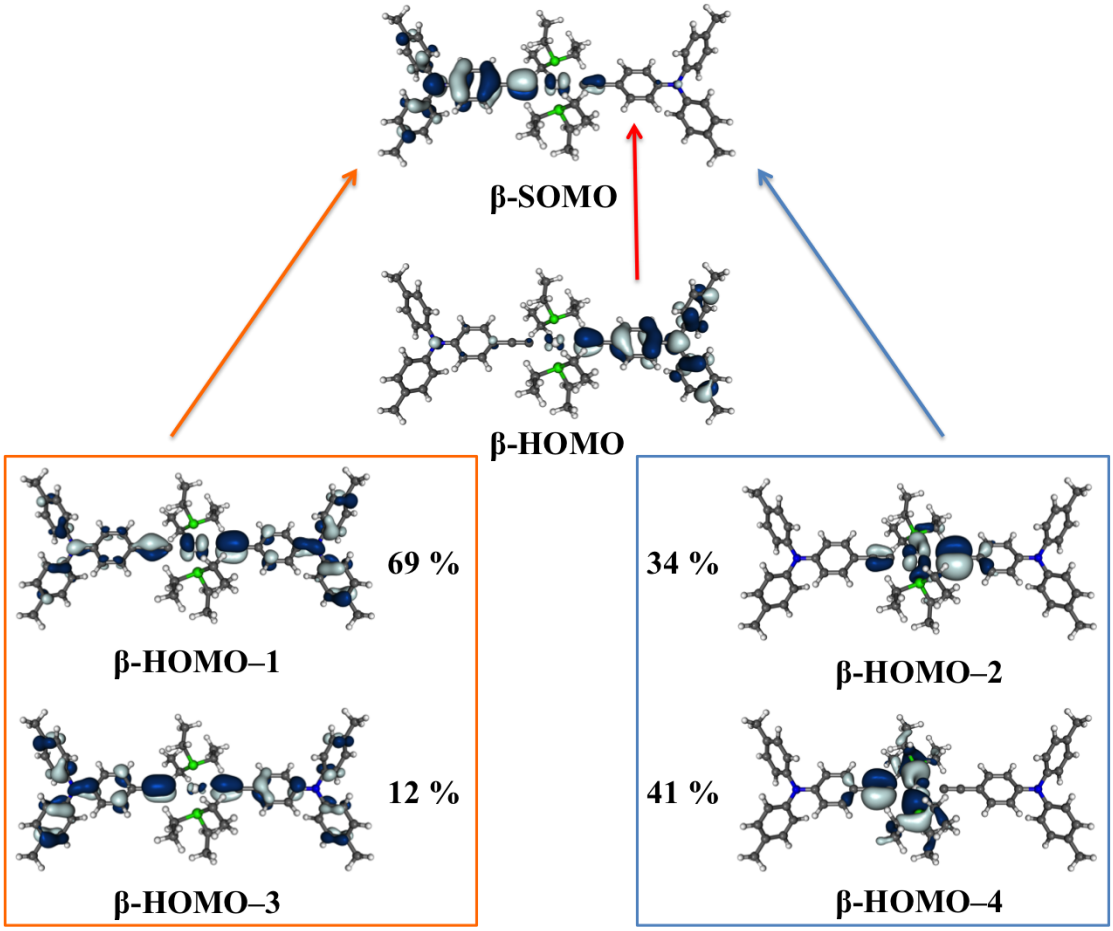

Figure 59: Isosurface plots (±0.03 a.u.) of the orbitals involved in the first three UV-vis-NIR transitions for monocationic radical [17′]$^+$; transition energies and transition dipole moments are given in parentheses.

The computed transitions between 15000 and 20000 cm^{-1} change appreciably when going from tolyl ([**17´**]$^+$) to anisyl ([**18´**]$^+$) substituents on the amine moieties (Table 27), consistent with experimental observation. The experimental data for **[18]**$^+$ in this region is dominated by an intense band centred at 14500 cm^{-1}, which compares with the less intense broad band in **[17]**$^+$ between 14000 and 20000 cm^{-1}. The TDDFT calculations for [**18´**]$^+$ feature two excitations of similar energy at 16000 cm^{-1} and 16529 cm^{-1}. While the first exhibits a relatively low transition dipole moment (μ_t = 1.6 D), the second is more intense (μ_t = 4.9 D) and thus is likely to be the major contributor to the experimentally observed absorption band. The character of these two transitions differs appreciably. The lower-energy, lower-intensity excitation at 16000 cm^{-1} originates from delocalised orbitals (244β and 246β) and goes to the β-SOMO (248β). Thus it is best described in terms of a $\pi \rightarrow N^+$ transition (Table 27). The higher-energy, more intense excitation at 16529 cm^{-1} originates from a single orbital, which is distributed over the same $Ar_2NC_6H_4C{\equiv}C$ moiety (94%) as the β-SOMO. The excitation thus exhibits no charge-transfer character and is better described as a localised transition arising from the amine radical cation (Table 27). The TDDFT calculations also predict three more low-intensity excitations at 17108, 19112, and 19562 cm^{-1} ($\mu_t \leq 0.6$ D), which are unlikely to have a significant role in determining the overall appearance of the absorption spectrum.

Table 27: Calculated excited state parameters for [17´]+ and [18´]+: UV-vis-NIR transition energies Etrans/cm–1 and transition dipole moments μt/D, and character of the excitation.

	[17´]$^+$		**[18´]$^+$**	
#	E_{trans}/cm$^-$ $_1$ (μ_t/D)	Character	E_{trans}/cm$^-$ $_1$ (μ_t/D)	Character
1	5572 (15.3)	N→N$^+$, intervalence CT	5628 (13.0)	N→N$^+$, intervalence CT
2	11252 (6.6)	π→N$^+$ bridge to amine CT	11062 (8.2)	π→N$^+$ bridge to amine CT
3	12046 (4.0)	Pt$^+$→N$^+$ metal to amine ligand CT	13588 (1.2)	Pt$^+$→N$^+$ metal to amine ligand CT
4	15790 (1.0)	Pt$^+$→N$^+$ metal to amine ligand CT	16000 (1.6)	π→N$^+$ bridge to amine CT
5	16162 (1.3)	π→N$^+$ bridge to amine ligand CT	16529 (4.9)	intra-ligand transition at triarylamine
6	17548 (0.2)	Pt$^+$→N$^+$ metal to amine ligand CT	17108 (0.2)	Pt$^+$→N$^+$ metal to amine ligand CT
7	19679 (1.7)	intra-ligand transition at triarylamine	19112 (0.2)	Pt$^+$→N$^+$ metal to amine ligand CT

Results for the triphenyl phosphine derivatives show similar composition to the triethylphosphine derivatives (Table 28). Orbital plots and details of the individual transitions involved in the principal transitions for all compounds are given in Table 29 - Table 32 and Figure 60 and Figure 61.

Table 28: Calculated excited state parameters for $[19']^+$ and $[20']^+$. UV-vis-NIR transition energies E_{trans}/cm^{-1}, and character for the first three excitations.

$[19']^+$		$[20']^+$	
E_{trans}/cm^{-1} (μ_t/D)	Character	E_{trans}/cm^{-1} (μ_t/D)	Character
5716 (13.8)	$N \rightarrow N^+$ IVCT	5626 (11.0)	$N \rightarrow N^+$ IVCT
11295 (5.5)	mixed $\pi \rightarrow N^+$ and $Pt^+ \rightarrow N^+$ MLCT	10928 (8.8)	mixed $\pi \rightarrow N^+$ and $Pt^+ \rightarrow N^+$ MLCT
11960 (5.8)	mixed $\pi \rightarrow N^+$ and $Pt^+ \rightarrow N^+$ MLCT	12798 (2.5)	mixed $\pi \rightarrow N^+$ and $Pt^+ \rightarrow N^+$ MLCT

Table 29: Calculated excited state parameters: UV-vis-NIR transition energies E_{trans}, transition dipole moments μ_t and main MO contributions for $[17']^+$.

#	E_{trans}/cm^{-1}	μ_t/D	Main contributions (%)
1	5572	15.3	231 β–> 232 β (96.0)
2	11252	6.6	230 β–> 232 β (68.7), 228 β–> 232 β (11.8)
3	12046	4.0	227 β–> 232 β (40.6), 229 β–> 232 β (34.2)
4	15790	1.0	229 β–> 232 β (54.5), 227 β–> 232 β (27.8)
5	16162	1.3	228 β–> 232 β (57.3), 230 β–> 232 β (15.8)
6	17548	0.2	223 β–> 232 β (97.4)
7	19679	1.7	221 β–> 232 β (48.4), 215 β–> 232 β (36.2)
8	20922	0.6	220 β–> 232 β (86.2), 219 β–> 232 β (5.3)
9	21021	2.5	221 β–> 232 β (45.0), 215 β–> 232 β (27.8)
10	21204	1.9	232 α–> 236 α (25.9), 231 β–> 236 β (18.5)

Table 30: Calculated excited state parameters: UV-vis-NIR transition energies E_{trans}, transition dipole moments μ_t and main MO contributions for [18´]$^+$.

#	E_{trans}/cm^{-1}	μ_t/D	Main contributions (%)
1	5628	13.0	247 β–> 248 β (96.8)
2	11062	8.2	246 β–> 248 β (74.2), 244 β–> 248 β (20.4)
3	13588	1.2	243 β–> 248 β (47.6), 242 β–> 248 β (43.5)
4	16000	1.6	244 β–> 248 β (70.7), 246 β–> 248 β (20.8)
5	16529	4.9	241 β–> 248 β (96.7)
6	17108	0.2	243 β–> 248 β (49.1), 242 β–> 248 β (48.8)
7	19112	0.2	239 β–> 248 β (95.6)
8	19562	0.6	245 β–> 248 β (99.1)
9	20993	0.6	233 β–> 248 β (70.2), 230 β–> 248 β (24.5)
10	21012	1.7	248 α–> 252 α (23.7), 247 β–> 251 β (18.6)

Table 31: Calculated excited state parameters: UV-vis-NIR transition energies E_{trans}, transition dipole moments μ_t and main MO contributions for [19´]$^+$.

#	E_{trans}/cm^{-1}	μ_t/D	Main contributions/%
1	5716	13.8	303 β–> 304 β (96.0)
2	11295	5.5	302 β–> 304 β (47.7), 301 β–> 304 β (25.9)
3	11960	5.8	300 β–> 304 β (35.1), 301 β–> 304 β (19.7)
4	15630	1.9	300 β–> 304 β (41.1), 301 β–> 304 β (30.8)
5	16791	0.2	299 β–> 304 β (37.7), 301 β–> 304 β (18.5)
6	18457	0.2	295 β–> 304 β (68.4), 282 β–> 304 β (7.6)
7	19194	0.3	299 β–> 304 β (45.7), 294 β–> 304 β (29.8)
8	19739	1.3	287 β–> 304 β (28.2), 277 β–> 304 β (25.5)
9	21069	1.8	303 β–> 305 β (11.7), 304 α–> 310 α (11.3)
10	21260	0.4	286 β–> 304 β (58.6), 285 β–> 304 β (13.0)

Table 32: Calculated excited state parameters: UV-vis-NIR transition energies E_{trans}, transition dipole moments μ_t and main MO contributions for $[20']^+$.

#	E_{trans}/cm^{-1}	μ_t/D	Main contributions/%
1	5626	11	319 β–> 320 β (97.1)
2	10928	8.8	318 β–> 320 β (64.6), 317 β–> 320 β (21.3)
3	12798	2.5	316 β–> 320 β (60.0), 317 β–> 320 β (14.4)
4	15379	1.6	317 β–> 320 β (53.3), 318 β–> 320 β (29.5)
5	16838	4.6	313 β–> 320 β (96.4)
6	18312	0.4	314 β–> 320 β (44.2), 310 β–> 320 β (16.4)
7	19651	0.2	312 β–> 320 β (65.4), 311 β–> 320 β (17.1)
8	19813	0.5	315 β–> 320 β (89.7), 314 β–> 320 β (4.8)
9	19835	0.2	314 β–> 320 β (41.4), 310 β–> 320 β (19.8)
10	20783	0.6	294 β–> 320 β (59.6), 292 β–> 320 β (23.7)

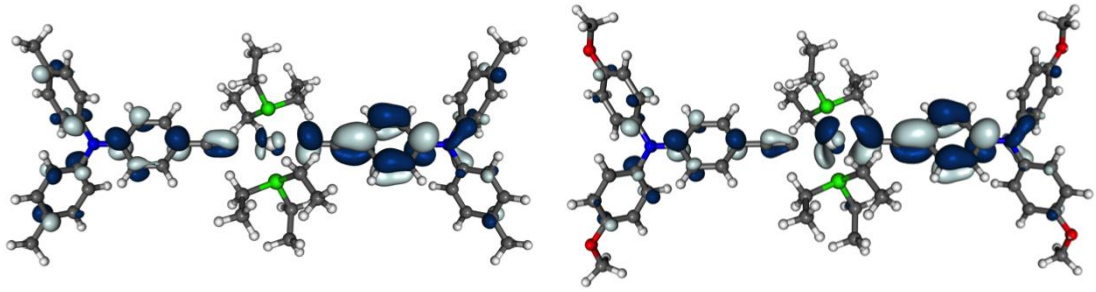

236β 252α

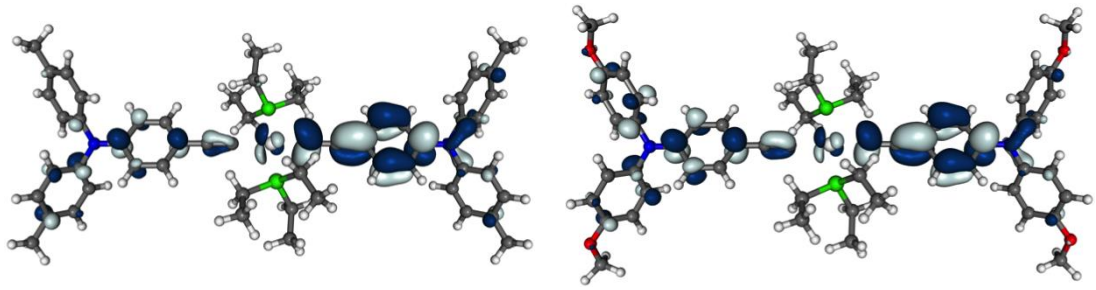

236α 251β

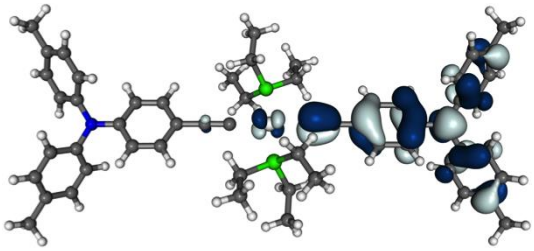

232α

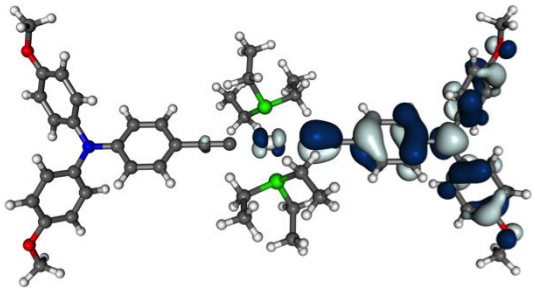

248α

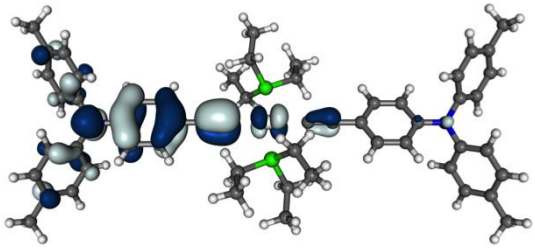

232β

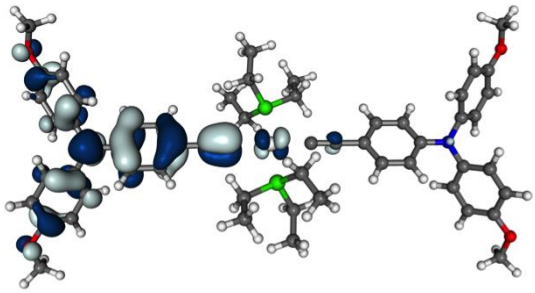

248β

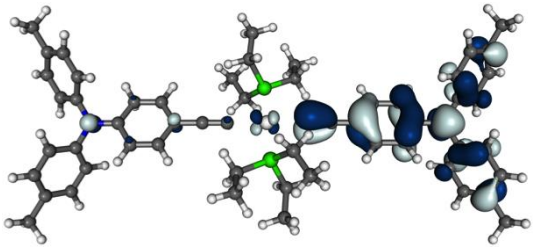

231β

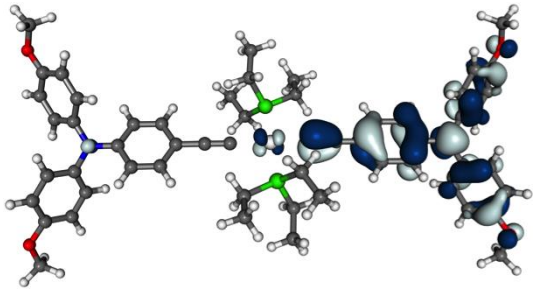

247β

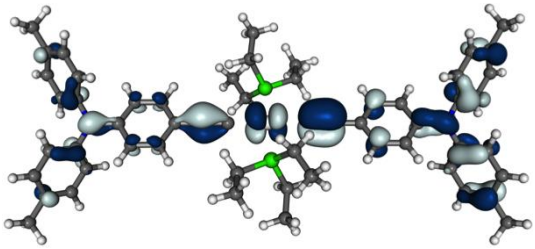

230β

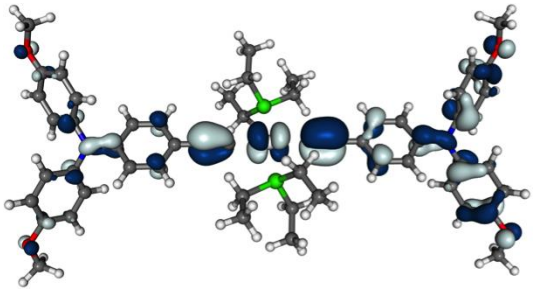

246β

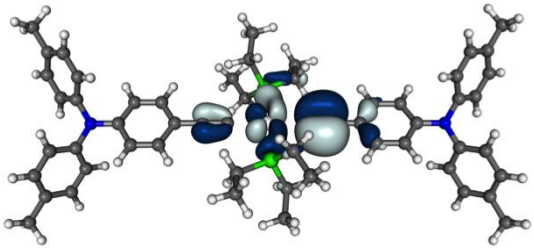

229β

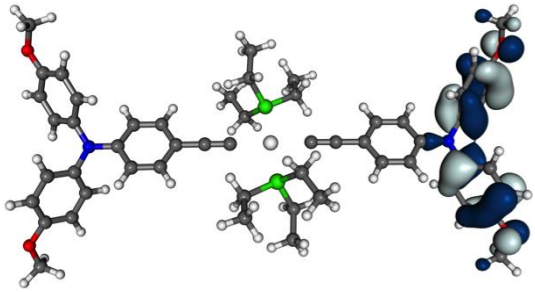

245β

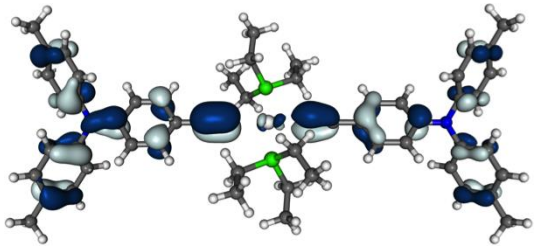

228β

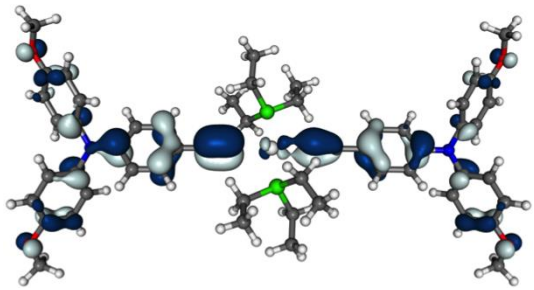

244β

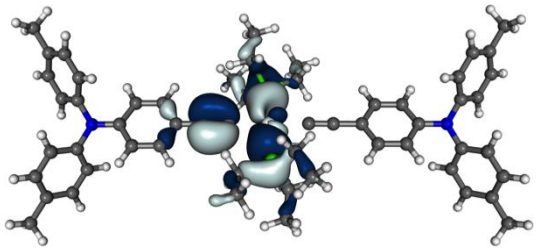

227β

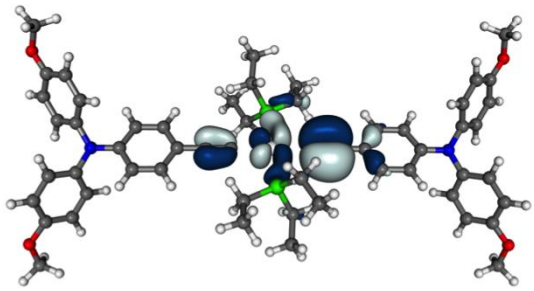

243β

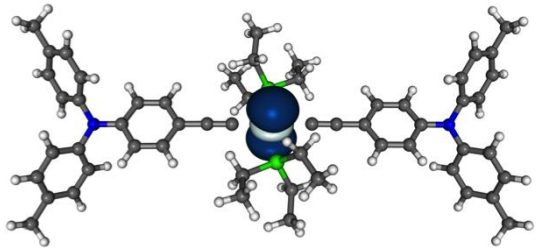

223β

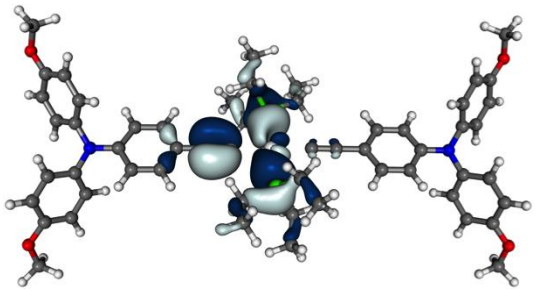

242β

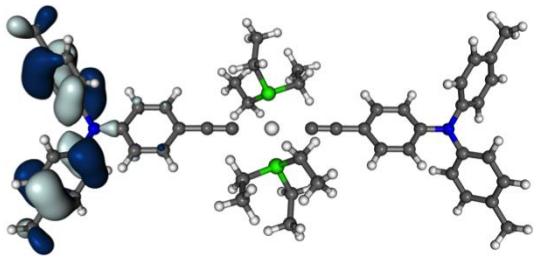

221β

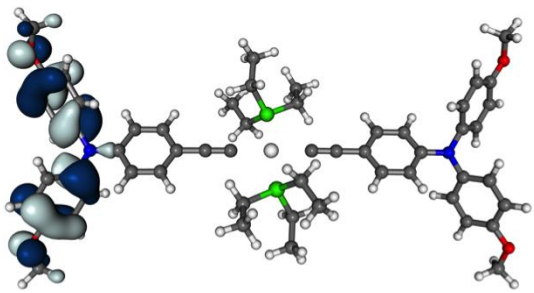

241β

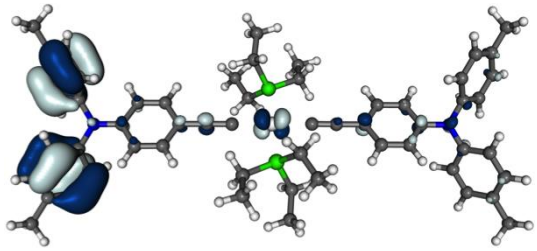

220β

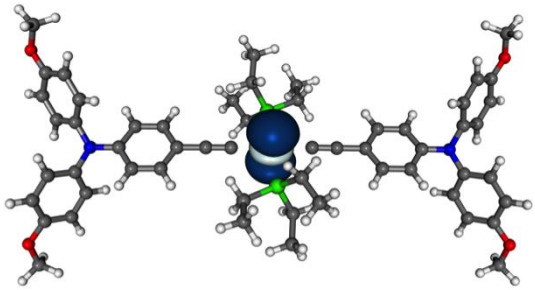

239β

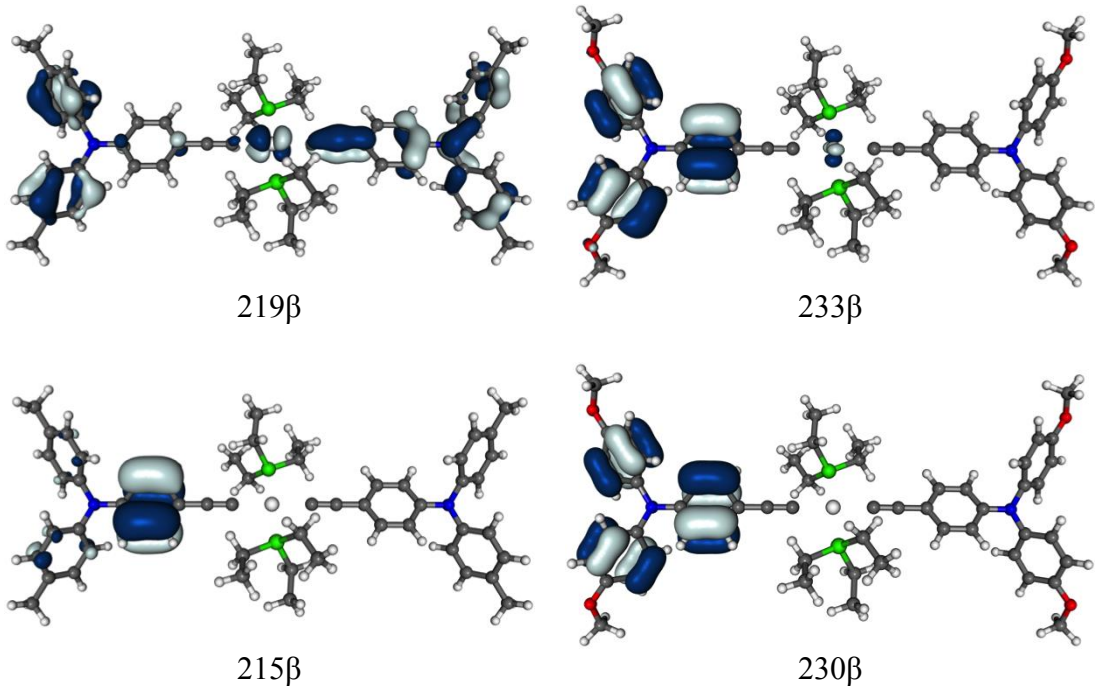

Figure 60: Isosurface plots (±0.03 a.u.) of the orbitals involved in the first 10 UV–vis–NIR transitions for monocationic radicals $[17']^+$ (left) and $[18']^+$ (right).

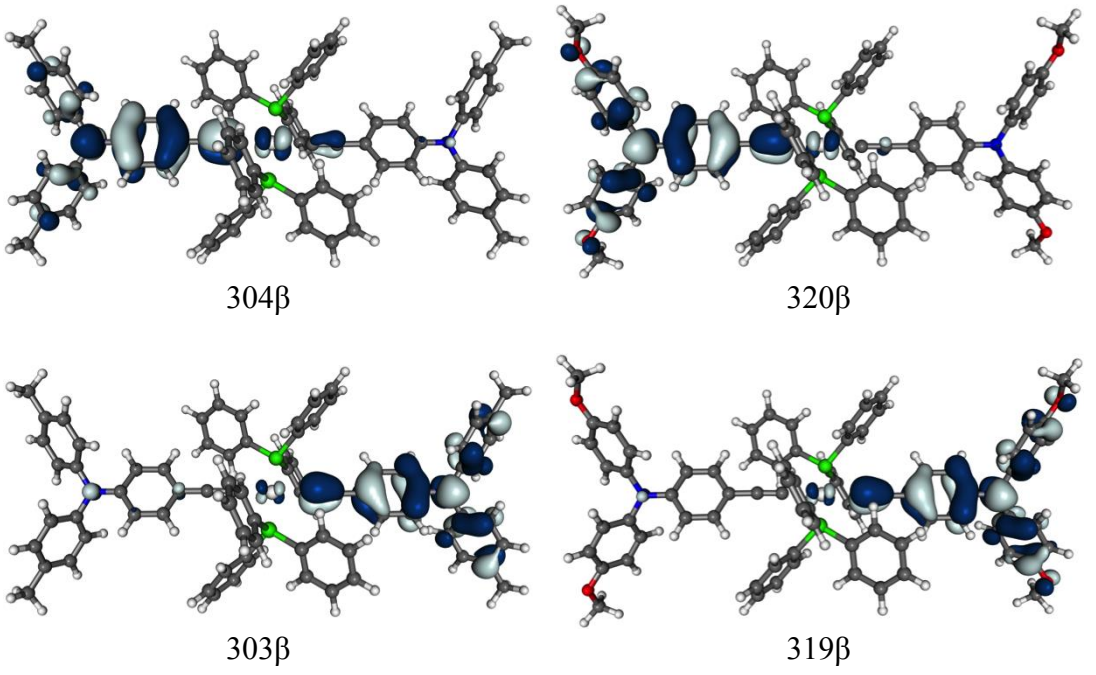

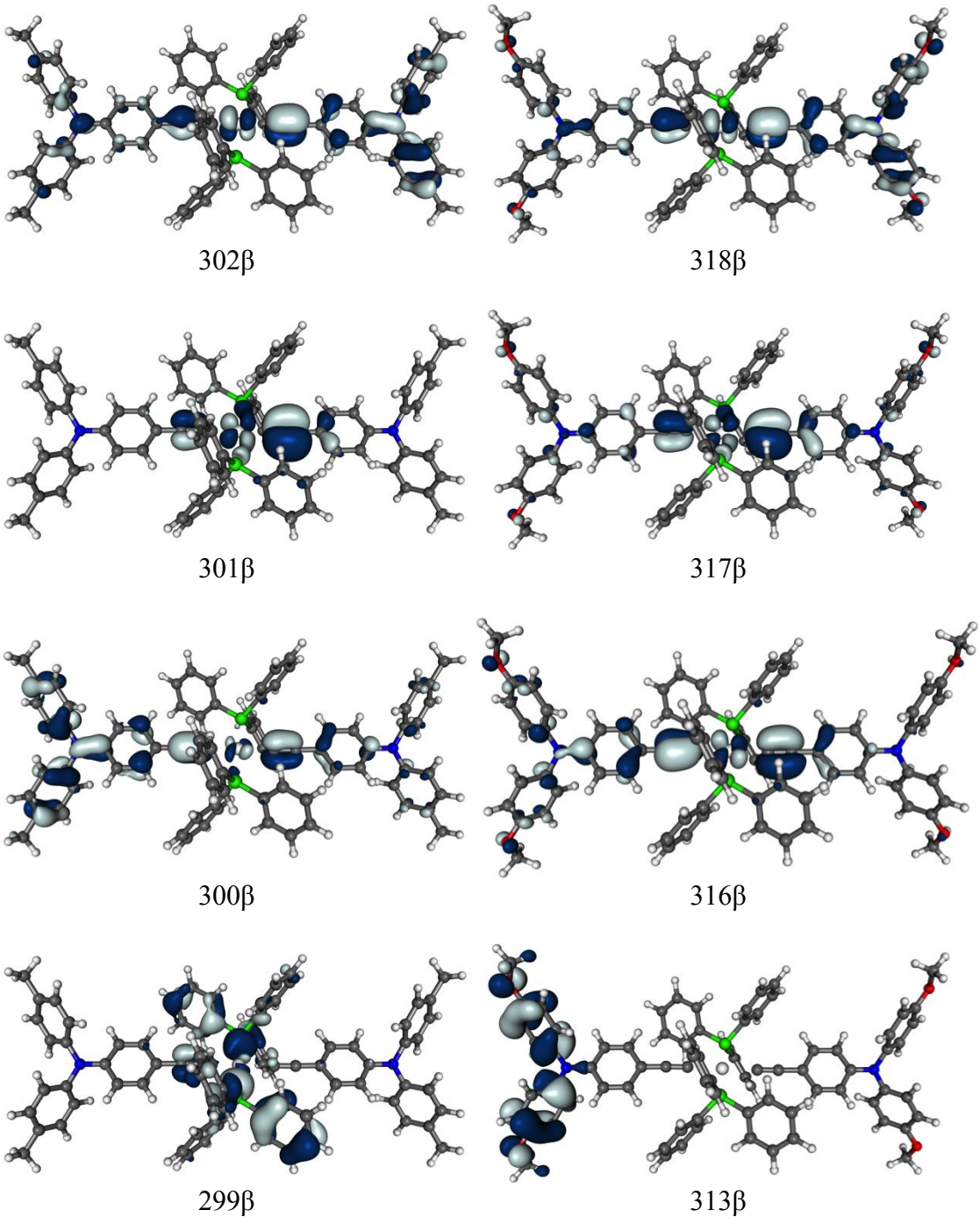

Figure 61: Isosurface plots (±0.03 a.u.) of the orbitals involved in the first 5 UV–vis–NIR transitions for monocationic radicals $[19']^+$ (left) and $[20']^+$ (right).

3.3.7. Conclusions

The synthesis of a range of different platinum-bridged bis-triarylamine compounds has been carried out, with the compounds bearing different amine and / or ancillary phosphine ligands. The compounds are prepared in good yield and the ethynyltriarylamine unit is suitable as an IR and UV-vis NIR probe. Electrochemical studies of the compounds **17 – 20** show that across the series the compounds undergo two closely positioned oxidations, and as such are suitable for further study by SEC. Spectroelectrochemical studies show that the nature of the UV-vis-NIR transitions observed upon oxidation of the platinum-bridged bis-triarylamine compounds **17** – **20** are consistent across the series, and that the effect of the phosphine ligand on most of them is relatively insignificant. The IR SEC reults demonstrate that there is limited involvement of the ethynyl linker in the frontier orbitals.

DFT calculations have shown that there is very little involvement of the phosphine moieties on the frontier orbitals of the compounds, thus changing the electron-donating ability of the phosphine has no appreciable effect on the electronic transitions observed. These transitions have been accurately modelled using a computational protocol, allowing a more detailed investigation than was possible a few years ago. As expected for localised MV systems, the lowest energy transition at around 5600 cm^{-1} corresponds to an IVCT excitation for all bis-triarylamine complexes [**17 - 20**]$^{+}$. Generally the agreement between computed and experimentally observed IVCT excitation energies is better for the tolyl complexes **[17´]**$^{+}$ and **[19´]**$^{+}$ than for the anisyl substituted compounds **[18´]**$^{+}$ and **[20´]**$^{+}$. While the assignment of the second excitation to a CT transition from a delocalised π

orbital and of the third to a CT from the platinum moiety to the cationic triarylamine unit is straightforward for **[17´]**$^{+}$ and **[18´]**$^{+}$, those excitations start to mix for the triphenylphosphine complexes **[19´]**$^{+}$ and **[20´]**$^{+}$.

The electronic properties of compounds **17** – **20** were accurately modeled and could be analyzed in detail using a computational protocol based on the BLYP35 functional and a suitable solvent model. The results show that despite the apparent simplicity of the electronic spectra the assignment of the transitions is more complex than previously recognized and as such suitable quantum chemical approaches provide a real insight in to the nature of such transitions. The combination of computational methods along with careful consideration of the redox substituents and bridging moieties thus allows compounds of mixed valence nature displaying facile intra-molecular charge transfer to be designed and prepared with specific properties in mind.

3.4. Experimental

3.4.1. General Conditions

Solvent purification and characterisation of compounds was carried out as detailed in Chapter 2. The compounds and complexes 4-trimethylsilylethynylenephenylenedi-p-tolylamine,[41] 4-ethynylenephenylenedi-p-anisylamine,[65] $Pt(PPh_3)_4$,[66] $PtCl_2(PPh_3)_2$,[67] $PtCl_2(PEt_3)_2$,[68] $Pd(PPh_3)_4$,[69] $Pt(C_6H_4CH_3\text{-}4)I(PPh_3)_2$,[70] and dppf[71] were prepared by the literature methods.

Electrochemical analyses were carried out using an EcoChemie Autolab PGSTAT-30 potentiostat, with platinum working, platinum counter and platinum pseudo

reference electrodes, from solutions in CH_2Cl_2 containing 0.1 M supporting electrolyte, $\nu = 100$ mV s^{-1}. The decamethylferrocene/decamethylferricenium ($FeCp^*_2$/ $FeCp^*_2{}^+$) couple was used as an internal reference for potential measurements such that the $FeCp_2$/ $FeCp_2{}^+$ couple falls at 0.00 V ($FeCp^*_2$/ $FeCp^*_2{}^+$ = –0.48 V). Spectroelectrochemical measurements were made in an OTTLE cell of Hartl design from CH_2Cl_2 solutions containing 0.1 M NBu_4PF_6 or NBu_4BArF_4 electrolyte. The cell was fitted into the sample compartment of the Thermo Nicolet 6700 IR or Lambda 900 UV-Vis NIR spectrophotometer, and electrolysis in the cell was performed with a PGSTAT-30 potentiostat.

3.4.2. Preparation of $[NH(C_6H_4CH_3\text{-}4)_2]$ (14)

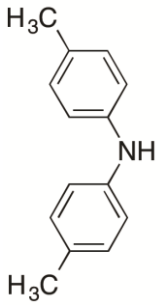

An oven dried Schlenk flask was charged with dry toluene (50 mL) and the solvent degassed. To the solvent, para-toluidine (2.23 g, 20.8 mmol), 4-iodotoluene (5.00 g, 22.9 mmol), $[Pd_2(dba)_3]$ (0.19 g, 0.21 mmol), dppf (0.35 g, 0.63 mmol) and sodium tert- butoxide (3.00 g, 31.2 mmol) were added and the mixture stirred at reflux for 20 h. The mixture was cooled, filtered and the solvent removed in vacuo. The residue was purified by silica column chromatography eluting with hexane increasing to a hexane:acetone (95:5) mixture. The eluent was concentrated in vacuo to 5 mL and the precipitated white solid collected and washed with cold hexane (3 x 5 mL) to give $[NH(C_6H_4CH_3\text{-}4)_2]$ (2.77 g, 68 %). ^{1}H NMR ($CDCl_3$): δ 2.30 (s, 6H, CH_3), 5.51

(s, 1H, NH), 6.95 (d, *J* = 8 Hz, 4H, Ar) 7.07 (d, J=8Hz, 4H, Ar). ^{13}C NMR($CDCl_3$): δ 20.6 (CH_3), 117.9 (Ar_o), 129.8 a(Ar_m), 130.2 (Ar_p), 141.1 (Ar_i). ES-MS(+) (m/z): 197.2 $[M+H]^+$.

3.4.3. Preparation of $[N(C_6H_4Br\text{-}4)(C_6H_4CH_3\text{-}4)_2]$ (15)

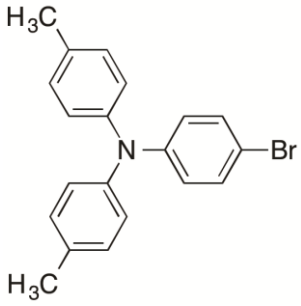

An oven dried Schlenk flask was charged dry toluene (50 mL) and the solvent degassed. To this solution, **14** (2.38 g, 12.0 mmol), 1-bromo-4-iodobenzene (3.76 g, 13.2 mmol), $[Pd_2(dba)_3]$ (0.11 g, 0.12 mmol), dppf (0.20 g, 0.36 mmol) and sodium tert-butoxide (1.74 g, 18.1 mmol) were added and the mixture stirred at reflux for 60 h. The mixture was cooled, filtered and the solvent removed in vacuo. The residue was treated with petroleum ether (30 mL) and the persistent solid removed by filtration, and the precipitate washed with petroleum ether (3 x 30 mL). The combined organic solutions were concentrated in vacuo to ca. 10 ml, which upon standing deposited a white precipitate. The precipitate was collected by filtration, and washed with cold petroleum ether (5 mL) to give **15** (2.84 g, 69 %). ^{1}H NMR ($CDCl_3$): δ 2.32 (s, 6H, CH_3), 6.90 (d, *J* = 9 Hz, 2H, Ar), 6.98 (d, J = 8 Hz, 4H, Ar), 7.08 (d, J = 8 Hz, 4H, Ar), 7.28 (d, *J* = 9 Hz, 2H, Ar). ^{13}C NMR ($CDCl_3$): δ 20.8 (CH_3), 113.6 (Ar_p'), 123.9 (Ar_o), 125.0 (Ar_o'), 130.3 (Ar_m), 131.9 (Ar_m'), 132.9 (Ar_p), 145.0 (Ar_i), 147.4 (Ar_i'). ESI-MS(+) (m/z): 351.1 $[M+H]^+$.

3.4.4. Preparation of $[N(C_6H_4\text{-}4\text{-}C{\equiv}CSiMe_3)(C_6H_4CH_3\text{-}4)_2]$

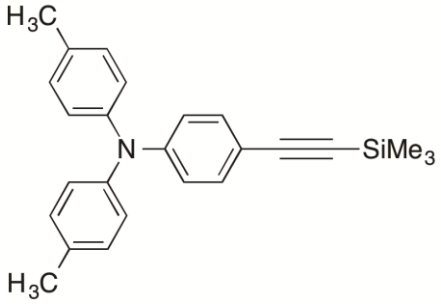

An oven dried Schlenk flask was charged dry triethylamine (75 mL) and the solvent degassed. To this solution, **15** (1.80 g, 5.12 mmol), $HC{\equiv}CSiMe_3$ (0.85 mL, 6.15 mmol), $[PdCl_2(PPh_3)_2]$ (0.18 g, 0.25 mmol) and copper(I) iodide (0.02 g, 0.13 mmol) were added and the mixture stirred under reflux for 17 h. The mixture was cooled, filtered and the solvent removed under high vacuum. The residue was treated with hexane (30 mL) and the precipitated solid removed by filtration and washed with hexane (3 x 10 mL). The solvent was removed from the combined filtrates in vacuo and the residue purified by silica column chromatography in hexane increasing polarity to a hexane:CH_2Cl_2 (8:2) mixture. The solvent was removed in vacuo to leave a yellow oil that solidifies on standing, affording $[N(C_6H_4\text{-}4\text{-}C{\equiv}CSiMe_3)(C_6H_4Me\text{-}4)_2]$ (1.37 g, 73 %). ^{1}H NMR ($CDCl_3$): δ 0.25 (s, 9H, $SiMe_3$), 2.33 (s, 6H, CH_3), 6.90 (d, J = 9 Hz, 2H, Ar), 6.98 (d, J = 8 Hz, 4H, Ar), 7.08 (d, J = 8 Hz, 4H, Ar), 7.28 (d, J = 9 Hz, 2H, Ar). ^{13}C NMR ($CDCl_3$): δ 0.00 ($SiMe_3$), 14.0 (CH_3), 92.5 (C:$CSiMe_3$), 105.6 (C:$CSiMe_3$) 114.8 ($Ar_{p'}$), 120.8 ($Ar_o{}^0$), 125.1 (Ar_o), 129.9 (Ar_m), 132.7 ($Ar_m{}^0$), 133.1 (Ar_p), 144.6 (Ar_i), 148.3 ($Ar_i{}^0$). ESI-MS(+) (m/z): 370.3 $[M+H]^+$.

3.4.5. Preparation of $[N(C_6H_4\text{-}4\text{-}CCH)(C_6H_4CH_3\text{-}4)_2]$ (16-CH_3)

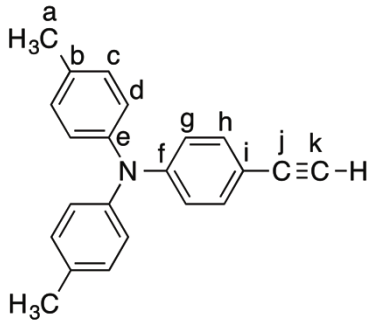

An oven dried Schlenk flask was charged with methanol (20 mL), THF (10 mL) and $[N(C_6H_4\text{-}4\text{-}C{\equiv}CSiMe_3)(C_6H_4Me\text{-}4)_2]$ (0.88 g, 2.39 mmol). To this solution, tetrabutylammoniumfluoride 1 M in THF (2.4 mL, 2.39 mmol) was added and the mixture stirred for 24 hours at room temperature. The solvent was removed in vacuo and the residue dissolved in CH_2Cl_2 (30 mL), washed with water (2 x 30 mL), separated, and the aqueous phase extracted with CH_2Cl_2 (3 x 30 mL). The combined organic phases were washed with brine (50 mL), dried over magnesium sulphate and the solvent removed in vacuo to yield an orange oil that solidifies on standing. Yield 0.60 g, 84%. ^{1}H NMR ($CDCl_3$): δ 2.33 (6H, s), 3.00 (1H, s), 6.91 (2H, m), 7.01 (4H, m), 7.09 (4H, m), 7.30 (2H, m); $^{13}C\{^1H\}$ NMR ($CDCl_3$): δ 20.87 (C_a, s), 75.85 (C_j, s), 84.16 (C_k, s) 113.65 (C_i, s), 120.77 (C_g, s), 125.30 (C_d, s), 130.06 (C_c, s), 132.94 (C_h, s), 133.41 (C_b, s), 144.59 (C_e, s), 148.74 (C_f, s); ESI-MS(+) *m*/*z*: 298.34 $[M+H]^+$

3.4.6. Preparation of *trans*-Pt{C≡CC$_6$H$_4$N(C$_6$H$_4$CH$_3$-4)$_2$}$_2$(PEt$_3$)$_2$ (17)

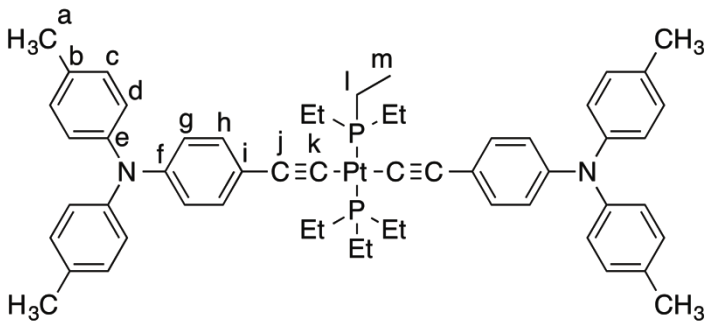

An oven dried Schlenk flask was charged with $HNEt_2$ (7 mL) and the solvent degassed. To this solution, $PtCl_2(PEt_3)_2$ (0.100 g, 0.199 mmol), **16-CH$_3$** (148 mg, 0.50 mmol) and CuI (1 mg, 0.006 mmol) were added and the mixture stirred for 15 h at room temperature. The solvent was removed in vacuo and the residue dissolved in CH_2Cl_2:Hexane (60:40) (2 mL) and purified by silica column chromatography using CH_2Cl_2:Hexane (60:40 → 70:30) The second fraction was collected and the solvent removed in vacuo to give a bright yellow solid. Yield 182 mg, 89 %. Crystals suitable for X-ray diffraction were grown from CH_2Cl_2:EtOH. ^{1}H NMR ($CDCl_3$) δ 1.34 (18H, m), 2.10 (12H, m) 2.22 (12H, s), 6.80 (4H, m), 6.89 (4H, m), 6.96 (8H, m), 7.05 (8H, m); ^{31}P NMR ($CDCl_3$) 11.0 (s, J(P-Pt) = 2385 Hz); ^{13}C{^{1}H} NMR ($CDCl_3$) δ 145.36 (C_e, s), 145.27 (C_f, s), 131.98 (C_b, s), 131.54 (C_h, s), 129.71 (C_c, s), 124.16 (C_d, s), 122.88 (C_g, s), 122.48 (C_i, s), 109.05 (C_j, s), 106.13 (C_k, s), 20.76 (C_a, s), 16.33 (C_l, t, J = 17.7 Hz), 8.37 (C_m, s). ASAP-MS(+) m/z: 1023.43 $[M]^+$. IR (CH_2Cl_2) ν(C≡C) 2100 cm^{-1}. Analysis found (calculated) %: C 65.54 (65.67), H 6.45 (6.50), N 2.79 (2.74).

3.4.7. Preparation of *trans*-Pt{C≡C$C_6H_4N(C_6H_4OCH_3$-4)$_2$}$_2$(PEt_3)$_2$ (18)

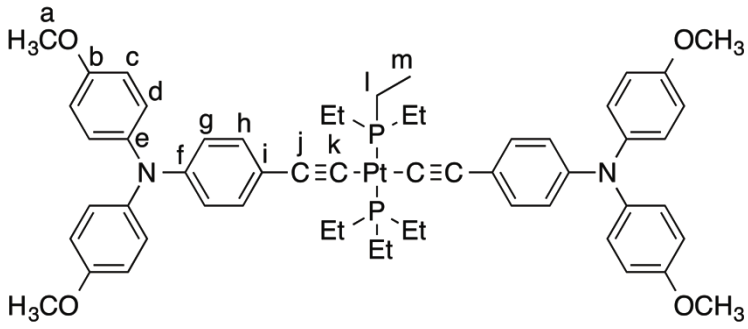

Compound **18** was prepared as described in the literature.[6] ^{1}H NMR ($CDCl_3$) δ 1.18 (18H, m), 2.14 (12H, m) 3.77 (12H, s), 6.78 (12H, m), 7.01 (8H, m), 7.09 (4H, m); ^{31}P NMR ($CDCl_3$) 11.5 (s, J(P-Pt) = 2383 Hz); ^{13}C{^{1}H} NMR ($CDCl_3$) δ 155.52 (C_b, s), 146.1 (C_e, s), 141.47 (C_f, s), 131.68 (C_h, s), 126.21 (C_c, s), 121.61 (C_i, s), 121.2 (C_g, s), 114.82 (C_d), 108.89 (C_j, s), 105.39 (C_k, s), 55.76 (C_a, s), 16.33 (C_l, vt, *J* = 17.7 Hz), 8.37 (C_m, s). ASAP-MS(+) *m*/*z*: 1087.41 $[M]^+$. IR (CH_2Cl_2) ν(C≡C) 2100 cm^{-1}.

3.4.8. Preparation of *trans*-Pt{C≡C$C_6H_4N(C_6H_4CH_3$-4)$_2$}$_2$(PPh_3)$_2$ (19)

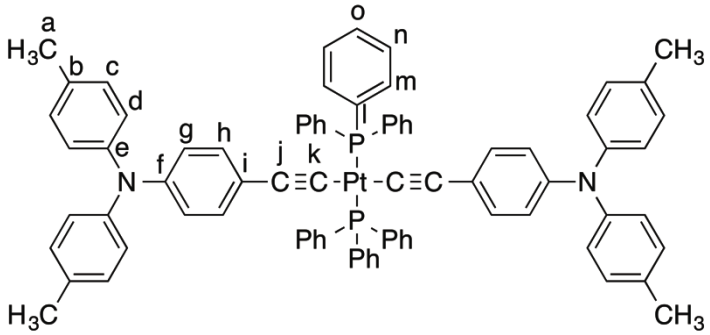

An oven dried Schlenk flask was charged with dry $HNEt_2$ (6 mL) and the solvent degassed. To the solution, $PtCl_2(PPh_3)_2$ (0.100 g, 0.126 mmol) was added to give a yellow suspension. Dry degassed DMF (3 mL), **16-CH$_3$** (94 mg, 0.316 mmol) and CuI (5 mg, 0.03 mmol) were added and the mixture stirred for 15 h under reflux to give a yellow precipitate. The mixture was cooled to ambient temperature and the solid filtered and washed with methanol (2 x 10 mL), hexane (2 x 10 mL) and ether

(2 x 10 mL). Yield 109 mg, 66 %. ^{1}H NMR ($CDCl_3$) δ 2.28 (12H, s, H_1), 6.07 (4H, m,), 6.56 (4H, m), 6.86 (8H, m), 6.99 (8H, m), 7.35 (18H, m), 7.80 (12H, m); ^{31}P NMR ($CDCl_3$) 18.73 (s, J(P-Pt) = 2663 Hz); ^{13}C{^{1}H} NMR ($CDCl_3$) 145.38 (C_e, s), 144.82 (C_f, s), 135.08 (C_n, vt, $J_{c\text{-}p}$ = 6.0 Hz), 131.78 (C_h, s), 131.61 (C_b, s), 130.03 (C_o, s), 129.59 (C_c, s), 127.75 (C_m, vt, $J_{c\text{-}p}$ = 5.4 Hz), 124.09 (C_d, s), 122.07 (C_g, s), 20.72 (C_a, s) other quaternary ^{13}C were not observed in the spectra; MALDI-MS(+) *m*/*z*: 1312.5 $[M]^+$. IR (CH_2Cl_2) ν(C≡C) 2106 cm^{-1}. Analysis found (calculated) %: C 73.12 (73.20), H 5.17 (5.07), N 2.21 (2.14).

3.4.9. Preparation of *trans*-Pt(C≡CC_6H_4N($C_6H_4OCH_3$-4)$_2$)$_2$(PPh_3)$_2$ (20)

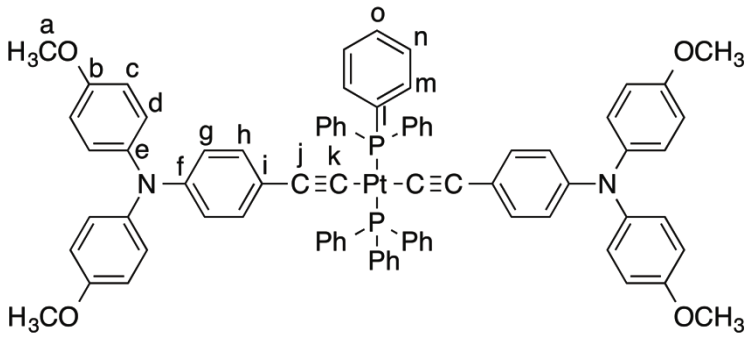

An oven dried Schlenk flask was charged with 4-ethynylenephenylenedi-p-anisylamine (229 mg, 0.696 mmol) in a solution of DCM (9.2 mL) and the solvent removed in vacuo. Dry degassed DMF (6 mL) and $HNEt_2$ (6 mL) were added and the solution degassed. To this solution, $PtCl_2(PPh_3)_2$ (0.250 g, 0.316 mmol) and CuI (5 mg, 0.03 mmol) were added and the mixture stirred for 15 h under reflux to give a yellow precipitate. The mixture was cooled to ambient temperature and the solid filtered and washed with methanol (2 x 10 mL), hexane (2 x 10 mL) and ether (2 x 10 mL). Yield 309 mg, 71 %. ^{1}H NMR ($CDCl_3$) δ 3.77 (12H, s), 6.06 (4H, d), 6.49 (4H, d), 6.75 (8H, d), 6.92 (8H, d), 7.35 (18H, m), 7.80 (12H, m); ^{31}P NMR ($CDCl_3$) 17.69 (s, J(P-Pt) = 2671 Hz); ^{13}C{^{1}H} NMR ($CDCl_3$) 155.30 (C_b, s), 145.40 (C_e, s),

141.23 (C_f, s), 135.09 (C_n, t, $J_{c\text{-}p}$ = 6.1 Hz), 131.81 (C_l, t, $J_{c\text{-}p}$ = 17.1 Hz), 131.54 (C_h, s), 130.01 (C_o, s), 127.74 (C_m, t, J = 5.4 Hz), 125.95 (C_c, s), 121.27 (C_i, s), 120.25 (C_g, s), 114.49 (C_d, s), 113.11 (C_j, s), 108.81 (C_k, s), 55.43 (C_a, s).; MALDI-MS(+) *m*/*z*: 1376.4 $[M]^+$. IR (CH_2Cl_2) ν(C≡C) 2106 cm^{-1}. Analysis found (calculated) %: C 69.79 (69.68), H 4.84 (4.84), N 2.04 (2.05).

3.5. References

1. For example: (a) Paul, F; Lapinte, C. *Coord. Chem. Rev*, **1998**, 341-509. (b) Quardokus, R. C; Lu, Y; Wasio, N. A; Lent, C. S; Justaud, F; Lapinte, C; Kandel, S. A. *J. Am. Chem. Soc*. **2012**, *134*, 1710. (c) Fitzgerald, E. C; Brown, N. J; Edge, R; Helliwell, M; Roberts, H. N; Tuna, F; Beeby, A; Collison, D; Low, P. J; Whiteley, M. W. *Organometallics*, **2012**, *31*, 157. (d) Low, P. J; Brown, N. J. *J. Clust. Sci*, **2010**, *21*, 235.
2. Heckmann, A; Lambert C. *Angew, Chem, Int, Ed*, **2012**, *51*, 326.
3. For example: (a) Touchard, D; Haquette, P; Guesmi, S; Le Pichon, L; Daridor, A; Toupet, L; Dixneuf, P. H. *Organometallics*. **1997**, *16*, 3640. (b) Albertin, G; Autoniutti, S; Bordignon, E; Cazzaro, F. *Organometallics*. **1995**, *14*, 4114. (c) Choi, M. Y; Chan, M. C. W; Peng, S. M; Cheung. K. K. *Chem Comm.* **2000**, 1250. (d) Khan, M. S; Kakkar, A. K; Ingham, S. L; Raithby, P. R; Lewis, J; Spencer, B; Wittmann, F; Friend. R. H. *J. Organomet. Chem*. **1994**, (e) 472. 247. McDonagh, A. M; Cifuentes, M. P; Whittall, I. R. *J. Organomet. Chem.* **1996**, *526*. 99.
4. (a) Marques-Gonzalez, S; Yufit, D. S; Howard, J. A. K; Martin, S; Osorio, H. M; Garcia-Suarez, V. M; Nichols, R. J; Higgins, S. J; Cea, P; Low, P. J. *Dalton Trans*, **2013**, *42*, 338. (b) Bruce M. I; Wong, F. S. *J. Organomet. Chem*, **1981**, *210*, C5. (c) Bruce, M. I; Wong, F. S; Skelton B. W; White, A. H. *J. Chem. Soc-Dalton Trans*, **1982**, 2203. (d) Bruce, M. I; Wong, F. S; Skelton B. W; White, A. H. *J.Chem Soc-Dalton Trans*, **1981**, 1398. (e) Mayor, M; Von Hannisch, C; Weber, H. B; Reichart, J; Beckmann, D. *Angew, Chem, Int, Ed*, **2002**, *41*, 1183.

5. Liddle, B. J.; Wanniarachchi, S.; Hewage, J. S.; Lindeman, S. V.; Bennett, B.; Gardinier, J. R. *Inorg. Chem*. **2012**, *51*, 12720.
6. Jones, S. C.; Coropceanu, V.; Barlow, S.; Kinnibrugh, T.; Timofeeva, T.; Bredas, J. L.; Marder, S. R. *J. Am. Chem. Soc*. **2004**, *126*, 11782.
7. Vacher, A.; Barriere, F.; Camerel, F.; Bergamini, J.F.; Roisnel, T.; Lorcy, D. *Dalton Trans*. **2013**, *42*, 383.
8. Vacher, A.; Barriere, F.; Roisnel, T.; Piekara-Sady, L.; Lorcy, D. *Organometallics* **2011**, *30*, 3570.
9. Vincent, K. B; Parthey, M; Yufit, D. S; Kaupp, M; Low, P. J. *Polyhedron*. **2014**. Manuscript accepted.
10. Bushby, R. J.; Kilner, C.; Taylor, N.; Williams, R. A. *Polyhedron* **2008**, *27*, 383.
11. Kohler, A.; Whittmann, H. F.; Friend, R. H.; Khan, M. S.; Lewis, J. *Synth. Met*. **1996**. *77*, 147.
12. Meng, F.; Hervault, Y.M.; Norel, L.; Costuas, K.; Van Dyck, C.; Geskin, V.; Cornil, J.; Hng, H. H.; Rigaut, S.; Chen, X. *Chem. Sci*. **2012**, *3*, 3113.
13. Luo, L.; Benameur, A.; Brignou, P.; Choi, S. H.; Rigaut, S.; Frisbie, C. D. *J. Phys. Chem. C.* **2011**, *115*, 19955.
14. Kim, B.; Beebe, J. M.; Olivier, C.; Rigaut, S.; Touchard, D.; Kushmerick, J. G.; Zhu, X. Y.; Frisbie, C. D. *J. Phys. Chem. C.* **2007**, *111*, 7521.
15. Mahapatro, A. K.; Ying, J.; Ren, T.; Janes, D. B. *Nano Lett*. **2008**, *8*, 2131.
16. Liu, K.; Li, G.; Wang, X.; Wang, F. *J. Phys. Chem. C* 2008, *112*, 4342.
17. Liu, K.; Wang, X.; Wang, F. *ACS Nano* **2008**, *2*, 2315.
18. Parthey, M; Gluyas, J. B. G; Schauer, P. A; Yufit, D. S; Howard, J. A. K; Kaupp, M; Low, P. J. *Chem. Eur. J.,* **2013**, *19*, 9780 .
19. Brown, N. J.; Lancashire, H. N.; Fox, M. A.; Collison, D.; Edge, R.; Yufit, D. S.; Howard, J. A. K.; Whiteley, M. W.; Low, P. J. *Organometallics* **2011**, *30*, 884.
20. Fox, M. A.; Roberts, R. L.; Baines, T. E.; Le Guennic, B.; Halet, J. F.; Hartl, F.; Yufit, D. S.; Albesa-Jové, D.; Howard, J. A. K.; Low, P. J. *J. Am. Chem. Soc*. **2008**, *130*, 3566.
21. Demadis, K. D.; Hartshorn, C. M.; Meyer, T. J. *Chem. Rev.* **2001**, *101*, 2655.
22. (a) Brunschwig, B. S.; Creutz, C.; Sutin, N. *Chem. Soc. Rev*. **2002**, *31*, 168. (b) Heckmann, A.; Lambert, C. *Angew. Chem. Int. Ed*. **2012**, *51*, 326.

23. (a) Costuas, K; Rigaut, S. *Dalton. Trans*. **2011**, *40*. 5643. (b) Bruce, M. I; Le Guennic, B. Scoleri, N; Zaitseva, N. N; Halet, J. F. *Organometallics*. **2012**. *31*. 4701.
24. Heckmann, A.; Lambert, C. *Angew. Chem. Int. Ed*. **2012**, *51*, 326.
25. Renz, M.; Theilacker, K.; Lambert, C.; Kaupp, M. *J. Am. Chem. Soc*. **2009**, *131*, 16292.
26. Kaupp, M.; Renz, M.; Parthey, M.; Stolte, M.; Würthner, F.; Lambert, C. *Phys. Chem. Chem. Phys*. **2011**, *13*, 16973.
27. Man, W. Y; Vincent, K. B; Spencer, H. J; Yufit, D. S; Howard, J. A. K; Low, P. J. *J. Clust. Sci.*, **2012**, *23*, 853.
28. Maiti, D; Fors, B. P; Henderson, J. L; Nakamura, Y; Buchwald, S. L. *Chem. Sci*, **2011**, *2*, 57.
29. Hartwig, J. F. *Acc. Chem. Res*, **2008**, *41*, 1534.
30. Chinchilla, R; Na jera, C. *Chem. Soc. Rev*, B. **2011,** *40*, 5084.
31. Xu, C; Gong, J. F; Wu, Y. J. *Tetrahedron Lett*, **2007**, *48*, 1619.
32. Li, G. Y; Zheng, G; Noonan, A. F. *J. Org. Chem*, **2001**, *66*, 8677.
33. Reddy, C. V; Kingston, J. V; Verkade, J. G. *J. Org. Chem*, **2008**, *73*, 3047.
34. Christmann, U; Pantazis, D. A; Benet-Buchholz, J; McGrady, J. E; Maseras, F; Vilar, R. *J. Am. Chem. Soc*, **2006**, *128*, 6376.
35. Maes, B. U; Loones, K. T. J; Lemiere, G. L; Dommisse, R. A. *Synlett*, **2003**, *12*, 1822.
36. Lipshutz B. H; Ueda, H. *Angew. Chem. Int. Ed*, **2000**, *39*, 4492.
37. Christmann, U; Vilar, R; White, A. J. P; Williams, D. J. *Chem. Commun*, **2004**, 1294.
38. Suresh, S. R; Swamy, K. C. K. *Tetrahedron Lett*, **2009**, *50*, 6004.
39. Pratt, D. A; DiLabio, G. A; Valgimigli, L; Pedulli, G. F; Ingold, K. U. *J. Am. Chem. Soc*, **2012**, *124*, 11085.
40. Liu, X; Zhang, S. *Synlett*, **2011**, 8, 1137.
41. Nandurkar, N. S; Bhanushali, M. J; Bhor, M. D; Bhanage, B. M. *Tetrahedron Lett*, **2007**, *48*, 6573.
42. Lambert, C; Noll, G; Schmalzin, E; Meerholz, K; Brauchle, C. *Chem. Eur. J.*, **1998**, *4*, 2129.
43. Plater, K. J; Jackson, T. *Tetrahedron*, **2003**, *59*, 4687.

44. Sonogashira, K; Yatake, T; Tohad, Y; Takahashi, S; Hagihara, N. *J. Chem. Soc, Chem Commun*, **1977**, *9*, 291.
45. Khairul, W. M; Fox, M. A; Zaitseva, N. N; Gaudio, M; Yufit, D. S; Skelton, B. W; White, A. H; Howard, J. A. K; Bruce, M. I; Low, P. J. *Dalton Trans*, **2009**, 610.
46. Low, P. J.; Paterson, M. A. J.; Goeta, A. E.; Yufit, D. S.; Howard, J. A. K.; Cherryman, J. C.; Tackley, D. R.; Brown, B. *J. Mater. Chem*. **2004**, *14*, 2516.
47. Low, P. J.; Paterson, M. A. J.; Puschmann, H.; Goeta, A. E.; Howard, J. A. K.; Lambert, C.; Cherryman, J. C.; Tackley, D. R.; Leeming, S.; Brown, B. *Chem. Eur. J*. **2004**, *10*, 83.
48. Low, P. J.; Paterson, M. A. J.; Yufit, D. S.; Howard, J. A. K.; Cherryman, J. C.; Tackley, D. R.; Brook, R.; Brown, B. *J. Mater. Chem*. **2005**, *15*, 2304.
49. Carpenter, J. P.; Lukehart, C. M. *Inorg. Chim. Acta* **1991**, *190*, 7.
50. Mayor, M.; von Hanisch, C.; Weber, H. B.; Reichert, J.; Beckmann, D. *Angew. Chem. Int. Edit*. **2002**, *41*, 1183.
51. Gagnon, K.; Aly, S. M.; Brisach-Wittmeyer, A.; Bellows, D.; Berube, J. F.; Caron, L.; Abd-El-Aziz, A. S.; Fortin, D.; Harvey, P. D. *Organometallics* **2008**, *27*, 2201.
52. Adams, C. J.; Bowen, L. E. *Dalton Trans*. **2005**, 2239.
53. Leininger, S.; Stang, P. J.; Huang, S. P. *Organometallics* **1998**, *17*, 3981.
54. Minh-Hai, N.; Yip, J. H. K. *Organometallics* **2011**, *30*, 6383.
55. Zhou, G.; Wong, W. Y.; Poon, S. Y.; Ye, C.; Lin, Z. *Adv. Funct. Mater*. **2009**, *19*, 531.
56. Lambert, C.; Nöll, G. *J. Am. Chem. Soc*. **1999**, *121*, 8434.
57. (a) D'Alessandro, D. M; Keene, R. *Dalton. Trans*. **2004**, 3950. (b) Low, P. J; Brown, N. J. *J. Clust. Sci*. **2010**, *21*, 235. (c) Arnold, D. P; Heath, G. A; James, D. A. *J.* Porphy. Phtalocya. **1999**, *3*, 5.
58. Barriere, F.; Camire, N.; Geiger, W. E.; Mueller-Westerhoff, U. T.; Sanders, R. *J. Am. Chem. Soc*. **2002**, *124*, 7262.
59. Barriere, F.; Geiger, W. E. *J. Am. Chem. Soc*. **2006**, *128*, 3980.
60. Richardson, D. E.; Taube, H. *Coord. Chem. Rev*. **1984**, *60*, 107.
61. Denis, R; Toupet, L; Paul, F; Lapinte, C. *Organometallics* **2000**, *19*, 4240.
62. (a) Richardson, D. E.; Taube, H. *Coord. Chem. Rev.* **1984**, *60*, 107. (b) Arnold, D. P.; Heath, G. A.; James, D. A. *J. Porph. Phtalocya.* **1999**, *3*, 5. (c)

Barrière, F.; Camire, N.; Geiger, W. E.; Mueller-Westerhoff, U. T.; Sanders, R. *J. Am. Chem. Soc.* **2002**, *124*, 7262.

63. Amthor, S.; Noller, B.; Lambert, C. *Chem. Phys*. **2005**, *316*, 141.
64. Barlow, S.; Risko, C.; Chung, S. J.; Tucker, N. M.; Coropceanu, V.; Jones, S. C.; Levi, Z.; Bredas, J. L.; Marder, S. R. *J. Am. Chem. Soc*. **2005**, *127*, 16900.
65. Hush, N. S. *Prog. Inorg. Chem.* **1967**, *8*, 391.
66. Blatter, K.; Schluter, A. *Synthesis* **1989**, *5*, 356.
67. Ugo, R.; Cariati, F.; Lamonica, G. *Inorg. Synth.* **1990**, *28*, 123.
68. Bailar, J. C.; Itatani, H. *Inorg. Chem.* **1965**, *4*, 1618.
69. Chen, L.; Davies, J. A.; Staples, R. *Inorg. Chim. Acta*. **1989**. 11.
70. Coulson, D. R. *Inorg. Synth*. **1972**, *13*, 121.
71. Sugita, N.; Minkiewicz, J. V.; Heck, R. F. *Inorg. Chem*. **1978**, *17*, 2809. Kawata, N.; Mizoroki, T.; Ozaki, A. *Bull. Chem. Soc. Jpn.* **1974**, *47*, 1807.

Chapter 4: Synthesis and Spectroelectrochemistry of Ferrocenylene-diynes

4.1. Synopsis

The readily available 1,1-dibromoethene derivative $FcCH=CBr_2$ can be cross-coupled with a range of 1-alkynes under Sonogashira-like conditions to yield 2-ferrocenyl-1,1-diethynylethenes. These compounds have been studied by (spectro)electrochemical methods revealing that the ferrocene moiety is essentially electronically isolated from the organic backbone of the molecules. The capacity for such point charged, cross-conjugated compounds to serve as transistor-like elements under a design proposed by Grozema is discussed.

4.2. Introduction

As has been indicated elsewhere in this thesis, redox-active moieties linked by linear conjugated backbones, and the mixed-valence complexes generated following one-electron redox processes, have been topics of immense interest for many decades.[1] Such '$[L_xM_A]$-bridge-$[M_BL_x]$' systems provide incentives for the development of synthetic methods, such as those used in the preparation of long linear polyyndiyl chains stabilized by end-capping metal complexes $[L_xM]\{\mu\text{-}(C{\equiv}C)_n\}[ML_x]$,[2] and explorations of electronic structure through studies of intramolecular electron-exchange processes mediated by the linear all-carbon bridge.[3-7] Cross-conjugated structures, which contain three or more unsaturated branches but where not all the branches are directly conjugated, are also attracting attention driven by similar ambitions concerning their redox properties as their linearly conjugated analogues.[8] The unique geometric properties of the prototypical 1,1-diethynylethene fragment have led to incorporation of this motif into a range of shape persistent macrocycles[9] and radiannulene derivatives.[10] Together, these families of cross-conjugated compounds comprise a series of materials with useful electronic and optical properties that complement those of the related linearly conjugated analogues.[11] In addition, cross-conjugated fragments are now being recognized as potential scaffolds through which to explore the influence of quantum interference effects on the promotion and mediation of trans-molecule conductance in molecules and nascent molecular electronic devices.[12] In turn, this has led to a growing number of studies in which cross-conjugated carbon-rich ligands are being incorporated into metal complexes,[13] and attracting interest in the potential for intramolecular electron transfer between metal centres through the cross-conjugated bridge.[14]

The versatility in the manipulation of the optoelectronic properties of cross-conjugated organic materials has been demonstrated by the Bunz group, who have synthesised a range of compounds with cross-conjugated cruciform motifs (XF, Scheme 14) which are based on aryl-substituted ethene groups and aromatic ethynyl moieties. These aryl substituted compounds are synthesised through successive Wittig and Sonogashira reactions (Scheme 14).[15]

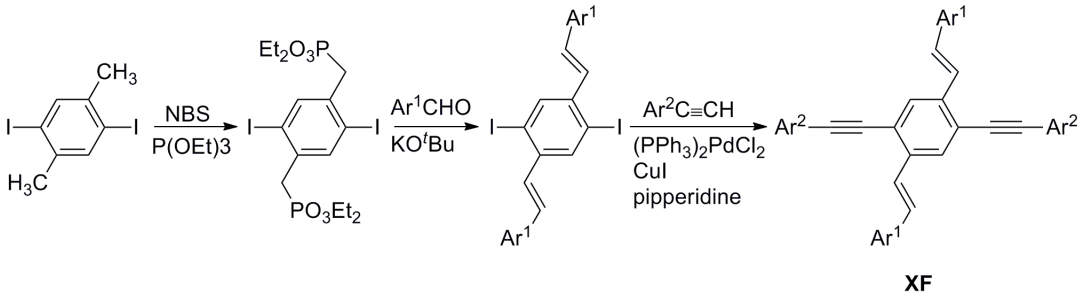

XF

Scheme 14: The synthetic strategy to cruciform compounds by the Bunz group

It has been shown that the nature of the distribution and energy of the HOMO and LUMO of these cruciform structures, and hence their electro-optical properties, can be manipulated by changing the donor-acceptor properties of Ar^1 and Ar^2, which allows, for example, the fluorescence properties to be tuned.[16]

In addition to the interest in cross-conjugated systems based on the cruciform motif, there has been increasing interest in the 1,1,2,2-tetraethynylethene (TEE) core (A, Figure 62) and related architectures as cross-conjugated scaffolds, due in no small part to the development of convenient synthetic routes to such structures. The C=C core of TEE compounds, which substitutes for the 1,2,4,5-aromatic cores in the cruciform, provides a wealth of synthetic possibilities that build on developments in the fabrication of simpler ene-yne and ene-diyne fragments (e.g. B and C, Figure 62).[17]

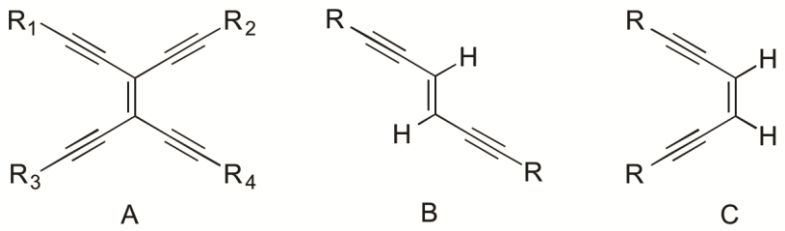

Figure 62: Typical structures of TEE and hexa-3-ene-1,5-diyne compounds

Recent work from the Low group has shown that simple symmetric TEE derivatives can be synthesised from Sonogashira reactions of tetrachloroethene with the respective terminal alkynes (Scheme 15). These compounds can then be used in the synthesis of redox-active organometallic complexes, most notably with cobalt-carbonyl cluster groups.[18] Asymmetric TEE derivatives have been prepared from the reaction of alkylformates with lithiated TMSA followed by sequential Corey-Fuchs and Sonogashira reactions and base catalysed deprotection (Scheme 16) to prepare compounds with two different geminal substituents. Other compounds with *trans* branches bearing the same substituent but with different geminal fragments have also been prepared (Scheme 17).

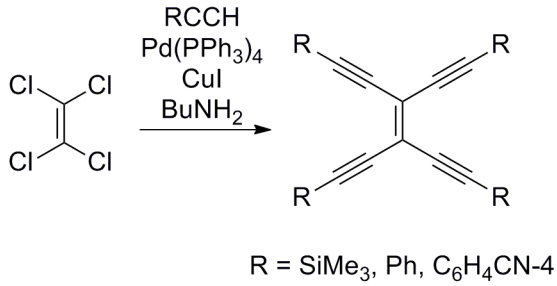

Scheme 15: Simplified synthesis of symmetrically tetra-substituted TEE derivatives

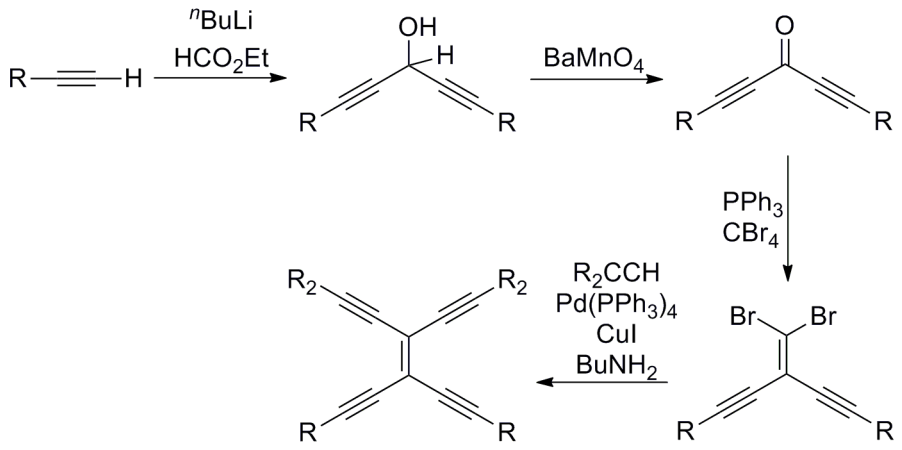

Scheme 16: Synthetic route employed by the Diederich group in synthesis of asymmetric TEE

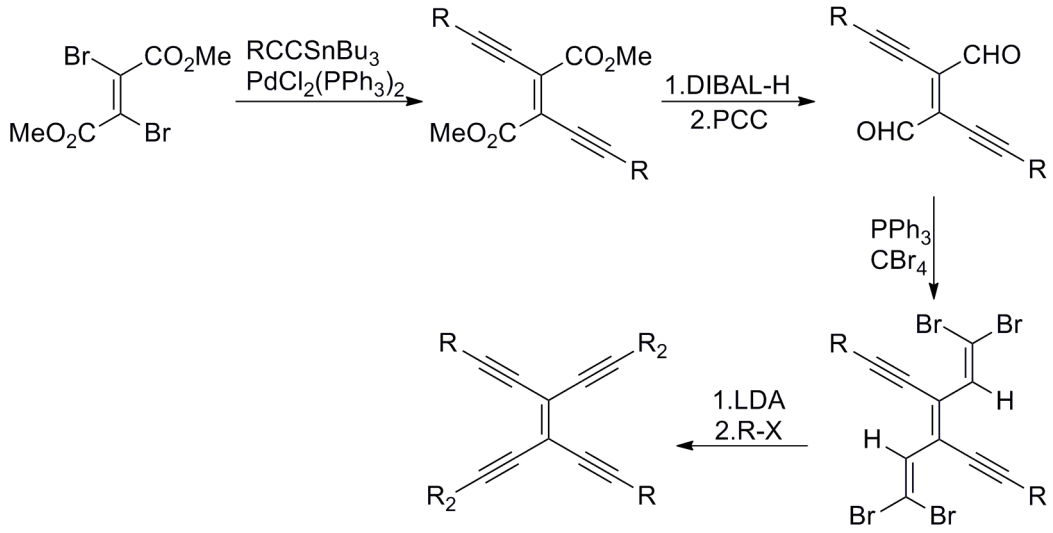

Scheme 17: Alternative synthetic route employed by the Low group in synthesis of asymmetric TEE. DIBAL-H = diisobutylaluminium hydride, PCC = pyridinium chlorochromate, X = halide

Selective removal of the $SiMe_3$ groups in the TEE (R= $SiMe_3$, R_2 = Si^iPr_3), Scheme 16 affords the partially protected TEE derivative, $(HC{\equiv}C)_2C{=}C(C{\equiv}CSi^iPr_3)_2$, which can be further reacted to give model polymeric species.[19] Polymeric species with conjugated ene-diyne / ene-tetrayne (Figure 63) are of synthetic interest as they give rise to a conjugated rod-like system that has the potential to be considered as a molecular wire suitable for use in molecular electronics.[20]

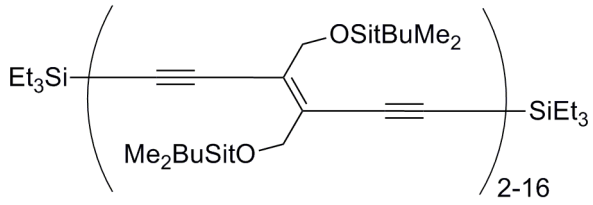

Figure 63: Example of polymeric DEE / TEE compounds.

It has been shown that the charge/electron transfer process can be augmented through manipulation of the electronic character of the R groups. When the R groups are π acceptor moieties (withdrawing) such as phenyl groups the molecule shows both solid and solution charge transfer. This can be greatly increased when the molecule is made of mixed donor and acceptor moieties.[21] Such donor-acceptor systems have also been shown to exhibit luminescent properties with the substituents *trans*- across the ethene moiety (Figure 64).[22]

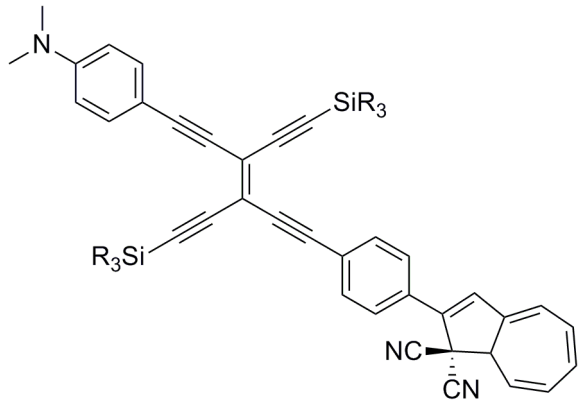

Figure 64: Example of a luminescent, D-A TEE.

While the electronic properties of such cross-conjugated materials are of considerable interest, there has also been interest in the biological potential of linearly conjugated ene-diyne materials (B and C, Figure 62), which form the key conceptual building blocks of the TEE structures. Perhaps the largest class of ene-diyne molecules studied for their biological activity are taxamycins, which contain

the *cis*-diethynylethene fragment (Figure 66). These compounds are naturally occurring materials that have been shown to undergo facile cyclisation reactions to give para-benzyne intermediate; Fallis and others have described the ene-diyne in these species as a 'warhead', as if these cyclisation reactions can be performed in related compounds in cells to form active biological materials then the compounds have potential to be used as antitumor treatments.[23] It has recently been reported that aryl substituted vinyl ferrocenes may also have potential applications in the treatment of cancers and offer increased anti-proliferative effect in some cells.[24]

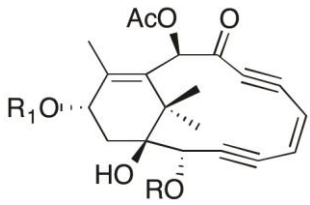

Figure 65: Typical taxamycin structure as used by Fallis.

The simplest molecular architectures of linearly-conjugated ene-diynes are hexa-3-ene-1,5-diyne compounds (B and C, Figure 62). Synthesis of these compounds can be achieved through the Sonogashira or Negishi coupling reactions of alkynes with the commercially available *cis*- or *trans*-CHCl=CHCl.[25] The hexa-3-ene-1,5-diyne scaffold has been incorporated into a range of different bi- and polymetallic compounds including $AuPCy_3$,[26] $Au(tpy)(PPh_3)_2$[27] and Fe(dppe)Cp* [28] derivatives and Co and Mo cluster compounds,[29] typical examples of these reactions are shown in Scheme 18.

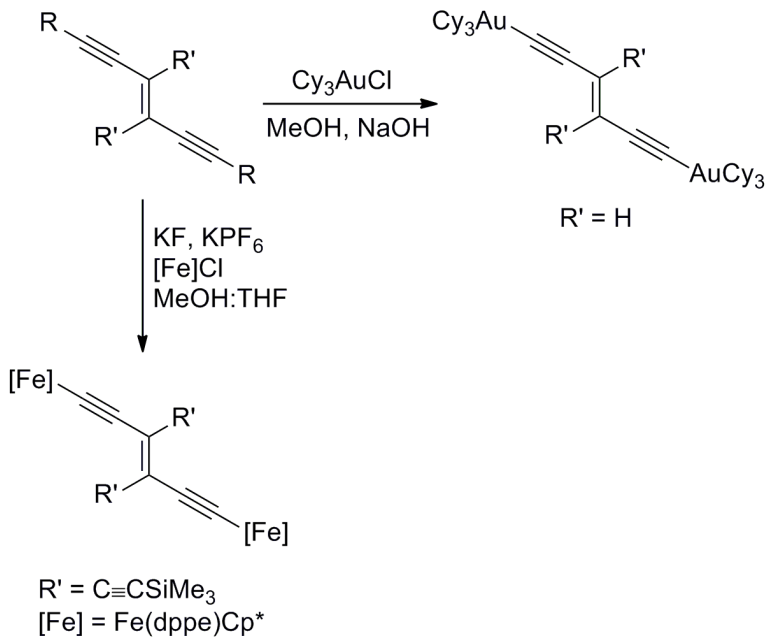

Scheme 18: Typical metallations of hexa-3-ene-1,5-diyne compounds.

The recent description of a chemically-gated quantum-interference based molecular transistor architecture based on a 1,1-diethynyl ethene (Figure 66) prompts renewed consideration of *cross-conjugated* ene-diyne structures. In the model put forward by Grozema, a donor *D* (or source electrode) is connected to an acceptor, *A* (or drain electrode) via a cross-conjugated ene-1,1-bis(alkyne) bridge (Figure 66). The gating component, *G*, is chosen to be capable of changing the charge state through chemical or electrochemical means. The cross-conjugated structure limits charge flow from *D* to *A* as the components of the charge carrier wave function propagating directly from *D* to *A* and that travelling via the channel to the gate *G* interact and form an interference pattern. This interference can be constructive or destructive depending on the chemical structure of the side chain; in the case of the structure shown in Figure 66, interference will be destructive and the transistor will normally be off. Chemical modification of the charge on the gating moiety (*G*) by (de)protonation or metal-ion binding to groups along the gate pathway changes the energy of the path,

and under favourable conditions will prevent a fully destructive interference pattern from being formed, and hence increasing the flow of charge from *D* to *A*. Redox-active gate groups were also noted as providing a suitable means for switching these interference effects.

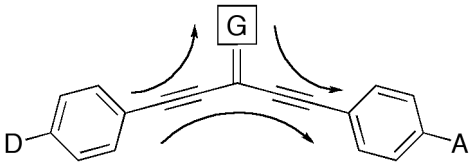

Figure 66: A schematic of the Grozema molecular transistor. The arrows show the propagation of the components of the wave function directly between donor, *D*, and acceptor, *A*, and also the portion travelling via the gate, *G*. The moieties *D* and *A* may be distinct chemical groups or the source and drain electrodes of a device.

Unsurprisingly, the most ubiquitous of all redox probes, ferrocene, has been incorporated into a wide-range of ene-1,1-diynes (e.g. **D** - **J**, Figure 67) with similar research aspirations in mind.[30] The synthesis of compounds with the general form of **F** where the ferrocenyl moiety can be replaced with other aromatic / organometallic fragments are often intermediates in the synthesis of larger polyyne systems. Compound **H** has been studied with the aim of investigating the extended chain length of the linear backbone although of greater interest was the solid state packing observed in the compound which highlights the potential of these compounds to undergo topochemical polymerisation in the solid state. Compounds **G** and **I** have been prepared with the Grozema design of wires and transistor type systems in mind with the aim of developing wire-like systems in which the communication is perturbed by QI effects of the cross-conjugated termini with results on the Ru complex comparable to that of the linear analogue $Ru(DMBA)_4(C{\equiv}CR)_2$. In the case of I it has been shown that the donating ability of the cross-conjugated termini promote the interaction of the Ru-d / C-π orbitals.

To this effect cross-coupling reactions of $FcCH{=}CBr_2$ (**22**) with terminal alkynes were investigated to generate the prototypical structures **D** (Figure 67) in which the ferrocene moiety can serve as an electrochemically addressable means of introducing a point charge to gate the flow of charge.

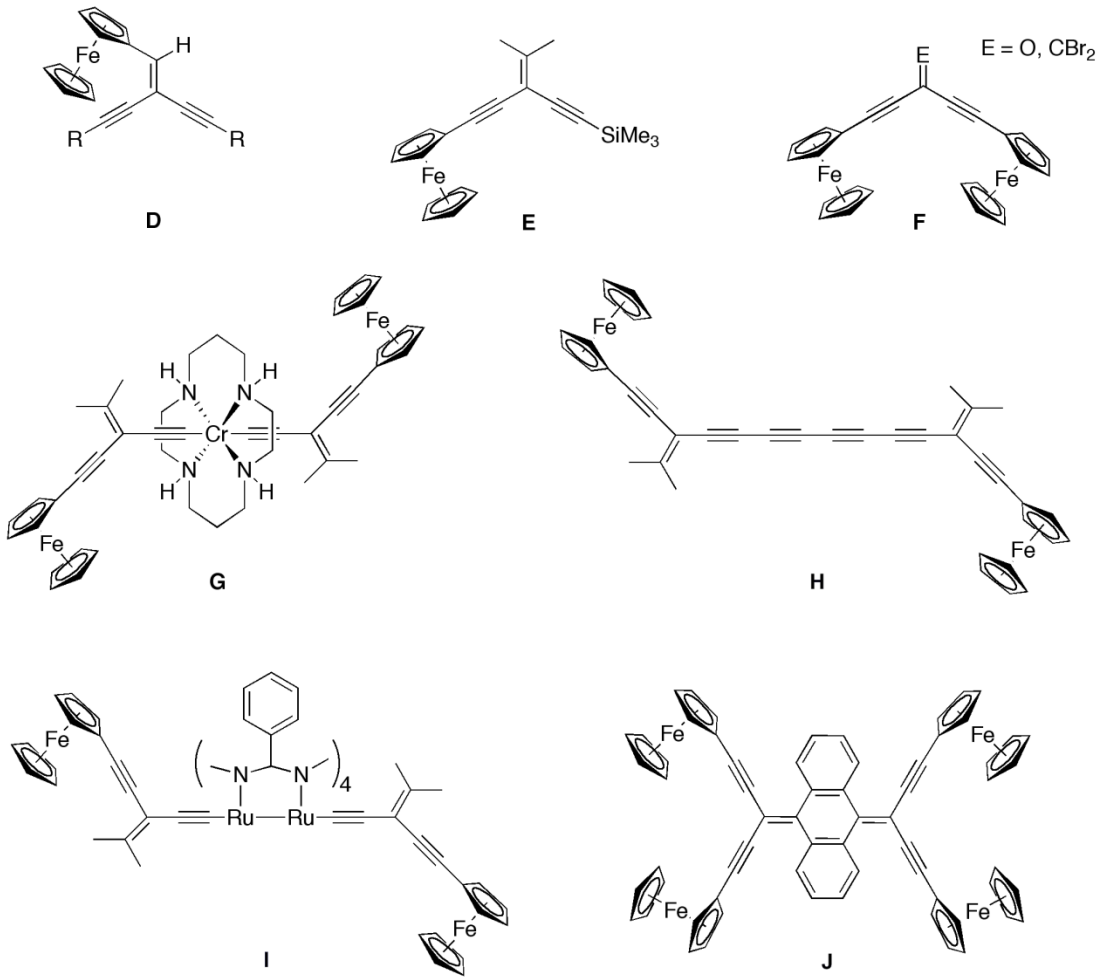

Figure 67: A selection of representative ferrocene-containing cross-conjugated compounds.

4.3. Results and discussion

4.3.1. Synthesis

The synthesis of 1,1-dibromo-2-ferrocenylethene (**22)** has been carried out using a previously reported procedure in good yield (Scheme 19).[31] Compound **22** is well-known as a precursor in the preparation of ethynylferrocene.[32] While **22** has been used in the synthesis of ferrocene substituted vinylic dithioethers and heterometallic oxidative addition products,[33] it is surprising that there have been no further developments of the synthetic uses of this organometallic 1,1-dihalo vinyl compound.

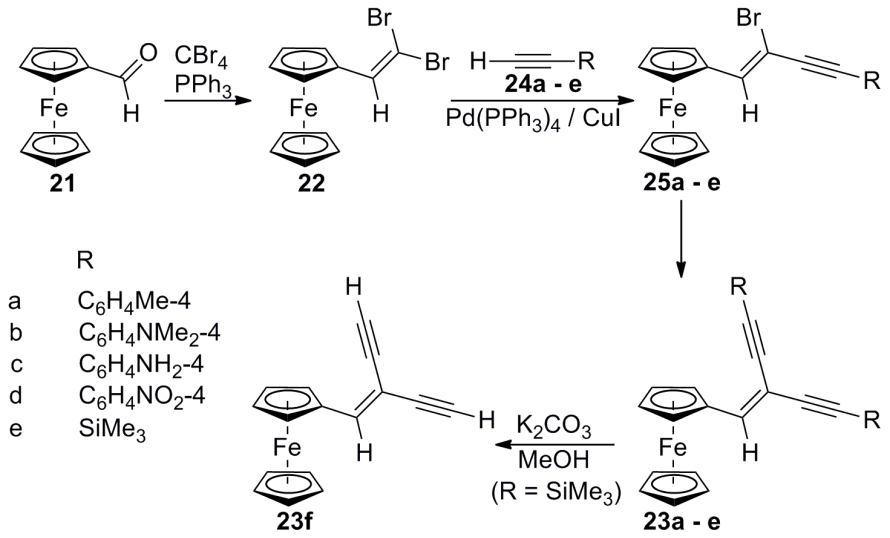

Scheme 19: The preparation of compounds 22 and 23 a - f from 21 via 25 a – e

Reaction of **22** with a large excess of terminal alkynes HC≡CC_6H_4R-4 (**24**: R = Me, **a**; NMe_2, **b**; NH_2, **c**; NO_2, **d**), or HC≡C$SiMe_3$ (**24e**) under Sonogashira cross-coupling conditions (NEt_3, $Pd(PPh_3)_4$ / CuI) gave moderate to good yields of the desired 1,1-di(alkynyl)-2-ferrocenyl ethenes **23a-e** (Scheme 19) as dark red solids (**23a - d**) or an oil (**23e**). Whilst **24a**, **24b**, and **24c** were chosen as representative

electro-neutral, -donating and -withdrawing substituents, the amino (**24c**) and trimethylsilyl (**24e**) groups are potential surface binding groups.[34] Desilylation of **23e** by treatment with K_2CO_3 / MeOH gave the fairly insoluble terminal dialkyne **23f** in good yield, which has potential for use as a reagent for the preparation of other derivatives featuring the 1,1-dialkynyl-2-ferrocenyl-alkene core.

During the purification of **23d** it was possible to isolate a pure sample of the intermediate ene-yne **25d** by column chromatography. The compound is isolated as a mixture of *cis*- and *trans*- isomers in an almost 50:50 mixture as shown by ^{1}H NMR spectroscopy. While **25d** crystallized as the *Z* isomer (*Z*-**25d** vinylic proton δ 7.19 ppm), in solution the compound undergoes equilibration over the course of several hours to give an approximately 1:1 mixture of *E*- and *Z*-**25d**, as shown by the appearance and integration of a second set of vinylic and $C_6H_4NO_2$-4 proton resonances (*E*-**25d** vinylic proton δ 7.05 ppm and aromatic resonances at δ 7.76, 8.30 ppm).

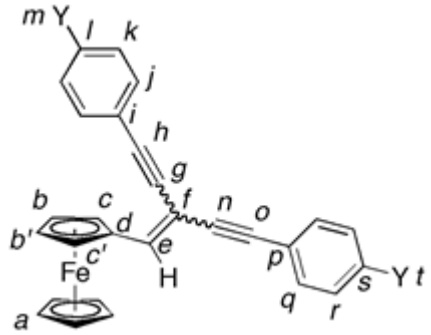

Figure 68: NMR labelling scheme for 23a-d.

Compounds **23a – f** were all characterized by the usual range of ^{1}H, ^{13}C{^{1}H} NMR spectroscopies, Atmospheric Solids Analysis Probe (ASAP) mass spectrometry,[35] elemental analyses and, in the case of **23d** and *Z*-**25d**, also by single crystal X-ray

diffraction. Each compound featured the expected pattern of ^{1}H resonances for a mono-substituted ferrocene, with a singlet for the C_5H_5 ring complemented by an unresolved pair of dd (apparent triplet) resonances. The equivalence of the H_b / $H_{b'}$ and H_c / $H_{c'}$ protons and the detection of a single cross peak from the H_c / $H_{c'}$ resonance to the vinylic proton (H_e) in the NOSEY spectrum indicated that there is free rotation of the ferrocenyl moiety around the C_d-C_e bond (see Figure 68). The two *para*-substituted aryl groups in **23a - d** gave rise to two pairs of resonances reflecting the different disposition across the double bond with respect to the ferrocenyl moiety, but individual pairs of resonances could not be unambiguously assigned to the *Z* or *E* branches of the ligand. The chemical shift of the H_c / $H_{c'}$ and vinylic (H_e) protons displayed some small dependence on the electronic nature of the alkynyl substituents, ranging from 4.55 and 7.18 for the NO_2 derivative **23d** to 4.41 and 6.95 for tolyl derivative **23a**, to 4.35 and 6.83 (**23b**) and 4.37 and 6.85 (**23c**) for the amine derivatives. Similarly, the vinyl carbon resonances C_e (identified by HSQC spectroscopy and the coupling to the vinyl proton H_e) and C_f (identified by HMBC to H_e) were also sensitive to the electronic character of the aryl substituent (C_e / C_f: 149.12 / 94.24, **23d**; 144.82 / 89.46, **23a**; 141.64 / 88.18, **23b**; 142.60 / 88.18, **23c**). The trimethylsilyl-protected and terminal alkyne derivatives **23e** and **23f** were similarly identified, with two $SiMe_3$ and C≡C-H resonances observed, respectively. However, whilst the sets of resonances belonging to the individual alkynyl fragments were unambiguously assigned through a combination of ^{1}H-^{1}H and ^{1}H-^{13}C 2D NMR experiments, as in the case of the phenylene protons, assigning these sets of ^{13}C resonances to either the *E* or *Z* arm was not possible. Nevertheless, the influence of the electronic nature of the aryl substituent on the NMR spectroscopic properties of the vinyl moiety clearly indicate that there is some

degree of electronic information being propagated through the cross-conjugated backbone.

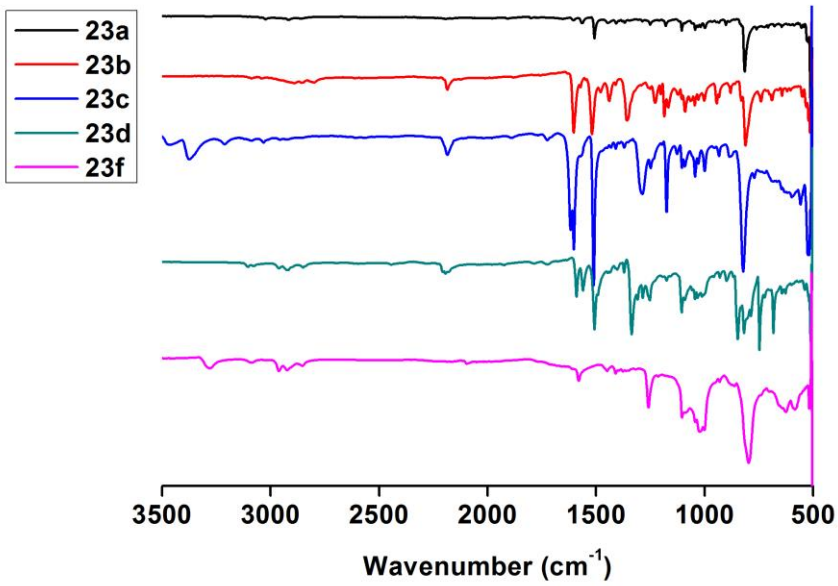

Figure 69: ATR- FTIR spectra for 23a-f

The IR spectra of **23a** - **e** were recorded in solution (CH_2Cl_2). Given the low solubility of **23f** spectra were also obtained in the solid state (ATR-FTIR) for comparison, with the exception of the oil **23e**. Results are summarized in Table 33, and Figures showing the ATR-FTIR spectra are given in Figure 69. All these compounds display ν(C−H) bands associated with the cyclopentadienyl rings and, in the case of **23a-d**, the phenylene rings, in the region of 2750–3200 cm^{-1} which were more clearly observed in the solid state spectra. For **23a** and **23b**, this region also involved ν(C−H) bands from the terminal methyl groups. In the solid state a weak ν(C≡C) band was observed around 2190 cm^{-1} for **23b** and **23c**; the band pattern became more complex for **23a** and especially **23d**, whilst in solution the ν(C≡C) bands appeared as relatively sharp bands near 2190 cm^{-1} with a higher frequency shoulder in the case of the aryl derivatives, possibly reflecting Fermi coupling.[36]

Table 33: Characteristic IR active vibrational modes (cm^{-1}) of 23a-e observed in solution (CH_2Cl_2), solid state (ATR-FTIR).

	ν(N−H)	*ν*(C−H)	*ν*(C≡C)	*ν*(C=C) aryl	*ν*(C=C) vinyl	*ν*(C−N)	*ν*(NO_2)
23a[a]	-	3155-2800	2209, 2196	1607, 1509	1577	-	
23a[b]	-	3150, 2800	2200, 2176	1604, 1508	1564	-	
23b[a]	-	3150-2774	2205, 2186	1608, 1523	not observed	1482, 1422, 1357	-
23b[b]	-	3100-2750	2189	1606, 1519	1576	1361	-
23c[a]	3394 [c]	3050-2800	2204-2190	1606, 1515	not observed		-
23c[b]	3400 [d]	3200-2800	2191	1605, 1514	1575	1296	-
23d[a]	-	2830-3035	2195, 2210	1593, 1493	1565	-	1518, 1344
23d[b]	-	3150-2800	2188, 2211	1592, 1499	1561	-	1509, 1339
23e[a]	-	3050-2800	2144	-	1577	-	-
23f[b]	-	3300,[g] 2775-3200	2100	-	1581	-	-

[a] CH_2Cl_2 solution state [b] Solid state [c] The corresponding bending vibration lies at 1622 cm^{-1} in pure CH_2Cl_2 and $CH_2Cl_2/10^{-1}$ M NBu_4PF_6 [d] The corresponding bending vibration lies at 1619 cm^{-1}. [g] ν(C≡C-H).

The aryl and vinyl ν(C=C) wavenumbers were modestly sensitive to the electronic character of the substituent, with a small shift to lower energy in the case of the donor-acceptor derivative **23d** arguably reflecting a contribution from a more cumulated resonance form (Figure 70). In the donor (ferrocene)-donor (amine) derivatives the **23b** and **23c** the ν(C=C) vinyl bands were not observed in solution likely due to the lack of a strong dipole. However, in the solid state, a band at 1575 (**23b**) / 1576 (**23c**) cm^{-1} was clearly observed and the gained intensity is likely to be due to local distortions brought about by solid state packing.

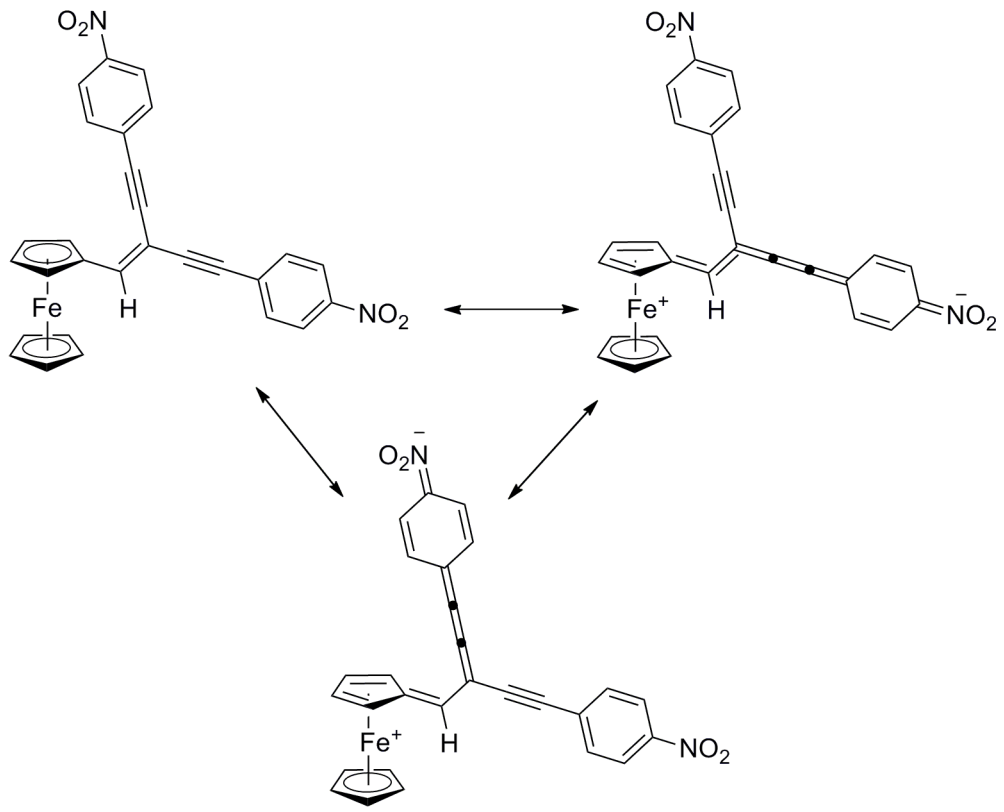

Figure 70: Resonance structures of the donor-acceptor compound 23d

4.3.2. Molecular Structures

Single crystals of **23d** (Figure 71) and *Z*-**25d** (Figure 72) suitable for X-ray diffraction were obtained by slow diffusion of ethanol into solutions of the compound in CH_2Cl_2. Important bond lengths and angles are summarised in the relevant figure captions. As expected, the 1,1-dialkynylethene portions of the molecules are planar within 0.03 Å deviation from the plane, and the key C=C (**23d** 1.355(3); *Z*-**25d** 1.335(4) Å), =C–C (**23d** 1.437(3), 1.434(3); *Z*-**25d** 1.422(4) Å), and C≡C (**23d** 1.199(3), 1.197(3); *Z*-**25d** 1.190(4) Å) bond lengths are consistent across both compounds. The C(1)−C(5) ring of the vinylferrocene moiety also lies close to this plane, evidencing a degree of delocalization between the metal and cross-conjugated fragments. Interestingly, in the molecule **23d** the C(1)−C(5) ring and the

aromatic group located *trans* across the double bond lie close to the same plane. The nitrophenyl groups *cis* to the vinylferrocene moiety are less obviously positioned to promote significant π conjugation.

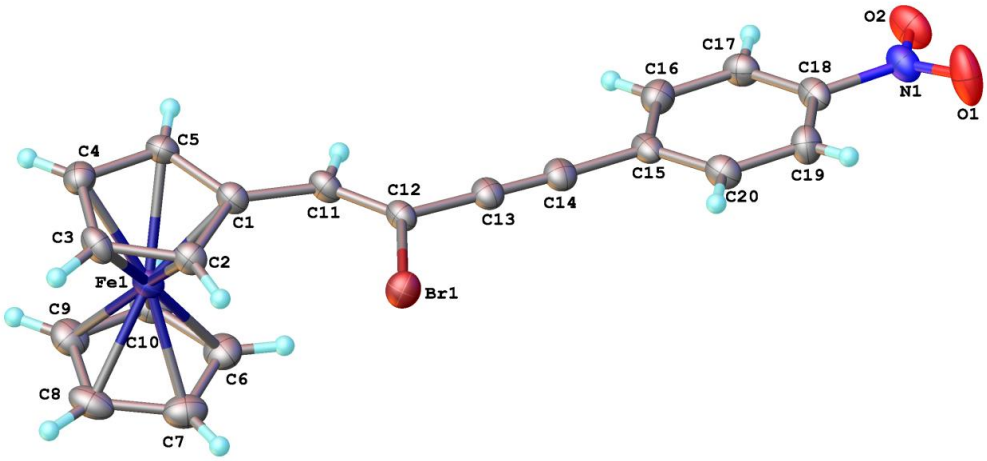

Figure 71: Molecular structure of *Z*-25d, thermal ellipsoids plotted at 50 %.

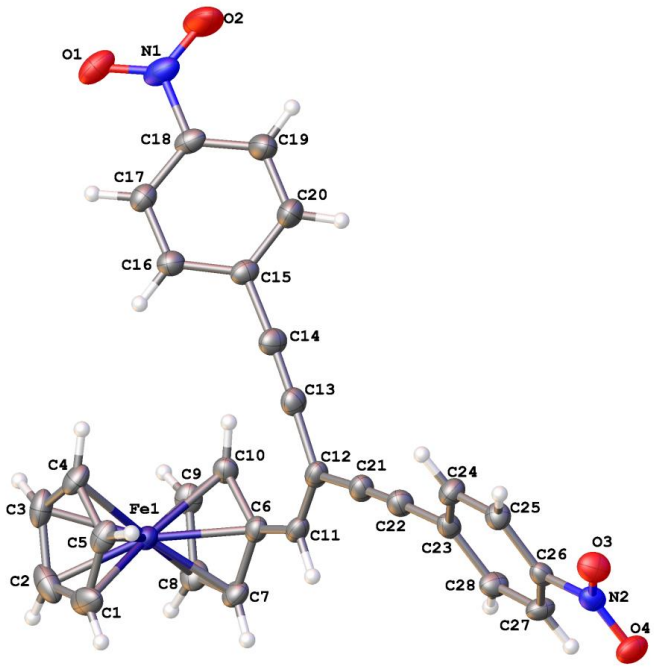

Figure 72: Molecular structure of 23d, thermal ellipsoids plotted at 50 %.

4.3.3. Electrochemistry

The electrochemical response of the ferrocenyl compounds **23a - f** were investigated by CV in a standard three-electrode cell (equipped with a Pt microdisc working electrode) from a CH_2Cl_2 solution containing the 10^{-1} M NBu_4PF_6 supporting electrolyte. All potentials are reported against the ferrocene/ferrocenium ($FeCp_2/FeCp_2^+$) couple by reference to an internal decamethylferrocene ($FeCp^*_2$) standard (–0.48 V vs $FeCp_2$/ $FeCp_2^+$) (Table 34). The CV of each of the monoferrocenyl complexes **23a - f** displayed a reversible one-electron oxidation wave consistent with the redox properties of the ferrocenyl moiety. The electron-withdrawing nature of the conjugated vinyl group was evidenced in the shift of these waves to more positive potentials relative to ferrocene. A representative plot of the CV of **23d** showing both the ferrocene-centred oxidation wave, which is similar to that observed for all compounds **23a - f**, and the reduction wave unique to this bis(nitroaromatic) derivative is shown in Figure 73. Across the series, the ferrocene redox potentials were also sensitive to the electronic character of the remote substituent, with the electron-withdrawing $–NO_2$ group giving rise to the most positive $E_{1/2}$ values (Table 34). As shown in Figure 73, the nitrophenyl groups in **23d** were also electroactive within the electrochemical window of the solvent, giving rise to two overlapping reduction waves ($E_{1/2}$ = −1.42 V, ΔE_p = 100 mV) and the formation of $[\mathbf{23d}]^{2–}$. There was no evidence for the stability of the organic mixed-valence form $[\mathbf{23d}]^{–}$.

Table 34: Oxidation half-wave potentials for 23a - 23f.[a]

Compound	$E_{1/2}$ / V	ΔE_p / V	i_{pa}/i_{pc}
23a	0.18	0.10	1
23b	0.09	0.16	1
23c	0.10	0.12	1
23d [b]	0.22	0.10	1
23e	0.16	0.29	1
23f	0.19	0.32	1

[a] CH_2Cl_2 / 10^{-1} M NBu_4PF_6; scan rate (ν) = 100 mV s^{-1}. Potentials reported against ferrocene ($FeCp_2$/ $FeCp_2^+$ = 0.0 V) by reference against an internal decamethylferrocene/decamethylferricenium couple ($FeCp^*_2$/ $FeCp^*_2{}^+$ = –0.48 V *vs* $FeCp_2$/ $FeCp_2^+$). [b] Compound **23d** undergoes reversible reduction at $E_{1/2}$ = −1.42V.

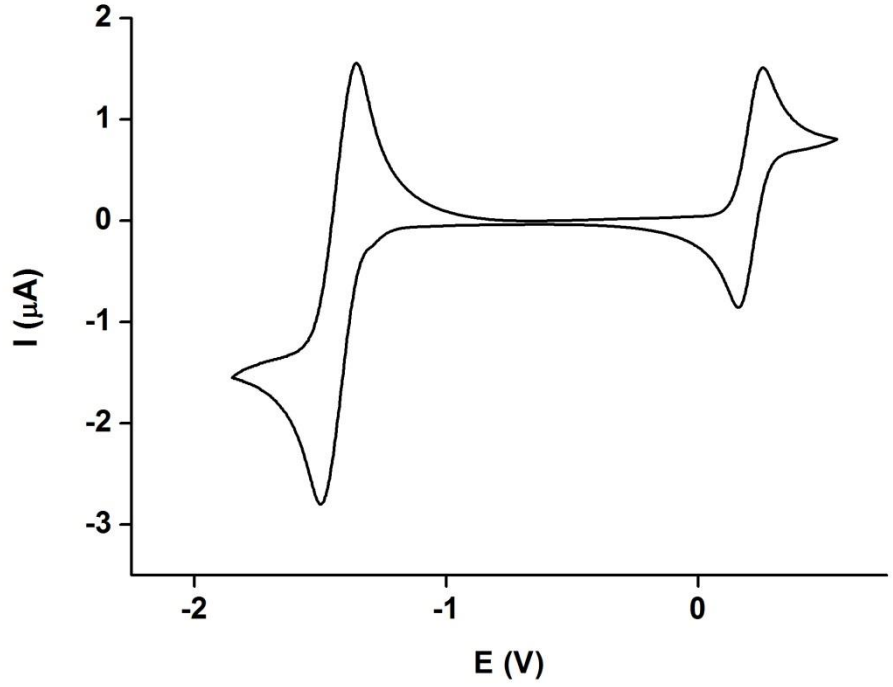

Figure 73: Cyclic voltammogram of 23d in CH_2Cl_2/10^{-1} M NBu_4PF_6; scan rate (ν) = 100 mV s^{-1}. Potentials are reported against ferrocene ($FeCp_2$/ $FeCp_2^+$ = 0.0 V) by reference against an internal decamethylferrocene/decamethylferricenium couple ($FeCp^*_2$/ $FeCp^*_2{}^+$ = −0.48 V vs $FeCp_2$/ $FeCp_2^+$)

4.3.4. IR Spectroelectrochemistry

IR spectroelectrochemical investigations were undertaken (in collaboration with Professor Franti Hartl's group in Reading, UK) to better assess the interactions between the ferrocenyl moieties and the 1,1-diethynylvinyl moiety in the most easily handled compounds **23a−d**. As **23d** exhibits both a reversible ferrocenyl-centered oxidation and a reduction localised on the terminal nitrophenyl substituents, it provided an ideal platform for spectroelectrochemical investigation of both the oxidation and reduction processes that promote understanding of the electronic interactions between the redox sites and the 1,1-dialkynyl vinyl moiety.

Reduction of the nitro groups in **23d** to [**23d**]$^{2-}$ induces a shift of the $\nu(NO_2)$ band at 1343 cm^{-1} to 1360 cm^{-1} and a decay of $\nu(NO_2)$ at 1520 cm^{-1} (Figure 74). Similar observations have been reported in comparisons of the IR spectra of nitrobenzene and its radical anion.[37] The $\nu(C{=}C)_{aryl}$ absorption at 1491 and 1594 cm^{-1} is very weak in [**23d**]$^{2-}$ while the $\nu(C{=}C)_{vinyl}$ and $\nu(C{\equiv}C)$ bands maintain the relatively high intensity. The spectral changes reveal a very small shift of the $\nu(C{=}C)_{vinyl}$ band at 1565 to 1570 cm^{-1} and a more significant low-energy shift of the $\nu(C{\equiv}C)$ absorption, with the band envelope between 2211 and 2195 cm^{-1} being replaced by a single broad band at 2152 cm^{-1}. It is clear from the change in spectral properties that the extra electron density is distributed over an area of the molecule that displays significant nitrophenyl and alkynyl character.

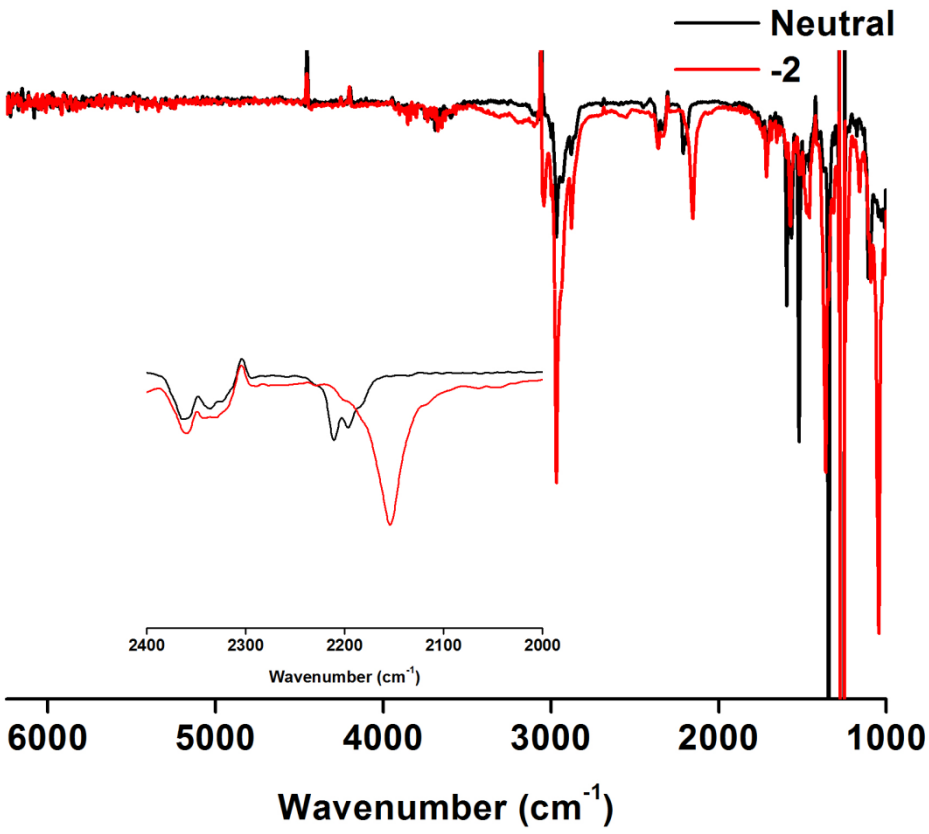

Figure 74: Reversible IR spectral changes accompanying reduction of the terminal nitrophenylene groups in 23d to $[23d]^{2-}$ in CH_2Cl_2 / 10^{-1} M NBu_4PF_6 within an OTTLE cell. Inset shows an expansion of the ν(C≡C) region.

Upon oxidation of **23d** to $[\mathbf{23d}]^+$ there are significantly different observations in the spectra compared to the reduction. The ferrocene based oxidation process to give $[\mathbf{23d}]^+$ does not affect $\nu(C{=}C)_{vinyl}$ or ν(C≡C) wavenumbers significantly, resulting in small blue shifts of less than 5 cm^{-1}, but with a substantial loss of intensity of these bands (inset Figure 75). These observations indicate that the ferrocene centre has only a small influence on the structure of the cross-conjugated fragment and therefore does not interact strongly with the 1,1-dialkynyl vinyl moiety. The ferrocene moiety can therefore be considered as electronically isolated from the cross-conjugated π-system, which is promising from the point of view of the design criteria of the Grozema transistor.

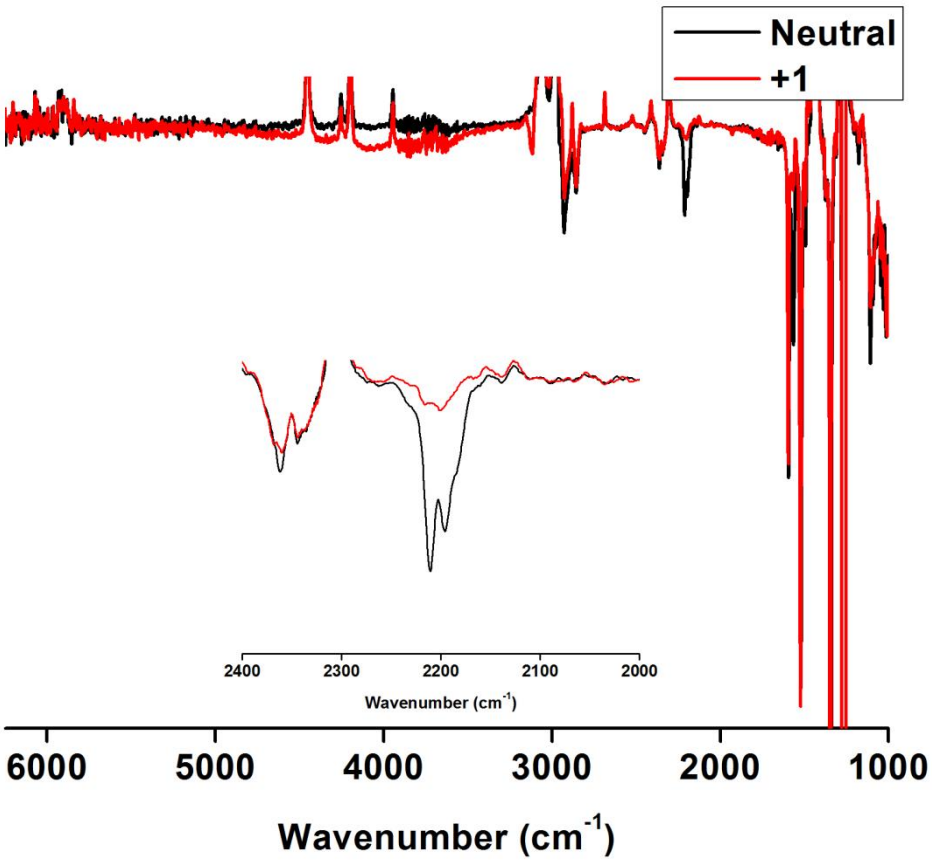

Figure 75: Reversible IR spectral changes accompanying oxidation of the ferrocene moiety in 23d in CH_2Cl_2 / 10^{-1} M NBu_4PF_6 within an OTTLE cell. Inset shows changes in the ν(C≡C) region.

The ν(C≡C) and ν(C=C)$_{vinyl}$ bands of **23a-c** with the donor substituents on the phenyl ring exhibit markedly different response to the 1e$^-$ oxidation when compared with **23d** (Table 35); these differences are discussed below. The new band centred at ca. 4000 cm^{-1} in [**23a-d**]$^+$ is consistent with a ferrocene centred transition and can be ascribed to a localised d-d type IC transition.[38]

Table 35: Characteristic IR active vibrational modes (cm^{-1}) of 23a-d observed in spectroelectrochemical studies by *in situ* oxidation of a $CH_2Cl_2/10^{-1}$ M NBu_4PF_6) solution for $[23a - 23d]^{n+}$ (n = 0, 1), and calculated vibrational frequencies $[23a´]^{n+}$, $[23b´]^{n+}$ and $[23d´]^{n+}$ (n = 0, 1).

	ν(N−H)	ν(C≡C)	ν(C=C) aryl	ν(C=C) vinyl	$\nu(NO_2)$
23a[b]		2208, 2194	1609, 1510	1575	
[**23a**]$^{+}$[b]		2208, 2194	1605, 1510	1559	
23a´[c]		2233, 2220	1619, 1617 1499, 1495	1585	
[**23a´**]$^{+}$[c]		2227, 2211	1615, 1556 1499	1561	
23b[b]		2188	1607, 1522	not observed	
[**23b**]$^{+}$[b]		2167	1605, 1524	1545	
23b´[c]		2223, 2210	1614, 1613 1514, 1511	–	
[**23b´**]$^{+}$[c]		2203, 2178	1611, 1604 1518, 1510	1527	
23c[b]	3395[e]	2185	1607, 1514	not observed	
[**23c**]$^{+}$[b]	3400	2173	1603, 1517	1545	
23d[b]		2211, 2195	1594, 1491	1565	1520, 1343
[**23d**]$^{+}$[b]		2215, 2201	1596, 1493	1565	1522, 1345
23d´[c]		2233, 2217	1601, 1566 1482, 1478	1568, 1567	1636, 1634 1395, 1393
[**23d´**]$^{+}$[c]		2237, 2223	1608, 1605 1573, 1572 1483, 1463	1576	1641, 1639 1403, 1401

[a] CH_2Cl_2 solution state [b] $CH_2Cl_2/10^{-1}$ M NBu_4PF_6 [c] calculated, with 0.95 correction factor applied [d] Solid state [e] The corresponding bending vibration lies at 1622 cm^{-1} in pure CH_2Cl_2 and $CH_2Cl_2/10^{-1}$ M NBu_4PF_6 [f] The corresponding bending vibration lies at 1619 cm^{-1}.

On oxidation of the most stable derivative **23a** to [**23a**]$^{+}$, the wavenumbers of the ν(C≡C) band maxima remain almost unchanged while the $\nu(C{=}C)_{vinyl}$ band at 1575 cm^{-1} shifts to lower energy by 16 cm^{-1} (Table 35) and the intensity of both ν(C≡C) and $\nu(C{=}C)_{vinyl}$ absorption bands strongly increasing in the cationic products (Figure

76). Again, these changes in band intensity are consistent with the changes in dipole moment across the molecule in response to localised changes in redox state. Again, in this and the other spectra described below the observation of an electronic absorption band near 4000 cm^{-1} (ferrocenium dd) is a clear marker for the ferrocene based oxidation of this and the other complexes.

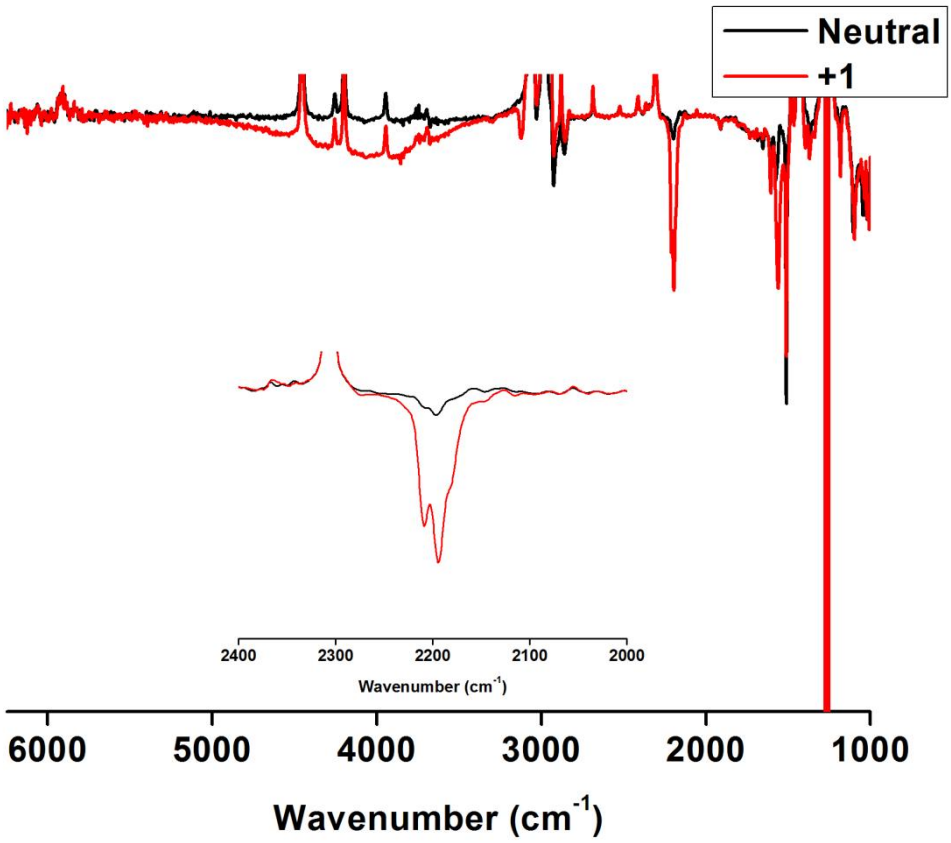

Figure 76: Reversible IR spectral changes accompanying oxidation of the ferrocene moiety in 23a in CH_2Cl_2 / 10^{-1} M NBu_4PF_6 within an OTTLE cell. Inset shows changes in the ν(C≡C) region.

Upon oxidation of **23c** to [**23c**]$^+$, the ferrocenyl-centred oxidation resulted in the gradual shift of the ν(C≡C) band envelope at 2185 cm^{-1} to a new structured band at 2173 cm^{-1} (Figure 77). However, in addition on forming [**23c**]$^+$, a new broad ν(C≡C) absorption at 2120 cm^{-1} was also observed to be independently growing, especially at later stages of the oxidation processes with concomitant decrease in the ν(C≡C)

absorption of [**23c**]$^{+}$. This behaviour reflects the reactivity of the aniline substituent in the cationic product, which may form an insoluble polyaniline-type structure. In contrast to the parent **23c**, the $\nu(C{=}C)_{vinyl}$ band of [**23c**]$^{+}$ is IR active in solution (1545 cm^{-1}) and found some 14 cm^{-1} lower than in [**23a**]$^{+}$ (Table 35).

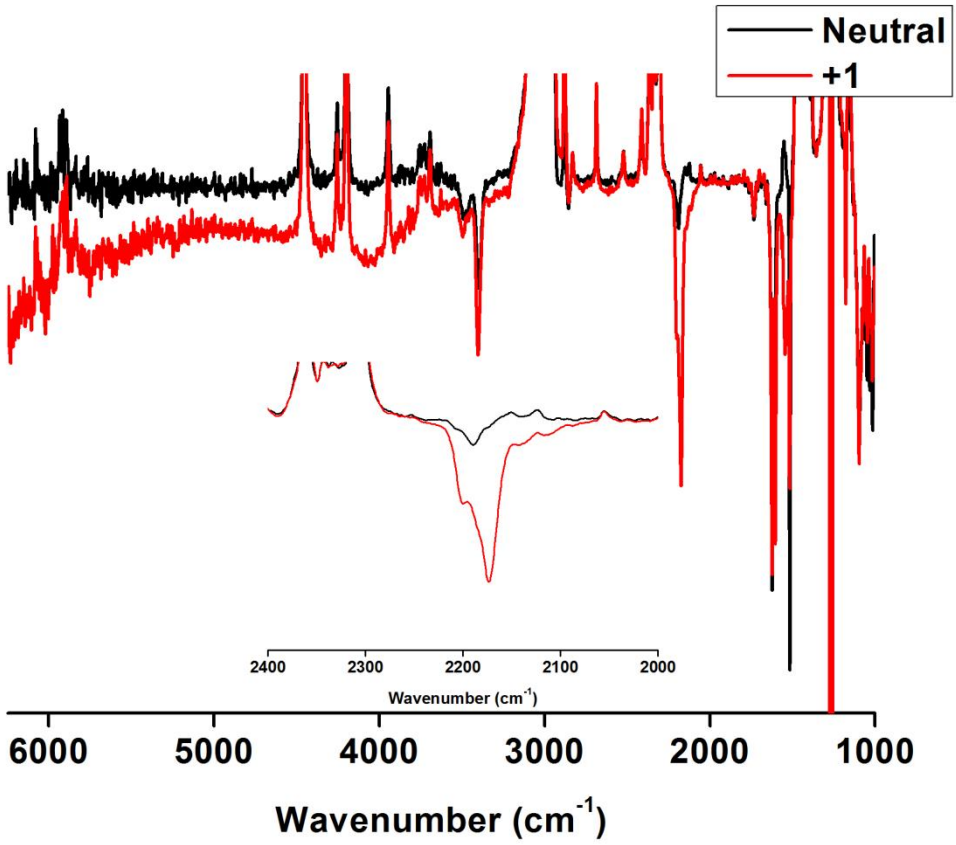

Figure 77: Reversible IR spectral changes accompanying oxidation of the ferrocene moiety in 23c in CH_2Cl_2 / 10^{-1} M NBu_4PF_6 within an OTTLE cell. Inset shows changes in the ν(C≡C) region.

Finally, for the dimethylamino derivative **23b**, the IR spectral changes due to the ferrocenyl-centred oxidation show a very similar trend as observed for **23c** (Table 35). Upon oxidation there was a gradual shift of the ν(C≡C) band envelope at 2188 cm^{-1} to a new structured band at 2167 cm^{-1}(Figure 78). In contrast to the parent **23b**, and consistent with the observations of [**23c**]$^{+}$, the $\nu(C{=}C)_{vinyl}$ band of [**23b**]$^{+}$ is IR

active in solution (1545 cm^{-1}) and, as with $[\mathbf{23c}]^+$, is found 14 cm^{-1} lower than in $[\mathbf{23a}]^+$. The secondary reactivity of $[\mathbf{23b}]^+$ is markedly less pronounced than noted above for $[\mathbf{23c}]^+$, which can be ascribed to higher steric demands of the *N*,*N*-dimethyl-aniline substituents which inhibits the polymerization reaction in the cationic product. Ultimately, this process complicates the spectroelectrochemical study of **23b** and **23c** due to severe passivation of the electrode surface. Nevertheless, as also seen in the solid-state ATR-FTIR spectra of the neutral systems, the $\nu(C{=}C)_{vinyl}$ wavenumbers in the oxidised forms exhibits some substituent effect and are more sensitive to the ferrocenyl oxidation than the $\nu(C{\equiv}C)$ and $\nu(C{=}C)_{aryl}$ modes, especially in the presence of a donor group on the phenyl rings.

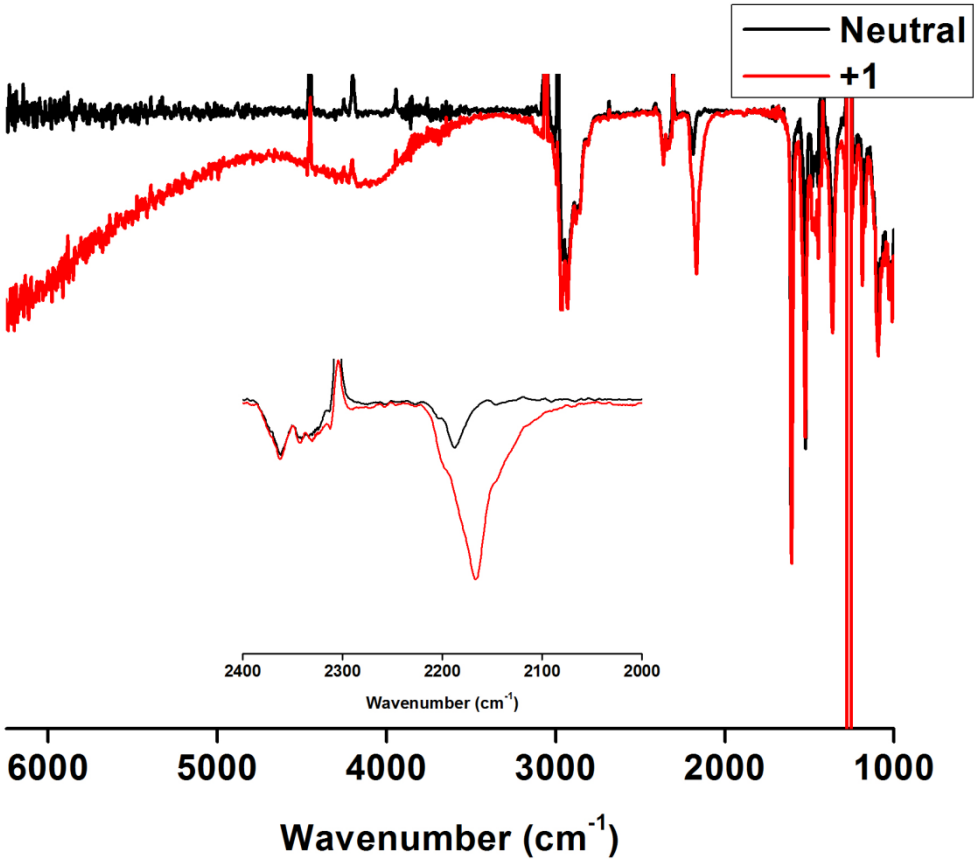

Figure 78: Reversible IR spectral changes accompanying oxidation of the ferrocene moiety in 23b in CH_2Cl_2 / 10^{-1} M NBu_4PF_6 within an OTTLE cell. Inset shows changes in the $\nu(C{\equiv}C)$ region.

4.3.6. Quantum Chemical Calculations

To gain further insight into the electronic structure and the character of the electronic transitions, calculations at the density functional theory (DFT) level were performed using compounds [**23a´**]^n, [**23b´**]^n and [**23d´**]^n (n = 0, +1) as representative examples (the ´ notation is employed to distinguish the *in silico* system from the experimental complex). Calculations were performed by Matthias Parthey in the Kaupp Group TU Berlin. The BLYP35 functional (35% exact exchange admixture) was used together with the COSMO continuum solvent model (CH_2Cl_2; ε = 8.93).[39] This combination of methods is known to provide a reasonable description of electronic localization/delocalization and excited-state properties of open shell organic and transition-metal systems, including the charge transfer characteristics of mixed-valence examples.[40]

The DFT calculations confirmed an essentially ferrocenyl-centered oxidation in each case [**23a´**]$^+$, [**23b´**]$^+$ and [**23d´**]$^+$, with spin density almost exclusively localised on the ferrocenyl moiety (Table 36 - Table 38). In the case of [**23b´**]$^+$ the calculated spin density on the ferrocenyl moiety (101 %) is matched with a small negative contribution form the two ethynyl units (-1 %) (Figure 79). Further details on the computational work carried out on these molecules is available in the published manuscript.[41]

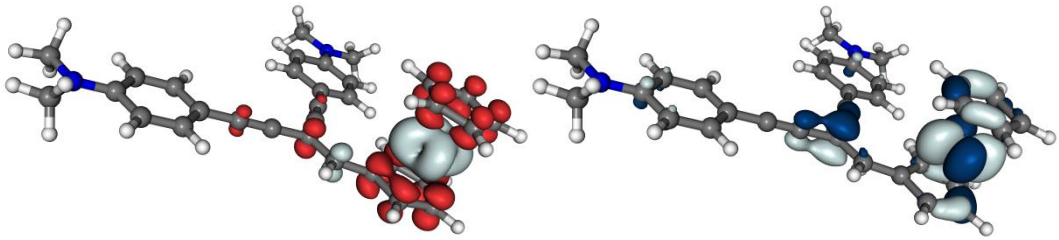

Figure 79: Isosurface plots of the spin-density (± 0.002 a.u., left) and the SOMO 113α (± 0.03 a.u., right) of [23b´]$^+$.

Harmonic vibrational frequency calculations were performed on each member of the series [**23a´**]^n, [**23b´**]^n and [**23d´**]^n (n = 0, +1) (Table 35). In agreement with experimental spectroelectrochemical results, the ν(C≡C) frequencies of the neutral and the oxidised form differ little. For each oxidation state, two ν(C≡C) bands are computed. Taking [**23b´**]$^{n+}$ as an example, while the ν(C≡C) bands appear at 2223 cm^{-1} and 2210 cm^{-1} for the neutral species **23b´**, upon oxidation to [**23b´**]$^+$ a small shift to lower energy to 2203 cm^{-1} and 2178 cm^{-1} occurs. While the ν(C≡C) frequencies of 2210 cm^{-1} (**23b´**) and 2203 cm^{-1} ([**23b´**]$^+$) are in good agreement with principal features of the experimental band envelopes (**23b** 2188 cm^{-1}; [**23b´**]$^+$ 2167 cm^{-1}), the additional features at 2223 cm^{-1} (**23b´**) and 2203 cm^{-1} ([**23b´**]$^+$) may explain in part the experimentally observed high-energy shoulder of the ν(C≡C) band. Overall, the calculations in each case overestimate the ν(C≡C) frequencies slightly (in spite of the customary scaling by an empirical factor of 0.95, cf. Computational Details).

The calculated ν(C=C)$_{aryl}$ frequencies are in excellent agreement with the experimental data across the series. Again, taking [**23b´**] by way of example, for neutral [**23b´**] the DFT calculations give two nearly degenerate frequencies corresponding to the experimental features at 1607 cm^{-1} (**23b′**: 1613 cm^{-1} and

1614 cm^{-1}), and 1522 cm^{-1} (**23b´**: 1514 cm^{-1} and 1511 cm^{-1}). The same holds true for the cation [**23b´**]$^{+}$, with very small shifts in the calculated $\nu(C=C)_{aryl}$ frequencies on oxidation ([**23b´**]$^{+}$ 1611 cm^{-1}, 1604 cm^{-1}, 1518 cm^{-1} and 1510 cm^{-1}). The main difference in the computed IR spectra of the neutral and oxidised forms is the appearance of an IR active $\nu(C=C)_{vinyl}$ frequency at 1527 cm^{-1} for [**23b´**]$^{+}$ which corresponds to the experimental band at 1545 cm^{-1}. Overall, the very good agreement between the calculated and experimental vibrational features permits a degree of confidence in the optimized conformations and hence significance of the calculated electronic structures.

Table 36: Orbital energies (E_{orb}) and contributions from Mulliken population analysis for [23a´]$^+$.

Orbital	E_{orb} (eV)	Contributions (%)					
		cis to ferrocene				*trans* to ferrocene	
		MeC_6H_4	C≡C	$HC{=}C_{vinyl}$	FcH	C≡C	C_6H_4Me
spin-density	/	0	0	0	99	0	0
117 β*	-1.24	0	0	0	98	0	0
117 α*	-2.59	0	0	0	98	0	0
116 β*	-1.98	5	6	20	56	4	4
116 α*	-3.20	2	4	14	68	5	2
115 β*	-2.97	2	4	14	68	4	2
115 α	-6.75	10	8	24	16	15	23
114 β	-6.70	11	9	24	12	15	23
114 α	-7.26	40	17	0	0	11	27
113 β	-7.26	39	16	0	0	11	28
113 α	-7.99	0	0	0	0	0	99
112 β	-7.99	0	0	0	0	0	99
112 α	-8.07	99	0	0	0	0	0
111 β	-8.08	99	0	0	0	0	0
111 α	-8.33	19	6	11	29	4	23
110 β	-8.39	20	9	13	21	7	24
110 α	-8.65	0	33	0	5	49	2
109 β	-8.66	1	32	0	0	52	3
109 α	-8.76	0	0	0	93	4	0
108 β	-8.96	0	0	0	97	0	0
108 α	-9.21	1	43	4	9	31	0
107 β	-9.21	0	33	3	31	24	0
107 α	-9.28	4	11	9	48	14	8
106 β	-9.23	0	18	3	54	13	0
106 α	-9.55	23	30	0	0	25	14
105 β	-9.56	16	24	0	12	23	14
105 α	-10.20	0	0	0	96	0	0
104 β	-9.62	0	4	0	83	5	0
104 α	-10.33	0	2	1	86	2	0
103 β	-9.66	0	0	0	93	0	0
103 α	-10.40	0	0	0	93	0	0
96 α	-11.30	0	0	0	90	0	1

*unoccupied orbital.

Table 37: Orbital energies (E_{orb}) and contributions from Mulliken population analysis for [23b´]$^+$.

Orbital	E_{orb} (eV)	Contributions (%) *cis* to ferrocene				*trans* to ferrocene	
		$Me_2NC_6H_4$	C≡C	$HC=C_{vinyl}$	FcH	C≡C	$C_6H_4NMe_2$
spin-density	/	0	0	0	101	-1	0
133 β*	-0.99	0	0	0	98	0	0
133 α*	-2.36	0	0	0	98	0	0
132 β*	-1.68	5	6	19	58	3	4
132 α*	-3.12	1	4	12	68	5	3
131 β*	-2.79	3	5	14	64	5	3
131 α	-5.95	0	0	10	5	11	66
130 β	-5.90	8	2	13	6	10	55
130 α	-6.06	72	11	4	0	1	6
129 β	-6.07	64	10	1	0	3	17
129 α	-7.36	11	7	21	21	11	17
128 β	-7.38	12	8	21	16	12	18
128 α	-7.95	0	0	0	0	0	99
127 β	-7.96	0	0	0	0	0	99
127 α	-8.04	99	0	0	0	0	0
126 β	-8.05	99	0	0	0	0	0
126 α	-8.31	29	21	0	0	18	21
125 β	-8.34	30	21	0	0	18	22
125 α	-8.43	1	38	0	0	52	3
124 β	-8.43	1	38	0	0	52	3
124 α	-8.61	0	0	0	96	0	0
123 β	-8.81	0	0	0	98	0	0
123 α	-8.81	11	4	5	60	3	10
122 β	-8.92	7	2	3	70	2	6
122 α	-9.01	3	48	3	0	36	0
121 β	-9.01	3	47	3	0	35	0
121 α	-9.51	21	2	12	18	5	29
120 β	-9.25	13	1	4	55	0	15
120 α	-9.95	27	17	0	7	17	21
119 β	-9.42	0	0	0	95	0	0
119 α	-10.00	0	1	0	86	2	0
118 β	-9.44	0	0	0	95	0	0
118 α	-10.17	0	0	0	94	0	0
117 β	-9.45	0	0	0	95	0	0
117 α	-10.27	1	4	2	82	3	0
113 α	-11.05	1	2	4	78	2	1

*unoccupied orbital.

Table 38: Orbital energies (E_{orb}) and contributions from Mulliken population analysis for [23d´]$^+$.

Orbital	E_{orb} (eV)	Contributions (%)					
		cis to ferrocene				*trans* to ferrocene	
		$O_2NC_6H_4$	C≡C	$HC{=}C_{vinyl}$	FcH	C≡C	$C_6H_4NO_2$
spin-density	/	0	0	0	99	0	0
134 β*	-1.12	4	4	11	67	1	2
131 β*	-2.46	0	0	2	18	5	52
131 α*	-2.79	0	0	0	98	0	0
130 β*	-2.54	48	5	3	28	0	0
130 α*	-3.48	5	5	17	53	5	4
129 β*	-3.34	9	6	18	48	5	6
129 α	-7.26	8	10	27	21	17	14
128 β	-7.23	9	11	27	17	17	15
128 α	-8.09	32	21	0	0	16	24
127 β	-8.09	32	21	0	0	16	25
127 α	-8.56	0	0	0	0	0	98
126 β	-8.56	0	0	0	0	0	98
126 α	-8.66	98	0	0	0	0	0
125 β	-8.66	98	0	0	0	0	0
125 α	-8.91	0	0	1	87	0	3
124 β	-8.99	3	30	2	7	42	6
124 α	-8.93	10	11	3	49	12	7
123 β	-9.09	7	6	4	53	11	10
123 α	-9.03	2	26	0	12	45	4
122 β	-9.12	3	0	0	85	4	0
122 α	-9.54	10	35	2	0	21	21
121 β	-9.51	6	1	6	67	2	9
121 α	-9.66	13	3	0	0	9	68
120 β	-9.54	11	35	2	0	20	20
120 α	-9.71	35	5	11	25	6	15
119 β	-9.66	13	3	0	0	9	68
119 α	-9.75	51	14	5	8	7	7
118 β	-9.74	67	13	0	1	6	3
118 α	-9.85	0	0	0	0	0	97
117 β	-9.78	0	0	0	93	0	0
117 α	-9.92	97	0	0	0	0	0
116 β	-9.86	0	0	0	0	0	97
116 α	-10.07	0	0	0	0	0	91
115 β	-9.87	0	0	0	94	0	0
115 α	-10.13	91	0	0	0	0	0
108 α	-11.47	0	0	1	92	0	0

*unoccupied orbital.

4.3.5. UV-vis NIR Spectroelectrochemistry and TDDFT Calculations

UV-Vis-NIR spectral changes recorded for compounds **23a-d** undergoing ferrocenyl-centered oxidation are shown in Figure 80 - Figure 83, and the wavenumbers of the absorption maxima of the neutral parent and oxidised cationic complexes are summarized in Table 39. More detailed analysis of the spectral changes and assignment of the absorption bands to particular vertical electronic transitions are facilitated by DFT and TDDFT calculations of the closed and open shell systems described below. The complications arising from the secondary reactivity of the oxidised anilinyl substituted compounds [**23b**]$^+$ and [**23c**]$^+$ observed in the IR spectroelectrochemical experiments are greatly reduced at the much lower concentrations used for the anodic UV-Vis spectroelectrochemical experiments (see Experimental).

Table 39: Electronic absorption spectra of 23a-d and their 1e- oxidised forms in CH_2Cl_2 /NBu_4PF_6.

Compound	Wavenumber (cm^{-1})
23a	43420, 40020, 35210, 33170, 29730, 28900, 20160
23a$^+$	39250, 34730 (sh), 32440 (sh), 30340, 23300, 17730, ~10970
23b	43240, 34850, 30250 (sh), 27900 (sh), 26750, 20160
23b$^+$	39250, 34390, 30790 (sh), 27460, 19900, 15610, ~10480
23c	43610, 35830, 31070, 27750, 20790
23c$^+$	38660 (sh), 35820, 32340, 29070, 25080, 22000, 16470, ~10500
23d	35090, 31840, 28510, 25640, 18590
23d$^+$	38370, 30250, 26020 (sh), 23300 (sh), 18750, ~11040

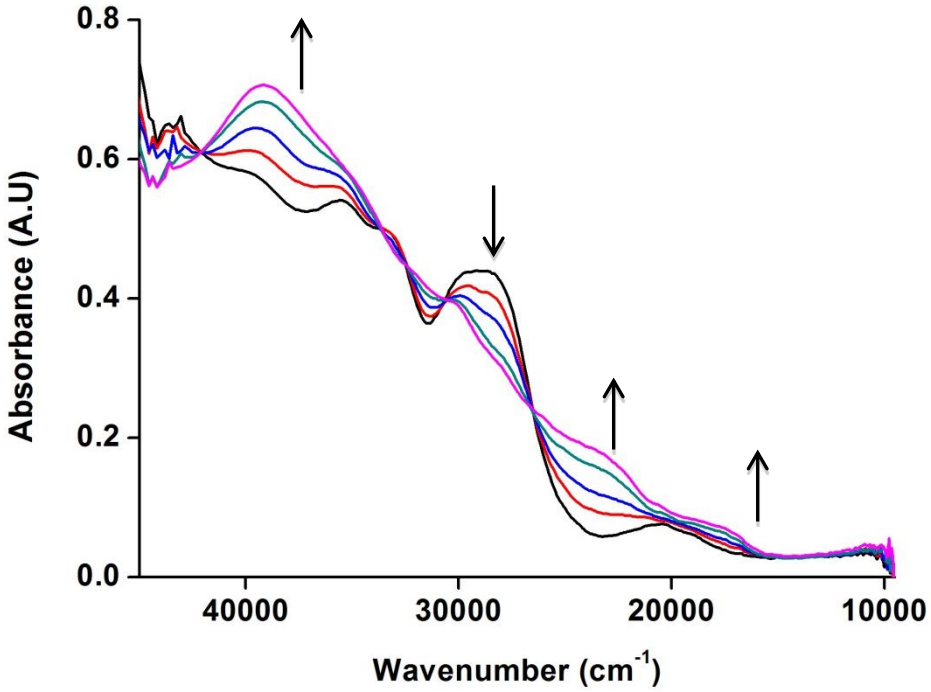

Figure 80: Reversible UV-Vis-NIR spectral changes resulting from the ferrocenyl-centered electrochemical oxidation of 23a in CH_2Cl_2 / 10^{-1} M NBu_4PF_6 within an OTTLE cell.

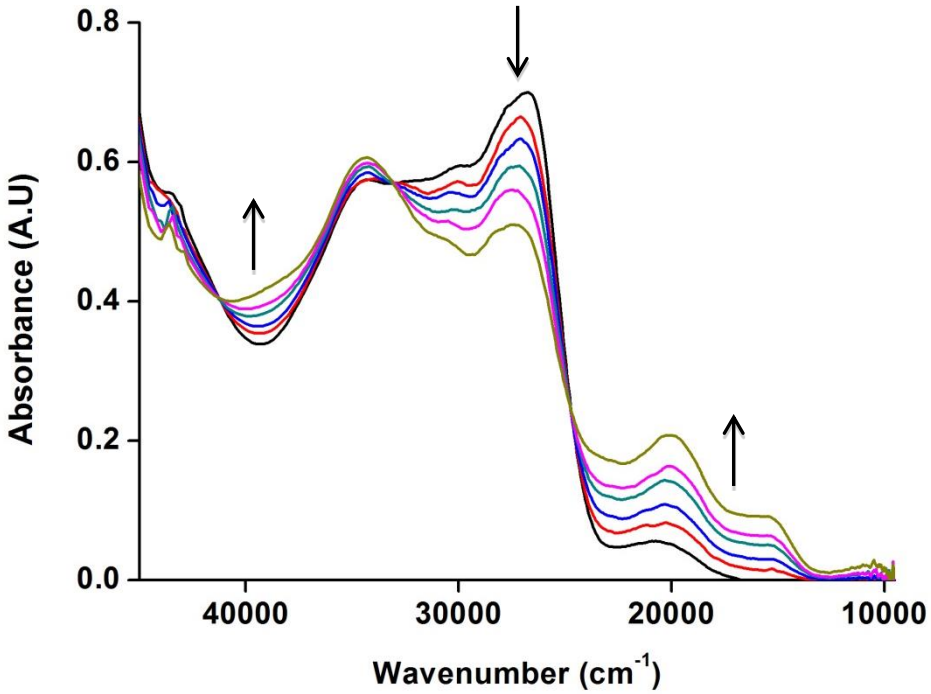

Figure 81: Reversible UV-Vis-NIR spectral changes resulting from the ferrocenyl-centered electrochemical oxidation of 23b in CH_2Cl_2 / 10^{-1} M NBu_4PF_6 within an OTTLE cell.

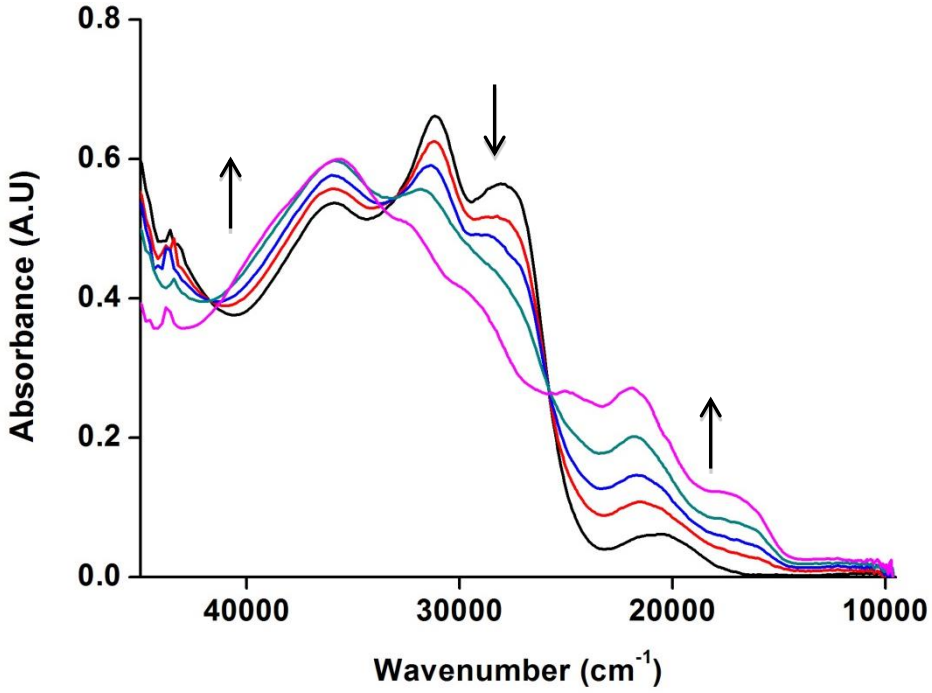

Figure 82: Reversible UV-Vis-NIR spectral changes resulting from the ferrocenyl-centered electrochemical oxidation of 23c in CH_2Cl_2 / 10^{-1} M NBu_4PF_6 within an OTTLE cell.

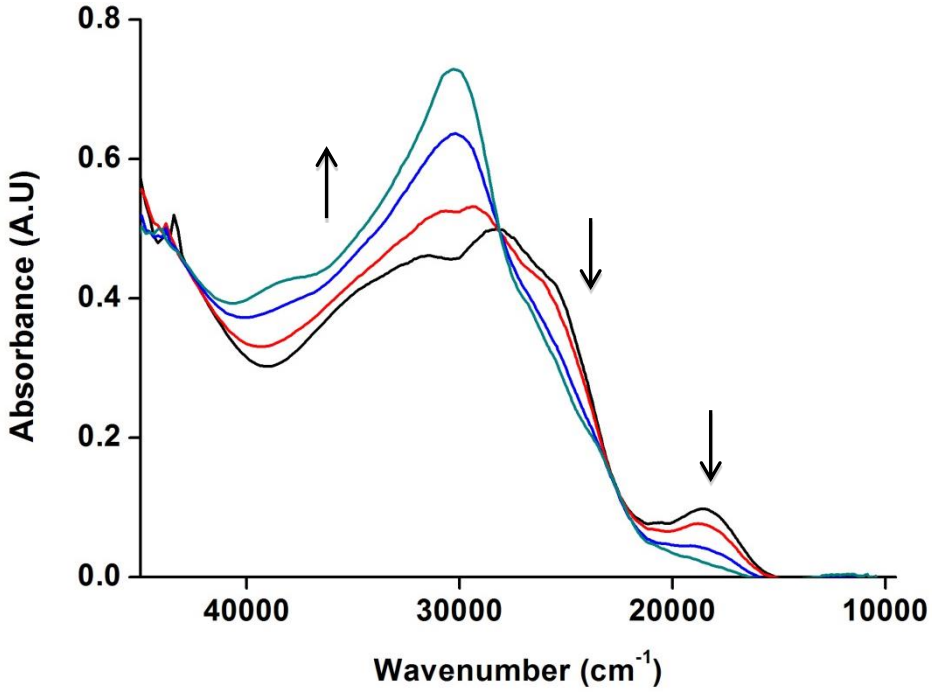

Figure 83: Reversible UV-Vis-NIR spectral changes resulting from the ferrocenyl-centered electrochemical oxidation of 23d in CH_2Cl_2 / 10^{-1} M NBu_4PF_6 within an OTTLE cell.

To assign the spectroelectrochemically observed UV-vis spectra, time-dependent DFT (TDDFT) calculations were performed for [**23a´**]$^+$, [**23b´**]$^+$ and [**23d´**]$^+$ (Table

40). In each case the lowest energy excitation of significant intensity is computed to be between 8200 and 8400 cm^{-1}, the other d-d transition at lower energy band observed at 4000 cm^{-1} not being calculated with any appreciable intensity. The 8200 - 8400 cm^{-1} transition also arises from a low-lying ferrocenyl-based MO and therefore also has interconfigurational (or pseudo-dd) character. The first electronic transition at energies greater than 10000 cm^{-1} is computed at 10123 cm^{-1} (μ_{trans} = 2.0 D) for [**23b´**]$^+$, which is in excellent agreement with the broad observed absorption at 10480 cm^{-1} for this complex and similar bands in the others (Figure 80 - Figure 83). Several orbitals contribute to the transition. The predominant character is that of a charge transfer from one ene-yne unit to the ferrocenyl cation, although the orbitals are more delocalised in the case of [**23d´**]$^+$ than the other systems.

Multiple transitions close in energy are computed around 16500 cm^{-1}.They can be assigned to the broad feature observed experimentally near 15000 cm^{-1}. In the case of [**23b´**]$^+$ the excitations at 16108 cm^{-1} (μ_{trans} = 2.9 D) and at 16560 cm^{-1} (μ_{trans} = 6.2 D) arise from transitions in which the hole is transferred from the vinyl ferrocenyl moiety to *cis*- and *trans*- branches of the cross-conjugated organic fragment. At 16309 cm^{-1} (μ_{trans} = 3.4 D) TDDFT gives a purely ferrocenyl centred excitation, which does not involve charge transfer. Precise assignment of the character of the excitation at 16678 cm^{-1} (μ_{trans} = 3.8 D) is not straightforward, as multiple transitions of both CT and IC character contribute to the absorption feature (Table 40).

The most intense excitation in [**23b´**]$^+$ (μ_{trans} = 7.2 D), computed at 19640 cm^{-1}, has again ene-yne to metal charge-transfer character. The excitation energy of

19640 cm^{-1} corresponds well with the band at 19900 cm^{-1} determined experimentally. This band exhibits a weak shoulder, which can be attributed to a computed low-intensity transition at 20127 cm^{-1} (μ_{trans} = 1.5 D). Similar conclusions can also be drawn from the TDDFT results for [**23a´**]$^+$ and [**23d´**]$^+$.

Table 40: Calculated excited state parameters in the range from 0 to 20000 cm^{-1}: UV-vis-NIR transition energies E_{trans}, transition dipole moments μ_{trans} and character of [23a´]$^+$, [23b´]$^+$ and [23d´]$^+$.[a]

	E_{trans} (cm^{-1})	μ_{trans} (D)	character
[23a´]$^+$	8242	0.7	interconfiguration
	11807	1.1	cross-conjugated fragment to vinyl ferrocene charge transfer
	19432	5.7	cross-conjugated fragment to vinyl ferrocene charge transfer
	19838	2.6	cross-conjugated fragment to ferrocene charge transfer
[23b´]$^+$	8381	1.3	interconfiguration
	10123	2.0	*trans* $Me_2NC_6H_4C{\equiv}C$ to vinyl ferrocene charge transfer
	16108	2.9	*cis* $Me_2NC_6H_4C{\equiv}C$ to vinyl ferrocene charge transfer
	16309	3.4	interconfiguration
	16560	6.2	*trans* $Me_2NC_6H_4C{\equiv}C$ to vinylferrocene charge transfer
	16678	3.8	mixed interconfiguration and charge transfer
	19640	7.2	*cis* $Me_2NC_6H_4C{\equiv}C$ to vinyl ferrocene charge transfer
[23d´]$^+$	8237	0.5	interconfiguration
	12168	0.7	delocalised π/π^* to vinyl ferrocene charge transfer

[a] Transitions with a μ_{trans} < 0.5 D are neglected.

4.3.7. Implications for Grozema Transistors.

The primary focus for investigations of the ferrocenyl-ene-diynes here was based on exploring systems related to the proposal by Grozema that cross-conjugated systems can be used to promote QI effects through the conjugated bridge leading to transistor like single molecule electronic performance. The modest shift in ν(C≡C) and $\nu(C{=}C)_{vinyl}$ bands in response to the oxidation state of the ferrocene moiety together with the presence of a number of charge transfer transitions in the spectra of [**23a**]$^{+}$, [**23b**]$^{+}$ and [**23d**]$^{+}$ also points to a small interaction between the metallocene and cross-conjugated fragments. However, strong ground state electronic coupling is not an essential criterion from the point of view of the Grozema molecular transistor designs and the limited structural rearrangement (evidenced by the small ν(C≡C) variations in response to charge state changes) may also help both preserving QI effects and aid integration into molecular electronic circuits where large structural changes during operation would be detrimental to long term device stability. The observation of a resonance form of **23d** in the ATR-FTIR gives promise that such systems, with careful consideration of the remote groups, will be suitable models for the Grozema design.

4.3.8. Conclusions

A simple preparative route to ferrocenyl substituted 1,1-dialkynyl-ethenes has been developed. The alkynyl substituents have a modest electronic influence on the ferrocenyl moiety, to which they are linearly coupled, as is evidenced by the sensitivity of the ferrocenyl oxidation potential to the electronic character of these remote groups. This interaction further goes to support the proposals highlighted

above that in the right conditions communication promoted by the cross-conjugated bridge can be achieved.

4.4. Experimental Details

4.4.1. General Conditions

Solvent purification and characterisation of compounds was carried out as detailed in Chapter 2. The compounds $Pd(PPh_3)_4$[42] and ethynylferrocene[31] were prepared by the literature methods.

The supporting electrolyte, tetrabutylammonium hexafluorophos- phate (NBu_4PF_6, Aldrich), was recrystallized twice from absolute ethanol and dried overnight under vacuum at 80 °C before use. IR and UV−vis spectra were recorded on a Bruker Vertex 70v FT-IR spectrometer and a Scinco S3100 diode array spectrophotometer, respectively. UV−vis−near-IR−IR spectroelectrochemical experiments at room temperature were conducted with an OTTLE cell equipped with a Pt-minigrid working electrode and CaF_2 windows.[43] The optical path of the cell was ca. 0.2 mm. Controlled-potential electrolyses within the OTTLE cell were carried out using a PA4 potentiostat (Laboratory Devices, Polna, Czech Republic). The concentrations of the ferrocenyl compounds and the supporting electrolyte used in these measurements were 1.3×10^{-2} and 3×10^{-1} mol dm^{-2} for IR spectroelectrochemical experiments and 10^{-3} and 3×10^{-1} mol dm^{-3} for the UV−vis−near-IR studies, respectively.

4.4.2. Preparation of FcCH=CBr_2 (22)

An oven dried Schlenk flask was charged with CH_2Cl_2 (50 mL) and the solvent degassed. To this solution CBr_4 (1.936 g, 5.84 mmol) and PPh_3 (3.062 g, 11.68 mmol) were added and stirred at 0 °C for 15 minutes until the solution was deep orange in colour. To this solution **21** (1.00 g, 4.67 mmol) was added and stirred for 30 min, the ice bath removed and stirring continued for a further 2 h. The mixture was then treated with hexane to precipitate the phosphine products and filtered. The solid was redissolved and precipitated again with hexane and the process repeated till the washings run clear. The hexane solutions were combined and the solvent was removed *in vacuo*. The crude material was purified by silica column chromatography eluting with hexane. The solvent was removed from the bright red band to give a red oil that solidified on standing. Yield 1.4 g, 82 %. Spectroscopic data were identical to those reported previously.[31]

4.4.3. Preparation of 23a-f

General procedure:

An oven dried Schlenk flask was charged with triethylamine (15mL) and the solvent degassed. To this solution, CuI (5 mg), $Pd(PPh_3)_4$ (32 mg, 0.027 mmol), **22** (200 mg, 0.054 mmol) and **24** were added and the mixture refluxed for 17 hours. The mixture was filtered and the solvent removed under reduced pressure. The crude mixture was purified with silica column chromatography eluting with hexane increasing to hexane: CH_2Cl_2 (70:30), removal of the solvent gives the desired compound.

23a:

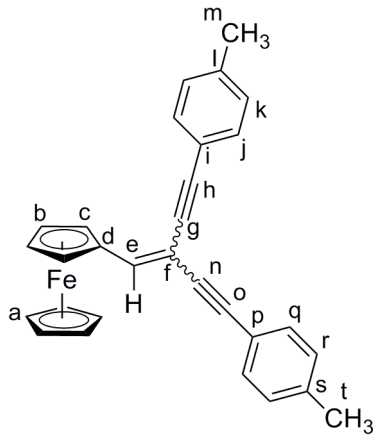

From **24a** (157 mg, 1.35 mmol), obtained as a dark red solid. Yield 109 mg, 46 %. ^{1}H NMR (CD_2Cl_2): δ 2.36 (3H, s, Me); 2.39 (3H, s, Me); 4.21 (5H, s, Cp); 4.41 (2H, apparent-t, *J* = 2 Hz, C_5H_4); 4.90 (2H, apparent-t, *J* = 2 Hz); 6.95 (1H, s, C*H*=); 7.14 (2H, d, *J* = 8 Hz, C_6H_4); 7.20 (2H, d, *J* = 8 Hz, C_6H_4); 7.41 (2H, d, *J* = 8 Hz, C_6H_4); 7.49 (2H, d, *J* = 8 Hz, C_6H_4). ^{13}C NMR (CD_2Cl_2): δ 21.80 (C_m); 21.85 (C_t); 70.20 (C_a); 70.37 (C_c); 71.10 (C_b); 80.28 (C_d); 87.75 (C_p); 87.84 ($C_{g/n}$); 89.46 (C_f); 94.09 (C_i); 99.76 ($C_{g/n}$); 120.74 (C_o); 120.76 (C_h); 129.74 (C_r); 129.87 (C_k); 131.72 (C_q); 131.75 (C_j); 139.09 (C_s); 139.50 (C_l); 144.82 (C_e). Found C 81.87, H 5.41% required C 81.81, H 5.50%. ASAP-MS(+): *m/z* 440.1 $[M]^+$.

23b:

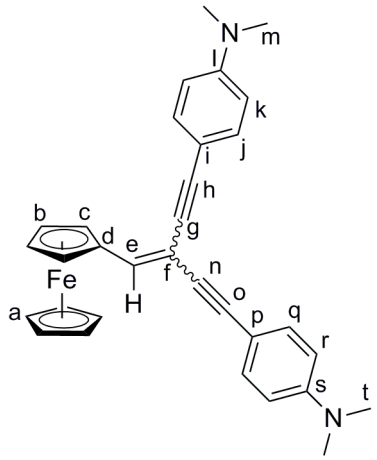

From **24b** (17 mg, 1.36 mmol), obtained as a red solid. Yield 109 mg, 40%. ^{1}H NMR (CD_2Cl_2): δ 2.98 (6H, s, NMe_2); 3.01 (6H, s, NMe_2); 4.20 (5H, s, Cp); 4.35 (2H, apparent-t, *J* = 2 Hz, C_5H_4); 4.89 (2H, apparent-t, *J* = 2 Hz, C_5H_4); 6.64 (2H, d, *J* = 9 Hz, C_6H_4); 6.70 (2H, d, *J* = 9 Hz, C_6H_4); 6.83 (1H, s, C*H*=); 7.39 (2H, d, *J* = 9 Hz, C_6H_4); 7.47 (2H, d, *J* = 9 Hz, C_6H_4). ^{13}C NMR (CD_2Cl_2): δ 40.38 (C_m, C_t); 69.93 (C_a); 70.45 (C_c); 80.87 (C_b); 86.59 ($C_{g/n}$); 88.18 (C_f); 88.51 (C_p); 95.01 (C_i); 100.89 ($C_{g/n}$); 110.24 (C_h); 110.25 (C_o); 112.20 (C_r); 112.26 (C_k); 132.75 (C_j); 132.78 (C_q); 141.64 (C_e); 150.56 (C_s); 150.77 (C_l). Found C 77.04, H 6.13, N 5.64% required C 77.09 H 6.07, N 5.62 %. ASAP-MS(+): *m/z* 498.1, $[M]^+$.

23c:

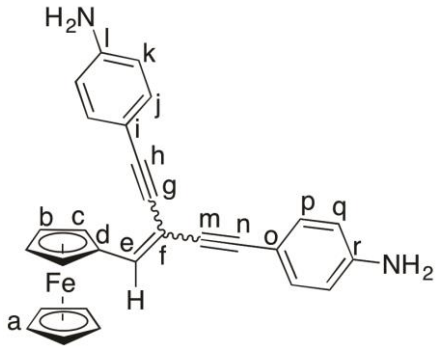

From **24c** (250 mg, 2.13 mmol), obtained as a bright red solid. Yield 236 mg, 55 %. ^{1}H NMR (CD_2Cl_2): δ 3.83 (4H, s, 2 x NH_2); 4.20 (5H, s, Cp); 4.37 (2H, apparent-t, *J* = 2 Hz, C_5H_4); 4.89 (2H, apparent-t, *J* = 8Hz); 6.62 (2H, d, *J* = 8 Hz, C_6H_4); 6.66 (2H, d, *J* = 8 Hz, C_6H_4); 6.85 (1H, s, C*H*=); 7.32 (2H, d, *J* = 8 Hz, C_6H_4); 7.39 (2H, d, *J* = 8 Hz, C_6H_4). ^{13}C NMR (CD_2Cl_2): δ 70.10 (C_a); 70.12 (C_c); 70.73 (C_b); 80.77 (C_d); 86.53 (C_f); 88.18 ($C_{g/n}$); 88.30 (C_h); 94.72 (C_o); 100.63 ($C_{g/n}$); 112.77 ($C_{l/s}$); 112.78 ($C_{l/s}$); 115.13 (C_k); 115.18 (C_r); 133.17 (C_q); 133.20 (C_j); 142.60 (C_e); 147.59 (C_i); 147.89 (C_p). Found C 75.87, H 4.91, N 6.44% required C 76.19, H 4.91, N 6.44 %. ASAP-MS(+): *m/z* 443.1 $[M+H]^+$.

23d:

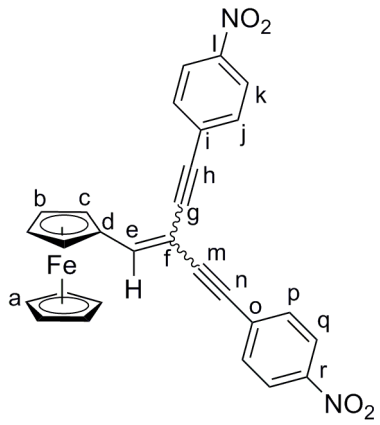

From **24d** (200 mg, 1.35 mmol), obtained as a dark red solid. Yield 121 mg, 45%. Crystals suitable for X-ray diffraction were grown from CH_2Cl_2:Ethanol. ^{1}H NMR (CD_2Cl_2): δ 4.25 (5H, s, Cp); 4.55 (2H, apparent-t, *J* = 2 Hz, C_5H_4), 4.90 (2H, apparent-t, *J* = 2 Hz, C_5H_4); 7.18 (1H, s, C*H*=), 7.65 (2H, d, *J* = 9 Hz, C_6H_4); 7.72 (2H, d, *J* = 9 Hz, C_6H_4); 8.22 (2H, d, *J* = 9 Hz, C_6H_4); 8.27 (2H, d, *J* = 9 Hz, C_6H_4). ^{13}C NMR (CD_2Cl_2): δ 69.92 (C_a); 70.28 (C_c); 71.67 (C_b); 78.66 (C_d); 86.03 (C_p); 91.70 (C_i); 92.29 ($C_{g/n}$); 94.24 (C_f); 96.85 ($C_{g/n}$); 123.63 (C_r); 123.76 (C_k); 129.85 (C_h); 130.07 (C_o); 131.91 (C_q); 131.94 (C_j), 146.83 (C_s), 147.10 (C_l), 149.12 (C_e); ASAP-MS(+) *m/z*: 502.1 $[M]^+$.

***Z*-25d**

Silica column chromatography of the previous reaction eluting with hexane increasing to hexane: CH_2Cl_2 (70:30), removal of the solvent gives the title compound as a dark red solid. Yield 49 mg. Due to the facile *E*/*Z*-isomerisation of the system ^{13}C NMR could not be obtained. Crystals suitable for X-ray diffraction were grown from CH_2Cl_2:Ethanol. ^{1}H NMR ($CDCl_3$): δ 4.23 (5H, s, Cp); 4.45 (2H, apparent-t, J = 2 Hz, C_5H_4), 4.85 (2H, apparent-t, J = 2 Hz, C_5H_4), 7.19 (1H, s, C*H*=), 7.62 (2H, d, *J* = 9 Hz, C_6H_4), 8.22 (2H, d, *J* = 9 Hz, C_6H_4).

23e:

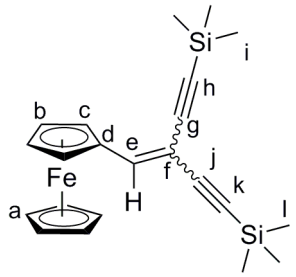

From **24e** (0.42 mL, 2.98 mmol), obtained as a dark red oil. Yield 416 mg, 76 %. ^{1}H NMR (CD_2Cl_2) δ 0.22 (9H, s, $SiMe_3$); 0.29 (9H, s, $SiMe_3$); 4.19 (5H, s, Cp); 4.38 (2H, apparent-t, J = 2 Hz), 4.83 (2H, apparent-t, J = 2 Hz); 6.89 (1H, s, C*H*=). ^{13}C NMR (CD_2Cl_2) δ 0.06 (C_l), 0.11 (C_i), 70.18 (C_a), 70.50 (C_c), 71.14 (C_b), 79.58 (C_d), 92.57 (C_k), 99.30 (C_h), 100.16 ($C_{g/j}$), 103.21 ($C_{g/j}$), 105.00 (C_f), 147.78 (C_e); ASAP-MS(+): *m/z* 404.1 $[M]^+$.

23f:

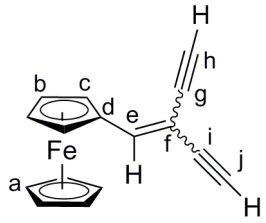

To a stirred solution of **23e** (0.345 g, 0.853 mmol) in MeOH (10 mL) and THF (10 mL) was added the K_2CO_3 (0.589 g, 4.265 mmol) and the reaction stirred for 2 hours. The mixture was poured into H_2O (20 mL) and extracted with CH_2Cl_2 (3 x 15 mL) and the organic phases combined, dried over $MgSO_4$ and filtered. The solvent was removed in vacuo to give a bright red oil that solidifies on standing. Yield: 209 mg, 94 %. ^{1}H NMR (CD_2Cl_2): δ 3.05 (1H, s, ≡C-H); 3.45 (1H, s, ≡C-H); 4.19 (5H, s, Cp); 4.42 (2H, apparent-t, J = 2 Hz), 4.84 (2H, apparent-t, J = 2 Hz); 7.00 (1H, s, C*H*=). ^{13}C NMR (CD_2Cl_2): δ 70.21 (C_a); 70.52 (C_c); 71.30 (C_b); 75.77 (C_j); 79.05

(C_d); 81.87 ($C_{g/i}$); 82.76 (C_h), 83.69 ($C_{g/i}$); 96.91 (C_f); 148.49 (C_e). ASAP MS(+): *m/z* 261.0 $[M+H]^+$.

4.5. References

1. (a) Creutz, C. *Prog. Inorg. Chem.* **1983**, *30*, 1. (b) Crutchley, R. J. *Adv. Inorg. Chem.* **1994**, *41*, 273. (c) Low, P. J.; Brown, N. J. *J. Cluster Sci*. **2010**, *21*, 235. (d) Launay. J. P. *Coord. Chem. Rev.* **2013**, *257*, 1544.
2. (a) Brady, M.; Weng, W.; Gladysz, J. A. *J. Chem. Soc. Chem. Commun.* **1994**, 2655. (b) Mohr, W.; Stahl, J.; Hampel, F.; Gladysz, J. A. *Inorg. Chem.* **2001**, *40*, 3263. (c) Mohr, W.; Stahl, J.; Hampel, F.; Gladysz, J. A. *Chem. Eur. J.* **2003**, *9*, 3324. (d) Owen, G. R.; Stahl, J.; Hampel, F.; Gladysz, J. A. *Organometallics* **2004**, *23*, 5889. (e) Zheng, Q.; Hampel, F.; Gladysz, J. A. *Organometallics* **2004**, *23*, 5896. (f) Owen, G.R.; Hampel, F.; Gladysz, J. A. *Organometallics* **2004**, *23*, 5893. (g) de Quadras, L.; Hampel, F.; Gladysz, J. A. *Dalton Trans.* **2006**, 2929. (h) Zheng, Q.; Bohling, J. C.; Peters, T.B.; Frisch, A. C.; Hampel, F.; Gladysz, J. A. *Chem. Eur. J.* **2006**, *12*, 6486. (i) de Quadras, L.; Bauer, E. B.; Stahl, J.; Zhuravlev, F.; Hampel, F.; Gladysz, J. A. *New J. Chem.* **2007**, *31*, 1594. (j) de Quadras, L.; Bauer, E. B.; Mohr, W.; Bohling, J. C.; Peters, T.B.; Martín-Alvarez, J. M.; Hampel, F.; Gladysz, J. A. *J. Am. Chem. Soc.* **2007**, *129*, 8296. (k) Stahl, J.; Mohr, W.; de Quadras, L.; Peters, T. B.; Bohling, J. C.; Martín-Alvarez, J. M.; Owen, G. R.; Hampel, F.; Gladysz, J. A. *J. Am. Chem. Soc.* **2007**, *129*, 8282. (l) Stahl, J.; Bohling, J. C.; Peters, T. B.; de Quadras, L.; Gladysz, J. A. *Pure Appl. Chem.* **2008**, *80*, 459. (m) Antonova, A. B.; Bruce, M. I.; Ellis, B. G.; Gaudio, M.; Humphrey, P. A.; Jevric, M.; Melino, G.; Nicholson, B. K.; Perkins, G. J.; Skelton, B. W.; Stapleton, B.; White, A. H.; Zaitseva, N. N. *Chem. Commun.* **2004**, 960. (n) Coat, F.; Lapinte, C. *Organometallics* **1996**, *15*, 477. (o) Xi, B.; Xu, G. L.; Fanwick, P. E.; Ren, T. *Organometallics* **2009**, *28*, 2338. (p) Xu, G. L.; Xi, B.; Updegraff, J. B.; Protasiewicz, J. D.; Ren, T. *Organometallics* **2006**, *25*, 5213.
3. (a) Lissel, F.; Fox, T.; Blacque, O.; Polit, W.; Winter, R. F.; Vekatesan, K.; Berke, H. *J. Am. Chem. Soc.* **2013**, *135*, 4051. (b) Semenov, S. N.; Taghipourian,

S. F.; Blacque, O.; Fox, T.; Venkatesan, K.; Berke, H. *J. Am. Chem. Soc.* **2010**, *132*, 7584. (c) Semenov, S. N.; Blacque, O.; Fox, T.; Venkatesan, K.; Berke, H. *J. Am. Chem. Soc.* **2010**, *132*, 3115.

4. (a) Low, P. J.; Rousseau, R.; Lam, P.; Udachin, K. A.; Enright, G. D.; Tse, J. S.; Wayner, D. D. M.; Carty, A. J. *Organometallics* **1999**, *18*, 3885. (b) Bruce, M. I.; Low, P. J.; Costuas, K.; Halet, J. F.; Best, S. P.; Heath, G. A. *J. Am. Chem. Soc.* **2000**, *122*, 1949. (c) Bruce, M. I.; Ellis, B. G.; Low, P. J.; Skelton, B. W.; White, A. H. *Organometallics* **2003**, *22*, 3184. (d) Bruce, M. I.; Costuas, K.; Davin, T.; Ellis, B. G.; Halet, J. F.; Lapinte, C.; Low, P. J.; Smith, M. E.; Skelton, B. W.; Toupet, L.; White, A. H. *Organometallics* **2005**, *24*, 3864. (e) Bruce, M. I.; Costuas, K.; Ellis, B. G.; Halet, J. F.; Low, P. J.; Moubaraki, B.; Murray, K. S.; Ouddai, N.; Perkins, G. J.; Skelton, B. W.; White, A. H. *Organometallics* **2007**, *26*, 3735. (f) Bruce, M. I.; Costuas, K.; Davin, T.; Halet, J. F.; Kramarczuk, K. A.; Low, P. J.; Nicholson, B. K.; Perkins, G. J.; Roberts, R. L.; Skelton, B. W.; Smith, M. E.; White, A. H. *Dalton Trans.* **2007**, 5387. (g) Fitzgerald, E. C.; Brown, N. J.; Edge, R.; Helliwell, M.; Roberts, H. N.; Tuna, F.; Beeby, A.; Collison, D.; Low, P. J.; Whiteley, M. W. *Organometallics* **2012**, *31*, 157. (h) Parthey, M.; Gluyas, J. B. G.; Schauer, P. A.; Yufit, D. S.; Howard, J. A. K.; Kaupp, M.; Low, P. J. *Chem. Eur. J.* **2013**. *19*. 9780.
5. (a) Le Narvor, N.; Toupet, L.; Lapinte, C. *J. Am. Chem. Soc.* **1995**, *117*, 7129. (b) Coat, F.; Lapinte, C. *Organometallics* **1996**, *15*, 477. (c) Coat, F.; Guillevic, M. A.; Toupet, L.; Paul, F.; Lapinte, C. *Organometallics* **1997**, *16*, 5988. (d) Guillemot, M.; Toupet, L.; Lapinte, C. *Organometallics* **1998**, *17*, 1928. (e) Paul, F.; Meyer, W. E.; Toupet, L.; Jiao, H. J.; Gladysz, J. A.; Lapinte, C. *J. Am. Chem. Soc.* **2000**, *122*, 9405. (f) Jiao, H. J.; Costuas, K.; Gladysz, J. A.; Halet, J. F.; Guillemot, M.; Toupet, L.; Paul, F.; Lapinte, C. *J. Am. Chem. Soc.* **2003**, *125*, 9511. (g) Ibn Ghazala, S.; Paul, F.; Toupet, L.; Roisnel, T.; Hapiot, P.; Lapinte, C. *J. Am. Chem. Soc.* **2006**, *128*, 2463. (h) Szafert, S.; Paul, F.; Meyer, W. E.; Gladysz, J. A.; Lapinte, C. *C.R. Chem.* **2008**, *11*, 693.
6. (a) Zhou, Y.; Seyler, J. W.; Weng, W.; Arif, A. M.; Gladysz, J. A. *J. Am. Chem. Soc.* **1993**, *115*, 8509. (b) Brady, M.; Weng, W.; Zhou, Y.; Seyler, J. W.; Amoroso, A. J.; Arif, A. M.; Böhme, M.; Frenking, G.; Gladysz, J. A. *J. Am. Chem. Soc.* **1997**, *119*, 775. (c) Zhuravlev, F.; Gladysz, J. A. *Chem. Eur. J.* **2004**,

10, 6510. (d) Herrmann, C.; Neugebauer, J.; Gladysz, J. A.; Reiher, M. *Inorg. Chem.* **2005**, *44*, 6174.

7. (a) Ren, T.; Zou, G.; Alvarez, J. C. *Chem. Commun.* **2000**, 1197. (b) Xu, G. L.; Zou, G.; Ni, Y. H.; DeRosa, M. C.; Crutchley, R. J.; Ren, T. *J. Am. Chem. Soc.* **2003**, *125*, 10057. (c) Xu, G. L.; Crutchley, R. J.; DeRosa, M. C.; Pan, Q. J.; Zhang, H. X.; Wang, X. P.; Ren, T. *J. Am. Chem. Soc.* **2005**, *127*, 13354. (d) Xi, B.; Ren, T. *C.R. Chem.* **2009**, *12*, 321. (e) Ying, J. W.; Liu, I. P. C.; Xi, B.; Song, Y.; Campana, C.; Zuo, J. L.; Ren, T. *Angew. Chem. Int. Ed.* **2010**, *49*, 954. (f) Xi, B.; Liu, I. P. C.; Xu, G. L.; Choudhuri, M. M. R.; DeRosa, M. C.; Crutchley, R. J.; Ren, T. *J. Am. Chem. Soc.* **2011**, *133*, 15094.
8. Ricks, A. B.; Solomon, G. C.; Colvin, M. T.; Scott, A. M. Chen, K.; Ratner, M. A.; Wasielewski, M. R. *J. Am. Chem. Soc.* **2010**, *132*, 7973.
9. (a) Campbell, K.; McDonald, R.; Tykwinski, R. R. *J. Org. Chem.* **2002**, *67*, 1133. (b) Campbell, K.; McDonald, R.; Tykwinski, R. R. *J. Porph. Phtalocya.* **2005**, *9*, 794. (c) Ooms, K. J.; Campbell, K.; Tykwinski, R. R.; Wasylishen, R. E. *J. Mater. Chem.* **2005**, *15*, 4318.
10. (a) Boldi, A. M.; Diederich, F. *Angew. Chem. Int. Ed. Engl* **1994**, *33*, 468. (b) Anthony, J.; Boldi, A. M.; Boudon, C.; Gisselbrecht, J. P.; Gross, M.; Seiler, P.; Knobler, C. B.; Diederich, F. *Helv. Chim. Acta* **1995**, *78*, 797. (c) Eisler, S.; Tykwinski, R. R. *Angew. Chem. Int. Ed.* **1999**, *38*, 1940. (d) Tobe, Y.; Umeda, R.; Iwasa, N.; Sonoda, M. *Chem. Eur. J.* **2003**, *9*, 5549. (e) Zhao, Y. L.; Liu, Q.; Zhang, J. P.; Liu, Z. Q. *J. Org. Chem.* **2005**, *70*, 6913. (f) Bandyopahyay, A.; Varghese, B.; Hopf, H.; Sankararaman, S. *Chem. Eur. J.* **2007**, *13*, 3813. (g) Chen, G.; Wang, L.; Thompson, D. W.; Zhao, Y. *Org. Lett.* **2008**, *10*, 657. (h) Gholami, M.; Chaur, M. N.; Wilde, M.; Ferguson, M. J.; McDonald, R.; Echegoyen, L.; Tykwinski, R. R. *Chem. Commun.* **2009**, 3038. (i) Chen G.; Dawe, L.; Wang, L.; Zhao, Y. *Org. Lett.* **2009**, *11*, 2736. (j) Hasegawa, M.; Takatsuka, Y.; Kuwatani, Y.; Mazaki, Y. *Tett. Lett.* **2012**, *53*, 5385. (k) Linkcke, K.; Frellsen, A. F.; Parker, C. R.; Bond, A. D.; Hammerich, O.; Nielsen, M. B. *Angew. Chem. Int. Ed.* **2012**, *51*, 6099.
11. (a) Burdett, J. K.; Mortara, A. K. *Chem. Mater.* **1997**, *9*, 812. (b) Gobbi, L.; Seiler, P.; Diederich, F.; Gramlich, V. *Helv. Chim. Acta* **2000**, *83*, 1711. (c) Gobbi, L.; Elmaci, N.; Nuran, H. P.; Diederich, F. *ChemPhysChem* **2001**, *2*, 423. (d) Zhao, Y.; Ciulei, S. C.; Tykwinski, R. R. *Tet. Lett.* **2001**, *42*, 7721. (e)

Moonen, N. N. P.; Boudon, C.; Gisselbrecht, J. P.; Seiler, P.; Gross, M.; Diederich, F. *Angew. Chem. Int. Ed.* **2002**, *41*, 3044. (f) Moonen, N. N. P.; Gist, R.; Boudon, C.; Gisselbrecht, J. P.; Seiler, P.; Kawai, T.; Kishioka, A.; Gross, M.; Irie, M.; Diederich, F. *Org. Biomol. Chem.* **2003**, *1*, 2032. (g) Mitzel, F.; Boudon, C.; Gisselbrecht, J. P.; Seiler, P.; Gross, M.; Diederich, F. *Helv. Chim. Acta* **2004**, *87*, 1130. (h) Auffrant, A.; Diederich, F.; Boudon, C.; Gisselbrecht, J. P.; Gross, M. *Helv. Chim. Acta* **2004**, *87*, 3085. (i) Zhao, Y.; Slepkov, A. D.; Akoto, C. O.; McDonald, R.; Hegmann, F. A.; Tykwinski, R. R. *Chem. Eur. J.* **2005**, *11*, 321. (j) Zhao, Y.; Zhou, N.; Slepkov, A. D.; Ciulei, S. C.; McDonald, R.; Hegmann, F. A.; Tykwinski, R. R. *Helv. Chim. Acta* **2007**, *90*, 909. (k) Bures, F.; Schweizer, W. B.; May, J.; Boudon, C.; Gisselbrecht, J. P.; Gross, M.; Biaggio, I.; Diederich, F. *Chem. Eur. J.* **2007**, *13*, 5378. (l) Andersson, A. S.; Kerndrup, L.; Madsen, A. O.; Kilsa, K.; Brondsted Nielsen, M.; La Porta, P. R.; Biaggio, I. *J. Org. Chem.* **2009**, *74*, 375. (m) Kato, S. I.; Kivala, M.; Schweizer, W. B.; Boudon, C.; Gisselbrecht, J. P.; Diederich, F. *Chem. Eur. J.* **2009**, *15*, 8687. (n) Lincke, K.; Christensen, M. A.; Diederich, F.; Nielsen, M. B. *Helv. Chim. Acta* **2011**, *94*, 1743. (o) Hasegawa, M.; Takatsuka, Y.; Kuwatani, Y.; Mazaki, Y. *Tet. Lett.* **2012**, *53*, 5385. (p) Bouit, P. A.; Marszalek, M.; Humphry-Baker, R.; Viruela, R.; Orti, E.; Zakeeruddin, S.; Graetzel, M.; Delgado, J. L.; Martin, N. *Chem. Eur. J.* **2012**, *18*, 11621.

12. Kocherzhenko, A. A.; Siebbeles, L. D. A.; Grozema, F. C. *J. Phys. Chem. Lett.* **2011**, *2*, 1753.
13. (a) Diederich, F.; Faust, R.; Gramlich, V.; Seiler, P. *J. Chem. Soc., Chem. Commun.*, **1994**, 2045. (b) Faust, R.; Diederich, F.; Gramlich, V.; Seiler, P. *Chem. Eur. J.* **1995**, *1*, 111. (c) Campbell, K.; McDonald, R.; Branda, N.R.; Tykwinski, R. R. *Org. Lett.* **2001**, *3*, 1045. (d) Siemsen, P.; Gubler, U.; Bosshard, C.; Gunter, P.; Diderich, F. *Chem. Eur. J.* **2001**, *7*, 1333. (e) Campbell, K.; McDonald, R.; Ferguson, M. J.; Tykwinski, R. R. *Organometallics*, **2003**, *22*, 1353. (f) Bruce, M. I.; Zaitseva. N. N.; Low, P. J.; Skelton, B. W.; White, A. H. *J. Organomet. Chem.* **2006**, *691*, 4273. (g) Akita, M.; Tanaka, Y.; Naitoh, C.; Ozawa, T.; Hayashi, N.; Takeshita, M.; Inagaki, A.; Chung, M. C. *Organometallics* **2006**, *25*, 5261.

14. (a) Cao, Z.; Ren, T. *Organometallics* **2011**, *30*, 245. (b) Xi, B.; Liu, I. P. C.; Xu, G. L.; Choduri, M. M. R.; De Rosa, M. C.; Crutchley, R. J.; Ren, T. *J. Am. Chem. Soc.* **2011**, *38*, 15094.
15. (a) Hauck, M; Schoenhaber, J; Zucchero, A. J; Hardcastle, K. I; Mueller, T. J. J; Bunz, U. H. F. *J. Org. Chem.* **2007**, *72*. 6714. (b) McGrier, P. L; Solntsev, K. M; Schoenhaber, J; Brombosz, S. M; Tolbert, L. M; Bunz, U. H. F. *Chem. Commun.* **2007**. *21*, 2127.
16. (a) Wilson, J. N; Smith, M. D; Enkelmann, V; Bunz, U. H. F. *Chem. Commun.* **2004**, *15*, 1700. (b) Zucchero, A. J; McGrier, P. L; Bunz, U. H. F. *Acc. Chem. Res*. **2010**, *43*, 397. (c) McGrier, P. L; Solntsev, K. M; Miao, S; Tolbert, L. M; Miranda, O. R; Rotello, V. M; Bunz, U. H. F. *Chem. Eur. J.* **2008**, *14*, 4503.
17. (a) Nielsen, M. B. Diederich, F. *Chem. Rev*. **2005**, *105*, 1837. (b) Gholami, M. Tykwinski, R. *Chem. Rev*. **2006**, *106*, 4997.
18. Koentjoro, O. F; Zuber, P; Puschmann, H; Goeta, A. E; Howard, J. A. K; Low, P. J. *J. Organomet. Chem*. **2003**, *670*, 178.
19. Boldi, A. M; Anthony, J; Knobler, C. B; Diedrich, F. *Angew. Chem. Int. Ed.* **1992**, *31*, 1240.
20. Martin R. E; Mader T; Diedrich F. *Angew. Chem. Int. Ed.* **1999**, *38*, 817.
21. Hilger, A; Gisselbrecht, J. P; Tykwinski, R. R; Boudon, C; Schreiber, M; Martin, R. E; Luthhi, H. P; Gross, M; Diederich, F. *J. Am. Chem. Soc*. **1997**, *119*, 2069.
22. Gobbi, L; Elmaci, N; Luthi, H. P; Diedrich, F. *ChemPhysChem.* **2001**, *2*, 423.
23. (a) Lu, Y. F; Harwig, C. W; Fallis, A. G. *J. Org. Chem*. **1993**, *58*, 4204. (b) Lu, Y. F; Harwig, C. W; Fallis, A. G. *Can. J. Chem*. **1995**, *73*, 2253.
24. Zekri, O; Hillard, E. A; Top, S; Vessieres, A; Pigeon, P; Plamont, M. A; Huche, M; Boutamine, S; McGlinchey, M. J; Muller-Bunz, H; Jaouen, G. *Dalton. Trans*. **2009**, 4318.
25. (a) Chemin, D; Linstrumelle, G. Tetrahedron. **1994**, *50*, 5335. (b) Carpita, A; Rossi, R. *Tet. Lett*. **1986**, *27*, 4351. (c) Lin, C. F; Lo, Y. H; Hsieh, M. C; Chen, Y. H; Wang, J. J; Wu, M. J. *Bioorganic and Medicinal Chemistry*. **2005**, *13*, 3565. (d) Andreini, B. P; Benetti, M; Carpita, A; Rossi, R. *Gazetta Chimica Italiana*. **1988**, *118*, 469. (e) Walker, J. A; Bitler, S. P; Wudl, F. *J. Org. Chem*. **1984**, *49*, 4733. (f) Vollhardt, K; Peter C; Winn, L. S. *Tet. Lett*. **1985**, *26*, 709. Gung, B. W; Gibeau, C; Jones, A. *Tetrahedron: Asymmetry*. **2005**, *16*, 3107.

26. Lin, Y; Yin, J; Yuan, J; Hu, M; Li, Z; Yu, G. A; Liu, Sheng H. *Organometallics*. **2010**, *29*, 2808.
27. Gao, L. B; Liu, S. H; Zhang, L. Y; Shi, L. X; Chen, Z. N. *Organometallics*. **2006**, *25*, 506.
28. Akita, M; Tanaka, Y; Naitoh, C; Ozawa, T; Hayashi, N; Takeshita, M; Inagaki, A; Chung, MC. *Organometallics*. **2006**, *25*, 5261.
29. Lindsell, W. E; Preston, P. N; Tomb, P. J. *J. Organomet. Chem*. **1992**, *439*, 201.
30. (a) Xu, G. L.; Xi, B.; Updegraff, J. B.; Protasiewicz, J. D.; Ren, T. *Organometallics* **2006**, *25*, 5213. (b) Zhao, Y.; Zhou, N.; Slepkov, A. D.; Ciulei, S. C.; McDonald, R.; Hegmann, F. A.; Tykwinski, R. R. *Helv. Chim. Acta* **2007**, *90*, 909. (c) Shoji, T.; Ito, S.; Okujima, T.; Morita, N. *Eur. J. Org. Chem.* **2011**, 5134. (d) Zhao, Y.; Luu, T.; Bernard, G. M.; Tearum, T.; McDonald, R.; Wasylishen, R. E.; Tykwinski, R. R. *Can. J. Chem.* **2012**, *90*, 994. (e) Forrest, W. P.; Cao, Z.; Hassell, K. M.; Prentice, B. M.; Fanwick, P. E.; Ren, T. *Inorg. Chem.* **2012**, *51*, 3261. (f) Forrest, W. P.; Cao, Z.; Hambrick, H. R.; Prentice, B. M.; Fanwick, P. E.; Wagenknecht, P. S.; Ren, T. *Eur. J. Inorg. Chem.* **2012**, *34*, 5616.
31. Courtney, D; McAdam, C. J; Manning, A. R; Müller-Bunz, H; Ortin, Y; Simpson, J. *J. Organomet. Chem*, **2012**, *705*, 7.
32. Luo, S. J; Liu, Y. H; Liu, C. M; Liang, Y. M; Ma, Y. X. *Synth. Commun*, **2000**, *30*, 1569.
33. Clément, S.; Guyard, L.; Knorr, M.; Villafañe, F.; Strohmann, C.; Kubicki, M. M. *Eur. J. Inorg. Chem.* **2007**, 5052.
34. (a) Frei, M.; Aradhya, S. V.; Hybertsen, M. S.; Venkataraman, L. *J. Am. Chem. Soc*. **2012**, *134*, 4003. (b) González, M. T.; Díaz, A.; Leary, E.; García, R.; Herranz, M. A.; Rubio-Bollinger, G.; Martín, N.; Agraït, N. *J. Am. Chem. Soc*. **2013**, *135*, 5420. (c) Pera, G.; Martín, S.; Ballesteros, L. M.; Hope, A. J.; Low, P. J.; Nichols, R. J.; Cea, P. *Chem. Eur. J*. **2010**, *16*, 13398. (d) Marqués-González, S.; Yufit, D. S.; Howard, J. A. K.; Martín, S.; Osorio, H. M.; García-Suárez, V. M.; Nichols, R. J.; Higgins, S. J.; Cea, P.; Low, P. J. *Dalton Trans*. **2013**, *42*, 338.

35. (a) McEwen, C. N.; McKay, R. G.; Larsen, B. S. *Anal. Chem.* **2005**, *77*, 7826. (b) Smith, M. J. P.; Cameron, N. R.; Mosely, J. A. *Analyst* **2012**, *137*, 4524.
36. Denis, R; Toupet, L; Paul, F; Lapinte, C. *Organometallics* **2000**, *19*, 4240.
37. Baronetskii, A. O.; Kuz'yants, G. M. *Russ. Chem. Bull.* **1980**, *29*, 1267.
38. (a) Kowalski, K; Linseis, M; Winter, R. F; Zabel, M; Zalis, S; Kelm, H; Kruger, H. J; Sarkar, B; Kaim, W. *Organometallics*. **2009**, *28*, 4196. (b) Warratz, R; Tuczek, F. *Inorg. Chem.* **2009**, *48*, 3591. (c) Warratz, R; Aboulfadl, H; Bally, T; Tuczek, F. *Chem. Eur. J.* **2009**, *15*, 1604.
39. Klamt, A.; Schüürmann, G. *J. Chem. Soc., Perkin Trans. 2* **1993**, *5*, 799.
40. (a) Renz, M.; Theilacker, K.; Lambert, C.; Kaupp, M. *J. Am. Chem. Soc.* **2009**, *131*, 16292. (b) Kaupp, M.; Renz, M.; Parthey, M.; Stolte, M.; Würthner, F.; Lambert, C. *Phys. Chem. Chem. Phys.* **2011**, *13*, 16973.
41. Vincent, K. B; Zeng, Q; Parthey, M. P; Yufit, D. S; Howard, J. A. K; Hartl, F; Kaupp, M; Low, P. J. *Organometallics*. **2013,** *32*, 6022-6032.
42. Coulson, D. R. *Inorg. Synth.* **1972**, *13*, 121.
43. Krejčík, M.; Daněk, M; Hartl, F. *J. Electroanal. Chem*. **1991**, *317*, 179.

Chapter 5: Synthesis and Spectroelectrochemistry of Hetero-Multimetallic Ferrocenylenediynes

5.1. Synopsis

Efforts to prepare trimetallic complexes of general form $FcCH=C(C\equiv CML_n)_2$ (ML_n= $Ru(PPh_3)_2Cp$, Ru(dppe)Cp* and Fe(dppe)Cp*) from reactions of $FcCH=C(C\equiv CH)_2$ or $FcCH=C(C\equiv CSiMe_3)_2$ with $MClL_n$ under a variety of conditions were largely unsuccessful, often yielding vividly coloured solutions containing compounds that could not be isolated or characterised. However, reaction of $FcCH=C(C\equiv CSiMe_3)_2$ with $AuCl(PPh_3)$ in the presence of NaOMe gave trimetallic $FcCH=C\{C\equiv CAu(PPh_3)\}_2$, and the heterobimetallic complex $FcCH=C\{CH=C[Ru(PPh_3)_2Cp]\}(C\equiv CH)PF_6$ could be obtained from stoichiometric reaction of $FcCH=C(C\equiv CH)_2$ with $RuCl(PPh_3)_2Cp$. In an attempt to unravel some of these complications, the related ligand 1,1-diphenyl-2,2-diethynylethene ($Ph_2C=C(C\equiv CH)_2$) was synthesised and double metallation reactions were explored. However, again, only mono-metallation with $RuCl(PPh_3)_2Cp$ was achieved, with the crystallographically determined structure of the intermediate vinylidene $Ph_2C=C\{CH=C[Ru(PPh_3)_2Cp]\}(C\equiv CH)$ suggesting that a combination of steric congestion and intramolecular reactions involving the putative vinylidene / acetylide intermediates were responsible for the synthetic difficulties encountered.

The extended ligands $Ph_2C=C(C\equiv CC_6H_4C\equiv CH)_2$ and $FcCH=C(C\equiv CC_6H_4C\equiv CH)_2$ were prepared with a view to alleviating steric congestion. This strategy was successful, allowing preparation of $Ph_2C=C(C\equiv CC_6H_4C\equiv C\{Ru(PPh_3)_2Cp\})_2$ and the

heterometallic derivatives $FcCH=C(C{\equiv}CC_6H_4C{\equiv}C\{Ru(PPh_3)_2Cp\})_2$ and $FcCH=C(C{\equiv}CC_6H_4C{\equiv}C\{Ru(dppe)Cp^*\})_2$. Whilst the oxidised forms of the $Ru(PPh_3)_2Cp$ derivatives decomposed on the timescale of the IR SEC experiments, the Ru(dppe)Cp* derivative of ferrocenylenediyne shows full reversibility of the first two oxidation processes in the IR SEC timescale. Interestingly, for both the $Ru(PPh_3)_2Cp$ and Ru(dppe)Cp* derivatives, the Ru moieties oxidise before the ferrocenyl fragment. IR spectroelectrochemistry shows that the monocation $[FcCH=C(C{\equiv}CC_6H_4C{\equiv}C\{Ru(dppe)Cp^*\})_2]^+$ (observed as part of a comproportionated mixture of the neutral and dicationic forms) gives rise to a low energy NIR band centred at ca. 5500 cm^{-1}. This band collapses when the full dicationic state is reached consistent with assignment to an IVCT process. The results suggest that if stereoselective control of the metallation can be achieved in an asymmetric system, with the right selection of cross-conjugated bridging ligand, communication between the remote centres can be achieved.

5.2. Background

The synthetic versatility of 1,1-dihaloethene substrates $R_2C{=}CX_2$ has led to the development of an array of preparative methods to these compounds, with preparation largely based on Corey-Fuchs di-bromination reactions[1] of aldehydes and ketones (Scheme 20) and elimination reactions (Scheme 21).[2] The key intermediate to 1,1-diethynyl-2,2-dihaloethenes, the diethynylketone $(Me_3SiC{\equiv}C)_2CO$, is often prepared through oxidation of $(Me_3SiC{\equiv}C)_2CHOH$, which in turn is prepared from reaction of formic esters with alkynyllithium reagents (Chapter 4.2. Introduction).[3] The dihaloethynyl moiety has been shown to undergo a range of different cross- coupling reactions with aryl[4] or ethynyl[5] partners.[6]

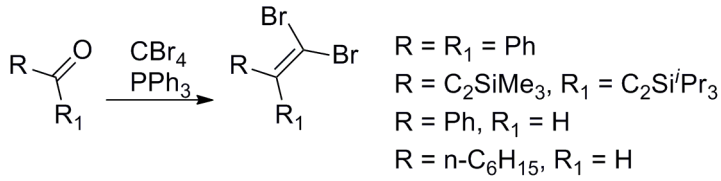

Scheme 20: Examples of the Corey-Fuchs reaction on aldehydes and ketones

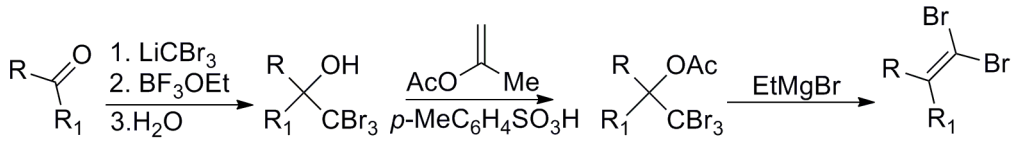

R = R_1 = ^{i}Pr
R = Ph, R_1 = Et

Scheme 21: Example of elimination reactions to 1,1-dibromoethenes

Despite the synthetic versatility shown by the organic 1,1-dihaloethene moiety, and hence the opportunities for the preparation of 1,1-ene derivatives, including ene-1,1-diethynylethenes, there are relatively few transition metal alkynyl complexes featuring a 1,1-ene fragment. Examples that have been prepared include $\{(Ph_3P)AuC{\equiv}C\}_2CO$,[7] $(FcC{\equiv}C)_2CO$,[8] and $FcC{\equiv}CC(O)C{\equiv}CSi^iPr_3$[9] (A, B and C

respectively in Scheme 22), while the Ren group has recently published a series of $Ru_2(DMBA)_4$, (DMBA = *N*,N'-dimethylbenzamidinate), complexes with donor/acceptor substituted diethynylethene moieties (Figure 84).[10] Bruce's group have also successfully synthesised ruthenium derivatives of penta-1,4-diyn-3-one. These compounds have been prepared by reaction of Ru(C≡CH)(dppe)Cp* and oxalyl chloride to give the bi-metallic ketone, $[Cp^*(dppe)RuC{\equiv}C]_2C{=}O$,[11] which is the first example of geminal-ene-diynes containing two directly bound ruthenium atoms, and explored the derivative chemistry of this complex. Interestingly, the Bruce team failed to prepare $\{Cp^*(dppe)RuC{\equiv}C)_2C{=}O$ from $Me_3SiC{\equiv}CC(=O)C{\equiv}CSiMe_3$ under a range of desilylmetallation conditions.

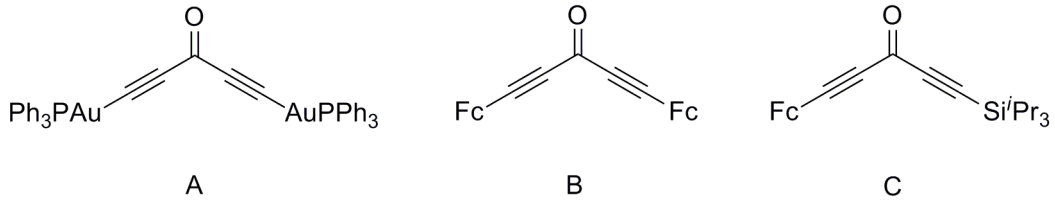

Scheme 22: Examples of cross-conjugated transition metal containing complexes

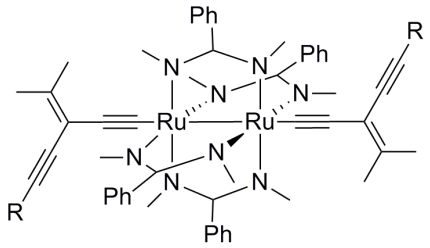

R = H, Si^iPr_3, Fc, $C_6H_4NO_2$-4, $C_6H_4NMe_2$-4

Figure 84: Ruthenium diethynylethenes prepared by the Ren group

Manipulation of the conjugated bridge in complexes of the form M-C≡C-Bridge-C≡C-M, where M is a redox-active metal fragment, can act to either promote or dampen any communication between the metal centres.[12] The increasing awareness

of the role that QI effects may play in determining the transport of charge through molecules[13] and proposals for transistors based on cross-conjugated scaffolds (Chapter 4.3.7. Implications for Grozema Transistors.) are key concepts now driving developments in the synthesis and understanding of this class of compounds.[14]

With these aspects in mind a series of cross-conjugated materials bearing redox-active ruthenium termini and a ferrocene / biphenyl appended organic bridged were prepared and studied by means of (spectro)electrochemistry. The redox-active nature of the ruthenium and ferrocene groups allow use as probes to explore the effect of charge transfer through the proto-typical ene-1,1-di(yne) cross-conjugated system, and may lead to small molecule solution models for QI effects that have been proposed to influence ET in cross-conjugated molecules when measured in a single molecule junction.[14]

5.3. Results and discussion

5.3.1. Synthesis

Having developed the synthesis of $FcCH=C(C{\equiv}CH)_2$ (Chapter 4)[15] and the corresponding organic derivatives, attention turned to the synthesis of compounds in the form of $FcCH=C(C{\equiv}CM)_2$ {M = $Ru(PPh_3)_2Cp$, Ru(dppe)Cp* and Fe(dppe)Cp*} to try to exploit the redox chemistry of the metal termini as tools for further exploration of electron-transfer in cross-conjugated systems. Recent reports have shown that *gem*-bis(rutheniumethynyl) compounds can be prepared and, as such, an array of coupling conditions were used to try and prepare compounds **26a-c** and **27a-c** (Scheme 23). The synthetic work towards the Fe(dppe)Cp* derivatives was carried

out in the laboratory of Professor Claude Lapinte in Rennes over a period of 3 months.

Various Ru and Fe half-sandwich groups have been used for many years in the study of (mostly linear) wire-like molecules, due to their ability to undergo reversible one-electron oxidation and to form MV complexes. The synthetic versatility of these compounds has been well explored and there are many different routes for the synthesis of the metal-acetylide systems based on these fragments. Most commonly a 1-alkyne HC≡CR' is reacted with the corresponding metal fragment $RuCl(L_2)(\eta^5\text{-}C_5R_5)$ (L_2 = $(PPh_3)_2$ R = H; L_2 = dppe R = Me) to form the vinylidene intermediate $[Ru(C{=}CHR')(L_2)(\eta^5\text{-}C_5R_5)]^+$ (L_2 = $(PPh_3)_2$ R = H; L_2 = dppe R = Me) and then deprotonated with base to give $Ru(C{\equiv}CR')(L_2)(\eta^5\text{-}C_5R_5)$ (L_2 = $(PPh_3)_2$, R = H; L_2 = dppe, R = Me). The synthetic strategies employed in these syntheses all follow the same principles but vary with regard to the actual reaction conditions. Commonly the reactions are carried out in MeOH with a salt such as NH_4PF_6 to promote halide ion abstraction leading to the formation of the vinylidene which is then treated with a base either *in situ* or after isolation and purification. This route has been employed to synthesise many compounds including Fe(C≡CPh)(dppe)Cp , $Fe(C{\equiv}CC_6H_4\text{-}CH_3\text{-}4)$(dppe)Cp,[16] Ru(C≡CPh)(dppe)Cp, [17] $Ru(C{\equiv}CC_6H_4\text{-}CH_3\text{-}4)(PPh_3)_2Cp$,[16] 1,4-$\{[Ru(PPh_3)_2Cp]C{\equiv}C\}_2C_6H_4$, [18] $Ru(C{\equiv}CNap)(PPh_3)_2Cp$[19] (Nap = naphthalene) and $Ru(C{\equiv}CC_6H_4\text{-}CN\text{-}4)(PPh_3)_2Cp$ [20] from 1-alkynes. Similar routes have also been employed from the silyl protected alkynes. The desilyation-metallation sequence, which is thought to proceed via a silyl-vinylidene intermediate, is promoted by fluoride sources such as KF or TBAF, and has been successfully used in the synthesis of 1,4-$\{[Ru(dppe)Cp^*]C{\equiv}C\}_2C_6H_4$,[21] 1,4-$\{[Ru(dppe)Cp]C{\equiv}C\}_2C_6H_4$,[21]

{[Ru(PPh$_3$)$_2$Cp]C≡C}$_2$[22] and 1,3,5-{[Ru(PPh$_3$)$_2$Cp]C≡C}$_2$C$_6$H$_3$.[18] Based on these previous experimental procedures, the synthesis of **27** was attempted by sequentially testing all the different reaction conditions used in these reports (Table 41), however for our system each set of conditions gave rise to a compound (or compounds) of bright blue / green colour that could not be characterised further.

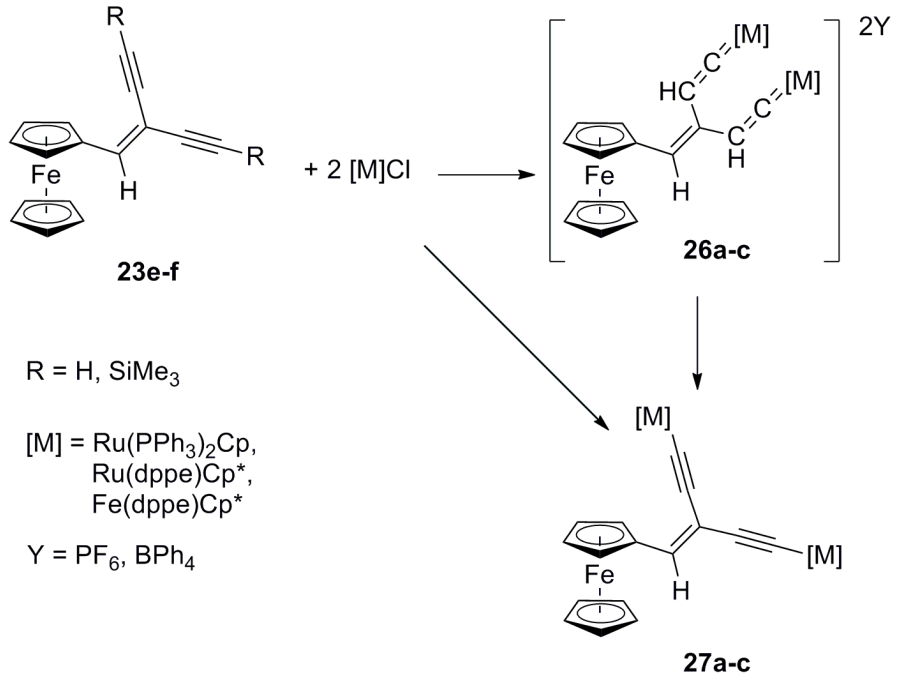

Scheme 23: Proposed synthesis of Ru and Fe substituted ferrocene-enediynes

Table 41: Attempted synthetic routes to bimetallic compounds 27a-c

Target Compound	R	M	Conditions
27a	$SiMe_3$	$Ru(PPh_3)_2Cp$	$THF:NEt_3$ $TBAPF_6$
	$SiMe_3$	$Ru(PPh_3)_2Cp$	$THF:NEt_3$ NaBPh4
	H	$Ru(PPh_3)_2Cp$	$THF:NEt_3$ $TBAPF_6$
	$SiMe_3$	$Ru(PPh_3)_2Cp$	MeOH, KF KPF_6
	$SiMe_3$	$Ru(PPh_3)_2Cp$	MeOH:THF, KF KPF_6
26a	H	$Ru(PPh_3)_2Cp$	THF $TBAPF_6$
	H	$Ru(PPh_3)_2Cp$	DCM $TBAPF_6$
	$SiMe_3$	$Ru(PPh_3)_2Cp$	MeOH KF KPF_6
27b	$SiMe_3$	Ru(dppe)Cp*	$THF:NEt_3$ $TBAPF_6$
27c	$SiMe_3$	Fe(dppe)Cp*	$THF:NEt_3$ $TBAPF_6$
	$SiMe_3$	Fe(dppe)Cp*	MeOH, KF KPF_6
	$SiMe_3$	Fe(dppe)Cp*	MeOH:THF, KF KPF_6
	H	Fe(dppe)Cp*	THF $TBAPF_6$
	H	Fe(dppe)Cp*	DCM $TBAPF_6$

With each reaction having failed to give **27a-c** it was hypothesised that a competing reaction was occurring at either the ferrocene moiety or the vinylic proton of the ligand system. It is well known that ferrocene, in the presence of a counter-ion, is susceptible to reaction with acidic protons to form ferricenium species most notably in the synthesis of common chemical oxidising agents, for example ferricenium hexafluorophosphate, while the vinylidene proton is mildly acidic.[23] As such we set out to develop a redox and chemically innocent ligand which would avoid these potential sites of reaction and clarify the causes of the synthetic difficulties.

The compound $(C_6H_5)_2C{=}CBr_2$ (**28**) has been shown to undergo cross-coupling reactions and deprotection sequences to give $(C_6H_5)_2C{=}C(C{\equiv}CR)_2$ (R = $SiMe_3$ (**29**), H (**30**)).[24] Given the analogous chemistry demonstrated by **28**, **29** and **30** to that of

the ferrocene ligand **23f** (Chapter 4) we adopted **28 - 30** as model systems related to the ferrocene ligand **23f**. Compounds **28**-**30** were synthesised in good yields from Corey-Fuchs, Sonogashira and deprotection reactions respectively (Scheme 24) and characterised with the usual spectroscopic techniques, with the data obtained consistent with the previously reported.

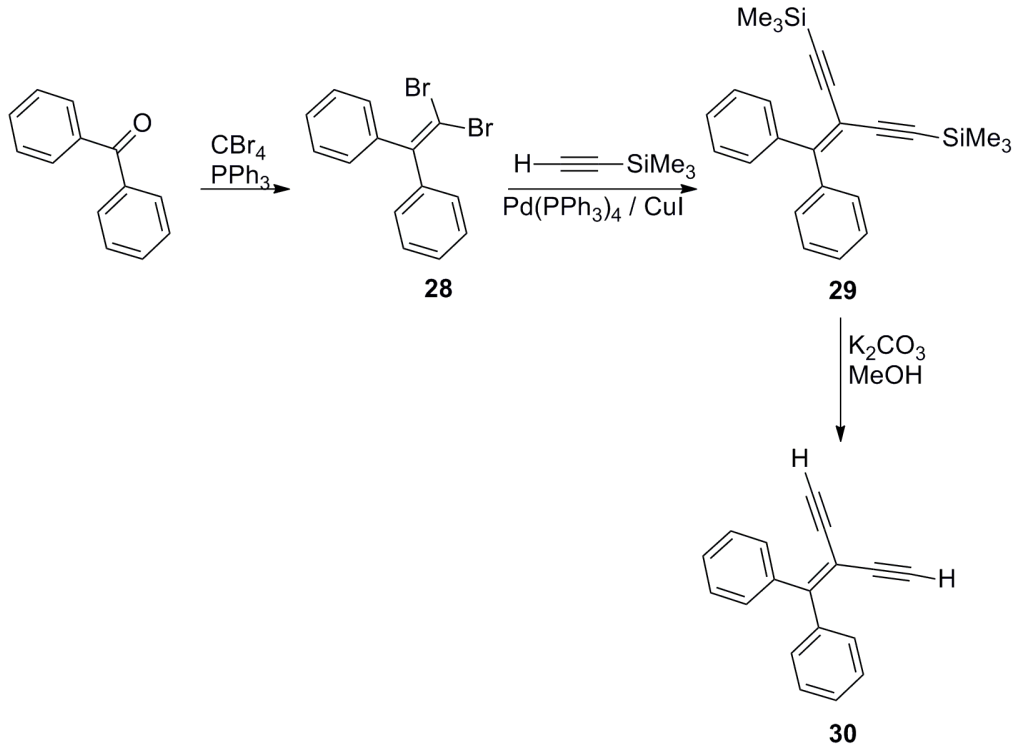

Scheme 24: Synthesis of 28-30

Having successfully synthesised **30**, $RuCl(PPh_3)_2Cp$ was used as a test substrate in the attempted synthesis of **31** with the hope of being able to isolate bimetallic compound **32**. Using standard conditions (CH_2Cl_2, KPF_6) the reaction between two equivalents of $RuCl(PPh_3)_2Cp$ and **30** at reflux was monitored over 24 hours. The ^{31}P NMR spectrum for the reaction showed a shift from δ ca. 37 ppm to ca. 42 ppm consistent with previously reported ruthenium vinylidene complexes[25] with ca. 50 % conversion. Following workup of the reaction mixture preliminary characterisation was carried out to reveal the presence of IR bands indicating that there was still a terminal alkyne present in the sample, ν(C≡*C*-*H*) 3300 cm^{-1}, as well as a signal

corresponding to the vinylidene product ca. 1600 cm^{-1}. Following further purification there was clear evidence for the presence of a mono-metallated species (discussed further below) and unreacted $RuCl(PPh_3)_2Cp$ (^{31}P NMR; 43 ppm and 37 ppm of equal intensities). Further attempts to force the reaction to completion yielded mixtures containing the same two species.

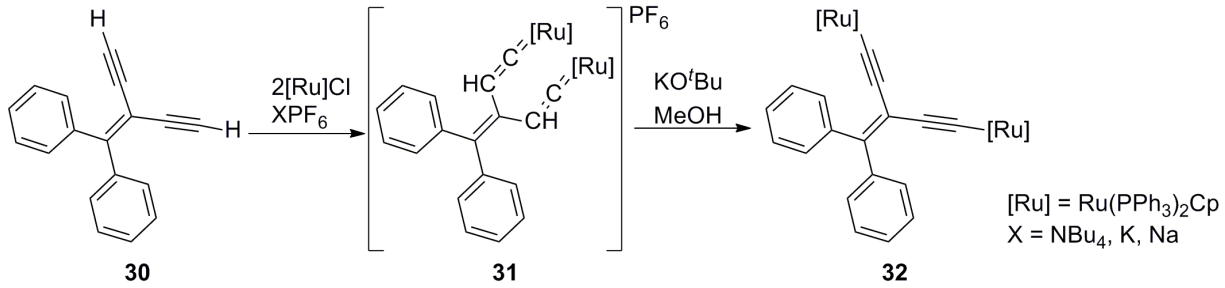

Scheme 25: Attempted synthesis of 31 and 32

Having identified a monometallic compound in the attempted synthesis of **32**, the reaction was repeated under the same reaction conditions but with only a single equivalent of $RuCl(PPh_3)_2Cp$. The reaction proceeded rapidly at reflux and the product vinylidene **33** was isolated as pink solid in good yield, 79 % (Scheme 26). The compound was characterised by the usual spectroscopic methods and suitable elemental analyses were obtained. The ^{31}P NMR spectrum shows a single signal at δ 41.62 ppm and the ^{1}H NMR data show the C_β proton at 4.92 ppm as a triplet, the Cp resonance at 5.23 ppm, consistent with a Ru-vinylidene complex, and the terminal alkyne as a singlet at δ 3.09 ppm. While the ^{31}P NMR data differs slightly from that observed in the synthesis of **32**, the slight shift can be attributed to the use of unlocked ^{31}P NMR for monitoring the reaction in the synthesis of **32**. The aromatic moieties give rise to a number of overlapping signals that were assigned on the basis of NOESY and COSY NMR. IR (CH_2Cl_2) gives rise to a ν(*CH*=*C*=Ru) 1629 cm^{-1},

ν(*C*≡*C*-H) 2109 cm^{-1} and ν(R_2C=CR_2) 1483 cm^{-1}. MALDI MS gave a signal corresponding to $[M+H]^+$ at 919.1 m/z.

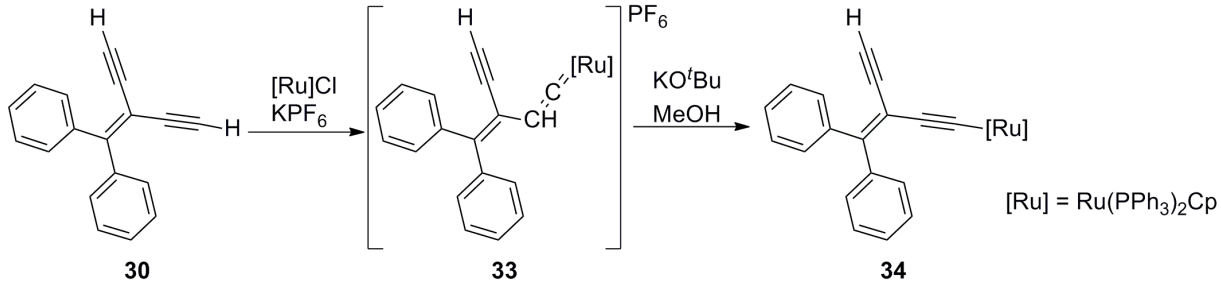

Scheme 26: Synthesis of 33 and 34

The monometallic acetylide compound **34** was synthesised in good yield (62 %) as a bright yellow solid through deprotonation of **33** by treatment of a methanolic suspension with potassium *tert*-butoxide. The ^{31}P NMR of **34** shows a single signal at δ 50.35 ppm and the ^{1}H NMR shows the terminal alkyne as a singlet at δ 2.77 ppm and the Cp resonance at 4.22 ppm, consistent with an acetylide complex of $Ru(PPh_3)_2Cp$, and disappearance of the C_β proton at 4.92 ppm. The aromatic moieties give rise to a number of overlapping signals that were assigned on the basis of NOESY and COSY NMR. IR (CH_2Cl_2) give rise to a ν(*C*≡*C*-Ru) 2044 cm^{-1}, ν(*C*≡*C*-H) 2105 cm^{-1} and ν(R_2C=CR_2) 1482 cm^{-1}. MALDI MS gave a signal corresponding to $[M]^+$ at 918.2 m/z. Further attempts to synthesise **31** or **32** from **33** or **34** respectively**,** using the conditions in Table 41, showed no further signs of reaction with the second equivalent of $RuCl(PPh_3)_2Cp$ failing to couple to the second arm of the ligand.

Having successfully synthesised monometallic compounds **33** and **34** it was decided to attempt the synthesis of the corresponding ferrocene analogue, complex **35**

(Scheme 27). The mono-vinylidene **35** was successfully obtained from **23f** with a single equivalent of $RuCl(PPh_3)_2Cp$ as a mixture of the *cis*- and *trans*- isomers, in contrast to the previous difficulties synthesising the diruthenium analogue. Attempts to synthesise **26a** from **35** gave similar results to that described earlier with the formation of a blue / green compound that could not be further identified. While the deprotonation of compound **35** to form the acetylide compound **35a** could be observed by following reactions of methanolic suspensions of **35** treated with KO^tBu with ^{31}P NMR the isolation of pure **35a** proved elusive.

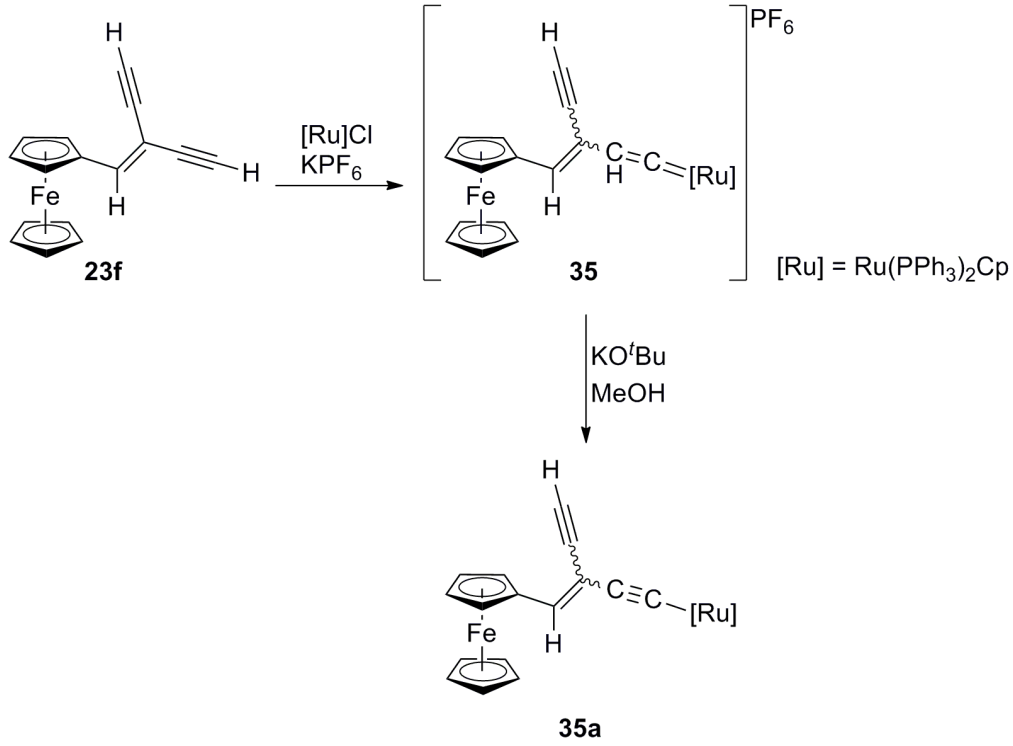

Scheme 27: Synthesis and deprotonation of 35

Having exhausted all routes to the bimetallic complexes from terminal alkyne **23f**, the silyl protected analogue **23e**, or **28** – **30,** or it was decided to revisit the transmetallation route exploited in the synthesis of a range of different compounds previously.[26] It has been shown that triphenylphosphine gold acetylide compounds are able to undergo reaction with metal chloride complexes (for example; $RuCl(PPh_3)_2Cp$, RuCl(dppe)Cp*, FeCl(dppe)Cp*, CuI, *cis*-$PtCl_2(PPh_3)_2$) to give the

corresponding metal acetylides, in good yield, and triphenylphosphine gold chloride.[26] The successful synthesis of **36** from **23e** was established from a reaction analogous to those previously reported[19] and the compound was obtained in good yield, 71 % (Scheme 28). The compound was characterised by the usual spectroscopic techniques and suitable elemental analyses were obtained. Complete assignment of the ^{13}C and ^{1}H NMR was achieved through the use of NOESY, COSY, HSQC and HMBC 2D techniques although signals could not be assigned specifically to the *cis*- and *trans*- arms of the compound. The ^{31}P NMR spectrum shows a single resonance for each inequivalent phosphorus centre at δ 42.20 and 42.41 ppm, though the signals could not be assigned specifically to the *cis*- and *trans*- arms. The ^{13}C NMR spectrum has C_α signals at δ 105.53 and 102.91 ppm that appear as doublet resonances with $J_{C\text{-}P}$ = 27 Hz. MALDI-MS give rise to a signal representing $[M]^+$ at 1176.1 *m/z*. IR (CH_2Cl_2) gave rise to a spectrum showing peaks for ν(*C*≡*C*-Au) 2102 cm^{-1} and ν(Fc*C*=*C*R_2) 1481 cm^{-1} consistent with the data reported previously for gold acetylide compounds[26] and *gem*-Fc compounds.[11]

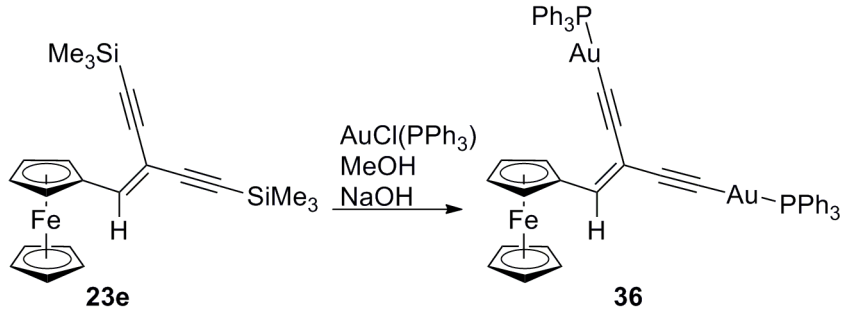

23e **36**

Scheme 28: Synthesis of 36

Unfortunately, further attempts to transmetallate **36** with $RuCl(L_2)(\eta^5\text{-}C_5R_5)$ (L_2 = $(PPh_3)_2$ R = H; L_2 = dppe R = Me) gave rise to solutions displaying the same

characteristics as previous attempts to synthesise **27a**, with generation of bright blue solution that could not be purified to identify any products.

Having been unsuccessful in all attempted synthesis of bi-metallic compounds **27a-c**, despite the successful synthesis of monometallic complexes of both organic (**33, 34)** and ferrocenyl (**35**) ligands as well as the bis-goldtriphenylphosphine complex **36** it was decided that the steric hindrance generated in these systems is too great to allow reaction at both alkyne arms (5.3.2. Molecular Structures). To further explore this synthesis the logical decision was to extend the arms of the ligand structure by inserting a $C_6H_4C{\equiv}C$-4 fragment. As such, the commercially available compound **37** was synthesised by the Sonogashira coupling of trimethylsilylacetylene ($HC{\equiv}CSiMe_3$, TMSA) and 4-iodobromobenzene catalysed by $PdCl_2(PPh_3)_2$ and CuI in basic media in good yield and the spectroscopic data were consistent with the literature.[27] The ^{1}H NMR has characteristic AB-coupling patterns for the aromatic signals giving rise to a set of apparent doublets at δ 7.44 and 7.32 ppm with coupling constants of 8 Hz and a singlet resonance for the $SiMe_3$ group at δ 0.24 ppm. The ^{13}C NMR has a characteristic $SiMe_3$ signal at δ -0.1 ppm.

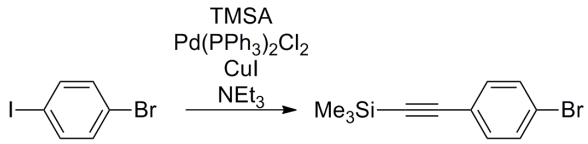

37

Scheme 29: Synthesis of 37

Further reaction of an excess of **37** with **30** under standard Sonogashira coupling conditions (Pd^0, CuI, amine solvent) gives compound **38** as a white solid following workup in good yield, 76 % (Scheme 30). ^{1}H NMR spectrum contained a series of overlapping signals that encompassed 10 H atoms within three broad signals at δ 7.41 – 7.47 ppm and two further multiplets each corresponding to 4 H at δ7.31 and

7.53 ppm that could be assigned on the basis of NOESY, COSY, HSQC and HMBC 2D-NMR. The ^{13}C spectrum can be assigned for all of the aromatic signals on the basis of the same 2D techniques although other quaternary signals could not be unambiguously assigned. The $SiMe_3$ group gives rise to ^{1}H NMR and ^{13}C NMR resonances at δ 0.23 and -0.1 ppm respectively. IR (CH_2Cl_2) give rise to a ν(*C*≡*C*-$SiMe_3$) 2156 cm^{-1}, ν(C-*C*≡*C*-Ar) 2208 cm^{-1} and ν(R_2C=*C*R_2) 1486 cm^{-1}. ASAP MS gave a signal corresponding to $[M+H]^+$ at 573.2 m/z.

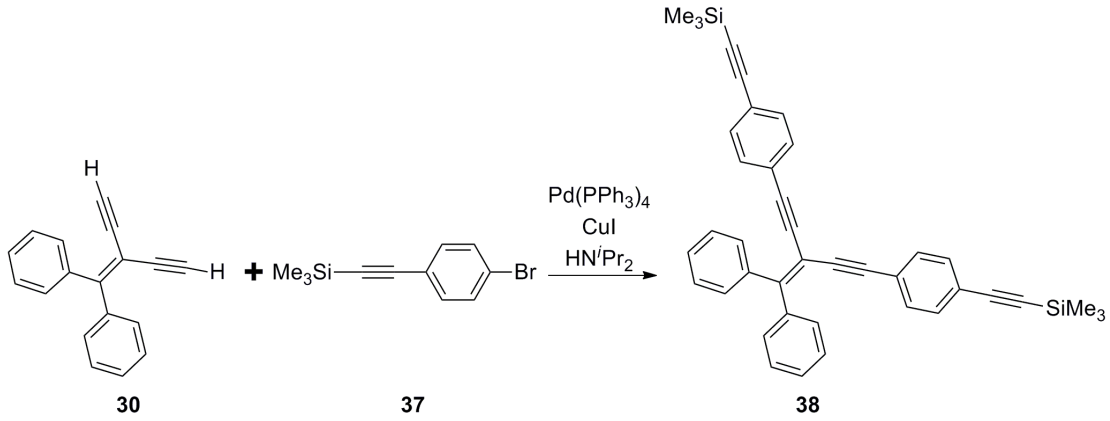

Scheme 30: Synthesis of 38

The synthesis of the dimetallic complex **39** was attempted using the *in situ* desilylation-metallation conditions (KF and MeOH) described above.[28] Under these conditions the hetero-dimetallic complex **39** was obtained as an orange solid in moderate yield (44 %) after workup. ^{1}H NMR data give rise to a series of overlapping signals that encompassed 10 H atoms from three signals at δ 7.38 – 7.43 ppm and two further multiplets each corresponding to 4 H at δ7.02 and 7.56 ppm for the ligand and three signals for the triphenylphosphine groups at δ 7.12, 7.23 and 7.46 ppm for C_m, C_p and C_o respectively, that could be assigned on the basis of NOESY, COSY, HSQC and HMBC 2D-NMR. The ^{13}C NMR spectrum gave rise to three triplets for the C_i, C_o, and C_m of the triphenylphosphine groups at δ 139.53 (J_{C-P}

= 21 Hz), 134.32 (J_{C-P} = 5 Hz) and 127.85 ppm (J_{C-P} = 4.5 Hz) respectively, Cα was observed at 116.55 ppm as a very weak multiplet although due to the signal-to-noise ratio no unambiguous splitting could be extracted. Collection of the spectrum using a long recycle and extended collection time gave rise to signals corresponding to all other quaternary carbons, although unambiguous assignment was not possible through the available 2D methods. ^{31}P NMR spectrum gave rise to a single resonance at δ 50.05 ppm, consistent with previously reported shifts of ruthenium acetylide complexes of this type and confirming the symmetric nature of the compound. In the IR (CH_2Cl_2) spectrum, ν(*C*≡*C*-Ru) 2067 cm^{-1}, ν(C-*C*≡*C*-Ar) 2204 cm^{-1} and ν(R_2C=CR_2) 1482 cm^{-1} were observed. The MALDI-MS gave an isotopic envelope corresponding to $[Ru(CO)(PPh_3)_2Cp]^+$ at 719.1 m/z, although the molecular ion could not be detected.

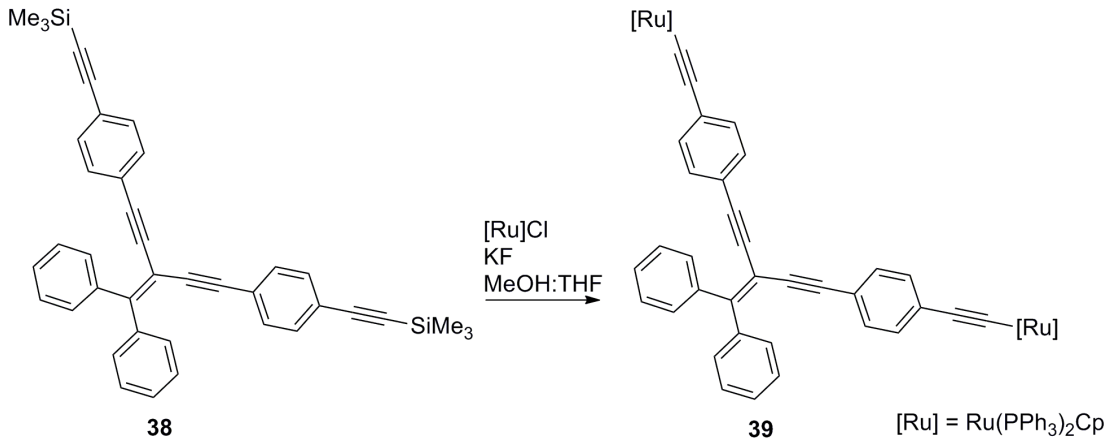

38 **39**

Scheme 31: Synthesis of 39

Having successfully managed to obtain the bimetallic compound **39,** the analogous ferrocene ligand **40** was obtained through similar Sonogashira reaction of **37** with the bis(terminal alkyne) **23f** (Scheme 32). After silica column purification, **40** was obtained as a bright red solid in moderate (51 %) yield. The ^{1}H NMR spectrum contained an overlapping set of signals in the aromatic region associated with the 8

H of the phenylene linkers, as well as the characteristic set of apparent triplets for the substituted Cp ring of the ferrocene moiety at δ 4.46 and 4.90 ppm with a singlet for the unsubstituted Cp ring at δ 4.23 ppm. Two singlet resonances were seen for the $SiMe_3$ moieties of the *cis*- and *trans*- arms of the ligand at δ 0.25 and 0.26 ppm. The singlet resonance for the vinylic proton was observed at δ 6.99 ppm consistent with the parent compound **23f** (Chapter 3). In the IR (CH_2Cl_2) ν(*C*≡*C*-Si) 2156 cm^{-1}, ν(C-*C*≡*C*-Ar) 2209 cm^{-1} and ν(R_2C=CR_2) 1576 cm^{-1} were observed. The ASAP-MS contained an isotopic envelope corresponding to $[M+H]^+$ at 605.2 *m/z*.

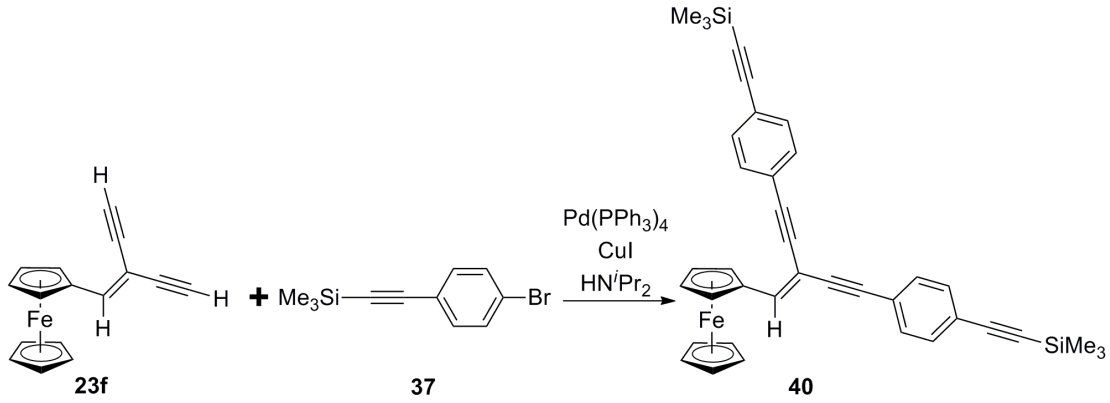

Scheme 32: Synthesis of 40

Following the successful synthesis of compound **39** an analogous method was used in the synthesis of compounds **41a-b** from the respective $RuCl(L_2)(\eta\text{-}C_5R_5)$ complex and **40** in moderate to good yields, 67 % (**41a**) and 70 % (**41b**), as bright orange solids. The compounds were characterised by the usual suite of spectroscopic methods and the NMR data assigned as fully as possible with NOESY, COSY, HSQC and HMBC 2D NMR. ^{1}H NMR for both compounds showed the characteristic signals for the mono-substituted ferrocene with triplets at δ 4.45 and 4.94 ppm (**41a**) and δ 4.41 and 4.88 ppm (**41b**) for the substituted Cp rings with singlets for the unsubstituted Cp rings at δ 4.24 and 4.20 ppm respectively. The resonance for the vinylic proton was mildly affected by the electron-donating nature

of the remote substituent with a negative shift of 0.07 ppm to 6.86 ppm for the more electron rich Cp* compound **41b**. ^{31}P NMR spectra shows two distinct signals for the *cis*- and *trans*- ruthenium fragments at δ 50.07 and 50.10 ppm for **41a,** which differs from the more electron rich **41b** that has a single ^{31}P resonance at δ 80.57 ppm suggesting that the extra electron density at the ruthenium centre negates the effect of being *cis*- and *trans*- on the phosphorus centres. In the IR (CH_2Cl_2) spectra, ν(*C*≡*C*-Ru) 2066 cm^{-1} (**41a**) and 2064 cm^{-1} (**41b**), ν(C-*C*≡*C*-Ar) 2180cm^{-1} (**41a**) and 2184 cm^{-1} (**41b**) and ν(R_2C=CR_2) 1593 cm^{-1} (**41a**) and 1588 cm^{-1} (**41b**) were observed. The MALDI-MS gave isotopic envelopes corresponding to $[M]^+$ for each compound at 1840.2 *m/z* (**41a**) and 1729.3 *m/z* (**41b**).

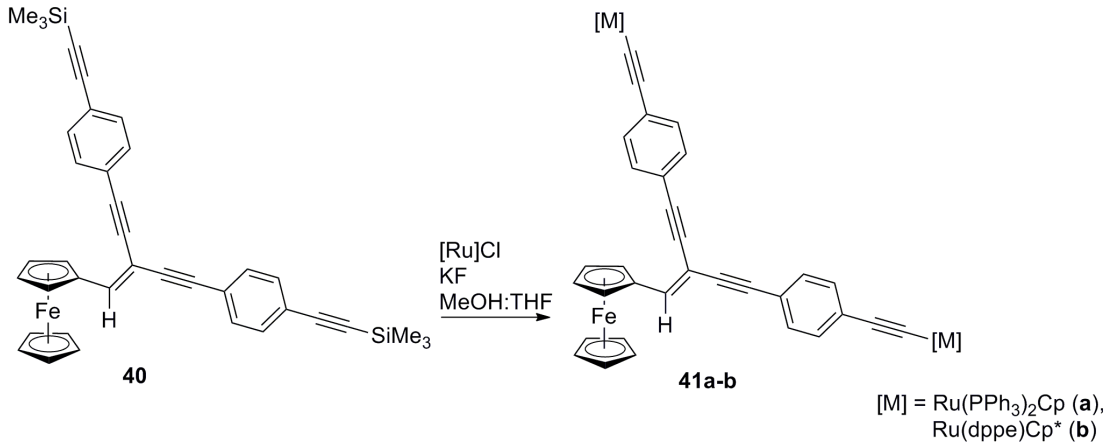

Scheme 33: Synthesis of 41a-b

5.3.2. Molecular Structures

Crystals of **33** and **34** were grown by slow diffusion of ether and methanol in CH_2Cl_2 solutions to give red plates and yellow plates respectively (Figure 85 and Figure 86) and selected bond lengths and angles are given in Table 41. The bond lengths and bond angles within **33** (Table 41) are generally unsurprising with short Ru=C [1.842(3) Å] and C=CH [1.328(4) Å] bonds and the Ru=C=C angle of 172.2(2) ° is

consistent with previously reported structures.[29] The acetylide compound **34** has bond lengths and angles consistent to those for similar reported compounds with Ru-C {2.0017(15) Å} and C≡C {1.2202(2) Å} bonds and the Ru-C≡C angle of 173.20(13) °.[30] The C=CAr_2 bond is consistent in both compounds **33** and **34** while the C2-C3-C4 bond angle is increased in the vinylidene compound **33** {115.1(2) ° and 114.74(14) ° respectively} this is consistent with the considerable change in the C2-C3-C6 in the vinylidene **33** {132.2(2) °} compared to the acetylide complex **34** {125.27(15) °} which is consistent with previously reported compounds.[31]

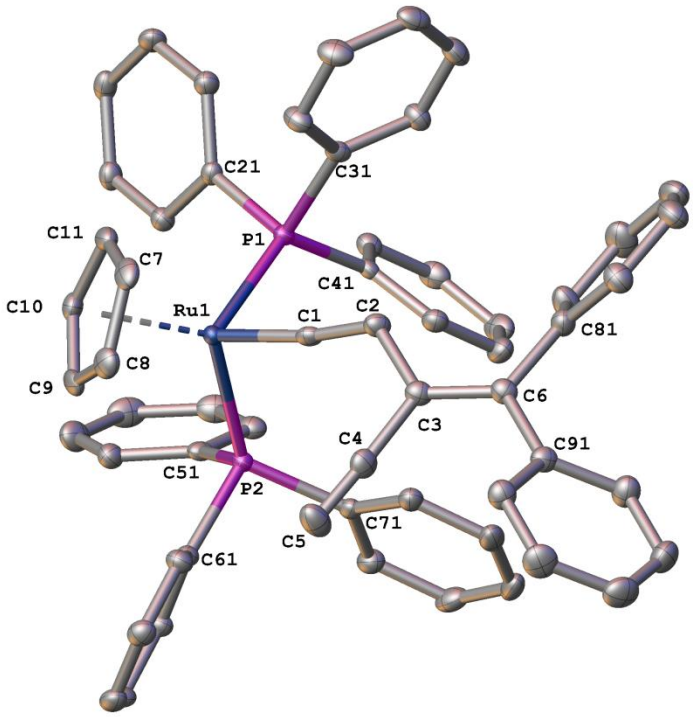

Figure 85: A plot of the molecular structure of 33 with thermal ellipsoids at 50%, showing the atom labelling scheme. Hydrogen atoms have been omitted for clarity.

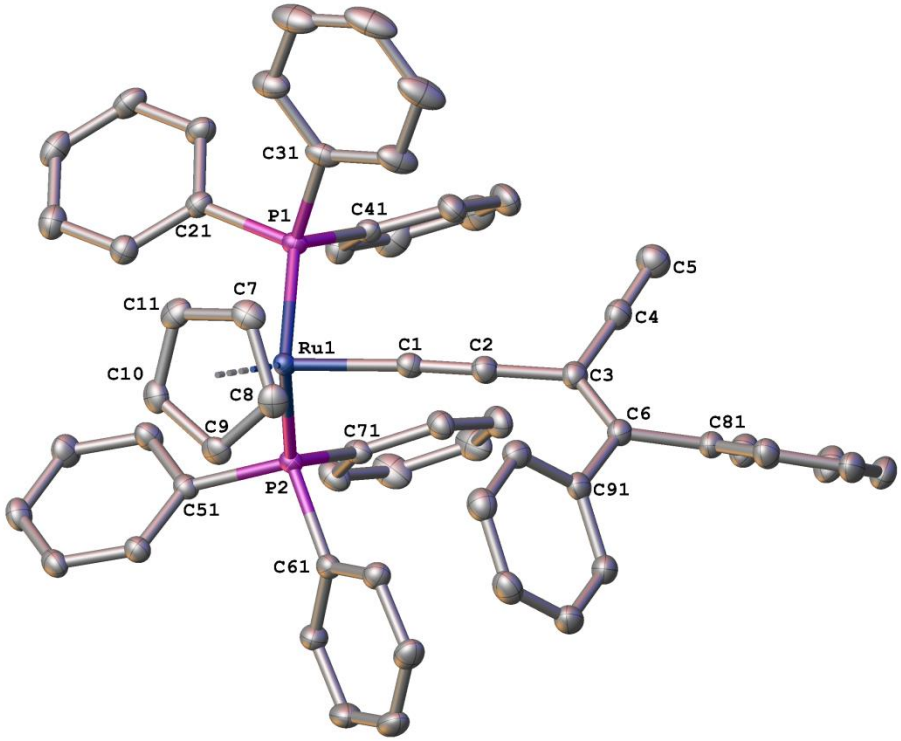

Figure 86: A plot of the molecular structure of 34 with thermal ellipsoids at 50%, showing the atom labelling scheme. Hydrogen atoms have been omitted for clarity.

Table 42: Selected bond lengths (Å) and angles (°) for 33 and 34

	33	**34**		**33**	**34**
Ru1-C1	1.842(3)	2.0017(15)	Ru1-C1-C2	172.2(2)	173.20(13)
C1-C2	1.328(4)	1.2202(2)	C1-C2-C3	125.6(2)	170.57(17)
C2-C3	1.475(3)	1.430(2)	C2-C3-C4	115.1(2)	114.74(14)
Ru1-P1	2.3290(6)	2.2831(4)	C2-C3-C6	132.2(2)	125.27(15)
Ru1-P2	2.3705(7)	2.2923(4)	P1-Ru1-C1	87.49(8)	89.09(4)
C3-C4	1.435(4)	1.444(2)	P2-Ru1-C1	98.39(8)	90.83(4)
C4-C5	1.190(4)	1.189(2)			
C3-C6	1.371(4)	1.375(2)			

5.3.3. Electrochemistry

In order to further explore the electronic properties of the metal-capped compounds **39**, **41a-b** and the model ferrocene ligand **40**, electrochemical analysis was carried out (Table 43). The CV of compound **39** shows a single redox process in 0.1 M NBu_4PF_6 that is consistent with two simultaneous one-electron oxidation processes, likely based at the ruthenium centres admixed with a considerable contribution from

the ethynyl-bridge (Figure 87). A single process was also observed in the weakly coordinating anion $[BarF_4]^-$ and, as such, it can be concluded that there is likely little or no through-bond or through-space interaction between the redox centres.

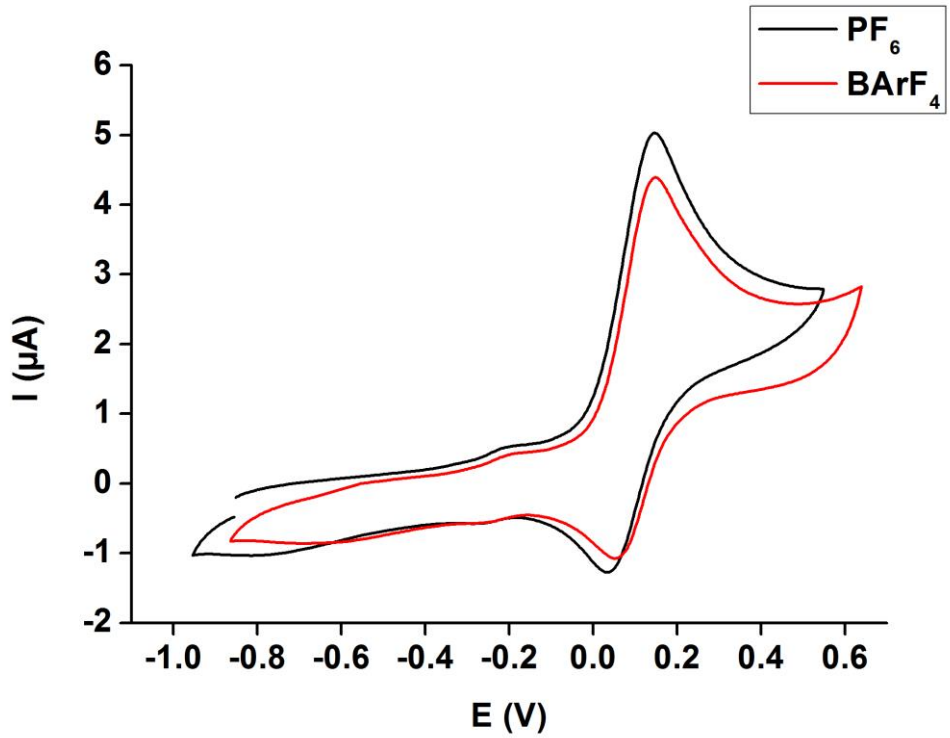

Figure 87: CV of 39 in CH_2Cl_2 with 0.1 M $NBu_4[X]$ in CH_2Cl_2 at a scan rate of 100 mV/s and referenced against $FeCp^*_2$ at -0.48 V *vs* $FeCp_2$ ($FeCp_2$= +0.0 V) (PF_6) and at -0.62 V *vs* $FeCp_2$ ($FeCp_2$ = +0.0 V) ($BArF_4$)

In order to try and understand the electrochemistry of the more complex compounds **41a** and **41b** the CV of the monometallic compound **40** in 0.1 M NBu_4PF_6 was obtained for reference. The CV shows a single reversible process at $\Delta E_{1/2}$ = 196 mV, which is consistent with the analogous mono-ferrocene compounds reported in Chapter 4 and indicates a single oxidation process at the ferrocene centre (Figure 88).

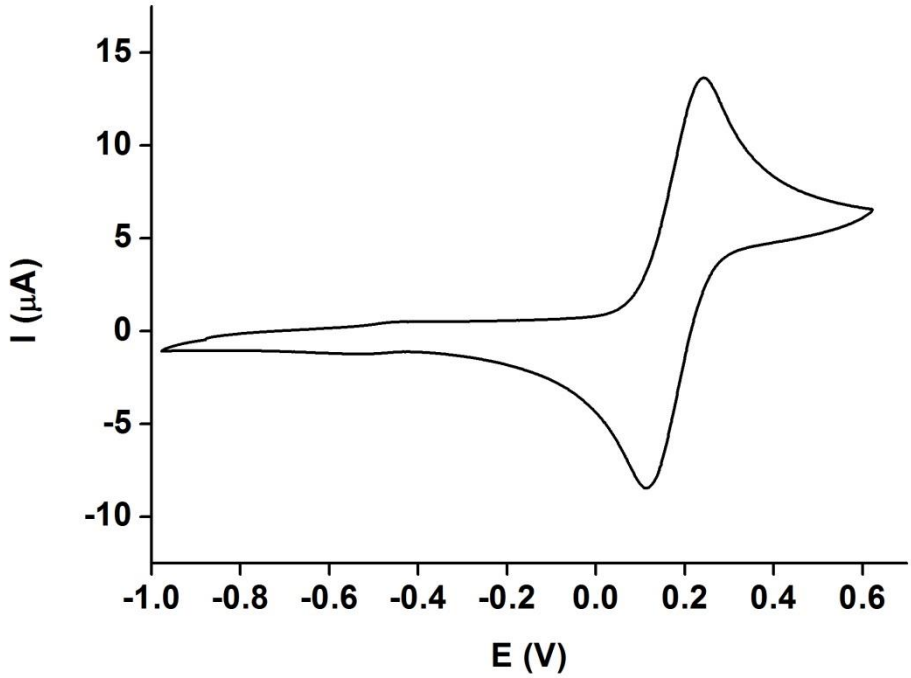

Figure 88: CV of 40 in CH_2Cl_2 with 0.1 M $NBu_4[PF_6]$ in CH_2Cl_2 at a scan rate of 100 mV/s and referenced against $FeCp_2$ at -0.48 V *vs* $FeCp_2$ ($FeCp_2$= +0.0 V).

The electrochemistry of compound **41a** shows a poorly resolved wave in 0.1 M NBu_4PF_6 that is consistent with overlapping one electron oxidation processes based at the ruthenium centres (with a considerable contribution from the ethynyl bridge) and the ferrocene oxidation (Figure 89). The simultaneous oxidation of the three redox centres is unexpected, and points at the very least to limited through-space interactions between the electrophores under these conditions. Moving to the weakly coordinating anion $[BArF_4]^-$ there is a change in the CV with the overlapping oxidations separating to two discernable redox process. Comparison with the model compound **39** in the same electrolyte (Figure 90) shows that the initial process in **41a** is consistent with the simultaneous oxidation of the two Ru centres and that the ferrocene oxidation occurs at higher potential. The separation of the redox waves in $[BArF_4]^-$ suggests that the change in electrolyte promotes a Coulombic interaction

between the ferrocene moiety and the oxidised ruthenium centres admixed with the ethynyl bridge.

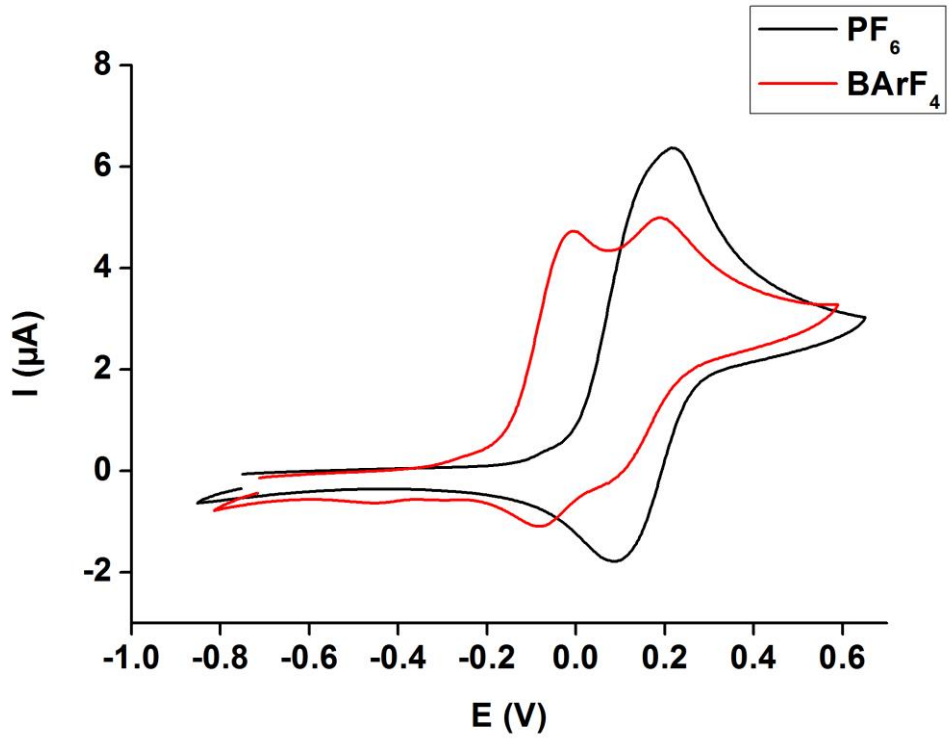

Figure 89: CV of 41a in CH_2Cl_2 with 0.1 M $NBu_4[X]$ in CH_2Cl_2 at a scan rate of 100 mV/s and referenced against $FeCp^*_2$ at -0.48 V *vs* $FeCp_2$ ($FeCp_2$ = +0.0 V) (PF_6) and at -0.62 V *vs* $FeCp_2$ ($FeCp_2$ = +0.0 V) ($BArF^{24}$)

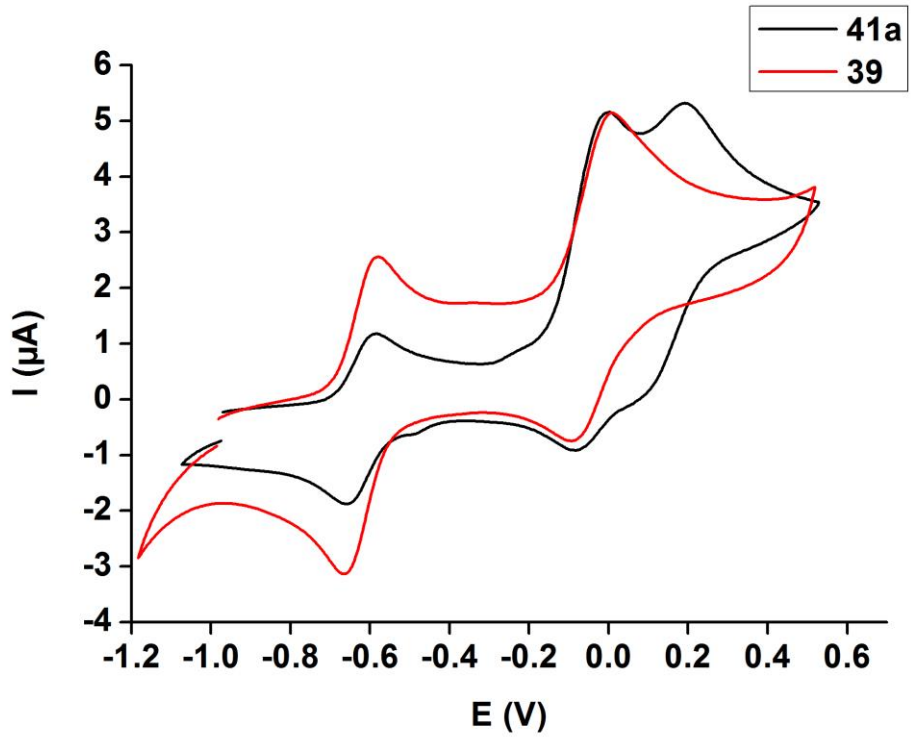

Figure 90: CV comparing 39 and 41a in CH_2Cl_2 with 0.1 M $NBu_4[BArF^{24}]$ in CH_2Cl_2 at a scan rate of 100 mV/s and referenced against $FeCp_2$ at -0.62 V *vs* $FeCp_2$ ($FeCp_2$ = +0.0 V)

The electrochemistry of compound **41b** shows two reversible redox processes in 0.1 M NBu_4PF_6 that are consistent with overlapping one electron oxidation processes based at the ruthenium centres and consistent with the two one-electron oxidation processes based at the ruthenium centres, admixed with a considerable contribution from the ethynyl bridge followed by the ferrocene oxidation (Figure 91). The more electron rich ligand structure around the Ru centre helps to stabilise the oxidation and make the oxidation potential less positive in comparison to the analogous compound **41a**. Moving to the weakly coordinating $[BArF_4]^-$ there is a change in the CV with an increase in the peak-to-peak separation (ΔE(1-2)) of the two process although there is still no separation of the Ru-C≡C- oxidation waves. As with compound **41a** the peak to peak separation indicates an increased Coulombic interaction between the ferrocene and oxidised Ru-C≡C- centres in the electrolyte containing the more weakly coordinating anion.

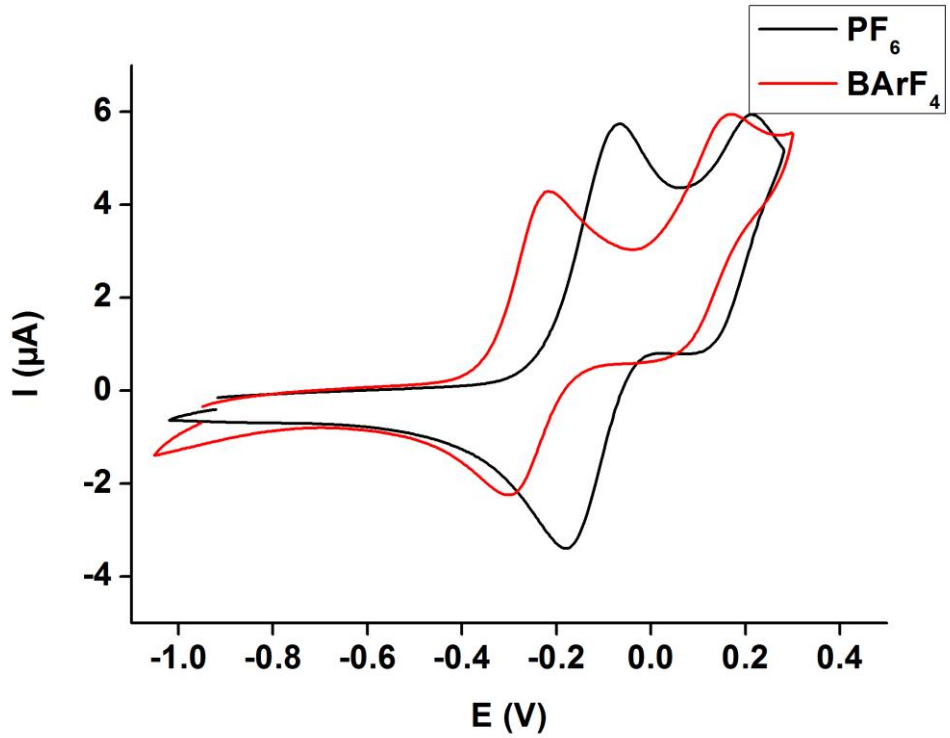

Figure 91: CV of 41b in CH_2Cl_2 with 0.1 M $NBu_4[X]$ in CH_2Cl_2 at a scan rate of 100 mV/s and referenced against $FeCp^*_2$ at -0.48 V *vs* $FeCp_2$ ($FeCp_2$ = +0.0 V) (PF_6) and at -0.62 V *vs* $FeCp_2$ ($FeCp_2$ = +0.0 V) ($BArF^{24}$)

Table 43: Oxidation potentials for complexes 39 - 41. CV in CH_2Cl_2 with 0.1 M $NBu_4[X]$ at a scan rate of 100 mV/s and referenced against $FeCp^*_2$ *vs* $FeCp_2$ ($FeCp_2$ = +0.0 V).

	$[X]^-$	$E_{1/2}(1)$ / V	$E_{1/2}(2)$ / V	ΔEv / V	ΔEp(1) / V	ΔEp(2) / V	ΔEp($FeCp^*_2$) / V
39	$[PF_6]^-$	0.078			0.120		0.080
	$[BAr^F{}_4]^-$	0.096			0.097		0.068
40	$[PF_6]^-$	0.176			0.105		0.090
41a	$[PF_6]^-$	0.151			0.150		0.074
	$[BAr^F{}_4]$	-0.045	0.144	0.189	0.94	0.81	0.068
41b	$[PF_6]^-$	-0.126	0.163	0.289	0.132	0.094	0.083
	$[BAr^F{}_4]^-$	-0.259	0.126	0.385	0.97	0.82	0.061

5.3.4. IR Spectroelectrochemistry

IR spectroelectrochemical investigations were undertaken to gain a better understanding of any interactions between the ferrocene and ruthenium moieties in compounds **39**, **41a** and **41b**. Unfortunately compound **39** was unstable on the IR SEC timeframe and upon oxidation showed rapid decomposition to the $[Ru(CO)(PPh_3)_2Cp][PF_6]$ species as indicated by presence of the characteristic $\nu(C\equiv O)$ at 1968 cm^{-1}.

Upon oxidation of **41a** (Figure 92, Table 44) there were significant changes in the spectra. As established from the electrochemistry the first oxidations occur at the ruthenium centres. Although the electrochemistry shows simultaneous oxidation of the two ruthenium centres it was possible to observe an intermediate spectra in the IR SEC consistent with a mixture of the neutral, mono- and di-cationic species. The intermediate spectrum for the mixture containing $[\mathbf{41a}]^+$ shows a decrease in the $\nu(C\equiv C\text{-}Ru)$ at 2065 cm^{-1} coupled with the growth of a new band at 1896 cm^{-1}consistent with the oxidised ruthenium centre. The change is coupled with the appearance of a new band of 1970 cm^{-1} consistent with a small amount of decomposition to $[Ru(CO)(PPh_3)_2Cp][PF_6]$. Further oxidation to $[\mathbf{41a}]^{2+}$ results in the collapse of the $\nu(C\equiv C\text{-}Ru)$ at 2065 cm^{-1} and the intermediate band at 1896 cm^{-1} to give a single band at 1920 cm^{-1} consistent with oxidised Ru-C≡C- fragments. The considerable shift of the $\nu(C\equiv C\text{-}Ru)$ upon oxidation suggests that there is considerable C≡C character in the orbitals involved in the oxidation. Upon oxidation to $[\mathbf{41a}]^{3+}$ there is a decrease in the intensity of all the major features of the spectrum, the compound then rapidly shows decomposition and all features collapse

in the IR. At higher energy for [**41a**]$^{+}$ and [**41a**]$^{2+}$ there is the appearance of a transition in the NIR region consistent with the tail of a band at higher energy.

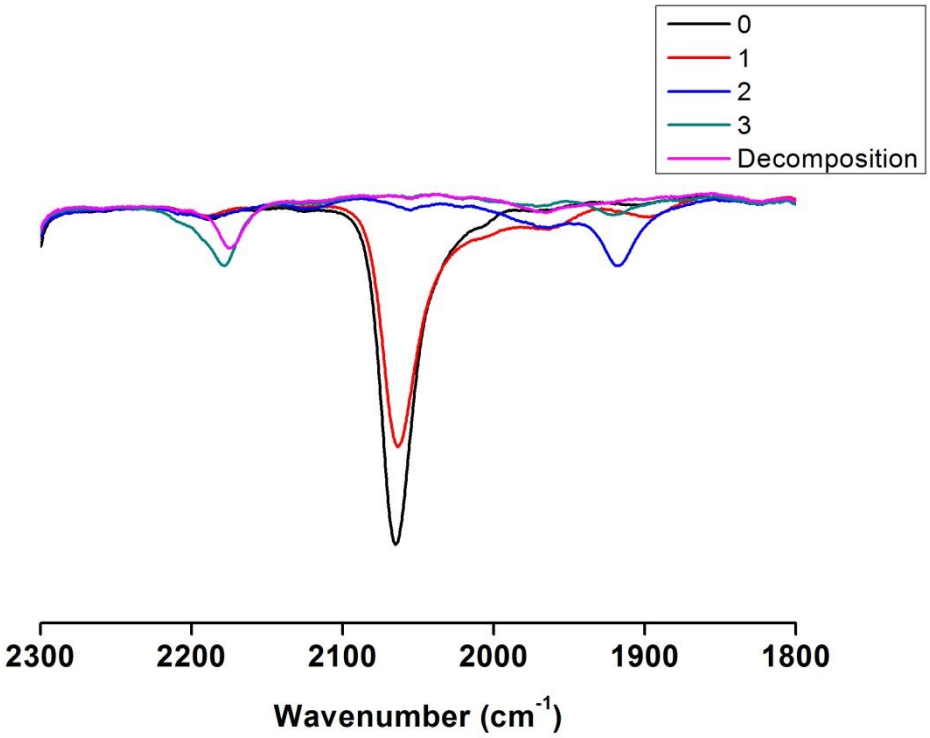

Figure 92: IR spectral changes accompanying oxidation of 41a in CH_2Cl_2 / 10^{-1} M NBu_4PF_6 within an OTTLE cell.

Similar IR spectral changes in the ν(C≡C-Ru) for compound [**41b**] (Figure 94, Table 44) where the intermediate spectrum for [**41b**]$^{+}$ shows a decrease in the ν(C≡C-Ru) at 2062 cm^{-1} coupled with the growth of new bands at 1892 cm^{-1} and 1925 cm^{-1} consistent with the oxidised ruthenium centre. There is also an unresolved feature at ca. 1980 cm^{-1} that collapses upon further oxidation. Accompanying these spectral changes is the growth of a NIR band with a band centre ca. 5500 cm^{-1}, and consistent with the oxidised forms of **41a** there is also the tail of a higher energy transition visible in this region (Figure 93). The band at ca. 5500 cm^{-1} is consistent with an IVCT type transition originating from the mixed valence nature of the –Ru-C≡C- fragments caused by the one electron oxidation process (red line, Figure 93). The

collapse of the band during oxidation to the dicationic species further supports the description of the band being of IVCT nature.

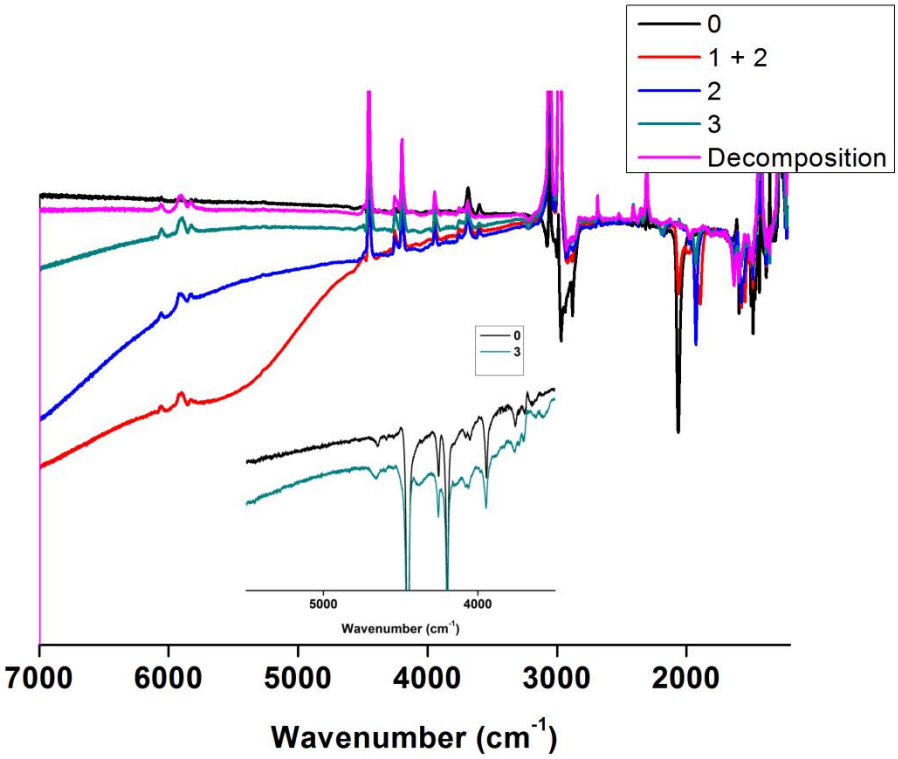

Figure 93: IR spectral changes accompanying oxidation of 41b in CH_2Cl_2 / 10^{-1} M NBu_4PF_6 within an OTTLE cell. Changes accompanying the 41b→$[41b]^+$→$[41b]^{2+}$ are reversible. Inset: expansion of the Fc d-d transition at ca 4150 cm^{-1}.

Further oxidation to [**41b**]$^{2+}$ results in the collapse of the ν(C≡C-Ru) at 2062 cm^{-1} and the intermediate band at 1892 cm^{-1} with an increase in the intensity of the band at 1920 cm^{-1} consistent with the oxidised ruthenium centres. Interestingly the electronic absorption band centred at ca. 5500 cm^{-1} collapses on oxidation to [**41b**]$^{2+}$ giving rise to features similar to [**41a**]$^{2+}$ with the tail of a band at higher energy, supporting the notion that the is the Ru→Ru^+ IVCT type transition (with due allowance in the description for the involvement of the ethynyl moieties in the redox-active orbitals). The appearance of the intermediate spectrum as a superposition of the neutral and dicationic spectra with unique features present only

in this state is consistent with a comproportionated mixture of the neutral, mono- and dicationic states.

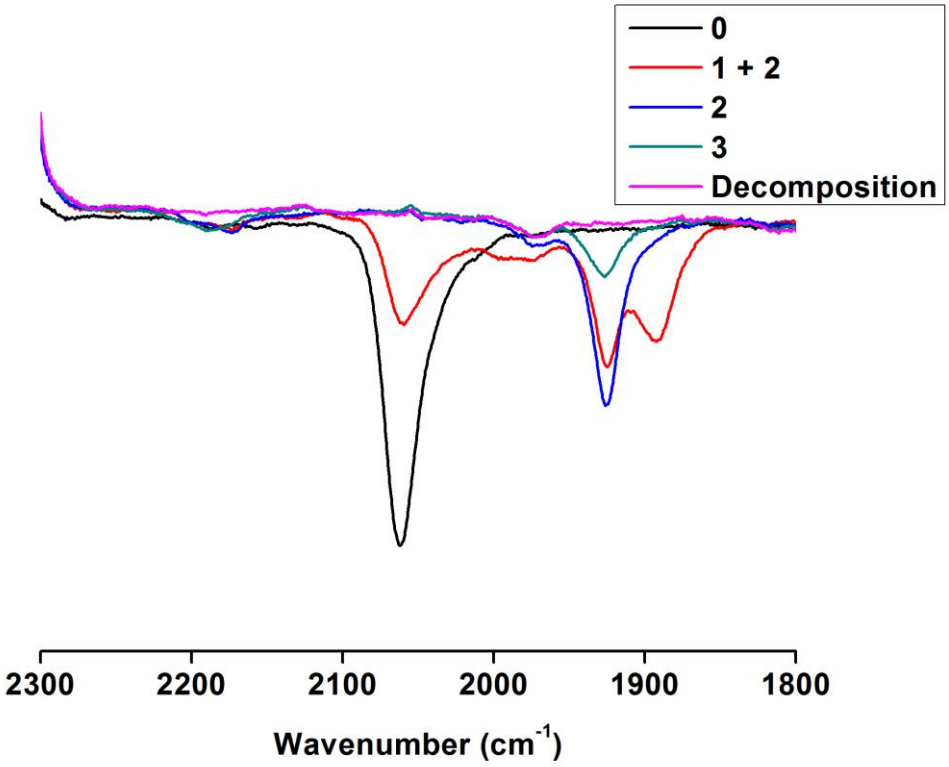

Figure 94: IR spectral changes accompanying oxidation of 41b in CH_2Cl_2 / 10^{-1} M NBu_4PF_6 within an OTTLE cell. Changes accompanying the 41b→[41b]$^+$→[41b]$^{2+}$ are reversible.

Table 44: Characteristic IR active vibrational modes (cm^{-1}) of 41a-b observed in spectroelectrochemical studies by *in situ* oxidation of a CH_2Cl_2/10^{-1} M NBu_4PF_6 solution.

	0	**+1**	**+2**	**+3**
41a	2065 (s)	1896 (s) 2065 (s)	1920 (s)	1920 (w)
41b	2062 (s)	1892 (s) 1925 (s) 1980 (w) 2062 (s)	1925 (s)	1925 (w)

The ferrocene-based oxidation to [**41a-b**]$^{3+}$ shows a decrease in the intensity of the tail of the higher energy band that extends in to the NIR region and a decrease in the intensity of the ν(C≡C) peak. However, on the SEC timescale the compound decomposes leading to a collapse of all signals as such no further analysis of the

tricationic states is possible. One feature that does become apparent is the appearance of a low intensity transition centred at ca. 4150 cm^{-1} (green line Figure 93 and inset) that is consistent with localised Fc d-d transitions as observed in Chapter 4 for the mono-metallic systems.

5.3.5. UV-vis NIR Spectroelectrochemistry

The increased stability of the sterically hindered compound **41b** makes it an ideal candidate for further investigation. UV-Vis-NIR spectral changes recorded for compound **41b** in CH_2Cl_2 / 10^{-1} M NBu_4PF_6 within an OTTLE cell are given in Figure 95 - Figure 96.

The neutral complex **41b** has a spectrum dominated by an intense band at 27500 cm^{-1}. Previous studies on Ru(C≡CR)(dppe)Cp* complexes have similar features and these have been attributed to a bridge-based π –π^* transition, albeit with the p-orbitals of the bridge admixed with some metal character (ML-LCT).[32] This band partially collapses upon one-electron oxidation accompanied the growth of a band envelope in the region 20000–17000 cm^{-1} and a broad band envelope at 10000–7000 cm^{-1}. The unresolved band profile in the visible region is consistent with those of related radical complexes.[33] Also seen in the spectrum for [**41b**]$^+$ is a distinct band centred at 12900 cm^{-1}, which is similar in profile to that of the previously reported [Ru(C≡CC_6H_4Me-4)(dppe)Cp*]$^+$ and, by analogy, can be assigned to a metal-to-metal/ligand (M-MLCT) transition. The broad low intensity band at 10000–7000 cm^{-1} can therefore be assigned to a transition between orthogonal orbitals with significant metal-d/ethynyl-π character by similar analogy.[34] Due to the low

concentrations used in the UV-vis NIR SEC the IVCT band at ca. 5500 cm^{-1}, seen in the IR SEC, is not seen in the NIR region.

.

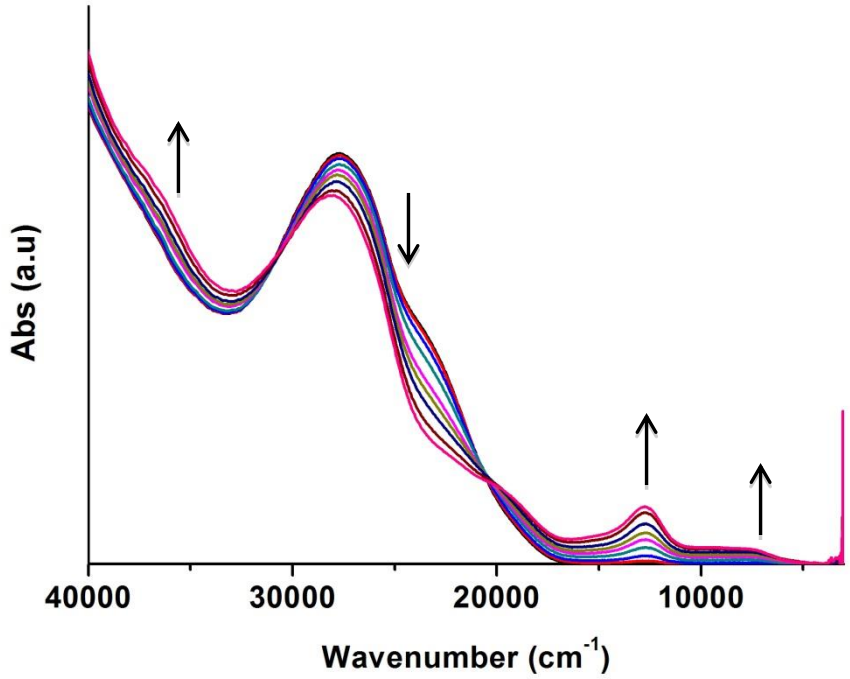

Figure 95: Reversible UV-vis NIR spectral changes accompanying oxidation of 41b in CH_2Cl_2 / 10^{-1} M NBu_4PF_6 within an OTTLE cell.

Further oxidation to [**41b**]$^{2+}$ shows a further decrease in intensity of the band at 27500 cm^{-1} with a small blue shift to 28300 cm^{-1}. This change is consistent with the first oxidation and can be ascribed to the sequential oxidation of the inequivalent Ru-C≡C- fragments. The band envelope at 20000–17000 cm^{-1} also shows a slight increase while the low intensity transition at 10000–7000 cm^{-1} shows a very small decrease in intensity. The feature at 12900 cm^{-1} which is attributed to the M-MLCT is unaffected by further oxidation.

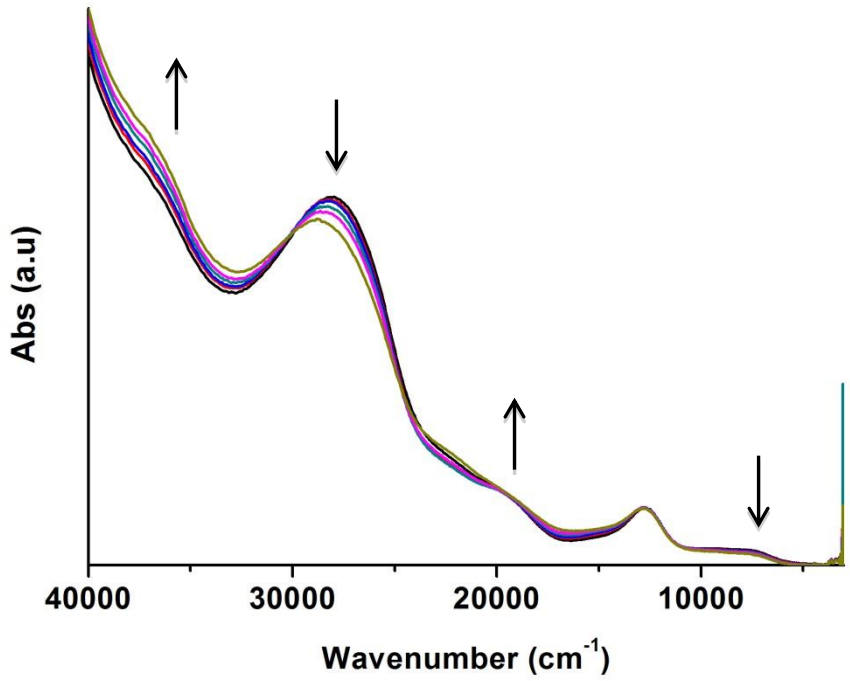

Figure 96: Reversible UV-vis NIR spectral changes accompanying oxidation to $[41b]^{2+}$ in CH_2Cl_2 / 10^{-1} M NBu_4PF_6 within an OTTLE cell.

Oxidation to [**41b**]$^{3+}$ gave rise to a spectrum with similar features to that of the dicationic species although decomposition of the sample occurred before a reliable spectrum could be obtained. The decomposition of the triply charged species is consistent with the IR SEC where decomposition after the final oxidation occurred before reliable data could be obtained.

The observation of bands in the visible region of the spectrum in the mono and dicationic states that are consistent with the oxidations at Ru-C≡C- further supports the assignment from the electrochemistry and the IR spectoelectrochemistry that it is these ruthenium ethynyl fragments that undergo oxidation process prior to the oxidation of the ferrocene moiety. These results, coupled with the observation of an electronic absorption band at ca 5500 cm^{-1} in the IR SEC that collapses on oxidation to the dicationic forms, suggest that it can be considered an Ru-C≡C- to [Ru-C≡C-]$^{+}$

IVCT transition. IVCT bands in mixed valence Ru(C≡CR)(dppe)Cp* complexes have previously been reported[32b] with a shift consistent (ca. 6000 cm^{-1}) to that observed here.

5.3.6. Conclusions

A simple synthetic route to di-ethynylethene compounds bearing 1,4-diethynyl benzene arms has been developed for compounds containing ferrocenylethene or 1,1-diphenylethene moieties. By combining the Corey-Fuchs reaction with subsequent cross-coupling reactions a range of cross-conjugated materials bearing ruthenium and iron remote moieties have been developed and their electronic structure probed by electrochemistry and UV-vis-NIR-IR SEC. The results show that the ferrocene moiety is essentially isolated from the remote centres and that there is no charge transfer between them. While results obtained for the model compound with $Ru(PPh_3)_2Cp$ show signs of rapid conversion to the carbonyl species the more sterically crowded centre, Ru(dppe)Cp*, offers increased stability on the SEC timeframe. Despite the lack of IVCT type transitions involving the ferrocene moiety in compounds **41a-b,** the more electron rich Ru compound $FcCH=C(C{\equiv}CC_6H_4C{\equiv}CRu(dppe)Cp^*)_2$ shows a distinct band of low intensity in the NIR region of the IR SEC that is present only in the mixture containing [**41b**]$^+$ and as such can be attributed as an IVCT type transition between the Ru-C≡C- and [Ru-C≡C-]$^+$ termini.

Despite recent reports of *gem*-bis-ruthenium acetylide complexes having been synthesised, the classical method of coupling terminal alkynes with metal chlorides

has proved unsuccessful for these compounds and molecular structures of the mono-metallic vinylidene and acetylide show that the second (vacant) site is heavily crowded.

Although not studied in detail herethe reaction of $FcCH=C(C\equiv CC_6H_4C\equiv CH)_2$ with FeCl(dppe)Cp* was undertaken in collaboration with Prof. Lapinte in Rennes, Fr., and preliminary data suggests that the complex $FcCH=C(C\equiv CC_6H_4C\equiv C\ [Fe])_2$ can be formed. This opens the way for further investigations of multi-metallic, cross-conjugated systems with different electronic properties at the remote centre can be explored.

5.4. Experimental Details

5.4.1. General Conditions

Solvent purification and characterisation of compounds was carried out as detailed in Chapter 2. The compounds $Pd(PPh_3)_4$,[35] $RuCl(PPh_3)_2Cp$[36] and RuCl(dppe)Cp*[29a] were prepared by the literature methods. CBr_4 was purified by sublimation before use.

The supporting electrolyte, tetrabutylammonium hexafluorophosphate (NBu_4PF_6, Aldrich), was recrystallized twice from absolute ethanol and dried overnight under vacuum at 80 °C before use. IR and UV−vis spectra were recorded on a Nicolet 6700 spectrometer and a Cary 5000 UV-vis NIR spectrophotometer, respectively. UV-vis-NIR-IR spectroelectrochemical experiments at room temperature were conducted with an OTTLE cell equipped with a Pt-minigrid working electrode and CaF_2

windows. The optical path of the cell was ca. 0.2 mm. The concentrations of the ferrocenyl compounds and the supporting electrolyte used in these measurements were 1.3×10^{-2} and 3×10^{-1} mol dm^{-3} for IR spectroelectrochemical experiments and 10^{-3} and 3×10^{-1} mol dm^{-3} for the UV-vis-NIR studies, respectively.

5.4.2. Preparation of $Ph_2C=CBr_2$ (28)

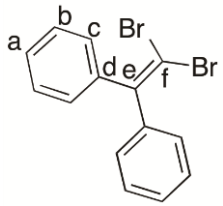

An oven dried Schlenk flask was charged with dry toluene (100 mL) and the solvent degassed. To this solution, CBr_4 (10.919 g, 32.927 mmol), PPh_3 (17.273 g, 65.854 mmol) and benzophenone (3.0 g, 16.463 mmol) were added and the mixture heated at reflux for 72 hours. The solvent was removed in vacuo, the residue extracted in CH_2Cl_2 and preabsorbed on to silica gel. Purification by silica column chromatography eluting with hexane and removal of the solvent in vacuo gives an off white solid. Yield 4.415 g, 79 %. Spectroscopic data were identical to those reported previously.[24]

5.4.3. Preparation of $Ph_2C=C(C\equiv CSiMe_3)_2$ (29)

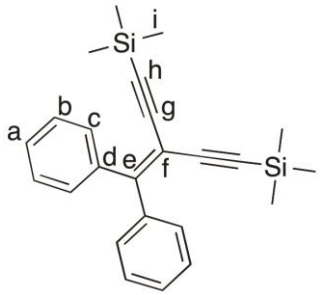

An oven dried Schlenk flask was charged with NEt_3 (100 mL) and the solvent degassed. To this solution **28** (3.00 g, 8.875 mmol), $Pd(PPh_3)_4$ (1.017 g, 0.887 mmol), CuI (0.169 g, 0.887 mmol) and TMSA (3.135 mL, 22.187 mmol) were added and the mixture heated at reflux for 72 hours, the solvent was removed in vacuo and the mixture extracted in to hexane (100 mL). The solvent was removed and the residue preabsorbed on to silica gel, purification by silica column chromatography eluting with hexane: CH_2Cl_2 (95:5) and removal of the solvent in vacuo gave an off white solid. Yield 2.767 g, 84 %. Spectroscopic data were identical to those reported previously.[24]

5.4.4. Preparation of $Ph_2C=C(C\equiv CH)_2$ (30)

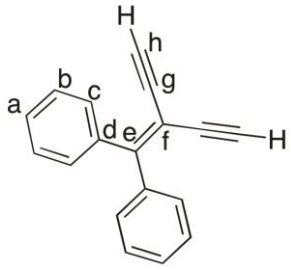

To a stirred solution of **29** (0.850 g, 2.281 mmol) in methanol (15 mL) was added K_2CO_3 (1.576 g, 11.405 mmol) and the mixture stirred for 90 minutes. The mixture was poured into H_2O (20 mL) and extracted with CH_2Cl_2 (3 x 15 mL) and the organic phases combined, dried over $MgSO_4$ and filtered. The solvent was removed

in vacuo to give the title compound as a white solid. Yield 496 mg, 95 %. Spectroscopic data were identical to those reported previously.[24]

5.4.5. Preparation of $Ph_2C=C(C\equiv CH)[CH=C=Ru(PPh_3)_2Cp]PF_6$ (33)

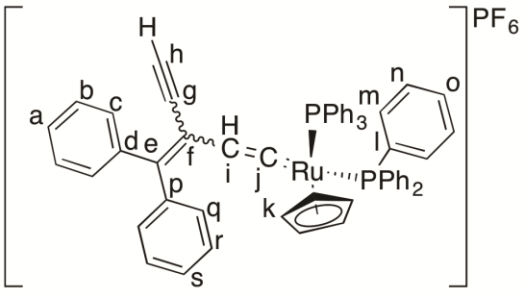

An oven dried Schlenk flask was charged with dry CH_2Cl_2 (15 mL) and the solvent degassed. To this solution, **30** (100 mg, 0.438 mmol), $RuCl(PPh_3)_2Cp$ (286 mg, 0.394 mmol) and KPF_6 (81 mg, 0.438 mmol) were added and the mixture heated at reflux for 20 hours. The solvent was concentrated in vacuo to 2 mL and added to vigorously stirring diethylehter at 0 °C, the precipitated pale red solid was filtered, washed with hexane (3 x 5 mL), ether (3 x 5 mL) and dried under air flow. Yield 329 mg, 79 %. Crystals suitable for X-ray diffraction were grown for slow diffusion of ether in to a CH_2Cl_2 solution of product. ^{1}H NMR (CD_2Cl_2): δ 3.09 (1H, s, H*h*), 4.92 (1H, t, J = 2.5 Hz, H*i*), 5.23 (5H, s, H*k*), 7.02 – 7.05 (12H, m, H*n*), 7.23 – 7.26 (15H, m, H*m* and H*o*), 7.29 – 7.34 (4H, m, H*b* and H*r*), 7.40 – 7.44 (6H, m, H*a*, H*c*, H*q* and H*s*). ^{31}P NMR (CD_2Cl_2): δ 41.62 (s). ^{13}C NMR (CD_2Cl_2): δ 81.75, 84.70, 90.66, 94.86 (t, J – 1.5 Hz), 104.23, 118.42, 127.77, 128.16 (d, J = 2.3 Hz), 128.46, 128.59 (t, j = 5.2 Hz), 128.82 (t, J = 5.2 Hz), 129.43, 130.37, 131.09, 132.87 (t, J = 5.3 Hz), 133.02 (t, J = 5.3 Hz), 139.94, 140.46, 145.91. MALDI MS(+): *m/z* 919.1 $[M]^+$. IR (CH_2Cl_2) ν(C≡C) 2108 cm^{-1}, ν(CH=CRu) 1629 cm^{-1}, ν(C=C) 1483 cm^{-1}. Found C 66.53, H 4.40 % required C 66.58, H 4.45 %.

5.4.6. Preparation of $Ph_2C=C(C\equiv CH)[C\equiv CRu(PPh_3)_2Cp]$ (34)

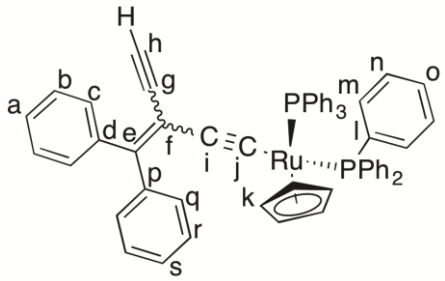

An oven dried Schlenk flask was charged with dry methanol (6 mL) and the solvent degassed. To this solution, **33** (85 mg, 0.08 mmol) and KO^{t}Bu (42 mg, 0.399 mmol) were added and the mixture stirred for 10 minutes. The precipitated yellow solid was filtered, washed with methanol (3 x 5 mL) and dried under air flow. Yield 45 mg, 62 %. Crystals suitable for X-ray diffraction were grown for slow diffusion of methanol in to a CH_2Cl_2 solution of product. ^{1}H NMR ($CDCl_3$): 7.44 - 7.39 (m, 14H), 7.36 (m, 2H), 7.32 - 7.28 (m, 4H), 7.16 (t, *J* = 7.4 Hz, 6H), 7.13 (m, 2H), 7.05 (t, *J* = 7.6 Hz, 12H), 4.22 (s, 5H), 2.77 (s, 1H). ^{13}C NMR ($CDCl_3$) ? 145.69 , 142.39 , 142.29 , 138.84 , 138.73 , 138.60 , 133.80 (t, *J* = 5.0 Hz), 131.01 , 130.66 , 130.43 , 130.03 , 128.30 , 128.24 , 127.21 (t, *J* = 4.5 Hz), 126.63 , 126.46 , 113.36 , 106.23 , 85.46 (t, *J* = 2.0 Hz).^{31}P NMR ($CDCl_3$) ? 50.35. MALDI MS(+): *m/z* 918.2 $[M]^+$. IR (CH_2Cl_2) ν(C≡CH) 2105 cm^{-1}, ν(C≡CRu) 2044 cm^{-1}, ν(C=C) 1482 cm^{-1}.

5.4.7. Preparation of [FcCH=C(C≡CH){ C≡CRu(PPh$_3$)$_2$Cp}]PF$_6$ (35)

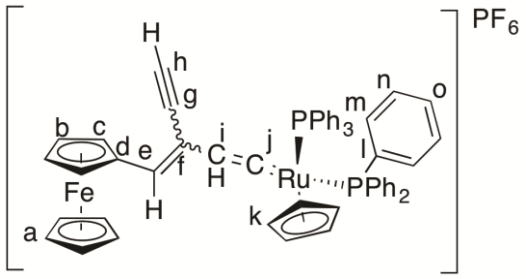

An oven dried Schlenk flask was charged with dry CH_2Cl_2 (5 mL) and the solvent degassed. To this solution, **23f** (0.1 g, 0.384 mmol), RuCl(PPh$_3$)$_2$Cp (0.252 g, 0.346 mmol) and KPF_6 (71 mg, 0.384 mmol) were added and the mixture heated at reflux for 16 hours. The solution was concentrated in vacuo to 3 mL and the filtered through celite into vigorously stirring diethylether (35 mL). The precipitate was filtered and washed with hexane (3 x 5 mL) and diethylether (3 x 5 mL). Yield 334 mg, 88% as a mixture of *cis* and *trans* isomers. MALDI MS(+): *m/z* 950.1 $[M-H]^+$. IR (CH_2Cl_2) ν(C≡CH) 1980 cm^{-1}, ν(CH=CRu) 1632 cm^{-1}, ν(C=C) 1586 cm^{-1}.

5.4.8. Preparation of FcCH=C(C≡CAuPPh$_3$)$_2$ (36)

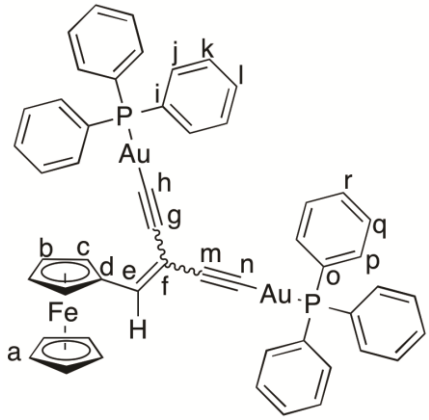

An oven dried Schlenk flask was charged with dry methanol (15 mL) and **23e** (0.1 g, 0.247 mmol, 25 mg/mL solution in THF) and the solution degassed. To this solution, NaOH (99 mg, 2.47 mmol) was added and the solution stirred for 30 minutes. AuCl(PPh$_3$) (0.247 g, 0.499 mmol) was added and the mixture stirred for 3 hours, filtered, washed with MeOH (3 x 10 mL) and hexane (3 x 10 mL) and dried under air flow for 1 hour. Yield 206 mg, 71 %. ^{1}H NMR (CD_2Cl_2): δ 4.16 (5H, s, H*a*), 4.26 (2H, vt, J = 2 Hz, H*c*), 4.96 (2H, vt, J = 2 Hz, H*b*), 6.56 (1H, s, H*e*), 7.49 (12H, m, H*j* and *p*), 7.54 (6H, m, H*l* and *r*), 7.55 – 7.62 (12H, m, H*k* and *q*). ^{31}P NMR (CD_2Cl_2): δ 42.20 (s), 42.41 (s). ^{13}C NMR (CD_2Cl_2): δ 139.22 (Ce, s), 134.90 (Ck, d, J = 5 Hz), 134.65 (Cq, d, J = 5 Hz), 132.06 (Cl, s), 132.04 (Cr, s), 130.75 (Ci, s), 130.44 (Co, s), 129.7- (Cj, d, J = 5Hz), 129.64 (Cp, d, J = 5Hz), 105.53 (Ch, d, J = 27 Hz), 103.39 (Cf, s), 102.91 (Cn, d, J = 27Hz), 82.37 (Cd, s), 70.02 (Cg, s), 69.99 (Cm, s), 69.84 (Ca, s), 69.78 (Cb, s), 69.65 (Cc, s). MALDI MS(+): *m/z* 1176.1 [M]$^+$. IR (CH_2Cl_2) ν(C≡CAu) 2102 cm^{-1}, ν(C=C) 1481 cm^{-1}. Analysis found C 52.93, H 3.34% required C 53.06, H 3.34%.

5.4.9. Preparation of $BrC_6H_4C{\equiv}CSiMe_3$ (37)

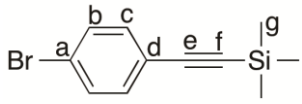

An oven dried Schlenk flask was charged with NEt_3 (50 mL) and the solvent degassed. To this solution, 4-iodobromobenzene (6.00 g, 21.208 mmol), $Pd(PPh_3)_2Cl_2$ (0.149 g, 0.212 mmol), CuI (0.040 g, 0.212 mmol) and TMSA (3.297 mL, 23.329 mmol) were added and the mixture stirred at room temperature for 1 hour. The solvent was removed in vacuo and the residue extracted in to hexane (50 mL) and filtered through a silica plug washing with hexane (50 mL). The organic fractions were combined and the solvent removed in vacuo to give a white solid. Yield 4.982 g, 93 %. Spectroscopic data were identical to those reported previously.[27]

5.4.10. Preparation of $Ph_2C{=}C(C{\equiv}CC_6H_4C{\equiv}CSiMe_3)_2$ (38)

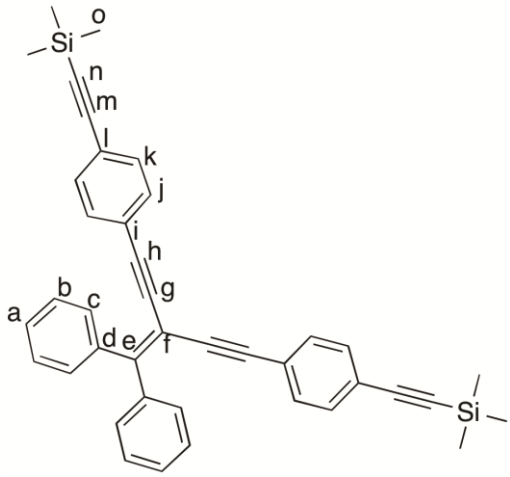

An oven dried Schlenk flask was charged with HN^iPr_2 (25 mL) and the solvent degassed. To this solution, **30** (0.200 g, 0.876 mmol), $Pd(PPh_3)_4$ (0.010 g, 0.01 mmol), CuI (0.002 g, 0.01 mmol) and **37** (0.466 g, 1.840 mmol) and the mixture

heated at reflux for 16 hours. The solvent was removed in vacuo and the residue extracted with hexane (50 mL). The solvent was removed in vacuo and the residue preabsorbed on to silica. Purification by silica column chromatography eluting with hexane:CH_2Cl_2 (70:30) and removal of the solvent in vacuo gave a white solid, Yield 379 mg, 76 %. ^{1}H NMR (CD_3COCD_3): δ 0.23 (18H, s, $SiMe_3$), 7.32 (4H, m, H*j*), 7.41-7.47 (10H, m, H*a*, H*c* and H*k*), 7.53 (4H, m, H*b*). ^{13}C NMR (CD_3COCD_3): δ -0.10 (C*o*), 91.11 (C*e*,*f*,*g* or *h*), 91.97 (C*e*,*f*,*g* or *h*), 97.02 (C*n*), 102.30 (C*e*,*f*,*g* or *h*), 105.28 (C*m*), 123.93 (C*l*), 124.11 (C*i*), 128.80 (C*c*), 129.84 (C*a*), 131.09 (C*b*), 132.17 (C*j*), 132.74 (C*k*), 141.05 (C*e*,*f*,*g* or *h*), 158.16 (C*d*). ASAP MS(+): *m/z* 573.2 $[M+H]^+$. IR (CH_2Cl_2): ν(C≡C) 2208, 2156 cm^{-1}, ν(C=C) 1486 cm^{-1}.

5.4.11. Preparation of $Ph_2C=C[C{\equiv}CC_6H_4C{\equiv}CRu(PPh_3)_2Cp]_2$ (39)

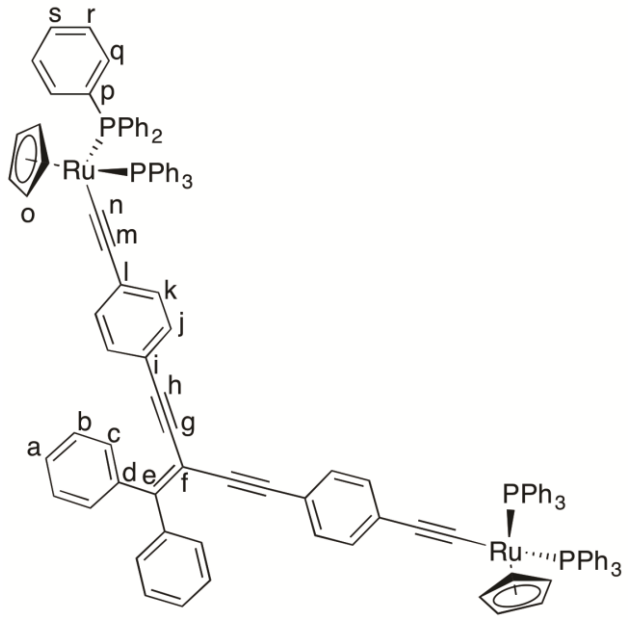

An oven dried Schlenk flask was charged with dry methanol (4 mL) and dry THF (4 mL) and the solvent degassed. To this solution, **38** (0.02 g, 0.035 mmol), $RuCl(PPh_3)_2Cp$ (0.051 g, 0.070 mmol) and KF (0.004 g, 0.070 mmol) were added and the mixture heated at reflux for 2 hours. The solvent was removed in vacuo and

the reside extracted in CH_2Cl_2 (3 mL), filtered through celite in to vigorously stirring methanol (30 mL) and the precipitated solid filtered, washed with hexane (3 x 5 mL) and methanol (3 x 5 mL) and dried under airflow. Yield 28 mg, 44 %. ^{1}H NMR (CD_2Cl_2): δ 4.34 (10H, s, H*o*), 7.02 (4H, t, J = 9 Hz, H*j*), 7.12 (24H, m, H*r*), 7.23 (12H, t, J = 7 Hz, H*s*), &.38-7.43 (10H, m, H*a,c and k*), 7.46 (24H, d, J = 8Hz, H*q*), 7.56 (4H, m, H*b*). ^{13}C NMR (CD_2Cl_2): δ 85.94 (C*o*), 89.55 (C*f*), 93.47 (C*e,g,h,l or m*), 116.55 (C*n*), 117.29 (C*i*), 127.85 (t, J = 4.5 Hz, C*r*), 128.82 (C*a,c or k*), 129.02 (C*e,g,h,l or m*), 129.09 (C*a,c or k*), 129.11 (C*s*), 130.81 (C*j*), 131.04 (C*b*), 131.54 (C*a,c or k*), 132.47 (C*e,g,h,l or m*), 132.52 (C*e,g,h,l or m*), 134.32 (t, J = 5 Hz, C*q*), 139.53 (t, J = 21Hz, C*r*), 141.34 (C*e,g,h,l or m*), 153.99 (C*d*). ^{31}P NMR (CD_2Cl_2): δ 50.05. MALDI MS(+): *m/z* 719.1 $[Ru(CO)(PPh_3)_2Cp]^+$.

5.4.12. Preparation of $FcCH=C(C{\equiv}CC_6H_4C{\equiv}CSiMe_3)_2$ (40)

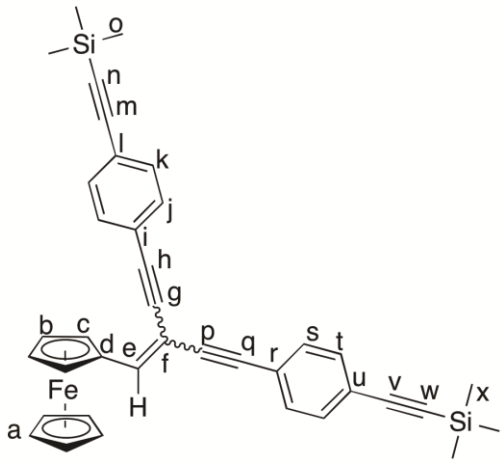

An oven dried Schlenk flask was charged with HN^iPr_2 (25 cm^3) and the solvent degassed. To this solution, **23f** (200 mg, 0.769 mmol), **37** (409 mg, 1.615 mmol), $Pd(PPh_3)_4$ (9 mg, 0.008 mmol) and CuI (2 mg, 0.016 mmol) were added and the solution stirred for 48 hours at reflux. The mixture was cooled and filtered and the solvent was removed in vacuo. The residue was preabsorbed on silica gel and

purified by silica column chromatography using CH_2Cl_2:hexane (10:90 → 50:50) The second fraction was collected and the solvent removed in vacuo to give a bright red solid. Yield 234 mg, 51 %. ^{1}H NMR ($CDCl_3$): δ 0.25 (9H, s, H*o or x*), 0.26 (9H, s, H*o or x*), 4.23 (5H, s, H*a*), 4.46 (2H, vt, J = 2 Hz, H*c*), 4.90 (2H, vt, J = 2 Hz, H*b*), 6.99 (5H, s, H*a*), 7.40 – 7.55 (8H, m, H*j, k, s or t*). ^{13}C NMR ($CDCl_3$): δ 69.76 (C*a*), 69.89 (C*b*), 70.78 (C*c*), 79.51 (C*h, g, m, p ,r or v*), 87.20 (C*h, g, m, p ,r or v*), 89.61 (C*d*), 91.40 (C*f*), 93.14 (C*h, g, m, p ,r or v*), 96.20 (C*n or w*), 96.50 (C*n or w*), 98.78(C*h, g, m, p ,r or v*), 104.60 (C*h, g, m, p ,r or v*), 104.72 (C*h, g, m, p ,r or v*), 122.65 (C*i, l, r or u*), 123.07 (C*i, l, r or u*), 123.32 (C*i, l, r or u*), 123.37 (C*i, l, r or u*), 131.10 (C*j, k ,s or t*), 131.18 (C*j, k ,s or t*), 131.85 (C*j, k ,s or t*), 131.99 (C*j, k ,s or t*), 145.45 (C*e*). IR (CH_2Cl_2) ν(C≡C) 2209 cm^{-1}, ν(C≡CSi) 2156 cm^{-1}, ν(C=C) 1576 cm^{-1}. ASAP MS(+) *m*/*z*: 605.2 $[M+H]^+$.

5.4.13. Preparation of FcCH=C[C≡CC$_6$H$_4$C≡CRu(PPh$_3$)$_2$Cp]$_2$ (41a)

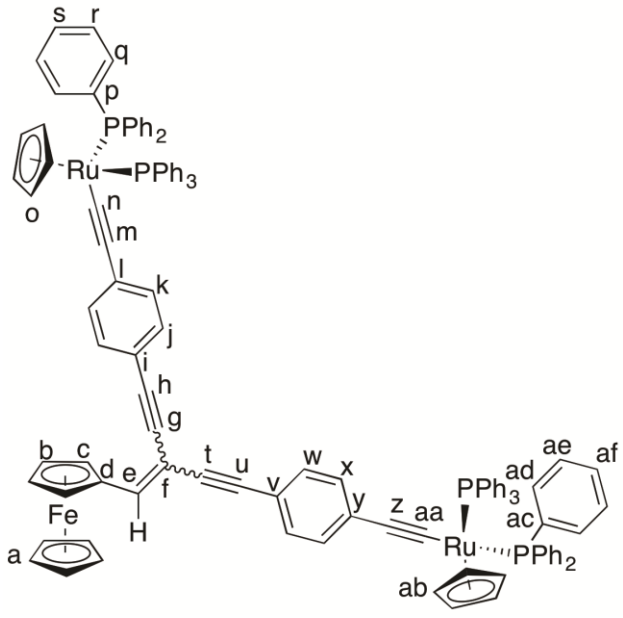

An oven dried Schlenk flask was charged with dry methanol and dry THF (6 mL) (1:1) and the solvent degassed. To this solution, **40** (30 mg), RuCl(PPh$_3$)$_2$Cp (74 mg) and KF (8 mg) was added and the mixture heated at reflux for 3 hours. The solvent

was removed in vacuo and the residue dissolved in CH_2Cl_2, filtered through celite and the solvent removed in vacuo. The residue was suspended in methanol, filtered and the solid dried under airflow for 30 minutes. Yield 66 mg, 67 %. ^{1}H NMR (CD_2Cl_2): δ 4.24 (5H, s, H*a*), 4.36 (5H, s, H*o*), 4.37 (5H, s, H*ab*), 4.45 (2H, t, J = 2Hz, H*c*), 4.94 (2H, t, J = 2Hz, H*b*), 6.93 (1H, s, H*e*), 7.08 (2H, d, J = 8Hz, H*j*), 7.13 (26H, m, H*r, w and ae*), 7.24 (12H, m, H*s and af*), 7.32 (2H, d, J = 8Hz, H*k*), 7.41 (2H, d, J = 8Hz, H*x*), 7.48 (24H, m, H*q and ad*). ^{31}P NMR (CD_2Cl_2): δ 50.07 (s), 50.10 (s). ^{13}C NMR (CD_2Cl_2): δ 69.59 (C*a*), 69.67 (C*b*), 70.30 (C*c*), 80.12 (C*d*), 85.34 (m, C*o and ab*), 88.08 (C*g, h, t or u*), 88.17 (C*m*), 89.78 (C*f*), 94.53 (C*z*), 99.91 (C*g, h, t or u*), 115.30 (C*g, h, t or u*), 115.38 (C*g, h, t or u*), 117.00 (C*i*), 117.03 (C*v*), 123.62 (t, J = 25Hz, C*n*), 124.44 (t, J = 25Hz, C*aa*), 127.25 (m, C*r and ae*), 128.51 (C*s*), 128.52 (C*af*), 130.28 (C*j*), 130.37 (C*w*), 130.84 (C*k*), 130.86 (C*x*), 131.85 (C*l*), 131.91 (C*y*), 133.72 (m, C*q and ad*), 138.80 (m, C*p and ac*), 142.70 (Ci). MALDI MS(+): *m/z* 1840.2 $[M]^+$. IR (CH_2Cl_2) ν(C≡C) 2180 cm^{-1}, ν(C≡CRu) 2066 cm^{-1}, ν(C=C) 1593 cm^{-1}.

5.4.14. Preparation of FcCH=C[C≡CC$_6$H$_4$C≡CRu(dppe)Cp*]$_2$ (41b)

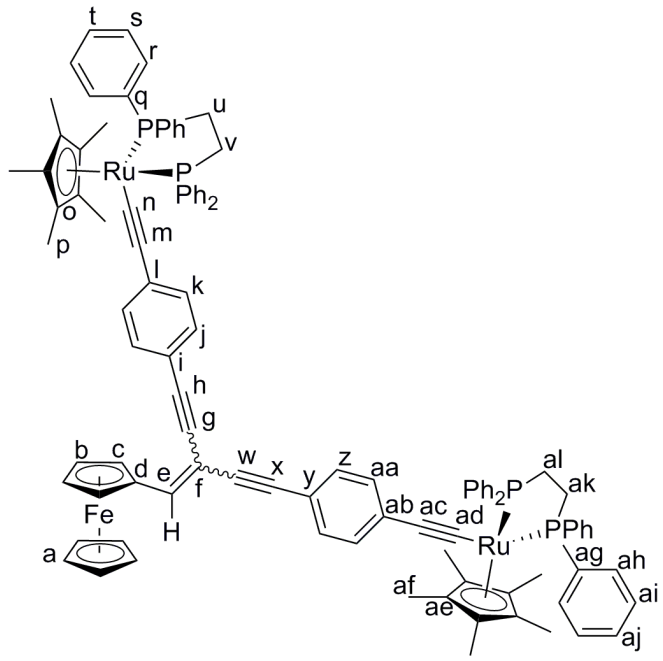

An oven dried Schlenk flask was charged with dry methanol and dry THF (6 mL) (1:1) and the solvent degassed. To this solution, **40** (30 mg), RuCl(dppe)$_2$Cp* (66 mg) and KF (6 mg) was added and the mixture heated at reflux for 15 hours. The mixture was cooled and treated with methanol (10 mL) the precipitated solid was filtered, washed with methanol (3 x 5 mL) and hexane (3 x 5 mL) and dried under airflow. Yield 60 mg, 70 %. ^{1}H NMR (CD_2Cl_2): δ 1.56 (15H, s, H*p*), 1.57 (15H, s, H*af*), 2.11 (4H, m, H*u and al* or H*v and ak*), 2.68 (4H, m, H*u and al* or H*v and ak*), 4.20 (5H, s, H*a*), 4.41 (t, J = 2Hz, H*c*), 4.88 (t, J = 2Hz, H*b*), 6.70 (2H, d, J = 8Hz, H*k*), 6.75 (2H,d, J = 8Hz, H*aa*), 6.86 (1H, s, H*e*), 7.14 (2H, d, J = 8Hz, H*j*), 7.23 (2H, d, J = 8Hz, Hz), 7.23, 7.33, 7.37, 7.80 (40H, m, H*r, s, t, ah, ai and aj*). ^{31}P NMR (CD_2Cl_2): δ 80.58 (s). ^{13}C NMR (CD_2Cl_2): δ 9.79 (C*p and af*), 29.15 (C*u and al* or C*v and ak*), 29.35 (C*u and al* or C*v and ak*), 69.53 (C*a*), 69.59 (C*b*), 70.20 (C_c), 8016 (C*d*), 87.83 (C*m*), 88.28 (C*h, g, w, or x*), 89.50 (C*f*), 92.67 (C*o*), 92.68 (C*ae*), 94.65 (C*ac*), 100.01 (C*h, g, w, or x*), 110.83 (C*h, g, w, or x*), 110.93 (C*h, g, w, or x*),

116.26 (C*i*), 116. 29 (C*y*), 127.17 (d, J = 3Hz, C*s*), 127.44 (d, J = 3Hz, C*ai*), 128.24 (C*t and aj*), 128.89 (C*n*), 129.89 (C*k*), 129.98 (C*aa*), 130.55 (C*j*), 130.57 (C*ad*), 130.58 (C_z), 131.20 (C*l*), 131.55 (C*ab*), 133.05 (t, J = 5Hz, C*r*), 133.61 (t, J = 5Hz, C*ah*), 138.55 (m, C*q*), 138.75 (C*ag*), 142.36 (C*e*). MALDI MS(+): *m/z* 1729.3 $[M+H]^+$. IR (CH_2Cl_2) ν(C≡C) 2184 cm^{-1}, ν(C≡CRu) 2064 cm^{-1}, ν(C=C) 1588 cm^{-1}.

5.5. References.

1. See for example: (a) Couty, S; Barbazanges, M; Meyer, C; Cossy, J. *Synlett*. **2005**, 905. (b) Corey, E. J; Fuchs, P. L. *Tetrahedron Lett*. **1972**, *13*, 3769. (c) Posner, G. H; Loomis, G. L; Sawaya, H. S. *Tetrahedron Lett*. **1975**, *16*, 1373. (d) Harada, T; Katsuhira, T; Hara, D; Kotani, Y; Maejima, K; Kaji, R; Oku, A. *J. Org. Chem*. **1993**, *58*, 4823. Olah, G. A; Wu, A. *Synthesis*. **1990**, 885. (e) Hassig, R; Seebach, D; Siegel, H. *Chem. Ber*. **1984**, *117*, 1877. (f) Newman, S. G; Aureggi, A; Bryan, C. S; Lautens, M. *Chem. Comm*. **2009**, 5236. (g) McIntosh, M. C; Weinreb, S. M. *J. Org. Chem*. **1993**, *48*, 4823. (h) Jiang, B; Ma, P. *Synth. Comm*. **1995**, *25*, 3641. (i) Donovan, P. M; Scott, L. T. *J. Am. Chem. Soc*, **2004**, *126*, 3108.
2. See for example: (a) Rezaei, H; Normant, J. F. *Synthesis*. **2000**, 109. (b) Ranu, B. C; Samanta, S; Das, A. *Tetrahedron Lett*. **2002**, *43*, 5993. (c) Galzunova, E. Y; Lutsenko, S. V; Efimova, I. V; Trostyanskaya, I. G; Kazankova, M. A; Beletskaya, I. P. *Russ. J. Org. Chem*. **1988**, *34*, 1104. (d) Azyat, K; Jahnke, E; Rankin, T; Tykwinski, R. R. *Chem. Commun*. **2009**, 433. (e) Rankin, T; Tykwinski, RR. *Org. Lett*. **2003**, *5*, 213.
3. Alberts, R. H; Wynberg, H. *Chem. Commun*. **1988**, 748.
4. (a) Roush, W. R; Riva, R. *J. Org. Chem*. **1988**, *53*, 710. (b) Roush, W. R; Brown, B. B; Drozda, S. E. *Tetrahedron Lett*. **1988**, *29*, 3541. (c) Miyaura, N; Suzuki, A. *Chem. Rev*. **1995**, *95*, 2457.
5. (a) Shi, J; Negishi, E. *J. Organomet. Chem*. **2003**, *687*, 518. (b) Sonogashira, K; Tohda, Y; Hagihara, N. *Tetrahedron Lett*. **1975**, *16*, 4467. (c) Uenishi, J; Matsui, K. *Tetrahedron Lett*. **2001**, *42*, 4353. (d) Uenishi, J; Matsui, K.; Ohmiya, H. *J. Organomet. Chem*. **2002**, *653*, 141. (e) Negishi, E; Shi, J; Zeng, X. *Tetrahedron*

2005, *61*, 9886. (f) Shi, J; Zeng, X; Negishi, E. *Org. Lett*. **2003**, *5*, 1825. (g) Metay, E; Negishi, E. *Org. Lett*. **2006**, *8*, 5773.

6. Chelucci, G. *Chem. Rev*. **2012**. *112*. 1269-2014.
7. Armitt, D. J; Bruce, M. I; Morris, J. C; Nicholson, B. K; Parker, C. R; Skelton, B. W; Zaitseva, N. N. *Organometallics*. **2011**, *30*, 5452.
8. (a) Moonen, N. N. P; Pomerantz, W. C; Gist, R; Boudon, C; Gisselbrecht, J. P; Kawai, T; Kishioka, A; Gross, M; Irie, M; Diederich, F. *Chem. Eur. J*. **2005**, *11*, 3325. (b) Auffrant, A; Diederich, F; Boudon, C; Gisselbrecht, J. P; Gross, M. *Helv. Chim. Acta*. **2004**, *87*, 3085. (c) Xu, GL; Xi, B; Updegraff, J. B; Protasiewicz, J. D; Ren, T. *Organometallics*. **2006**, *25*, 5213.
9. Antony, J; Boldi, A. M; Rubin, Y; Hobi, M; Gramlich, V; Knobler, C. B; Seiler, P; Diederich, F. *Helv. Chim. Acta*. **1995**, *78*, 13.
10. Forrest, W. P; Cao, Z; Hassell, K .M; Prentice, B. M; Fanwick, P. E; Ren, T. *Inorg. Chem*. **2012**, *51*, 3261.
11. Bruce, M. I; Burgun, A; Fox, M. A; Jevric, M; Low, P. J; Nicholson, B. K; Parker, C. R; Skelton, B. W; White, A. H; Zaitseva, N. N. *Oganometallics*. **2013**, *32*, 3285.
12. (a) Bruce, M. I; Low, P. J; Hartl, F; Humphrey, P. A.; de Montigny, F; Jevric, M; Lapinte, C; Perkins, G. J; Roberts, R. L; Skelton, B. W; White, A. H. *Organometallics*. **2005**, *24*, 5241. (b) Bruce, M. I; Humphrey, P. A; Jevric, M; Perkins, G. J; Skelton, B. W; White, A. H. *J. Organomet. Chem*. **2007**, *692*, 1748. (c) Bruce, M. I; Jevric, M; Perkins, G. J; Skelton, B. W; White, A. H. *J. Organomet. Chem*. **2007**, *692*, 1757. (d) Lohan, M; Ecorchard, P; Ruffer, T; Justaud, F; Lapinte, C; Lang, H. *Organometallics*. **2009**, *28*, 1878. (e) Lohan, M; Justaud, F; Roisnel, T; Ecorchard, P; Lang, H; Lapinte, C. *Organometallics*. **2010**, *29*, 4804. (f) Lohan, M; Justaud, F; Lang, H; Lapinte, C. *Organometallics*, **2012**, *31*, 3565. (g) Bruce, M. I; Le Guennic, B; Scoleri, N; Zaitseva, N. N; Halet, J. F. *Organometallics*. **2012**, *31*, 4701. (h) Bruce, M. I; Halet, J. F; Le Guennic, B; Skelton, B. W; Smith, M. E; White, A. H. *Inorg. Chim. Acta*. **2003**, *350*, 175. (i) Low, P. J; Brown, N. J. *J. Cluster Sci*. **2010**, *21*, 235. Costuas, K; Rigaut, S. *Dalton Trans*. **2011**, *40*, 5643.
13. Markussen, T; Stadler, R; Thygensen, K. S. *Nano Lett*. **2010**, *10*, 4260.

14. (a) Kocherzhenko, A. A; Siebbeles, L. D. A; Grozema, F. C. *J. Phys. Chem. Lett*. **2011**, *2*, 1753. (b) Kocherzhenko, A. A; Grozema, F. C; Siebbeles, L. D. A. *Phys. Chem. Chem. Phys*. **2011**, *13*, 2096.
15. Vincent, K. B; Zeng, Q; Parthey, M. P; Yufit, D. S; Howard, J. A. K; Hartl, F; Kaupp, M; Low, P. J. *Organometallics*. **2013,** *32*, 6022.
16. Long, E. M.; Brown, N. J.; Man, W. Y.; Fox, M. A.; Yufit, D. S.; Howard, J. A. K.; Low, P. J. *Inorg. Chim. Acta*. **2012**, *380*, 358.
17. Consiglio, G; Morandini, F; Ciani, G; Sironi, A. *Organometallics*. **1986**, *5*, 1976.
18. Huang, C. C; Lin, Y. C; Huang, S. L; Liu, Y. J; Wang, Y. *Organometallics*, **2003**, *22*, 1512.
19. Fox, M. A.; Roberts, R. L.; Khairul, W. M.; Hartl, F.; Low, P. J. *J. Organomet. Chem.* **2007**, *692*, 3277.
20. Cordiner, R. L.; Albesa-Jove, D.; Roberts, R. L.; Farmer, J. D.; Puschmann, H.; Corcoran, D.; Goeta, A. E.; Howard, J. A. K.; Low, P. J. *J. Organomet. Chem*. **2005**, *690*, 4908.
21. Armitt, D. J; Bruce, M. I; Gaudio, M; Zaitseva, N. N; Skelton, B. W; White, A. H; Le Guennic, B; Halet, J. F; Fox, M. A; Roberts, R. L; Hartl, F; Low, P. J. *Dalton. Trans.* **2008,** 6763.
22. Bruce, M. I; Low, P. J. Costuas, K; Halet, J. F; Best, S. P; Heath, G. A. *J. Am. Chem. Soc*. **2000**, *122*, 1949.
23. Barras, J. P; Davies, S. G.; Metzler, M. R.; Edwards, A. J.; Humphreys, V. M.; Prout, K. *J. Organomet. Chem.* **1993**, *461*, 157.
24. Donovan, P. M; Scott, L. T. *J. Am. Chem. Soc*, **2004**, *126*, 3108.
25. (a) Tsai, F. Y; Ma, H. W; Huang, S. L; Lin, Y. C; Wang, Y; Liu, Y. H. *Chem. Eur. J*. **2012**, *18*, 3399. (b) Lui, M. C; Chung, C. P; Chang, W. C; Lin, Y. C; Wang, Y; Liu, Y. H. *Organometallics*. **2009**, *28*, 5204. (c) Tamm, M; Jentzsch, T; Werncke, W. *Organometallics*. **1997**, *16*, 1418. (d) Mishra, A; Pandey, D. S; Mishra, K; Agarwala, U. C. *Ind. J. Chem. A.* **1990**, *29*, 251. (e) Bruce, M. I; Hameister, C; Swincer, A. G; Wallis, R. C. *Inorg. Synth*. **1992**, *21*, 78. (f) Bruce, M. I; Wallis, R. C. *Aus. J. Chem*. **1979**, *32*, 1471. (g) Bruce, M. I; Wallis, R. C. *J. Organomet. Chem*. **1978**, *161*, C1.
26. (a) Abu Salah, O. M; Bruce, M. I. *Aust. J. Chem*, **1977**, *30*, 2639. (b) Miguel D; Riera, V. *J. Organomet. Chem*. **1985**, *293*, 379. (c) Khairul, W. M; Fox, M. A;

Zaitseva, N. N; Gaudio, G; Yufit, D. S; Skelton, B. W; White, A. H; Howard, J. A. K; Bruce, M. I; Low, P. J. *Dalton. Trans.* **2009**, 610.

27. Rahaim, R. J; Shaw, J. T. *J. Org. Chem.*, **2008**, *73*, 2912.
28. (a) Bruce, N. I; Hall, B. C; Kelly, B. D; Low, P. J; Skelton, B. W; White, A. H. *J. Chem. Soc. Dalton. Trans*. **1999**, 3719. (b) Parthey, M; Gluyas, J. B. G; Schauer, P. A; Yufit, D. S; Howard, J. A. K; Kaupp, M; Low, P. J. *Chem. Eur. J.* **2013**, *19*, 9780. (c) Bruce, M. I; Jevric, M; Perkins, G. J; Skelton, B. W; White, A. H. *J. Organomet. Chem*. **2007**, *692*, 1757. (d) Bruce, M. I; Low, P. J; Hartl, F; Humphrey, P. A; De Montigny, F; Jevric, M; Lapinte, C; Perkins, G. J; Roberts, R. L; Skelton, B. W; White, A. H. *Organometallics.* **2005**, *24*, 5241.
29. (a) Bruce, M. I; Ellis, B. G; Low, P. J; Skelton, B. W; White, A. H. *Organometallics*. **2003**, *22*, 3184. (b) Cowley, M. J; Lynam, J. M; Moneypenny, R. S; Whitwood, A. C; Wilson, A. J. *Dalton. Trans*. **2009**, 9529. (c) Bruce, M. I. *Chem. Rev*. **1991**, *91*, 197. (d) Puerta, M. C; Valerga, P. *Coord. Chem. Rev*. **1999**, *977* 193. (e) Cowley, M. J; Lynam, J. M; Whitwood, A. C. *Dalton. Trans*. **2007**, 4427.
30. (a) Bruce, M. I; Humphrey, M. G; Snow, M. R; Tiekink, E. R. T. *J. Organomet. Chem*. **1986**, *314*, 213. (b) Wu, I. Y; Lin, J. T; Wen, Y. S. *Oganometallics*. **1999**, *18*, 320.
31. Gholami, M; Chaur, M. N; Wilde, M; Ferguson, M. J; McDonald, R; Echegoyenb, L; Tykwinski, R .R. *Chem. Commun*. **2009**, 3038.
32. (a) Armitt, D. J; Bruce, M. I; Gaudio, M; Zaitseva, N. N; Skelton, B. W; White, A. H; Le Guennic, B; Halet, J. F; Fox, M. A; Roberts, R. L; Hartl, F; Low, P. J. *Dalton Trans*. **2008**, *47*, 6763. (b) Fox, M. A; Le Guennic, B; Roberts, R. L; Brue, D. A; Yufit, D. S; Howard, J. A. K; Manca, G; Halet, J. F; Hartl, F; Low, P. J. *J. Am. Chem. Soc.* **2011**, *133*, 18433.
33. Klein, A; Lavastre, O; Fiedler, J. *Organometallics*, **2006**, *25*, 635.
34. Fox, M. A; Roberts, R. L; Khairul, W. M; Hartl, F; Low, P. J. *J. Organomet. Chem*. **2007**, *692*, 3277.
35. Coulson, D. R. *Inorg. Synth.* **1972**, *13*, 121.
36. Bruce, M. I; Hameister, C; Swincer, A. G; Wallis, R. C. *Inorg. Synth*. **1990**, *18*. 270.

Chapter 6: Synthesis and Spectroelectrochemistry of Multi-ferrocenylenediynes

6.1. Synopsis

The compounds $Ph_2C=C(C\equiv CFc)_2$ (**43**), $FcCH=C(C\equiv CFc)_2$ (**44**) and $(FcC\equiv C)_2C=C(C\equiv CFc)_2$ (**48**) have been prepared in 46, 68 and 19 % yield respectively from reactions of $FcC\equiv CH$ with $Ph_2C=CBr_2$, $FcCH=CBr_2$ and $(FcC\equiv C)_2C=CBr_2$ respectively under classical Sonogashira coupling conditions. The CV of **43** in NBu_4PF_6 is characterised by a single broad wave arising from the overlapping oxidation process of the two Fc moieties. In contrast, in the weakly coordinating anion (WCA) containing electrolyte NBu_4BArF_4 the electrostatic effects between the ferrocenyl moieties are enhanced, leading to a greater separation of the individual redox processes and the observation of two distinct, and only partially overlapping waves. Similarly, the heavily overlapped redox waves observed for **44** and **48** in NBu_4PF_6 are separated to give three and four distinct redox processes in NBu_4BArF_4 respectively.

These observations coupled with results from IR SEC that show that the ferrocenyl moiety is essentially electronically isolated from the backbone, as indicated by the small changes in spectra caused by the sequential oxidations, highlight the potential of these materials, in particular **48**, as possible candidates for use in a molecular Quantum-dot Cellular Automata (MQCA) device. Unfortunately UV-vis NIR SEC studies undertaken to try and help electronically characterise these materials appear to be severely broadened and contain little information directly pertaining to any underlying electron-transfer processes. As such further studies on these compounds

to fully characterise the electronic structure, such as low temperature spectroscopy (to attempt to limit conformational degrees of freedom), EPR and magnetic measurements on isolated samples of the compounds in their various oxidation states are required.

6.2. Background

Ferrocene has long been used in the study of mixed valence compounds of linear, wire-like composition. It was shown in the 1970s that biferrocene (A, Figure 97) was able to undergo one electron oxidation to form a mixed valence compound that gives rise to an electronic transition in the NIR (ca. 1900 nm) that can be attributed to an IVCT type transition between the two ferrocene moieties.[1] These results were followed by studies on 1,2-diferrocenylethene analogues (FcCR=CRFc, R=H, CH_3) which contain a bridge larger than a single bond between the ferrocenyl moieties. Despite the greater physical separation of the redox centres, electrochemical studies have shown that for both *cis*- and *trans*-FcCH=CHFc (B and C, Figure 97) two one-electron processes separated by 170 mV can be observed.[2] In the case of the methyl substituted analogues, *E*-1,2-dimethyldiferrocenylethylene (B, Figure 97) and *Z*-1,2-dimethyldiferrocenylethylene (C, Figure 97), the *Z*-isomer gave a slightly greater separation of the two redox processes (170 vs 159 mV). However, whilst the thermodynamically more stable *E*-isomer was able to be studied spectroscopically the *Z*-isomer could not be fully studied due to complications arising from isomerisation.[3] Nevertheless, for this family of 1,2-bis(ferrocenyl)ethenes, the mixed valence form is sufficiently thermodynamically stable to be studied, revealing IVCT type transitions at ca. 6000 cm^{-1} in each available case.

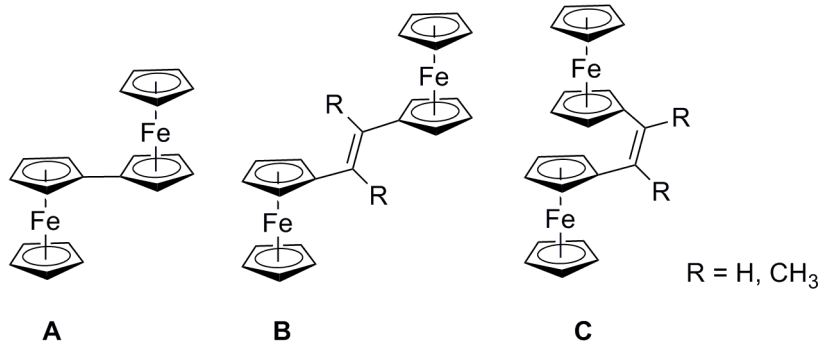

Figure 97: Biferrocene and diferrocenylethylene complexes that display mixed valence structures

Given that the different isomers of the diferrocenylethylene can add additional complexity to the analysis of the MV states, it is desirable to try and prevent these issues. One way of doing this is to move to a strictly linear system such as those formed from acetylene linkers, Fc-$(C\equiv C)_n$-Fc. Results have shown that in common electrolyte solutions the n = 1, 2 compounds undergo two reversible one-electron processes, although for Fc-$(C\equiv C)_2$-Fc the waves are poorly resolved with a high degree of overlap. The corresponding MV mono-cations have been prepared and the Uv-vis NIR spectra show a distinct band in the NIR for $[Fc\text{-}C\equiv C\text{-}Fc]^+$ with a band centre of ca. 6500 cm^{-1}. This IVCT band undergoes a dramatic blue shift in the extended bridged $[Fc\text{-}(C\equiv C)_2\text{-}Fc]^+$ being found at ca. 8500 cm^{-1}, to give a modest H_{ab} value of ca. 250 cm^{-1}.[4] The thermodynamic stability of the mixed-valence forms of bis(ferrocenyl)polyynes decreases with increasing length of the polyyne segment, and with common electrolytes the 1,6-bis(ferrocenyl)hexa-1,3,5-triyne Fc-$(C\equiv C)_3$-Fc gives rise to only a single redox wave in the CV, although consideration of ΔE_p with respect to an internal standard identifies this as two overlapping oxidations rather than a single two-electron process.[5] While the Fc-$(C\equiv C)_4$-Fc has been prepared there have been no electrochemical or spectroscopic studies of its electronic structure.[6] However, when going to the C_{12} bridged derivative (Fc-$(C\equiv C)_6$-Fc) the CV now

reveals a genuine single two-electron process highlighting the thermodynamic instability of the MV species in NBu_4PF_6.[7]

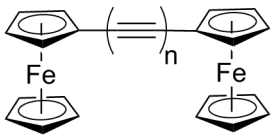

Figure 98: Linear α,ω-ferrocene(poly)yne complexes.

While linear ferrocene compounds represent one of the most studied organometallic fragments from which to explore electron transfer, it is clear that in common electrolyte solutions the mixed valence state is not always sufficiently thermodynamically stable to permit study of its electronic properties. As such there has recently been an increase in the use of WCA solutions to exploit these effects in mixed-valence ferrocene systems. As outlined in the Introduction (Chapter 1: Introduction) the use of such electrolyte solutions can stabilise a degree of through-space (Coulombic) interaction that is not observed in more strongly coordinating systems due to the ion-pairing of the counter-ion. For example, Barriere and Geiger have shown that by altering the nature of the medium they were able to increase the peak separation between the different oxidation processes in a tetra-ferrocene compound (Figure 99) from 292 mV (ca. 130 mV per process) separating the first and fourth anodic processes to 682 mV (ca. 228 mV per process), the latter being sufficiently large that study of the mixed valence forms should be possible.[8]

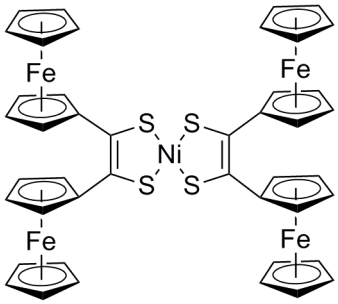

Figure 99: Tetraferrocenyl(nickel dithiolene)

In a similar manner, Lang has recently prepared a range of different bis(ferrocene) complexes (Figure 100) with varying heterocyclic bridges (E = S,[9] O,[10] NR,[11] PR,[12] P(O)R, [12] SiR_2[13]) that have shown that use of a WCA has been able to stabilise the mixed valence state of these material, identified by an IVCT type transition in the NIR.[14]

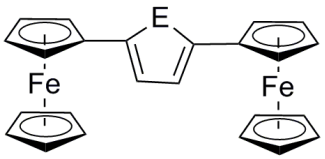

E = S, O, NR, PR, P(O)R, SiR_2

Figure 100: Recent ferrocene based materials developed by the Lang group

To further support the results from the Lang group the synthesis of a range of ethynylferrocene terminated benzene compounds has also been reported. The Long group in collaboration with the group of Zanello has previously published the synthesis and electrochemical analysis of 1,3,5- tris(ferrocenylethynyl)benzene (D, Figure 101) and have shown that in NBu_4PF_6 electrolyte solutions all of the ferrocene moieties oxidise simultaneously.[15]

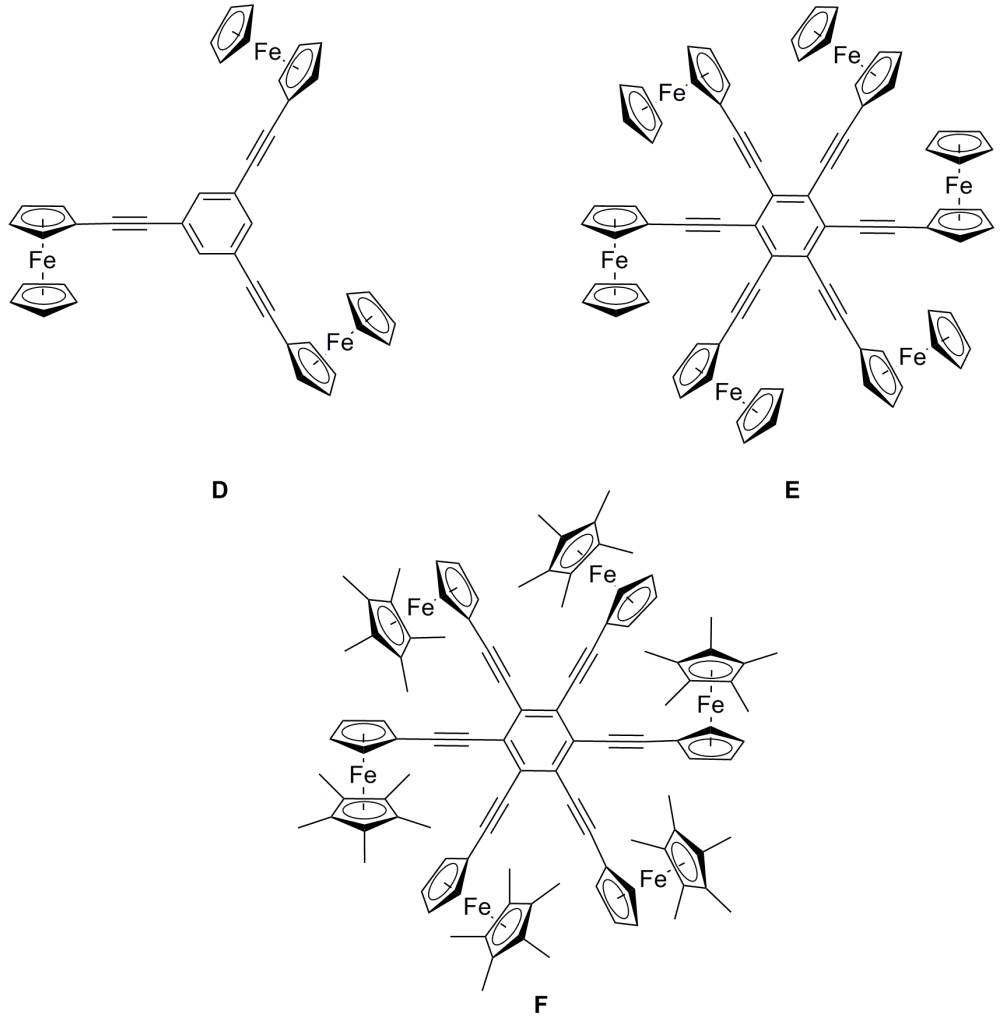

Figure 101: Examples of multi-ethynylferrocene compounds

More recently examples have appeared from the Astruc group that contain six ethynylferrocene moieties.[16] These compounds, including hexa(ferrocenylethynyl)benzene (E, Figure 101), are shown to undergo a single oxidation in NBu_4PF_6 but in the case of the pentamethylferrocene derivative the use of a WCA gives rise to six individual processes (E, Figure 101).

The results obtained from Chapter 5 in this Thesis have shown that with careful selection of electrolyte it is possible to elicit a modest degree of stabilisation of the mixed valence complexes derived from cross-conjugated complexes $FcCH=C(C{\equiv}CC_6H_4C{\equiv}CML_n)_2$ (ML_n= $Ru(PPh_3)_2Cp$, Ru(dppe)Cp* and

Fe(dppe)Cp*) that is sufficient to detect a small amount of communication between the remote electrophores through the cross-conjugated bridge. Given these findings and the recent work on multi-ferrocenyl systems, a series of compounds containing ethynylferrocene fragments incorporated into cross-conjugated bridging structures were prepared and studied by spectroelectrochemical methods, with aims of exploiting the ferrocene group's ability to generate, and serve as a probe of, mixed-valence character.

6.3. Results and discussion

6.3.1. Synthesis

Ethynylferrocene, **42**, was prepared in good yield through one of the literature methods (Scheme 34) and characterised by the usual spectroscopic techniques with analyses consistent with those reported elsewhere.[17] The ^{1}H NMR spectrum shows the characteristic signals of a substituted ferrocene with pseudo triplet resonances at 4.19 and 4.46 ppm triplet (presumably caused by an ABB' spin system in which the strong second order coupling gives rise to $J_3 \approx J_4$) for the substituted Cp ring and a singlet resonance at 4.21 ppm for the unsubstituted ring. Solution IR (CH_2Cl_2) give characteristic ν(C≡C−H) 3300 cm^{-1} and ν(C≡C) 2109 cm^{-1} bands.

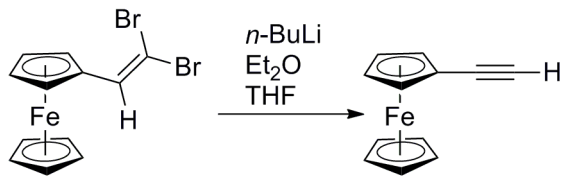

22 **42**

Scheme 34: Synthesis of ethynylferrocene

Compound **42** reacted smoothly with $Ph_2C{=}CBr_2$ (**28**) under Sonogashira cross-coupling conditions to form the geminal bis-ferrocenyl compound $Ph_2C{=}C(C{\equiv}CFc)_2$ (**43**) in moderate yield (48 %) as a bright orange solid (Scheme 35). Compound **43** was characterized by the usual range of ^{1}H, $^{13}C\{^{1}H\}$ NMR spectroscopies, and ASAP mass spectrometry.[18] Full assignment of the NMR spectroscopic data was possible through NOESY, COSY, HSQC and HMBC methods. The ^{1}H NMR spectrum shows the characteristic signals of a mono-substituted ferrocene with apparent triplet resonances at 4.22 and 4.36 ppm for the substituted Cp ring and a singlet resonance at 4.15 ppm for the unsubstituted Cp ring.[10-13] The phenyl moieties gave rise to two multiplet resonances. The IR spectrum (CH_2Cl_2) exhibits characteristic signals for the C≡C and C=C functional groups with ν(C≡C) at 2202 cm^{-1} and ν(C=C) at 1481 cm^{-1}. The purity of the isolated sample was confirmed with satisfactory elemental analysis (Analysis found C 76.38, H 4.61 % required C 76.52, H 4.74 %.)

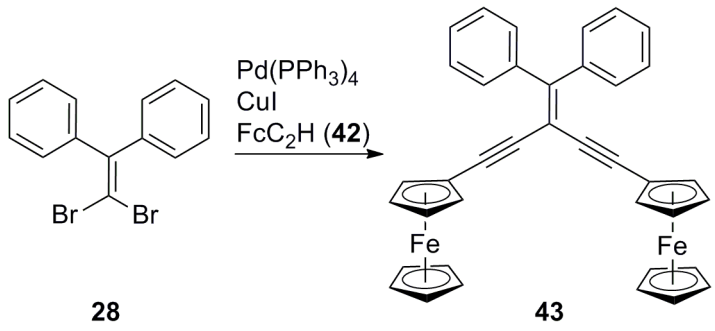

Scheme 35: Synthesis of bis-ferrocene compound 43

In an analogous manner to the synthesis of compound **43,** FcC≡CH (**42**) reacted smoothly with the ferrocenyl-substituted dibromoethene $FcCH{=}CBr_2$ (**22**) under Sonogashira cross coupling conditions to form the tris-ferrocenyl compound **44** in

good yield (68 %) as a bright red solid (Scheme 36). The compound was characterised by the usual spectroscopic techniques and a satisfactory elemental analysis was obtained (C 68.82, H 4.50 % required C 68.70, H 4.61 %). Full assignment of the ^{1}H and ^{13}C NMR spectra was possible through a combination of NOESY, COSY, HSQC and HMBC techniques and whilst the sets of resonances belonging to the individual alkynyl fragments were unambiguously assigned, attributing these sets of resonances to either the *E* or *Z* arm was not possible. The ^{1}H NMR spectrum has a singlet resonance at 6.85 ppm consistent with the vinylic proton of the ferrocenylethene fragment in the same range as those seen for the organic and ruthenium compounds in Chapter 4 and Chapter 5 respectively. The three inequivalent ferrocenyl groups give rise to three sets of two triplet resonances for the three substituted Cp rings and three singlet resonances for the unsubstituted Cp rings. The two ethynyl substituted ferroccenyl moieties give rise to apparent triplets at 4.24, 4.49 and 4.29, 4.58 ppm, and two singlet resonances at 4.22 and 4.27 ppm in the ^{1}H NMR spectrum. The vinyl ferrocene moiety gives the usual pseudo resonances at 4.41 and 4.92 ppm and a singlet resonance at 4.32 ppm for the unsubstituted Cp ring. ASAP-MS(+) shows the $[M+H]^{+}$ ion and the IR (CH_2Cl_2) spectrum gives ν(C≡C) bands at 2195 and 2203 cm^{-1} corresponding to the two inequivalent arms in addition to ν(C=C) at 1551 cm^{-1}.

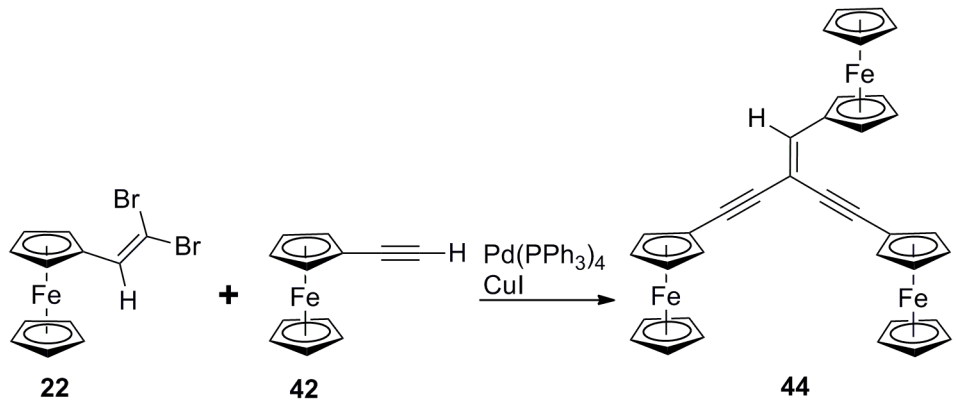

Scheme 36: Synthesis of tris-ferrocene compound 44

In seeking to extend this synthetic methodology, the cross-conjugated *gem*-dibromoethene $(FcC{\equiv}C)_2C{=}CBr_2$ (**47**) was quickly identified as a useful cross-coupling partner. As highlighted previously (Chapter 4 Introduction) compound **47** has previously been synthesised for use in the preparation of 1,6-bis(ferrocenyl)-1,3,5-hexatriyne via a Fritsch-Buttenberg-Wiechell rearrangement.[5 and 19] The preparation of **47** is outlined in Scheme 37, with the slight modifications of procedures reported in the literature being detailed in the experimental section. Initial deprotonation of **42** with BuLi gives FcC≡CLi, which upon treatment with methylformate gives bis(ferrocenylethynyl) methanol **45**. Subsequent oxidation of the secondary alcohol **45** with MnO_2 gave the bis(ferrocenylethynyl) ketone **46** from which Corey-Fuchs di-bromo olefination is used to give the desired cross-conjugated *gem*-dibromoethene **47**. Each compound along this synthetic sequence was characterised with the usual spectroscopic techniques giving data that were consistent with those reported in the earlier literature. The ^{1}H NMR spectra for all the compounds have the usual pseudo triplet resonances for the substituted Cp ring (**45**; 4.22 and 4.48 ppm, **46**; 4.42 and 4.66 ppm, **47**; 4.26 and 4.52 ppm) and the singlet resonance for unsubstituted Cp (**45**; 4.25 ppm, **46**; 4.29 ppm, **47**; 4.25 ppm).

The diethynylmethanol derivative **45** also gives rise to a set of doublet resonances for the –CH(OH)- fragment at 2.38 and 5.37 ppm for the CH and OH protons respectively.

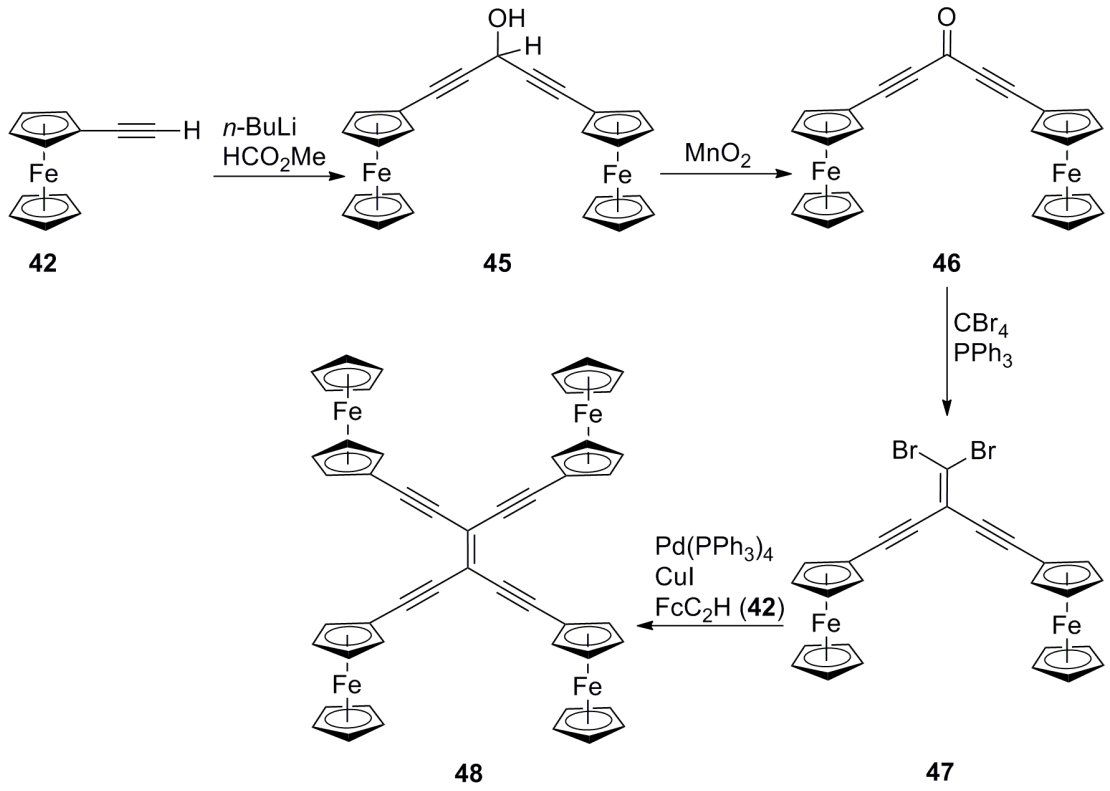

Scheme 37: Synthesis of tetra-ferrocene compound 48

Cross-coupling of compound **42** with **47** under Sonogashira conditions gave the desired tetra-ferrocenyl ethene $(FcC{\equiv}C)_2C{=}C(C{\equiv}CFc)_2$ **48** in moderate yield (19 %) as a dark purple solid after workup. The compound was characterised by the usual spectroscopic techniques and ASAP-HRMS. Full assignment of the ^{1}H and ^{13}C NMR spectra was possible through a combination of NOESY, COSY, HSQC and HMBC techniques. Consistent with the previous examples of mono-substituted ferrocene compounds, the ^{1}H NMR spectrum contains characteristic singlet and triplet resonances for the unsubstituted (4.27 ppm) and substituted (4.30 and 4.59

ppm) Cp rings. ASAP-MS(+) shows the $[M]^+$ ion and the IR spectrum contains both ν(C≡C) (2198 cm^{-1}) and ν(C=C) (1482 cm^{-1}) bands.

The synthetic issues surrounding compounds with four ethynyl ferrocene moieties in an approximately four-fold symmetric arrangement have previously been observed in the Raithby group while trying to prepare 1,2,4,5-tetrakis(ferrocenylethynyl)benzene.[20] It was shown that the most efficient route to this compound was through the Stille coupling with (tributylstannylethynyl)ferrocene and 1,2,4,5-tetrabromobenzene, and not the Sonogashira conditions. The observations of the Raithby group where the mono, bis, tris and tetra ferrocenyl products along with homo-coupled ethynylferrocene are produced may help to explain the poor reaction yields observed here. However, chromatography failed to separate and conclusively identify partially coupled materials in the case of the preparation of **48**.

6.3.2. Molecular Structures

Single crystals of the tris(ferrocene) complex **44** suitable for X-ray diffraction were obtained by slow evaporation of a CH_2Cl_2 solution. Important bond lengths and angles are given in Table 45. As expected, the 1,1-dialkynyl ethene portion of the molecule is essentially planar, consistent with the structures obtained in Chapter 4 and 5. The key C=C (1.366(5) Å), and C≡C (1.193(5) and 1.198(5) Å) bond lengths are consistent with the compounds reported in Chapter 4 and for other ethynyl ferrocene compounds (1,3,5-$[FcC{\equiv}C]_3C_6H_3$; 1.182(11) - 1.187(11) Å, FcC≡CC≡CC≡CFc; 1.211(1) Å and $[FcC{\equiv}C]_2C{=}CBr_2$; 1.207(2) Å). Interestingly, the C11 – C15 ring and C3 ≡ C4 arm located *trans* across the double bond lie close to the same

plane, with a *syn* relationship in the case of the two ferrocenyl moieties and the groups *cis* to the vinyl ferrocene is much less obviously positioned to promote significant π-conjugation.

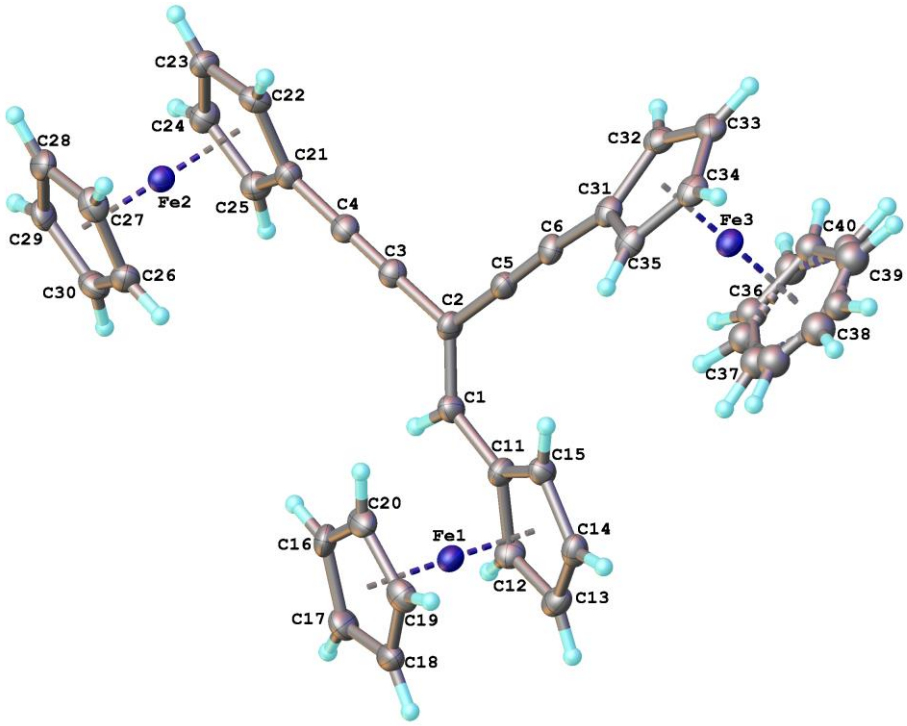

Figure 102: A plot of the molecular structure of 44 , showing the atom labelling scheme.

Table 45: Selected bond lengths (Å) and angles (°) for 44.

C1-C11	1.454(5)	C11-C1-C2	128.2(3)
C11-C15	1.435(5)	C1-C2-C3	120.0(3)
C1-C2	1.366(5)	C1-C2-C5	124.1(3)
C2-C3	1.437(5)	C2-C3-C4	178.5(4)
C3-C4	1.193(5)	C2-C5-C6	176.2(4)
C4-C21	1.425(5)	C3-C4-C21	179.5(4)
C2-C5	1.431(5)	C5-C6-C31	175.7(4)
C5-C6	1.198(5)		
C6-C31	1.431(5)		

6.3.3. Electrochemistry

In order to explore the redox chemistry of the bis (**43**), tris (**44**) and tetra (**48**) ferrocenyl compounds, cyclic voltammetry (CV) was carried out in a standard three-electrode cell (equipped with a Pt microdisc working electrode) from a CH_2Cl_2 solution containing the 10^{-1} M $NBu_4[X]$ supporting electrolyte, X = $[PF_6]$ or $[BArF_4]$.[8 and 21] The CV of compounds **43** and **48** with $[PF_6]$ containing electrolyte each show a single reversible process comprised of the overlapping redox waves of the ferrocenyl moieties. In contrast, in this electrolyte, the tris-ferrocenyl compound $FcCH=C(C{\equiv}CFc)_2$ (**44**) shows two close lying peaks with current intensities in the ratio 1:2 consistent with the vinyl and ethynyl-substituted ferrocene fragments undergoing oxidation at measurably different potentials (Table 46 and Table 47).

Turning more detailed attention to each compound in turn, the single reversible redox process observed in the CV of the bis(ferrocene) $Ph_2C=C(C{\equiv}CFc)_2$ (**43**) in NBu_4PF_6 electrolyte (denoted $E_{1/2}(1)$, Table 46) has a rather large (134 mV) value of $\Delta E_p(1)$ (Table 47, Figure 103). As noted in Chapter 2 the observation of ΔE_p values that are approaching twice that of the internal reference (ca. 59 mV) indicate that the redox couple is more consistent with two closely positioned $1e^-$ processes. Studies in electrolyte containing the very weakly coordinating $[BAr^F{}_4]$ anion show a remarkable change on the nature of the CV with two distinct reversible processes present and separated by some 110 mV. The increase in peak separation in the $[BAr^F{}_4]^-$ experiment suggests that there is better prospect of observing the intermediate mono-cation $[\mathbf{43}]^+$ in SEC experiments conducted in the WCA-containing electrolyte.

Table 46: Oxidation potentials for complexes 43, 44 and 48. CV in CH_2Cl_2 with 0.1 M $NBu_4[X]$ at a scan rate of 100 mV/s and referenced against $FeCp^*_2$ *vs* $FeCp_2$ ($FeCp_2$ = +0.0 V).

	$[X]^-$	$E_{1/2}(1)$/V	$E_{1/2}(2)$/V	$E_{1/2}(3)$/V	$E_{1/2}(4)$/V	$\Delta E_p(1)$/ V	$\Delta E_p(2)$/ V	$\Delta E_p(3)$/ V	$\Delta E_p(4)$/ V	$\Delta E_p(FeCp_2^*)$ / V
43	$[PF_6]^-$	0.202				0.134				0.089
	$[BAr^F{}_4]^-$	0.089	0.201			0.063	0.062			0.060
44	$[PF_6]^-$	0.057	0.202			0.079	0.121			0.074
	$[BAr^F{}_4]^-$	0.074	0.290	0.471		0.139	0.146	0.144		0.120
48	$[PF_6]^-$	0.233				0.084				0.078
	$[BAr^F{}_4]$	0.108	0.222	0.347	0.478	0.064	0.065	0.069	0.068	0.061

Table 47: Comproportionation constants for 43, 44 and 48.

	$[X]^-$	$\Delta E(1\text{-}2)$/ V	K_c	$\Delta E(2\text{-}3)$/ V	K_c	$\Delta E(3\text{-}4)$/ V	K_c
43	$[PF_6]^-$	<0.050	4				
	$[BAr^F{}_4]^-$	0.112	78				
44	$[PF_6]^-$	0.145	283				
	$[BAr^F{}_4]^-$	0.216	4500	0.181	1151		
48	$[PF_6]^-$	<0.050	4				
	$[BAr^F{}_4]$	0.114	85	0.125	130	0.131	165

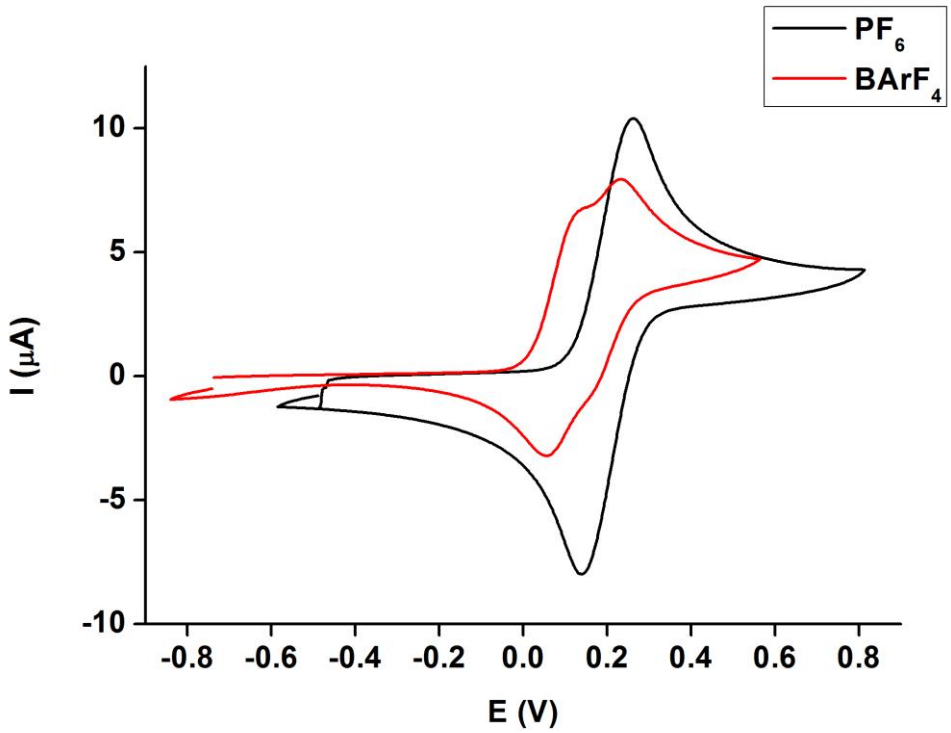

Figure 103: Cyclic voltammograms of 43 in $CH_2Cl_2/10^{-1}$ M $NBu_4[X]$; scan rate v = 100 mV s^{-1}. Potentials are reported against ferrocene ($FeCp_2/FeCp_2^+$ = 0.0 V) by reference against an internal decamethylferrocene/decamethylferricenium couple.

The tris ferrocenyl compound **44** undergoes a reversible, apparently 1-e oxidation ($E_{1/2}$(1) 0.057 V, ΔE_p = 0.079 V)) which can be assigned on the basis of comparison with the potentials observed for oxidation of $FcCH{=}C(C{\equiv}CR)_2$ (R = $C_6H_4CH_3$-4, $C_6H_4NH_2$-4, $C_6H_4NMe_2$-4, $C_6H_4NO_2$-4) (Chapter 4) to the vinyl-substituted ferrocenyl moiety. The second redox process in NBu_4PF_6 electrolyte arises from overlapping oxidation of the ethynylferrocene groups as suggested by the ΔE_p of this wave approaching twice that of the internal reference and a halfwave potential consistent with the ethynyl ferrocenyl moieties in **43** (ca. 0.2 V in each case). As may be expected, studies of the voltammetric response of the tris(ferrocenyl)

compound **44** in $[BAr^{F}_{4}]^{-}$ solutions are consistent with results from **43** and other poly(ferrocene) compounds in electrolytes containing WCAs, with an increase in separation of the individual redox events to give three reversible one electron process that can be attributed to the vinyl-ferrocene oxidation followed by sequential oxidation of the ethynylferrocene fragments.

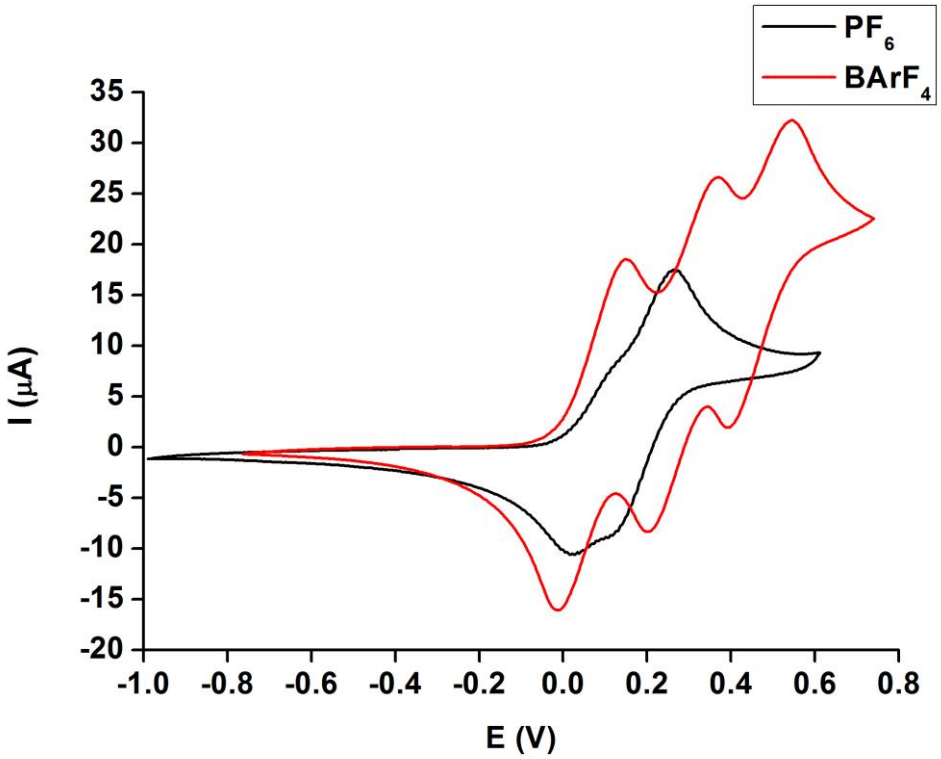

Figure 104: Cyclic voltammograms of 44 in $CH_2Cl_2/10^{-1}$ M $NBu_4[X]$; scan rate v = 100 mV s^{-1}. Potentials are reported against ferrocene ($FeCp_2/FeCp_2^+$ = 0.0 V) by reference against an internal decamethylferrocene/decamethylferricenium couple.

Curiously, in contrast to the wave shapes observed for the bis(ferrocenylethynyl) portions of both **42** and **44** which suggest overlapping (unresolved) oxidation processes associated with each FcC≡C fragment, the single reversible redox process in the tetrakis(ferocenylethynyl) compound **48** has the shape of a 1-e process, which

indicates independent and simultaneous oxidation of all four ferrocenyl groups in NBu_4PF_6 electrolyte (Figure 105). However, as with other poly(ferrocenyl) compounds reported here and elsewhere, in electrolyte solutions containing $[BAr^F{}_4]^-$ anions there is an increase in the separation of the individual redox events, to give four reversible one electron process that can be attributed to the sequential oxidation of the four ethynylferrocenyl moieties, the comproportionation constants for each separation are given in Table 47.

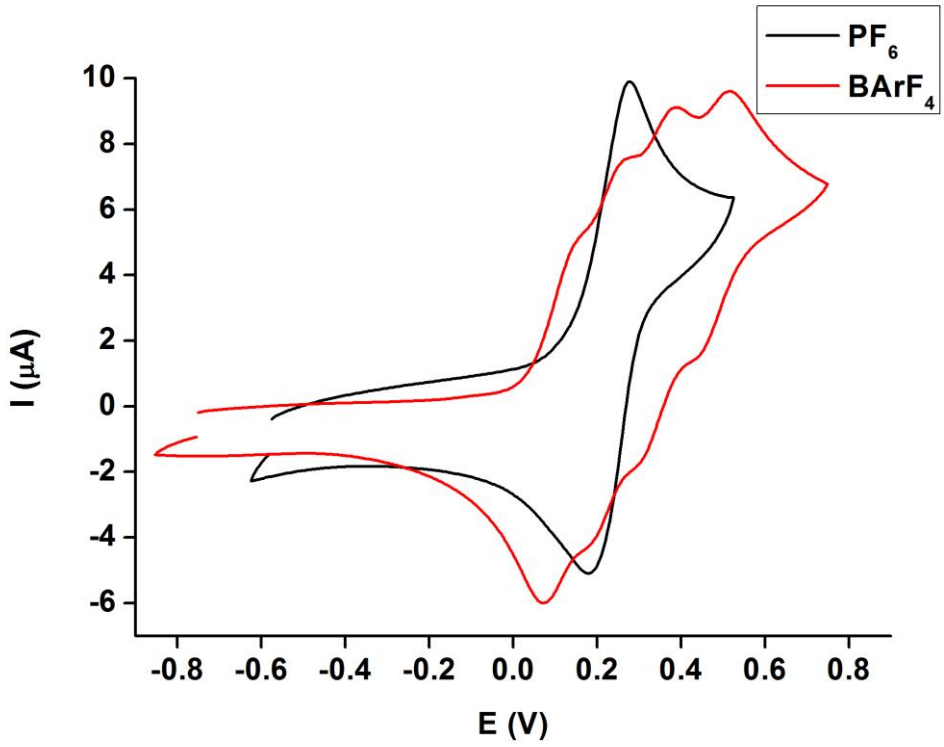

Figure 105: Cyclic voltammograms of 48 in $CH_2Cl_2/10^{-1}$ M $NBu_4[X]$; scan rate v = 100 mV s^{-1}. Potentials are reported against ferrocene ($FeCp_2/FeCp_2^+$ = 0.0 V) by reference against an internal decamethylferrocene/decamethylferricenium couple.

6.3.4. IR Spectroelectrochemistry

IR spectroelectrochemical investigations were undertaken (in collaboration with Professor Franti Hartl's group in Reading, UK.) to better assess the interactions between the ferrocenyl moieties in **43**, **44** and **48**. Spectroelectrochemical experiments were carried out in electrolyte solutions of $NBu_4[BArF_4]$ in order to maximize the stability of the intermediate redox states.

The IR spectra of the tris (**44**) and tetrakis (**48**) ferrocenyl compounds give rise to sharp ν(C≡C) bands at 2203 and 2189 cm^{-1} respectively. In contrast the bis(ferrocenyl) compound $Ph_2C{=}C(C{\equiv}CFc)_2$ (**43**) gives rise to a broader ν(C≡C) band envelope which may be due to a number of conformers in solution. Similar effects have been observed recently in 2,5-Fc_2-3,4-Ph_2-C_4SiR (R = Me, Ph).[13] All three compounds have a single vinyl ν(C=C) band (**43**; 1481, **44**; 1552, **48**; 1481 cm^{-1}), and it is interesting to note that this spectroscopic feature is unchanged as a function of the redox state of the molecule. Consistent with the oxidation of the complexes **23a-f** and **41a-b** (Chapter 4 and 5 respectively) upon oxidation of complexes **43**, **44** and **48** to [**43**, **44** and **48**]$^{n+}$ (n = 0, 1, 2, 3 or 4 as appropriate) there is the appearance of a new electronic absorption band centred at ca. 4150 cm^{-1} consistent with a localised d-d transition of the oxidised ferrocene moiety, highlighted in Figure 106 for [**43**]$^{n+}$ (n = 0, 1, 2).[22]

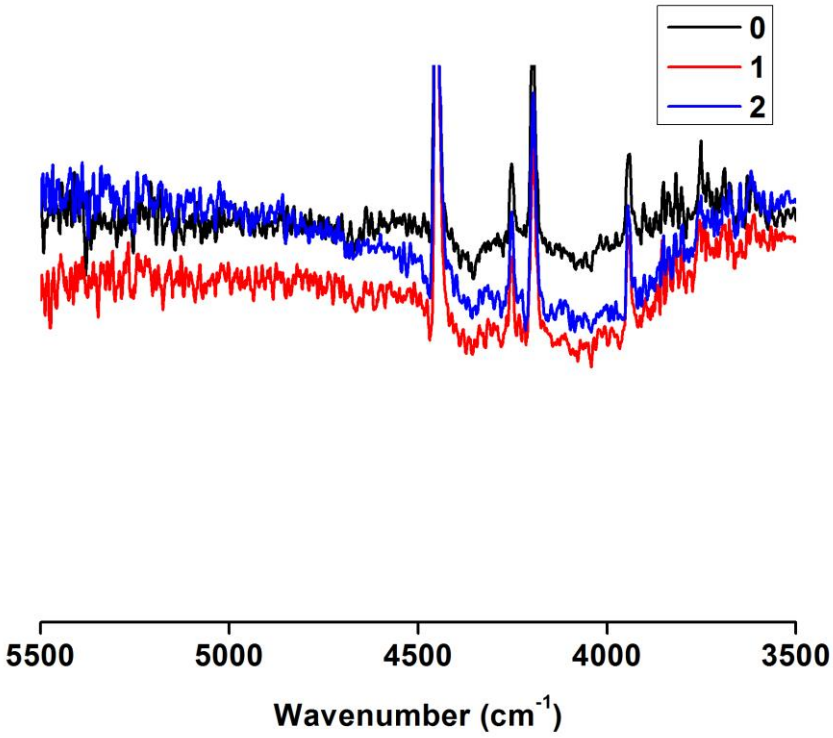

Figure 106: Reversible IR spectral changes accompanying highlighting the localised d-d transition of the oxidised ferrocene moieties. Figure shows $[43]^{n+}$ (n = 0, 1, 2) as an example.

Turning to each complex in more detail, the sequential oxidation of the two ferrocene moieties in **43** to give $[\mathbf{43}]^{+}$ and $[\mathbf{43}]^{2+}$ has little effect on the nature of the ν(C≡C) with an increase in the intensity on formation of $[\mathbf{43}]^{+}$ and a slight decrease on formation $[\mathbf{43}]^{2+}$ coupled with an almost imperceptible blue shift about 3 cm^{-1} (noting the spectrometer resolution of 0.5 cm^{-1}) (Figure 107). The results indicate that the oxidation is localised at the ferrocene centre and that there is little contribution from the ethynyl group to the oxidised fragment.

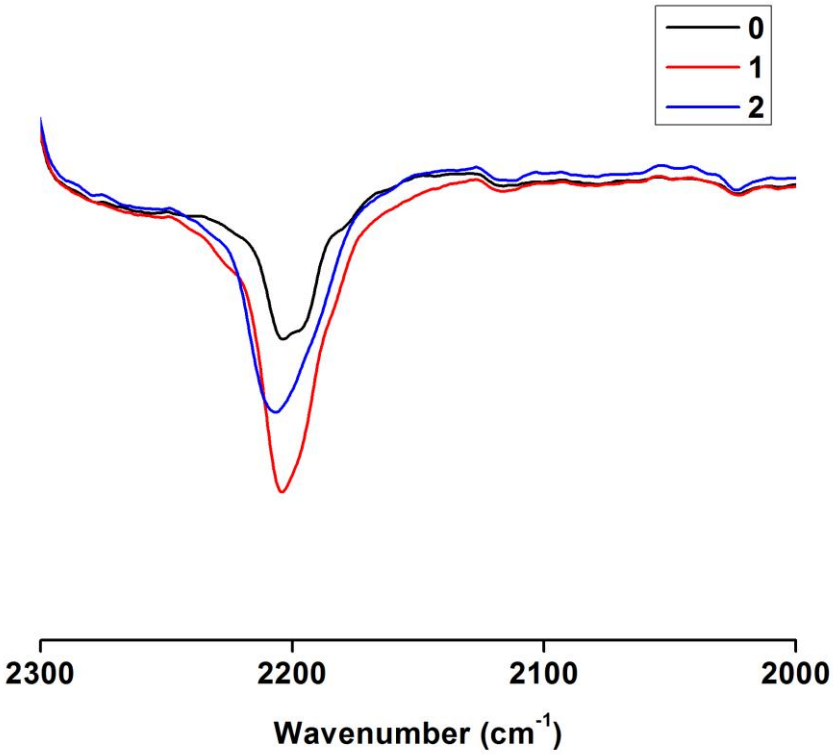

Figure 107: Reversible IR spectral changes in the ν(C≡C) region accompanying oxidation of the ferrocene moiety in 43 in CH_2Cl_2 / 10^{-1} M NBu_4BArF_4 within an OTTLE cell.

The oxidation of **44** to [**44**]$^+$ (i.e. oxidation of the vinyl ferrocene moiety) has little effect on the IR spectrum and the ν(C≡C) band remains largely unchanged with a the appearance of a shoulder on the low energy side of the peak (Figure 108). Upon oxidation to [**44**]$^{2+}$ the spectral changes are consistent with the oxidation of an ethynylferrocene moiety with a slight increase in intensity of the ν(C≡C) band, accompanied with a shift of ca. 20 cm^{-1} to lower energyand the appearance of a shoulder on the high energy side of the band. The third oxidation to [**44**]$^{3+}$ gives a further small increase in intensity of the ν(C≡C) band with no other notable spectral changes in the IR region.

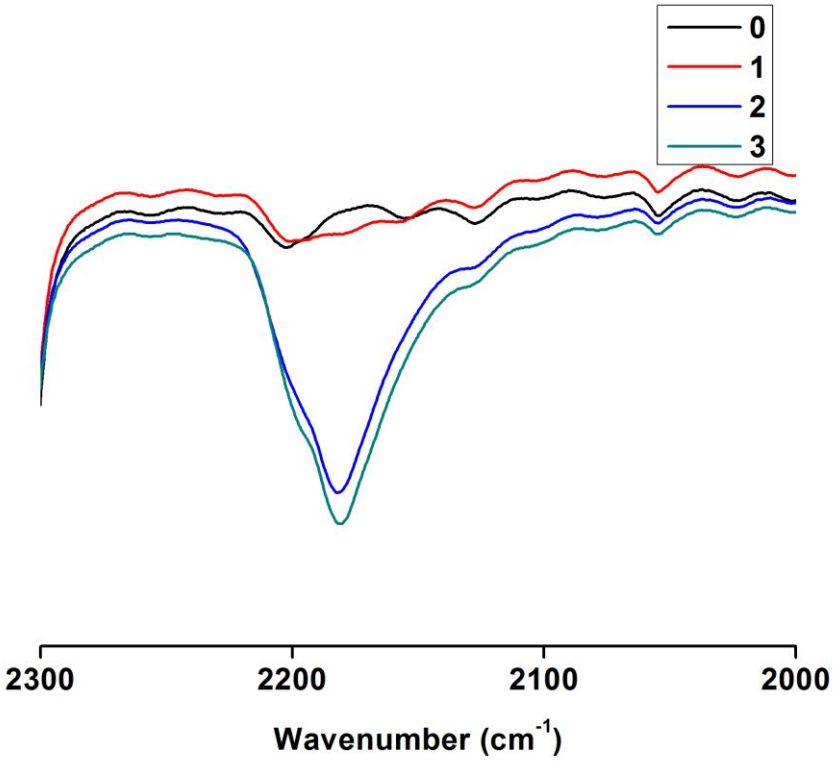

Figure 108: Reversible IR spectral changes in the ν(C≡C) region accompanying oxidation of the ferrocene moiety in 44 in CH_2Cl_2 / 10^{-1} M NBu_4BArF_4 within an OTTLE cell.

The oxidation of **48** to [**48**]$^{+}$ gives spectral changes that are consistent with the oxidation of an ethynylferrocene moiety with a slight increase in intensity of the ν(C≡C) band, accompanied with a shift of ca. 20 cm^{-1} to lower energyand the appearance of a shoulder on the high energy side of the band (Figure 109). The sequential oxidations to [**48**]$^{2+}$ and [**48**]$^{3+}$ show a further shift to lower energy of ca. 4 cm^{-1} of the principal ν(C≡C) band accompanied with a decrease in intensity. This decrease in intensity continues on oxidation to [**48**]$^{4+}$ where the ν(C≡C) band is no longer detected in the spectrum consistent with the symmetric nature of the structure and the loss of a dipole across the system. It is important to note here that although the description of a symmetric system accounts for the loss of the ν(C≡C) band in

the higher oxidation states the poor solubility of the complex in these states may lead to precipitation of the charged material from solution.

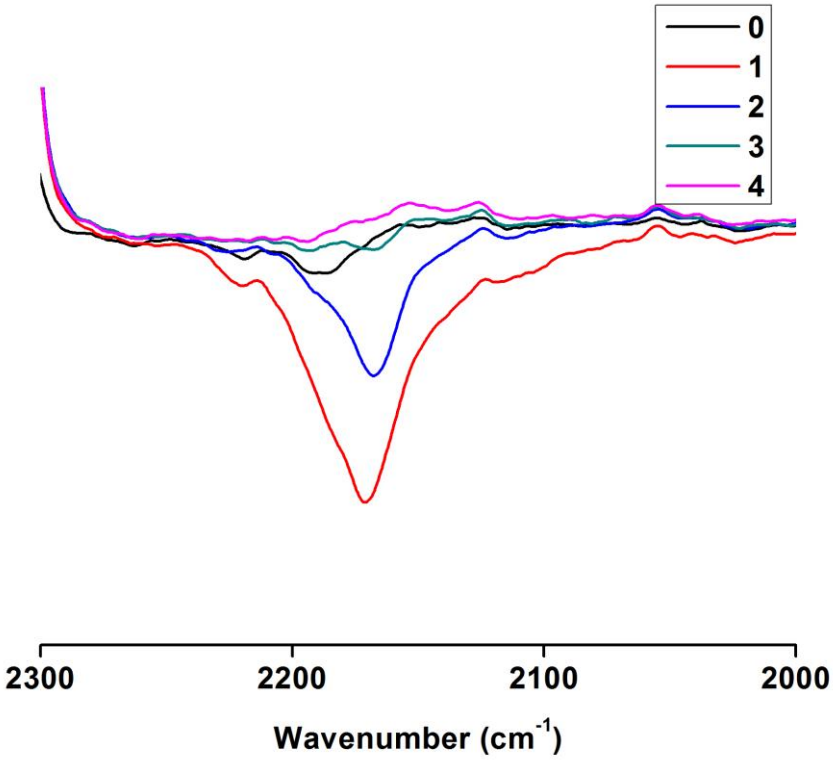

Figure 109: Reversible IR spectral changes in the ν(C≡C) region accompanying oxidation of the ferrocene moiety in 48 in CH_2Cl_2 / 10^{-1} M NBu_4BArF_4 within an OTTLE cell.

Table 48: Characteristic IR active vibrational modes (cm^{-1}) of 43, 44 and 48 observed in spectroelectrochemical studies by in situ oxidation of a $CH_2Cl_2/10^{-1}$ M NBu_4BArF_4 solution for [43, 44 and 48]$^{n+}$ (n = 0, 1, 2, 3, 4).

	ν(C≡C)	*ν*(C=C) vinyl
43	2203(s), 2198(s)	1481(s)
[43]$^{+}$	2204(s), 2198(sh)	1481(s)
[43]$^{2+}$	2206(s), 2192(sh)	1481(s)
44	2203(s)	1552(s)
[44]$^{+}$	2201(s), 2178(sh)	1551(s)
[44]$^{2+}$	2180(s), 2201(sh)	1551(s)
[44]$^{3+}$	2180(s), 2199(sh)	1540(b)
48	2189(s)	1481(s)
[48]$^{+}$	2171(s), 2196(sh)	1481(s)
[48]$^{2+}$	2167(s), 2190(sh)	1481(s)
[48]$^{3+}$	2167(w), 2193(w)	1481(s)
[48]$^{3+}$	Not observed	1481(s)

6.3.5. Implications in the design of QCA devices

As highlighted in the introduction to this work (Chapter 1) the need to develop molecular materials that can act as components in device technology is growing rapidly as we reach a point were Moore's law can no longer be reached. There has been a large drive recently in the design of materials that can be used for Quantum-dot Cellular Automata (QCA). In QCA data are no longer stored in binary code but in the specific charge configuration of the cell.[23] Materials suitable for QCA are often of a four component nature and require the presence of two holes / electrons that can be transferred around the cell (Figure 110), these different configurations are representative of the classical 0 and 1 states in binary systems. The antipodal

arrangement of the holes / electrons is caused by the Coulombic interactions in the cell, and the polarisation of adjacent cells will be the same due the Coulombic repulsion.

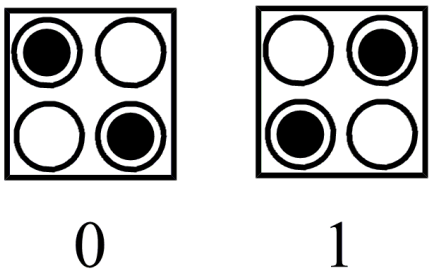

Figure 110: Degenerate ground states of a QCA cell and their binary representations.

If these cells can then be placed in a linear series to each other then it is possible to create wires based on these materials (Figure 111). Through modification of the charge configuration in either of the end cells the line will be switched so the ends are the same.[24]

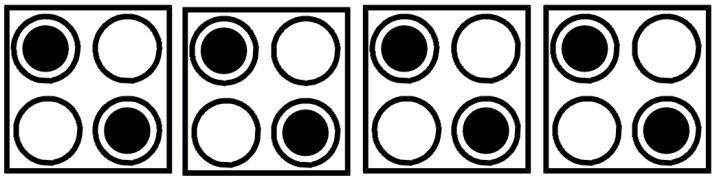

Figure 111: Wire-like structure based on QCA materials.

It thus stands that molecular QCA (MQCA) have a number of requirements:

1. Four redox sites with four-fold symmetry
2. Ability for charge localisation
3. Ability for charge switching.

The electrochemical and IR spectroelectrochemical results suggest that $(FcC{\equiv}C)_2C{=}C(FcC{\equiv}C)_2$, **48**, offers the required geometry and charge transfer properties to be a MQCA candidate structure. However, in order to be suitable for

use as MQCA, the electronic (charge) structure of the compounds has to be explored and their ability to undergo charge migration / switching which has been demonstrated previously in multi-ferrocenyl complexes by the observation of IVCT type transitions in the NIR region of spectrum. [25]

Giving some further consideration to device-like concepts, the Kandel group has recently managed to co-adsorb diferrocenylacetylene on to an Au(111) surface with benzene. Their studies have shown that the molecule sits in the *syn*- geometry and that there is very little contribution from the C≡C to the HOMO with the electron density centred on the ferrocene moieties.[26] Further recent work published by the Kandel and Lapinte groups has shown that the electronic structure of molecules (1,3,5-{Cp*(dppe)Fe(C≡C)}$_3$C$_6$H$_3$), in various oxidation states, can be probed by STM.[27] The reports highlight the ability to study the charge state of molecules in the various oxidation states whilst immobilised on a surface. The study of ferrocene based mixed-valence materials by this technique is clearly possible and as such would provide a suitable method of probing the configuration of the most relevant compound in terms of MQCA applications, [**48**]$^{2+}$.

6.3.5.1. Electronic Structure

UV-vis NIR spectroelectrochemical investigations were undertaken (in collaboration with Hartl's group) to better assess the electronic interactions in the various oxidation states, and with a particular interest in attempting to identify an IVCT transition that might provide more information concerning the charge distribution and transfer through the ene(poly-yne) scaffolds. The spectra for **43**, **44** and **48** all

show characteristic absorption bands for ferrocenyl compounds with maxima at ca. 20000 and 27000 cm^{-1} (Table 49). As might be expected for closed shell compounds with deep purple / red colours, the low energy part of the spectrum for these complexes is featureless in all cases.[10, 11, 14 and 28]

Table 49: Characteristic UV-vis NIR absorption maxima (cm^{-1}) of 43, 44 and 48.

43	44	48
29411, 27027	29069, 20408	31847(sh), 30303, 24752, 19455

Unfortunately, the data collected provide a series of spectra that display a number of broad, and heavily overlapped transitions in the visible and NIR region for the complexes [**43**, **44** and **48**]$^{n+}$ (n = 1,2,3 and 4) (Figure 113 - Figure 115). While the exact cause of this broadening has not yet been established there are a number of reasons that have to be considered. As identified in the IR SEC results for [**48**]$^{4+}$ the insolubility of the highly charged species may lead to the adsorption of solid material on the electrode surface. In addition, the presence of various geometric forms (an example for **48** is given in Figure 112) of the compounds may lead to broadening due to the different transitions associated with each conformation as identified in the IR SEC for **43**. The charged species [**48**]$^{n+}$ are also able to occupy different spin states; this has been reported previously for Fe compounds by the Lapinte group for [Cp*(dppe)Fe=C(OCH_3)-CH=CHC-(OCH_3)=Fe-(dppe)Cp*][PF_6]$_2$,[29] [{Cp*(dppe)Fe(C≡C)}$_2$(1,3-C_6H_4)][PF_6] [30] and [{Cp*(dppe)Fe(C≡C)}$_2$(2,5-C_4H_2S)][PF_6] where the singlet triplet conversion barrier is found to be in the order of ca. 150 cm^{-1}.[31]

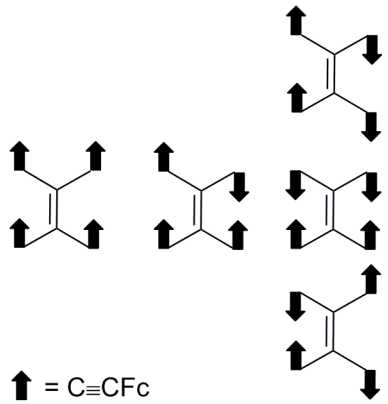

Figure 112: Schematic representation of the different geometries that ferrocenyl moieties can adapt in 48.

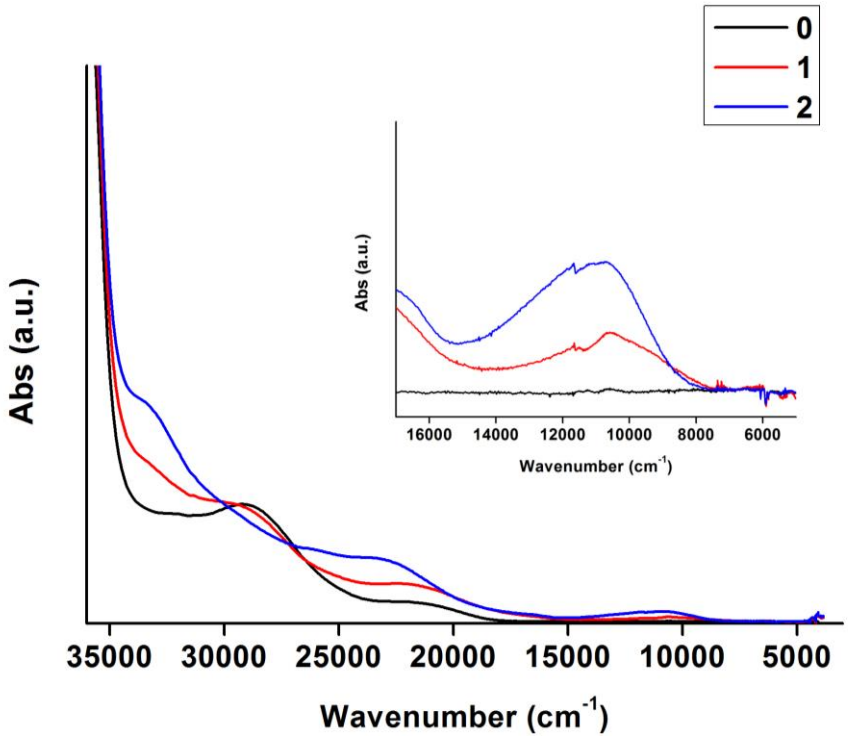

Figure 113: UV-vis NIR spectral changes accompanying oxidation of the ferrocene moiety in 43 in CH_2Cl_2 / 10^{-1} M $NBu_4[BArF_4]$within an OTTLE cell.

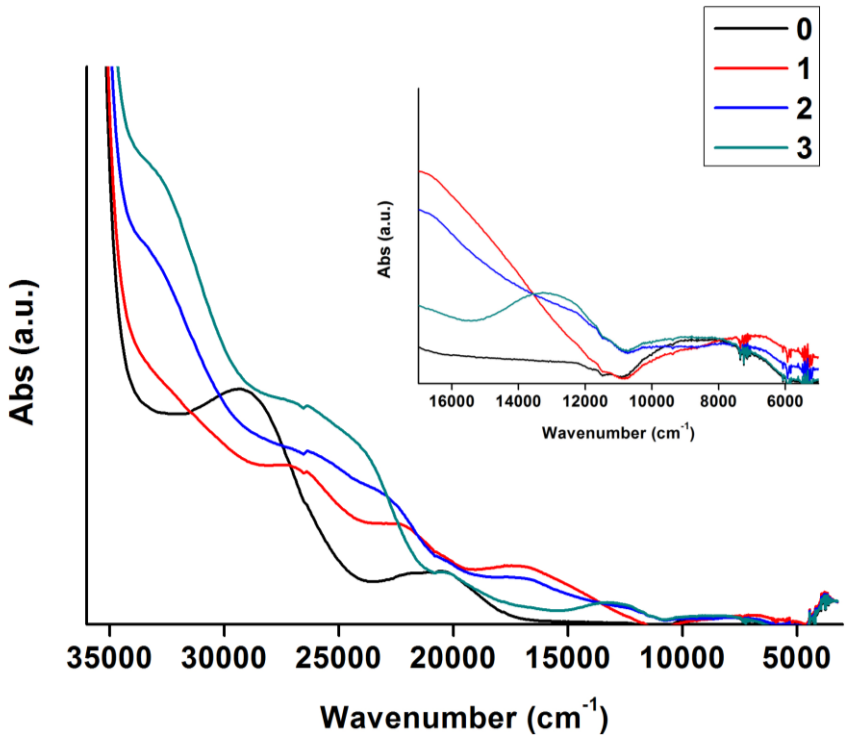

Figure 114: UV-vis NIR spectral changes accompanying oxidation of the ferrocene moiety in 44 in CH_2Cl_2 / 10^{-1} M $NBu_4[BArF_4]$within an OTTLE cell.

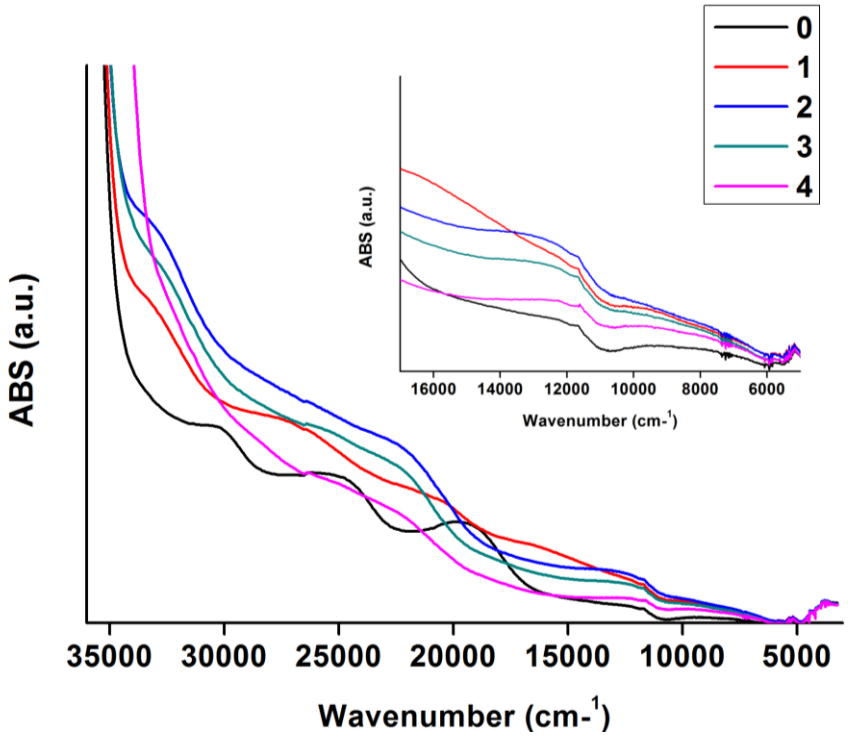

Figure 115: UV-vis NIR spectral changes accompanying oxidation of the ferrocene moiety in 48 in CH_2Cl_2 / 10^{-1} M $NBu_4[BArF_4]$within an OTTLE cell.

6.3.6. Conclusions

A simple synthetic route to di-ethynylethene compounds bearing ethynylferrocene arms has been developed for compounds containing 1,1-diphenylethene, ferrocenylethene or 1,1-di(ferrocenylethynyl)ethene moieties. By combining the Corey-Fuchs reaction with subsequent cross-coupling reactions a range of cross-conjugated materials bearing two, three or four ferrocene moieties have been developed and their electronic structure probed by electrochemistry and IR spectroelectrochemistry. Despite the previous reports of IVCT type transitions having been observed in ferrocenyl compounds the results here, hampered by the complex and broadened UV-vis NIR SEC, are unable to identify such transitions. In order to fully understand the electronic structure of these compounds and the nature of any transitions that can be extracted from experimental data further analysis needs to be carried out on the oxidised compounds. This has particular implications for compound **48** as the electronic structure needs to be fully understood before its viability as a MQCA type material can be fully assessed.

In trying to address the problems that have arisen in the UV-vis NIR SEC it is desirable for the compounds to undergo further testing including the use of low temperature UV-vis NIR SEC experiments in order to try and freeze out the most stable geometries of the complexes and reduce the broadening of the transitions as well as EPR and magnetic measurements to identify the specific charge configuration of the most applicable system [**48**]$^{2+}$.

6.4. Experimental Details

6.4.1. General Conditions

Solvent purification and characterisation of compounds was carried out as detailed in Chapter 2. The compounds $Pd(PPh_3)_4$,[32] and $Pd(PPh_3)_2Cl_2$ [33] were prepared by the literature methods. CBr_4 was purified by sublimation before use.

IR and UV−vis spectra were recorded on a Bruker Vertex 70v FT-IR spectrometer and a Scinco S3100 diode array spectrophotometer, respectively. UV-vis-NIR-IR spectroelectrochemical experiments at room temperature were conducted with an OTTLE cell equipped with a Pt-minigrid working electrode and CaF_2 windows. The optical path of the cell was ca. 0.2 mm. The concentrations of the ferrocenyl compounds and the supporting electrolyte used in these measurements were 1.3×10^{-2} and 3×10^{-1} mol dm^{-3} for IR spectroelectrochemical experiments and 10^{-3} and 3×10^{-1} mol dm^{-3} for the UV-vis-NIR studies, respectively.

6.4.2. Preparation of FcC≡CH (42)

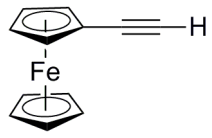

An oven dried Schlenk flask was charged with dry THF (25 mL) and Et_2O (50 mL) and the solvent degassed. To this solution, **22** (5.138 g, 13.892 mmol) was added and the mixture cooled to -78 °C. to the mixture a 2.5 M solution of ^{n}BuLi (11.67 mL, 29.172 mmol) in hexane was added dropwise and the mixture stirred for 1 h and then allowed to warm to room temperature. The reaction was quenched with H_2O (50

mL) and extracted with CH_2Cl_2 (3 x 40 mL) and the organic layers were combined, dried over MgSO4, filtered and the solvent removed in vacuo. The residue was pre-absorbed on to silica gel and purified purified by silica column chromatography eluting with hexane increasing to hexane: CH_2Cl_2 (50:50) to give the title compound as an orange solid. Yield 2.816 g, 97 %. ^{1}H NMR ($CDCl_3$): δ 2.70 (1H, s). 4.19 (2H, t, J = 2 Hz), 4.21 (5H, s), 4.46 (2H, t, J = 2 Hz). Literature: ^{1}H NMR ($CDCl_3$): δ 4.45 (2H, t, C_5H_4Fe), 4.21 (5H, s, C_5H_5Fe), 4.18 (2H, t, C_5H_4Fe), 2.71 (1H, s, C≡C*H*).[17]

6.4.3. Preparation of $Ph_2C=C(C{\equiv}CFc)_2$ (43)

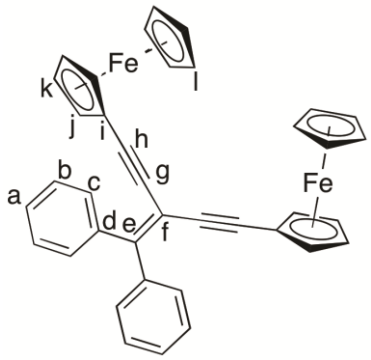

An oven dried Schlenk flask was charged with NEt_3 (25 mL) and the solvent degassed. To this solution, Ph_2CCBr_2 (0.5 g, 1.479 mmol), ethynylferrocene (0.652 g, 3.106 mmol), $Pd(PPh_3)_4$ (85 mg, 0.05 mmol) and CuI (6 mg, 0.02 mmol) were added and the solution heated at reflux for 17 hours. The solvent was removed in vacuo, the residue was preabsorbed on silica gel and purified by silica column chromatography eluting with hexane increasing to hexane: CH_2Cl_2 (50:50). Removal of the solvent in vacuo gives the title compound as an orange solid. Yield 418 mg, 48 %. ^{1}H NMR (CD_2Cl_2) δ 4.15 (10H, s, H*l*), 4.22 (4H, vt, J = 1.8 Hz, H*k*), 4.36 (4H, vt, J = 1.8 Hz, H*j*), 7.41 (6H, m, H*a*, H*c*), 7.53 (4H, m, H*b*). ^{13}C NMR (CD_2Cl_2) δ

64.78 (C*i*), 68.98 (C*k*), 69.85 (C*l*), 71.12 (C*j*), 84.66 (C*f,g* or *h*), 91.12 (C*f,g* or *h*), 102.91 (C*f,g* or *h*), 127.68 (C*c*), 128.17 (C*a*), 130.06 (C*b*), 140.80 (C*e*), 153.07 (C*d*). ASAP MS(+): *m/z* 597.1 $[M+H]^+$. Analysis found C 76.38, H 4.61% required C 76.52, H 4.74%.

6.4.4. Preparation of $FcCH=C(C\equiv CFc)_2$ (44)

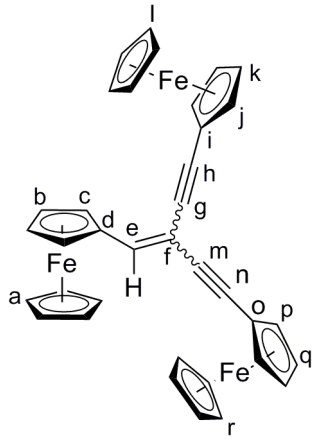

An oven dried Schlenk flask was charged with dry triethylamine (20 mL) and the solvent degassed. To this solution CuI (5 mg, 0.027 mmol), $Pd(PPh_3)_4$ (32 mg, 0.027 mmol), **22** (200 mg, 0.54 mmol) and **42** (250 mg, 1.19 mmol) were added and the mixture heated at reflux for 20 hours. The mixture was cooled to ambient temperature and the solvent removed *in vacuo*. The crude mixture was purified by silica column chromatography eluting with hexane increasing to hexane:CH_2Cl_2 (50:50), removal of the solvent gave the title compound as a bright red solid. Yield 231 mg, 68 %. Crystals suitable for X-ray diffraction were grown from slow evaporation of a CH_2Cl_2 solution. ^{1}H NMR (CD_2Cl_2) δ 4.22 (5H, s, H*l*), 4.24 (2H, t, J = 2 Hz, H*j*), 4.27 (5H, s, H*r*), 4.29 (2H, t, J = 2 Hz, H*p*), 4.32 (5H, s, H*a*), 4.41 (2H,t, J = 2 Hz, H*c*), 4.49 (2H, t, J = 2 Hz, H*k*), 4.58 (2H, t, J = 2 Hz, H*q*), 4.92 (2H,

t, J = 2 Hz, H*b*), 6.85 (1H, s, H*e*); ^{13}C NMR (CD_2Cl_2) δ 65.24 (Ci), 65.31 (Co), 68.85 (Ck), 69.12 (Cq), 69.47 (Cc), 69.53 (Ca), 69.88 (Cl), 69.91 (Cr), 70.09 (Cb), 71.13 (Cj), 71.19 (Cp), 80.17 (Cd), 84.36 (Cg/m), 85.77 (Cf), 85.97 (Cg/m), 92.80 (Cn), 100.09 (Ch), 142.06 (Cf); Found C 68.82, H 4.50% required C 68.70, H 4.61%. ASAP-MS(+):*m/z* 629.0 $[M+H]^+$.

6.4.5. Preparation of $CH(OH)(C{\equiv}CFc)_2$ (45)

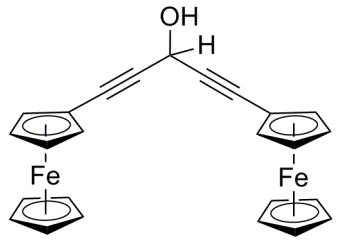

An oven dried Schlenk flask was charged with dry THF (30 mL) and the solvent degassed. To this solution, **42** (1.50 g, 7.14 mmol) was added and the mixture cooled to 0 °C. To the mixture a 2.5 M solution of ^{n}BuLi (3.00 mL, 7.40 mmol) in hexane was added dropwise and the mixture stirred for 2 h and methyl formate (0.22 mL, 3.57 mmol) added. The reaction was stirred at 0 °C for 1 hour, and then quenched with saturated aqueous NH_4Cl, added to H_2O (15 mL) and extracted with CH_2Cl_2 (3 x 40 mL) and the organic layers were combined, dried over $MgSO_4$, filtered and the solvent removed in vacuo. The residue was pre-absorbed on to silica gel and purified purified by silica column chromatography eluting with hexane increasing to hexane: CH_2Cl_2 (30:70) to give the title compound as an orange solid. Yield 1.026 g, 64 %. ^{1}H NMR (CD_2Cl_2): δ 2.38 (1H, d, *J* = 7.5 Hz), 4.22 (4H, t, J = 2 Hz), 4.25 (10H, s), 4.48 (4H, t, J = 2 Hz), δ 5.37 (1H, d, *J* = 7.5 Hz).

Literature: ^{1}H NMR ($CDCl_3$): δ 2.21 (1H, d, *J* = 7.5 Hz), 4.21 (4H, t, J = 2 Hz), 4.24 (10H, s), 4.47 (4H, t, J = 2 Hz), δ 5.55 (1H, d, *J* = 7.5 Hz).[5 and 19]

6.4.6. Preparation of C(=O)(C≡CFc)$_2$ (46)

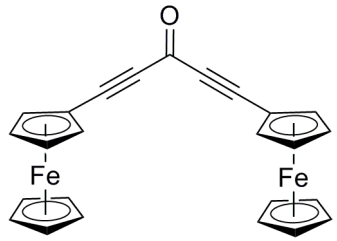

An oven dried Schlenk flask was charged with dry Et_2O (50 mL) and the solvent degassed. To this solution, **45** (1.026 g, 2.29 mmol) and MnO_2 (1.493 g, 17.172 mmol) were added and the mixture stirred for 15 hours, filtered through celite and washed with Et_2O until the washings run colourless (ca 150 mL). The solvent was removed in vacuo to give the title compound as a dark red solid. ^{1}H NMR (CD_2Cl_2): δ 4.29 (10H, s), 4.42 (4H, t, J = 2 Hz), 4.66 (4H, t, J = 2 Hz).

Literature: ^{1}H NMR($CDCl_3$): δ 4.30 (10H, s), 4.43 (1H, t, J = 2 Hz), 4.66 (4H, t, J = 2 Hz).[5 and 19]

6.4.7. Preparation of $(FcC{\equiv}C)_2C{=}CBr_2$ (47)

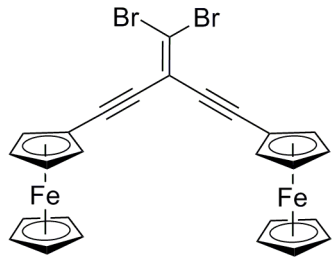

An oven dried Schlenk flask was charged with dry benzene (40 mL) and the solvent degassed. To this solution, **46** (0.450 g, 1.009 mmol), PPh_3 (1.058 g, 4.035 mmol) and CBr_4 (0.669 g, 2.017 mmol) were added and the mixture stirred for 17 hours. The solvent was removed in vacuo and the residue pre-absorbed on to silica gel and purified by silica column chromatography eluting with hexane increasing to hexane: CH_2Cl_2 (60:40). The solvent was removed in vacuo to give the title compound as an orange solid. Yield 0.548 g, 90 %. ^{1}H NMR ($CDCl_3$): δ 4.25 (10H, s), 4.26 (4H, t, J = 2 Hz), 4.52 (4H, t, J = 2 Hz).

Literature: ^{1}H NMR($CDCl_3$): δ 4.26 (14H, m), 4.52 (4H, s).[5 and 19]

6.4.8. Preparation of $(FcC{\equiv}C)_2C{=}C(C{\equiv}CFc)_2$ (48)

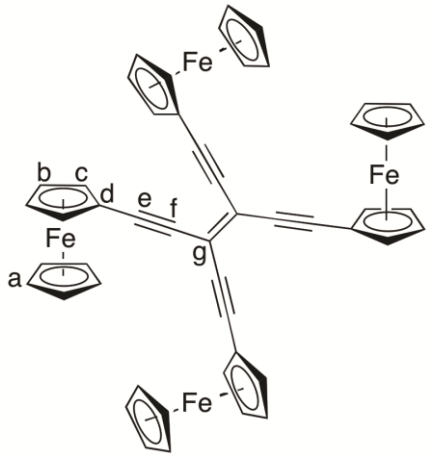

An oven dried Schlenk flask was charged with HN^iPR_2 (10 mL) and the solvent degassed, To this solution, $(FcC{\equiv}C)_2C{=}CBr_2$ (**47**) (60 mg, 0.1 mmol), $FcC{\equiv}CH$ (63 mg, 0.3 mmol), $Pd(PPh_3)_4$ (7 mg, 0.005 mmol) and CuI (2 mg) were added and the mixture stirred at room temperature for 16 hours. The precipitate was filtered, extracted in to hexane:CH_2Cl_2 (50:50). The solvent removed in vacuo and the residue was taken up in CH_2Cl_2 and purified on column chromatography (hexane $\rightarrow$hexane:CH_2Cl_2 (70:30)) carefully eluting 3 close running bands. The solvent was removed from the 3rd band (rf = 0.35 in hexane:CH_2Cl_2 (70:30)) to give a dark purple solid. Yield 16 mg, 19 %. ^{1}H NMR ($CDCl_3$): 4.27 (s, 20H, H*a*), 4.30 (vt, J = 2Hz, 8H, H*c*), 4.59 (vt, J = 2Hz, 8H, H*b*). ^{13}C NMR ($CDCl_3$): 64.91 (s, C*d*), 69.54 (s, C*b*), 70.46 (s, C*a*), 71.87 (s, C*c*), 84.99 (s, C*f*), 97.65 (s, C*e*), 110.17 (s, C*g*). ASAP MS(+): *m/z* 861.1 $[M]^+$. ASAP-HRMS(+) *m/z*: 860.0228 (found); 860.0215 (calculated for $C_{50}H_{36}{}^{56}Fe_4$) (860.0214).

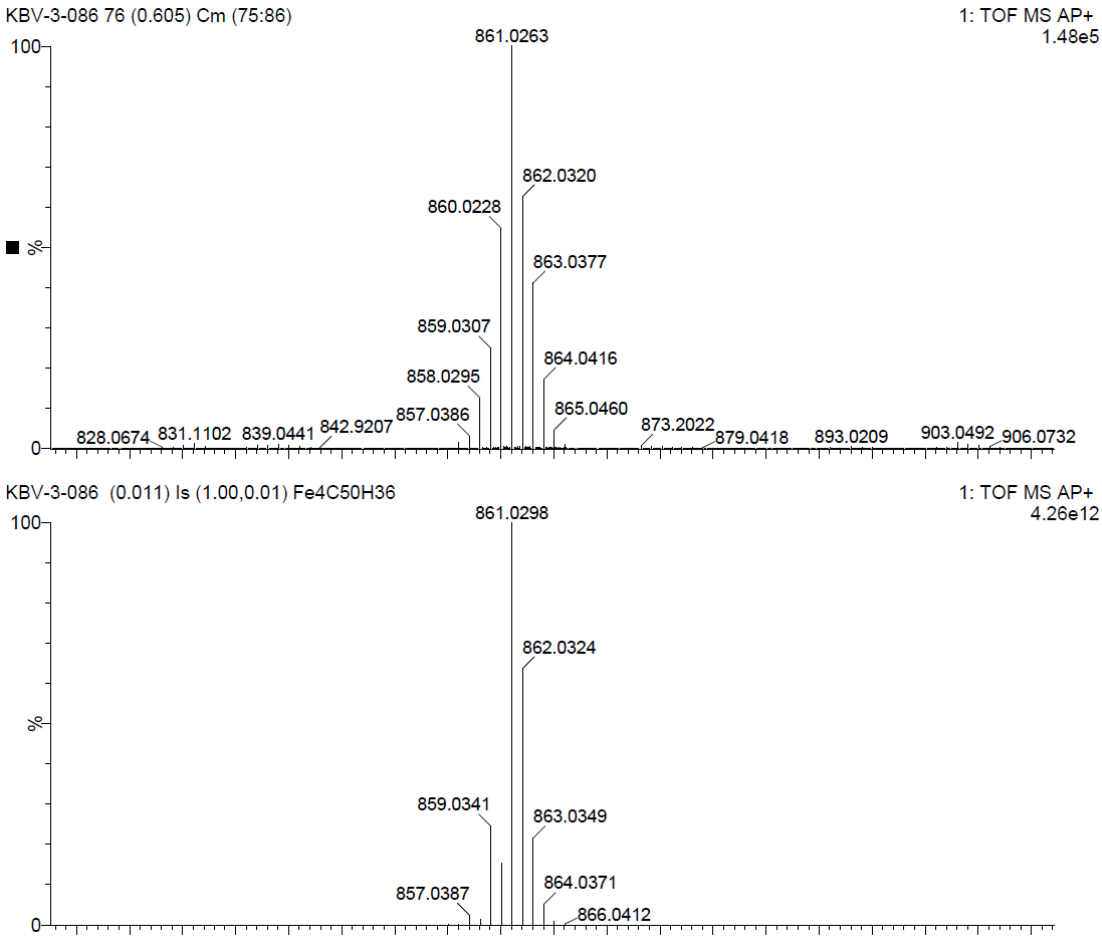

Figure 116: ASAP HRMS(+) for 48. Top shows obtained and bottom shows predicted spectra.

6.5. References

1. (a) Cowan, D. O; Park, J; Pittman, C. U; Sasaki, Y; Mukerjee, T. K; Diamond, N. A; *J. Am. Chem. Soc*, **1972**, 5110. (b) Cowan, D. O; LeVanda, C; Park, J; Kaufman, F. *Acc. Chem. Res*. **1973**, *6*, 1. (c) Talham, D. R; Cowan, D. O. *Organometallics*, **1984**, *3*, 1712.
2. (a) Ribou, A. C.; Launay, J. P.; Sachtleben, M. L.; Li, H.; Spangler, C. W. *Inorg. Chem*. **1996**, *35*, 3735. (b) Delgado-Pena, F; Talham, D. R; Cowan, D. O. *J. Organomet. Chem*, **1983,** *253*, C43.
3. Chen, Y. J; Pan, D. S; Chiu, C. F; Su, J. X; Lin, S. J; Kwan, K. S. *Inorg. Chem*. **2000**, *39*, 953.
4. (a) Levanda, C.; Bechgaard, K.; Cowan, D. O. *J. Org. Chem*. **1976**, *41*, 2700. (b) Shah, H. H; Al-Balushi, R. A; Al-Suti, M. K; Khan, M. S; Woodall, C. S; Molloy, K. C; Raithby, P. R; Robinson, T. P; Dale, S. E. C; Marken, F. *Inorg. Chem*. **2013**, *52*, 4898.
5. Xu, G. L.; Xi, B.; Updegraff, J. B.; Protasiewicz, J. D.; Ren, T. *Organometallics* **2006**, *25*, 5213.
6. Yuan, Z; Stringer, G; Jobe, I. R; Kreller, D; Scott, K; Koch, L; Taylor, N. J; Marder, T. B; *J. Organomet. Chem*, **1993**, *452*, 115.
7. Adams, R. D.; Qu, B.; Smith, M. D. *Organometallics.* **2002**, *21*, 3867.
8. Barriere, F; Camire, N; Geiger, WE; Mueller-Westerhoff, UT; Sanders, R. *J. Am. Chem. Soc*. **2002**, *124*, 7262.
9. Speck, J. M; Claus, R; Hildebrand, A; Ruffer, T; Erasmus, E; Van As, L; Swarts, J. C; Lang, H. *Oragnometallics*, **2012**, *31*, 6373.
10. Hildebrandt, A.; Schaarschmidt, D.; Claus, R.; Lang, H. *Inorg. Chem*. **2011**, *50*, 10623.
11. Hildebrandt, A.; Schaarschmidt, D.; Lang, H. *Organometallics* **2011**, *30*, 556.
12. Miesel, D; Hildebrandt, A; Korb, M; Low, P. J; Lang, H. *Organometallics*, **2013**, *32*, 2993.
13. Lehrich, S. W; Hildebrandt, A; Rüffer, T; Korb, M; Low, P. J; Lang, H. *Organometallics*. **2014**, DOI: 10.1021/om500072q.
14. Hildebrandt, A.; Rüffer, T.; Erasmus, E.; Swarts, J. C.; Lang, H. *Organometallics* **2010**, *29*, 4900.

15. Fink, H; Long, N. J; Martin, A. J; Opromolla, G; White, A. J. P; Williams, D. J; Zanello, P. *Organometallics*, **1997**, *16*, 2646.
16. (a) Diallo, A. K; Dara, J. C; Varret, F; Ruiz, J; Astruc, D. *Angew. Chem. Int. Ed*, **2009**, *48*, 3141. (b) Diallo, A. K; Absalon, C; Ruiz, J; Astruc, D. *J. Am. Chem. Soc*. **2011**, *133*, 629.
17. Courtney, D; McAdam, C. J; Manning, A. R; Müller-Bunz, H; Ortin, Y; Simpson, J. *J. Organomet. Chem*, **2012**, *705*, 7.
18. (a) McEwen, C. N.; McKay, R. G.; Larsen, B. S. *Anal. Chem.* **2005**, *77*, 7826. (b) Smith, M. J. P.; Cameron, N. R.; Mosely, J. A. *Analyst* **2012**, *137*, 4524.
19. Auffrant, A; Diederich, F.; Boudon, C; Gisselbrecht, J. P; Gross, M. *Helv. Chim. Acta*, **2004**, *87*, 3085.
20. Davies, H. M. (2008) *Synthesis and Characterisation of Molecular Materials*. Ph.D. Thesis. University of Bath, UK.
21. Barriere, F; Geiger, W. E. *J. Am. Chem. Soc*. **2006**, *128*, 3980.
22. (a) Kowalski, K; Linseis, M; Winter, . ; Zabel, M; Zalis, S; Kelm, H; Kruger, H. J; Sarkar, B; Kaim, W. *Organometallics*. **2009**, *28*, 4196. (b) Warratz, R; Tuczek, F. *Inorg. Chem.* **2009**, *48*, 3591. (c) Warratz, R; Aboulfadl, H; Bally, T; Tuczek, F. *Chem. Eur. J.* **2009**, *15*, 1604.
23. Lent, C. S. *Science*, **2000**, 288,1597.
24. (a) Li, Z; Beatty, A. M; Fehlner, T. P. *Inorg. Chem*. **2003**, *42*, 5707. (b) Lent, C. S; Isaksen, B; Lieberman, M. *J. Am. Chem. Soc.* **2003**, *125*, 1056.
25. (a) Auger, J; Muller, A. J; Swarts, J. C. *Dalton Trans*. **2007**, 3623. (b) Pfaff, U; Hildebrandt, A; Schaarschmidt, D; Rufffer, T; low, P. J; Lang, H. *Organometallics*. **2013**, *32*, 6106.
26. Quardokus, R. C; Wasio, N. A; Forrest, R. P; Lent, C. S; Corcelli, S. A; Christie, J. A; Henderson, K. W; Kandel, S. A. *Phys. Chem. Chem. Phys*, **2013**, *15*, 6973.
27. Wasio, N. A; Quardokus, R. C; Forrest, R. P; Corcelli, S. A; Lu, Y. Lent, C. S; Justaud, F; Lapinte, C; Kandel, S. A. *J. Phys. Chem. C*. **2012,** *116*, 25486.
28. (a) Hildebrandt, A.; Schaarschmidt, D.; van As, L.; Swarts, J. C.; Lang, H. *Inorg. Chim. Acta* **2011**, *374*, 122. (b) Hildebrandt, A.; Pfaff, U.; Lang, H. *Inorg. Chem*. **2011**, *31*, 111. (c) Hildebrandt, A.; Lang, H. *Dalton Trans*. **2011**, *40*, 11831. (d) Kaleta, K.; Hildebrandt, A.; Strehler, F.; Arndt, P.; Jiao, H.; Spannenberg, A.; Lang, H.; Rosenthal, U. *Angew. Chem., Int. Ed*. **2011**, *50*, 11248. (e) Speck, J.

M.; Schaarschmidt, D.; Lang, H. *Organometallics* **2012**, *31*, 1975. (f) Auger, J.; Muller, A. J.; Swarts, J. C. *Dalton Trans*. **2007**, 3623.

29. Guillame, V; Mahias, V; Mari, A; Lapinte, C. *Organometallics*, **2000**, *19*, 1422.
30. Weyland, T; Costuas, C; Toupet, L; Halet, J. F; Lapinte, C. *Organometallics*, **2000**, *19*, 4228.
31. Roué, S; Le Stang, S; Toupet, L; Lapinte, C. *C. R. Chimie*, **2003**, *6*, 353.
32. Coulson, D. R. *Inorg. Synth.* **1972**, *13*, 121.
33. Miyaura, N; Suzuki, A. *Org. Syth. Coll*, **1993**, *8*, 532.